
Estudio hidroquímico y de isótopos estables
en un sistema acuífero en el neógeno de la
Cuenca del Guadiana Menor
(Sureste de España)

Combined hydrochemical and stable isotope
study of an aquifer system in the neogene
Guadix-Baza basin in southern Spain

Index

I. List of figures	
II. List of tables	
III. List of abbreviations	
IV. Summary	
1. Introduction.....	1
1.1. Motive.....	1
1.2. Regional Setting:.....	1
1.2.1. Spain.....	1
1.2.2. The Betic Cordillera.....	2
1.2.3. Climate, Meteorology	4
1.3. Study Area	6
1.3.1. Geological Setting	6
1.4. Geomorphology.....	9
1.5. Hydrogeology	10
1.5.1. Hydrogeology Aquifer Duda-La Sagra	10
1.5.1.1. Carbonate terrains	11
1.5.1.2. Pliocene/Quaternary basin deposits	12
1.6. Agriculture, Land-use, Soils	12
1.7. Climate, Meteorology	13
1.7.1. Climate, Temperature, Precipitation, Groundwater recharge	13
1.7.2. Evapotranspiration, hydrological balance.....	15
1.8. Hydrology	16
1.8.1. Principle river and San Clemente Reservoir.....	16
2. Stable Isotopes.....	18
2.1. Isotope fractionation	18
2.1.1. Equilibrium fractionation.....	19
2.1.2. Non-equilibrium (kinetic) fractionation	19
2.1.3. Rayleigh fractionation and Meteoric Water lines	20
2.2. Isotope effects.....	22
2.3. Previous stable isotope studies.....	23
3. Methods.....	25
3.1. Sampling Strategy and Sampling Network	25
3.2. Sampling Methods.....	28
3.3. Analysis.....	30
3.3.1. Ions	30
3.3.2. Stable Isotopes	30
3.4. Climatology, evapotranspiration, groundwater recharge	31
3.5. Catchment, Digital Elevation Model (DEM)	32
3.6. Hydrochemistry	32
3.6.1. Reliability check	32
4. Results and Discussion	33
4.1. Hydrochemistry	33
4.1.1. Concepts.....	34
4.1.1.1. Carbonate Dissolution.....	34
4.1.1.2. Saturation Index.....	34
4.1.2. Classification	36
4.1.2.1. Group 1	37
4.1.2.2. Group 2.....	39

4.1.2.3.	Group 3.....	40
4.1.3.	Discussion and conceptual model.....	41
4.2.	Stable Isotopes.....	45
4.2.1.	Precipitation, GNIP.....	45
4.2.2.	Stable Isotopes ($\delta^{18}\text{O}$, δD)	47
4.2.2.1.	Springs.....	49
4.2.2.1.1.	Group 1 “Sierra de la Sagra”	50
	(SP-GM-017; -020; -021; -022)	50
4.2.2.1.2.	Group 2 “Sierra Seca” (SP-GM-001; -013).....	51
4.2.2.1.3.	Group 3 “Guardal Basin” (SP-GM-002; -023; -026).....	52
4.2.2.1.4.	“Group” 4 “Thermal” (SP-GM-007)	54
4.2.2.2.	Surface water.....	55
4.2.2.3.	Wells	57
4.2.2.3.1.	Group Huescar	58
4.2.2.3.2.	Group San Clemente.....	59
4.2.2.3.3.	Group Fatima	59
4.2.2.3.4.	Conclusions.....	60
5.	Outlook.....	61
6.	References.....	62
7.	Appendix (data & sampling sites info)	64

I. List of Figures

- Figure 1.1 Outline map of mainland Spain and the Balearic Islands showing the brought division into “Variscan” and “Alpine” Spain. White areas in Spain are Cenozoic Basins Box indicates region of the study area (Gibbons & Moreno, 2002).
- Figure 1.2 Geologic evolution of the Betic-Rif mountain belt (LONERGAN & WHITE, 1997).
- Figure 1.3 Geologic sketch map of the Betic Cordillera (Azañón et. al., 2002). a- Iberian Massif, b- Subbetic zone, c- Prerif, Mesorif, d- Prebetic zone, e- olistostroms and brecciasf- Flysch, g- Nevado-Filábride complex, h- Alpujárride complex, i- Malaguidej- flysch, k- Neogene basins (Azañón et al., 2002).
- Figure 1.4 Deviations of mean seasonal precipitation in Andalusia(colored areas) in A) winter 2004/05 and B) spring 2005. The red droplets indicate negative deviations of the hydrological balance to the period of 1971-2000, the blue ones positive deviations. The outlined area is the Baza and Huescar-Puebla region representing the upper Guadiana Menor catchment. (www.juntadeandalucia.es, 5/9/2006)
- Figure 1.5 Geological sketch map of Andalusia showing the division of the Betics into External, Internal and Flysch Zones. Black outline indicates Study area Duda-La Sagra near Huescar (simplified after IGME, 2005)
- Figure 1.6 Overview map of the Upper Guadiana Menor shows the geological and hydrogeological Setting. The study area is in the NW corner where the Guardal River Catchment is indicated. A schematic geological cross-section displays the transition zone of the S mountains and the basin with horst and graben structures where faults establish possible pathways for groundwater to the surface (e.g. thermal springs). The empty areas are the central parts of the basin where the sediments are impermeable.
- Figure 1.7 Simplified structural map of the study area. Indicated are the Guardal River sampling site (blue) and Fuencaliente (red) where the water is highly mineralized. Modified from ITGE, 1994
- Figure 1.8 Contour map of the study area with the main morphologic features of the transition zone from the mountainous northern part to the southwards open basin, the Guardal River and Catchment. Generated with ESRI ArcMap 8.3; data source: Mapa Digital de Andalusia 1:100.000, 1999.
- Figure 1.9 Mean annual temperature and precipitation values for the years 2000 – 2006 for the meteorological stations in Baza (X: 520628; Y: 4157712), Puebla de Don Fadrique (X: 554482; Y: 4192456) and 2000 – 2004 in Huescar (X: 539946; Y: 4184099)[Data: www.juntadeandalucia.es, 5/9/2006].
- Figure 1.10 Climatic water balance for Baza station: mean monthly values 2000-2006 (left) and hydrological year (2005) of field campaigns (right) and for 2000-2006 at Puebla de Don Fadrique station.

-
- Figure 1.11 Extraction tower and dam of San Clemente Reservoir (Height of tower: ca. 30m).
- Figure 2.1 Isotopic enrichment in evaporating water and the effect of humidity (h). Slopes (s) are approximations of each curve near the GMWL (heavy line) (from CLARK AND FRITZ, 1997).
- Figure 2.2 Elevation effect and groundwater mixing for spring water (modified after www.iaea.org).
- Figure 3.1 Sampling Network.
- Figure 3.2 Electro Neutrality vs. Number of Samples.
- Figure 4.1 Linear correlations of EC and sum of cations (top) and anions (bottom) of measured samples.
- Figure 4.2 Piper diagram of all samples.
- Figure 4.3 Correlation of carbonate (left) and sulfate (right) dissolution of the 3 groups.
- Figure 4.4 Concentration [meq/l] vs. constituents plot of Group 2 members.
- Figure 4.5 Concentration [meq/l] vs. constituents plot of all three groups.
- Figure 4.6 Schematic cross-section of the mountain-intramontane basin transition zone with flow paths of shallow groundwater from recharge areas in the elevated regions and of groundwater from the basin along tectonic faults to a mixing zone of the two (sketch not to scale).
- Figure 4.7 Simplified geological maps with overview of the spatial distribution of Ca-Mg ratio (left) and the major chemical constituents presented as Stiff-Diagrams (right).
- Figure 4.8: Developing of saturation indices (calcite & dolomite) from spring to autumn 2005 for the study area.
- Figure 4.9 Mean weighted monthly values for $\delta^{18}\text{O}$ (middle) and d-excess (top), both in ‰ vs. VSMOW and with individual scales, are plotted with meteorological data for Gibraltar (left, 1962-2001) and Barcelona (right, 1985-1991). The lower diagram displays mean monthly precipitation in mm (bars, left ordinate) and temperature in °C (line, right ordinate) Data: GNIP, IAEA, 27/10/2006.
- Figure 4.10 The amplitude of the seasonal variation of the ^{18}O values of precipitation can be observed in groundwater (exponential model by STICHLER AND HERRMANN, 1983. source: IAEA, VOLUME IV).
- Figure 4.11 Overview of $\delta^{18}\text{O}$ and δD values of all samples (n=48) with GWML and WMMWL reference and magnified section (A) of the plot for better identification. Some of the members of spring Group 1 “Sierra Sagra” (solid triangles) are assumed to be affected by “secondary” evaporation and are possibly located closer to the rest of this group as indicated by the arrow (for explanation see description of group section below).
- Figure 4.12 Overview of $\delta^{18}\text{O}$ and δD values of all samples (n=48) with GWML and WMMWL reference and magnified section (A) of the plot for better identification. Some of the members of spring Group 1 “Sierra Sagra” (solid triangles) are assumed to be affected by “secondary” evaporation

and are possibly located closer to the rest of this group as indicated by the arrow (for explanation see description of group section below).

- Figure 4.13 $\delta^{18}\text{O}$ and δD -correlation of sampled springs in reference to the Global and Western Mediterranean MWL.
- Figure 4.14 Temporal variations of $\delta^{18}\text{O}$ and d-excess of Group 1 springs with mean monthly temperatures 2005 Huescar. The dotted lines indicate a phase shift between the input (summer precipitation) and the response signal (enriched isotope compositions). (www.juntadeandalucia.es, 2006)
- Figure 4.15 Temporal variations of $\delta^{18}\text{O}$ (left) and δD (right) with mean monthly temperatures 2005 (Huescar, www.juntadeandalucia.es, 2006).
- Figure 4.16 Group 3 values and temporal variations of $\delta^{18}\text{O}$ and d-excess with mean monthly temperatures 2005 (Huescar, www.juntadeandalucia.es 2006) Line indicates change of sampling location for SP-GM-002.
- Figure 4.17 $\delta^{18}\text{O}$ vs. δD plot of the previously described groups of springs and the slightly thermal spring which is shifted on both axes.
- Figure 4.18 Different processes that shift the δ -values for ^{18}O and D away from the MWL. Local MWL corresponds to Mediterranean Water Line (Source: IAEA, 2006).
- Figure 4.19 $\delta^{18}\text{O}$ and δD -correlation of sampled surface water in reference to the global and western Mediterranean MWL.
- Figure 4.20 Temporal variations of $\delta^{18}\text{O}$ of all river sites compared to a contributing spring with the monthly precipitation 2005 (grey bars) to visualize rain amounts.
- Figure 4.21: Location of river sampling sites upstream and downstream from the reservoir.
- Figure 4.22 $\delta^{18}\text{O}$ vs. time plot for all surface water sites with the mean monthly temperature at the Huescar station in the background. Two sites (SP-GM-015 & -019) are located upstream and one site (SP-GM-016) downstream from the reservoir.
- Figure 4.23: Schematic flow conditions upstream and downstream from the reservoir
- Figure 4.24: $\delta^{18}\text{O}$ vs. δD plot of the sampled wells with MWL as reference (left) and with river and reservoir to visualize the evaporation trend in the study area (right).

II. List of Tables

- Table 1.1 Mean annual temperature T and precipitation P for the Baza station (data: Junta de Andalucia, 5/9/2006).
- Table 3.1 Site types.
- Table 3.2 Data of Sampling Sites.
- Table 3.3 Methods and devices of sampled parameters.
- Table 3.4 Analytical Methods Hydrogeochemistry.
- Table 4.1 Summary of Group 1 physical parameters and saturation indices (SI).
- Table 4.2 Summary of Group 2 physical parameters and saturation indices (SI).

III. List of Abbreviations

°	degree
°C	degree centigrade (Celsius scale)
‰	per mil
2H	D or Deuterium
approx.	approximately
avg.	average
Barr.	Barranco (creek, valley)
Cjo.	Cortijo (homestead)
D	2H or Deuterium
d-excess	deuterium excess
Emb.	Embalse (reservoir)
ETA	actual evapotranspiration
Eq	equation
FAO	Food and Agriculture Organization of the United Nations
Fte.	Fuente (spring)
FUB	Freie Universität Berlin
GMWL	Global Meteoric Water Line
GNIP	Global Network of Isotopes in Precipitation
GWR	groundwater recharge
IAEA	International Atomic Energy Agency
ICP	Inductively Coupled Plasma
IGME	Instituto Geologico y Minero España
Man.	Manantial (spring)
masl	meter above sea level
max.	maximum
min.	minimum
MWL	Meteoric Water Line
Nac.	Nacimiento (source)
R	runoff
SI	saturation index
UGR	Universidad Granada
vs.	versus
VSMOW	Vienna Standard Mean Ocean Water
WMMWL	Western Mediterranean Meteoric Water Line

V. Summary

This work is trying to approach the improvement in understanding the hydrogeological mechanisms of an aquifer system in a semiarid climate where the necessity for an economic and sustainable water management becomes increasingly urgent.

The study area is located at the northern margin of the Guadix-Baza-Basin, a neogene intermontane depression 150 km north-east of Granada, Southern Spain. It is part of the upper catchment of the Guadalquivir River, one of the largest streams in Spain. The study area covers part of the transition zone between the basin and the surrounding sierras where groundwater recharge mainly occurs.

The study is divided into two main aspects, the characterization of the Duda-La Sagra Aquifers in terms of time and space. To achieve this, it was essential to develop a grid of water sampling points in different types of water sources (springs, rivers, wells and reservoir) while a good spatial distribution of sampling sites is important to cover the area of the aquifers in a representative way.

The spatial characterization required a larger sampling campaign where a number of sampling points were chosen that are distributed widely across the study area and that were sampled once or twice within the hydrological year. For the characterization of the variations over time, a smaller number of important springs, rivers, the reservoir and wells were sampled at least monthly. The data relevant for this study includes discharge, depth to water table, field parameters, alkalinity and ion and stable isotope analysis.

The access to wells was particularly problematic, since most of the wells are private pumping wells for irrigation purpose. The few domestic wells are either on private property or in form of older dug wells that fell dry within the last decade. This could be taken as evidence for the growing number of agricultural pumping wells precipitating the lowering of the water table locally. Additionally a potential quantity of unregistered wells also might have some significance in this matter.

The sampling followed a routine where a number of field parameters were determined at each site. These included temperature, pH-value, electric conductivity, Eh-value and dissolved oxygen measurement as well as alkalinity, nitrate and nitrite determination. Three individual samples were taken and shipped to the FU Berlin Hydrochemistry Laboratory for selected major and minor ion analysis (Ca^{2+} , Mg^{2+} ,

Summary

Na⁺, K⁺, Fe²⁺, Mn²⁺, Sr²⁺, Cl⁻, SO₄²⁻, NO₃⁻) and to the AWI isotope laboratory in Potsdam for stable isotope analysis (¹⁸O and ²H).

The results of the analyses could then be interpreted and the samples and sampling sites could be classified according to their hydrochemical and isotopegeochemical properties.

Three hydrochemically distinct groups could be determined. The first group comprises springs, creeks, a reservoir and three wells and can be associated with the sierras in the northern part of the catchment area where hydrogen carbonate-type waters prevail (Ca-Mg-HCO³). The temperature ranges from 8-21 °C, the pH from 7-9 and electric conductivities from 300-760 μS/cm. The positive trend in saturation indices with respect to calcite reflects the declining discharge rates as summer proceeds. This fact confirms the assumption that groundwater recharge occurs mainly in winter.

The second group is associated with the basin and includes two springs and two wells with sulfate-bearing water (Ca-Mg-SO₄-CO³). The temperatures range between 15° and 17°C with pH around 7 and of 700 to 900 μS/cm. Some wells in the transition zone show chemical compositions that represent a mixture of these two water types. A third group comprises a spring and a river in the basin that show similar chemical compositions as the second group but exceed their concentration by far. The temperatures for this group range between 16° to 20° and the electric conductivities from 1500-1800 μS/cm. These relatively high mineralized waters can be associated with fault zones.

The hydrochemical interpretation concludes in a conceptual model, that the shallow hydrogen carbonate waters from the mountains mix with the deeper sulfate-type waters from the basin.

The classification of the springs could be extended by means of the stable isotope analyses. The groups of springs that were determined are distinguished by orographic conditions like different altitude and slope exposition. They are a northern group (Sierra Sagra), a western group (Sierra Seca), a southern group (basin) and a thermal spring. Altogether the δ-values are in the relatively narrow range of -8‰ (thermal) and -9.3‰ (mountain spring) for ¹⁸O and -57‰ and -62‰ for D respectively. Variations according to summer/winter seasonality in precipitation could be detected with a phase shift of approximately 2-3 months between input and output signal.

Summary

The reservoir obtains a peculiar part in the group of surface water. The isotope data show a trend line typical for evaporation from open surfaces with the reservoir as an end member. The δ -values range from -8.99 to -5.96 and -60 to -45.6 for ^{18}O and D respectively. The influence of the reservoir with its strong evaporation does not show in the river water downstream as expected. While the Guardal River upstream from the reservoir that runs dry during summer is subject to losing river conditions, it is a gaining river downstream from it. As a result, the evaporation signal in the rivers isotopic composition is superposed by the exfiltration of groundwater.

The isotope signals in the sampled wells differ locally; however, some difficulties are encountered trying to interpret the spatial relations. The southward expanding basin enfolds a variety of factors capable of altering isotope signals that can not be accounted for within the scope of this work. It can be assumed though that mixing processes as well as evaporation occupy a significant position in isotopic composition of groundwater.

1. Introduction

1.1. Motive

This Diploma Thesis and Mapping were devised and carried out under the patronage of collaboration between the Freie Universität Berlin, Alfred Wegener Institut Potsdam, the Universidad de Granada and the Instituto GeoMinero de España. Objectives of the collaboration are hydrogeological studies in regions with semi arid climate where water supply increasingly depends on groundwater as a resource and ways to produce drinking water in an effective way. Recent climatic development shows a trend towards warmer winters and drier summers and demands for secure access to water and sustainable groundwater resource management obtains crucial significance. The field work in Spain was between February and October 2005.

1.2. Regional Setting:

1.2.1. Spain

The geology of Spain (GIBBONS & MORENO, 2002) can be simplified and divided into Mesozoic-Cenozoic rocks deformed by Alpine orogeny in the eastern part of the

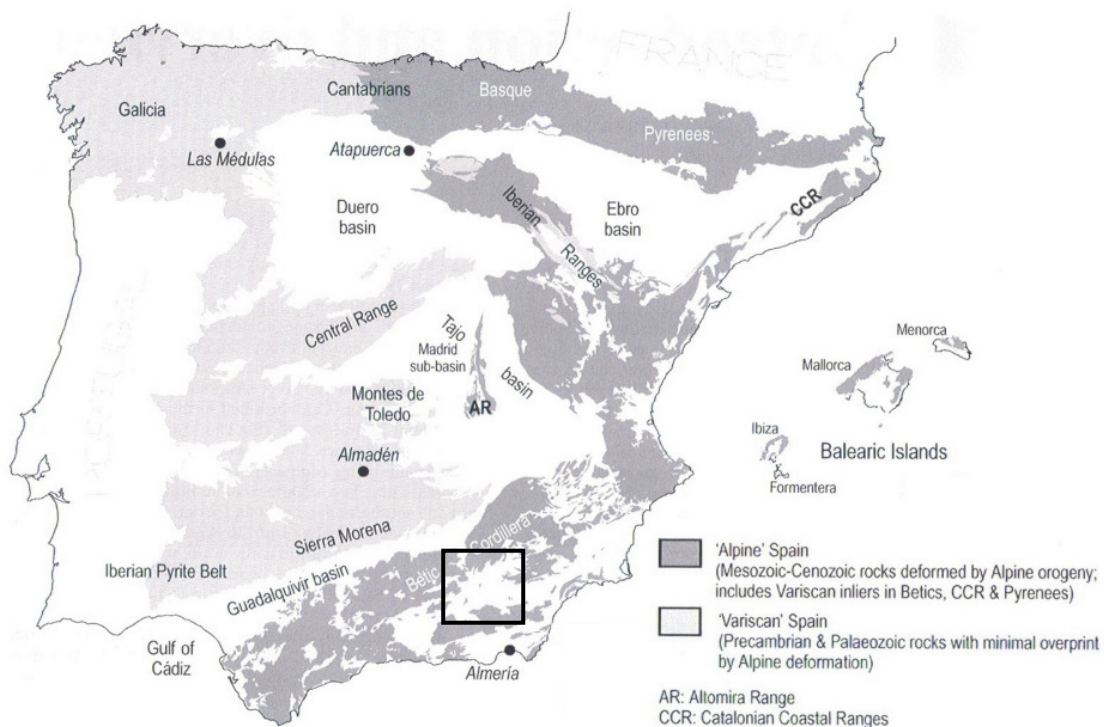


Figure 1.1: Outline map of mainland Spain and the Balearic Islands showing the brought division into “Variscan” and “Alpine” Spain. White areas in Spain are Cenozoic Basins Box indicates region of the study area (Gibbons & Moreno, 2002).

Iberian peninsula and Precambrian and Paleozoic rocks deformed by Variscan orogeny in the western half (Figure 1.1) . Spain is bordered by two great mountain chains, the Pyrenees-Basque-Cantabria belt to the north and the Betic Cordillera to the south, that also mark the margins of the Iberian continental plate that existed prior to Cenozoic orogeny. Alpine collision initially occurred in the north where the Iberian plate partly became subducted beneath the Eurasian plate, and then the focus of deformation changed to the southern margin, where the Betic Cordillera was formed through ibero-african collisional movement. This mountain range was exposed to strong extensional movement. Classic examples of foreland basins were generated like the Ebro basin south of the Pyrenees and the Guadalquivir basin north of the Betics. The Iberian Ranges south of the Ebro basin are an example of Alpine intraplate deformation while the Sierra Morena north of the Guadalquivir shows less alpine overprint. Central Spain is dominated by the Central Range formed by Alpine intraplate deformation and two large Cenozoic basins that form high areas north and south of the Central Range. The Iberian Ranges are composed of an inverted Mesozoic sedimentary basin while the Central Range is characterized by Paleozoic granitic and metamorphic basement which also appears west of the Tajo and Duero Basins and thus defines the simplified division into Variscan and Alpine Spain (Figure 1.1) although effects of Alpine orogeny are detectable across Variscan Spain as well as inliers of pre-Mesozoic Variscan rocks in parts of the Pyrenees, Iberian Ranges and the Betics overprinted by various degrees of Alpine deformation. Spain was assembled from three (Cadomian, Variscan, Alpine) orogenic cycles, although relatively little is preserved of the Cadomian orogeny along an ancient active plate margin.

1.2.2. The Betic Cordillera

Separated by the Alborán Sea, the Betic-Rif mountain belt is an arc-shaped orocline that extends from northern Morocco across the Strait of Gibraltar to southern Spain that was formed from late Mesozoic to Cenozoic during convergent movement between Africa and Iberia (AZAÑÓN ET. AL., 2002). The evolution of the Betic –Rif mountain belt along with the rest of the western Mediterranean orogens was embossed by late-orogenic coeval extension and shortening (LONERGAN & WHITE, 1997) and is, together with the development of the Alborán Sea, associated with a

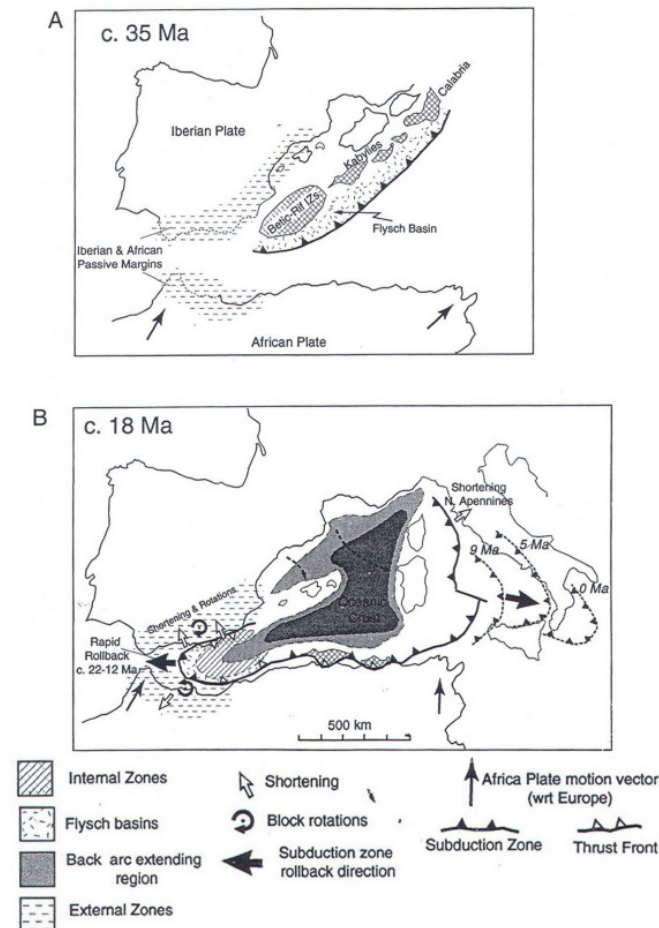


Figure 1.2: Geologic evolution of the Betic-Rif mountain belt (LONERGAN & WHITE, 1997).

subduction-zone rollback in the western Mediterranean during early to middle Miocene (Fig 1.2 A). In the Betic-Rif arc three main pre-Miocene tectonic domains have been identified, and traditionally the rocks are divided into a) Internal Zones, b) External Zones and c) Flysch nappes (Fig 1.2 B).

The Internal Zone or Alborán domain comprehends a nappe structure built up of three different complexes of variable metamorphic grade. These are from bottom to top: the Nevado-Filábride, the Alpujárride and Maláguide complexes (Figure 1.3). The Flysch Nappes are deformed Cretaceous

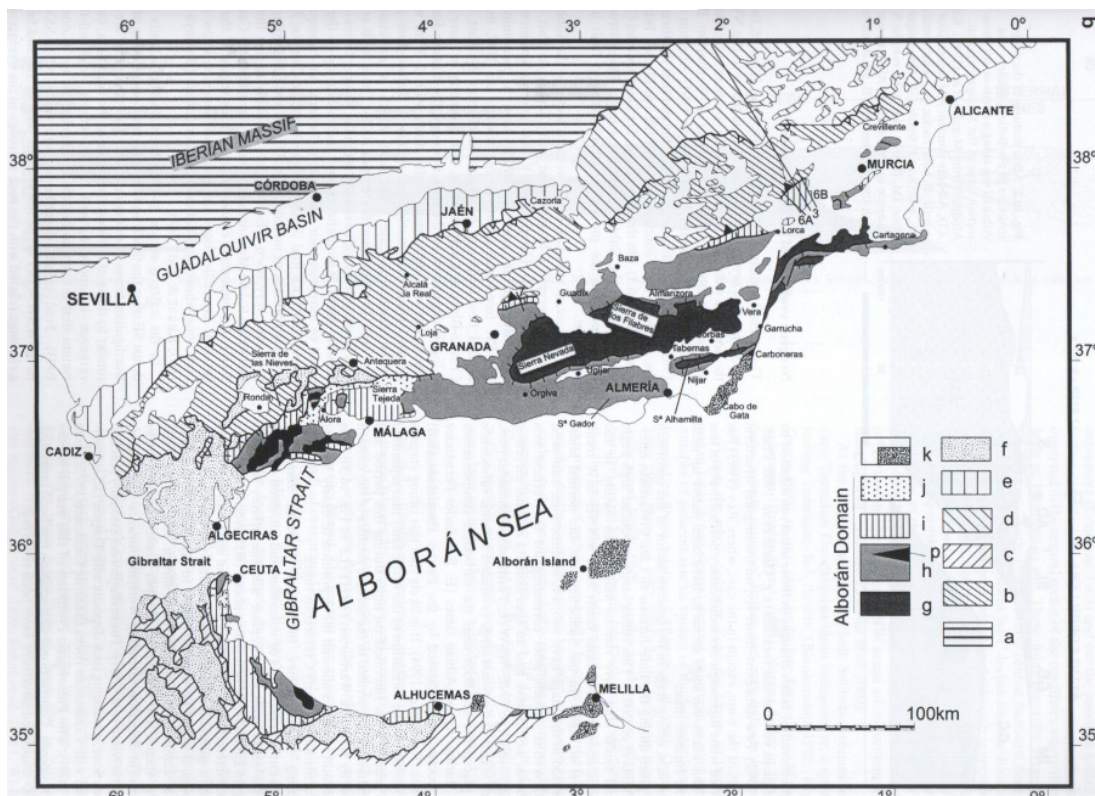


Figure 1.3: Geologic sketch map of the Betic Cordillera (Azañón et. al., 2002). a- Iberian Massif, b- Subbetic zone, c- Prerif, Mesorif, d- Prebetic zone, e- olistostroms and brecciasf- Flysch, g- Nevado-Filábride complex, h- Alpujárride complex, i- Malaguidej- flysch k- Neogene basins (Azañón et al., 2002).

and Miocene deep-water sediments deposited in a basin between Africa and Iberia. The External zone consists of Mesozoic and Tertiary sedimentary rocks deposited in basinal (Subbetics) and shelf (Prebetics) environments on the Iberian margin of the Tethyan Ocean. These rocks were deformed by northwest directed, thin skinned thrusting and folding during early to late Miocene. Shortening was accompanied by the development of the Guadalquivir foreland basin (LONERGAN & WHITE, 1997). The Prebetic rocks are mainly Triassic to lower Tortonian platform carbonates with some continental siliciclastic deposits (shelf). The rocks of the Subbetic zone further south comprise Triassic to Burdigalian (Miocene, 20Ma) basinal carbonates and few basalts.

The tectonic evolution of the External Zone is dominated by Mesozoic rifting stages. Rifting during Lower to Middle Jurassic caused a break-up of the shallow carbonate platform into smaller fault blocks separated by basin areas. From Late Jurassic to Late Cretaceous this part of the Cordillera underwent rifting that produced high angle normal faults that produced half-graben basins. The directions of this extensional faulting are NNE-SSW in the Prebetic units and E-W and NNW-SSE respectively in the Subbetic units. The eastern part of the External Zone is dominated by a NW-SE directed fold-and-thrust belt where during Neogene the Subbetic units were thrust on Prebetic units. During Tortonian a large part of the Betic Cordillera was covered by the Alborán Sea while subsequent uplift produced emergent areas parted by sedimentary basins. The intermontane basins in the central Betic Cordillera are intensely deformed and interpreted as piggy-back basins most of which are developed as synforms locally bordered by faults. The NW border of the Guadix-Baza basin (Figure 1.3) is partly deformed by faulting while little is known about the deep structure apart from the influence of Pliocene folding in Sierra Nevada and Sierra de los Filabres.

1.2.3. Climate, Meteorology

Typical factors that control the seasonal weather pattern for winter are high pressure areas over Eastern Europe and the North Atlantic and low pressure areas over Iceland producing air pressure circulations bringing rain bearing air masses from the North Atlantic.

The hydrological year 2005 (from November 2004 to October 2005) was the driest in a time period of 65 years (CONSEJERÍA DE MEDIO AMBIENTE, JUNTA DE ANDALUCIA). Figure 1.4 shows the deviation of precipitation with respect to the observed time period of 1971-2000 for Andalusia in winter (A) and spring (B) of 2004/05, when 60% of the average annual rainfall occurs.

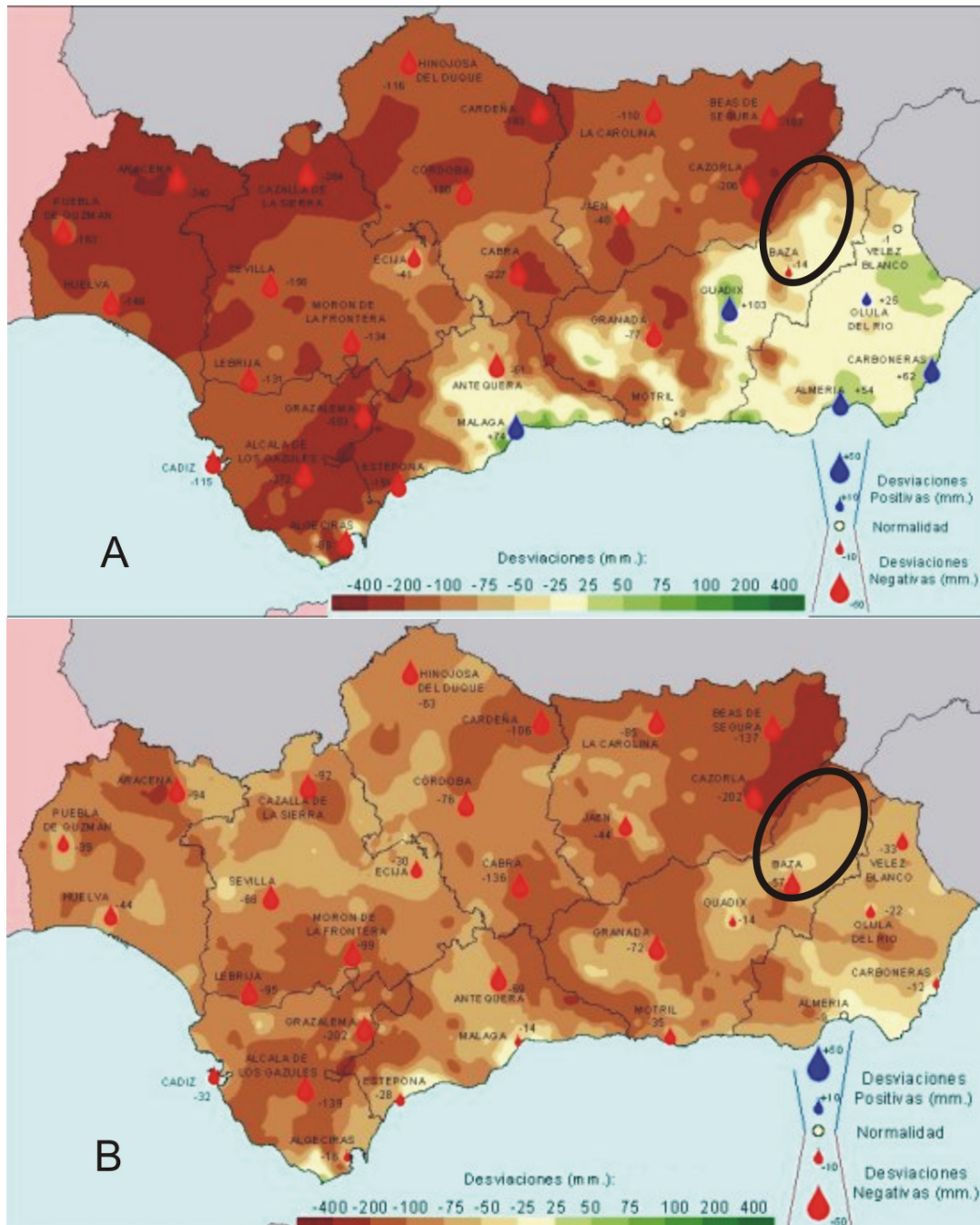


Figure 1.4: Deviations of mean seasonal precipitation in Andalusia(colored areas) in A) winter 2004/05 and B) spring 2005. The red droplets indicate negative deviations of the hydrological balance to the period of 1971-2000, the blue ones positive deviations. The outlined area is the Baza and Huescar-Puebla region representing the upper Guadiana Menor catchment (www.juntadeandalucia.es, 5/9/2006).

1.3. Study Area

1.3.1. Geological Setting

The study area (Duda-La Sagra area) is situated at the margin of a neogene intermontane basin and its bordering sierras near the town of Huescar at the eastern limits of the Granada Province (Figure 1.4). This basin is part of the Guadix-Baza Depression (SORIA ET. AL., 1999) and geologically belongs to the External Zone of the Betic Cordillera and is located on the contact of Prebetic and Subbetic units (Figure 1.3, 1.5) The depositional sequence of the Guadix-Baza Depression starts with a transgressive pattern during Lower Tortonian (11.5 Ma) with shallow platform sedimentation caused by strong subsidence. The middle Tortonian (9 Ma) sedimentation is dominated by shallow shelf prograding into pelagic basin deposits. Upper Tortonian tectonic uplift processes (7 Ma) caused shallowing of the basin and marks the beginning of continental influence on sedimentation with alluvial cones along with shallow marine deposits. Continuing uplift during Tortonian-Messinian is characterized by the development of continental environments throughout the basin with sedimentation in an endorheic context and alluvial fan, lacustrine fan delta, mud flat, and lacustrine deposits. Pliocene to Quaternary sedimentation is determined by detrital continental depositions.

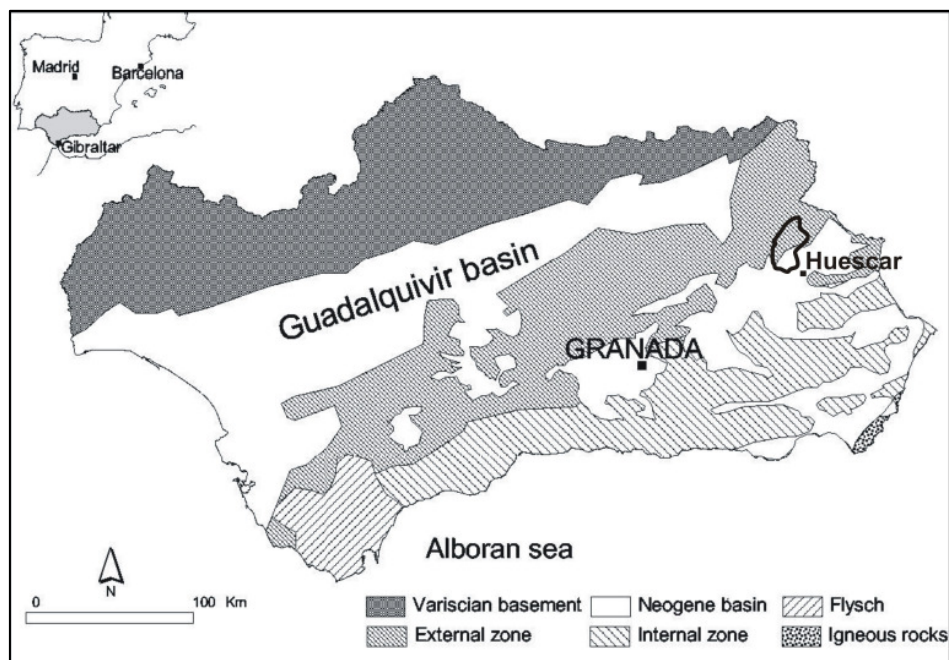


Figure 1.5: Geological sketch map of Andalusia showing the division of the Betics into External, Internal and Flysch Zones. Black outline indicates Study area Duda-La Sagra near Huescar (simplified after IGME, 2005).

The sediments in the central basin are tending to be fine-grained and therefore less permeable while the sediments at the margins are coarser and permeable. Figure 1.6 shows the distribution of the permeable materials in the Baza-Basin where no aquifers are developed in the central parts.

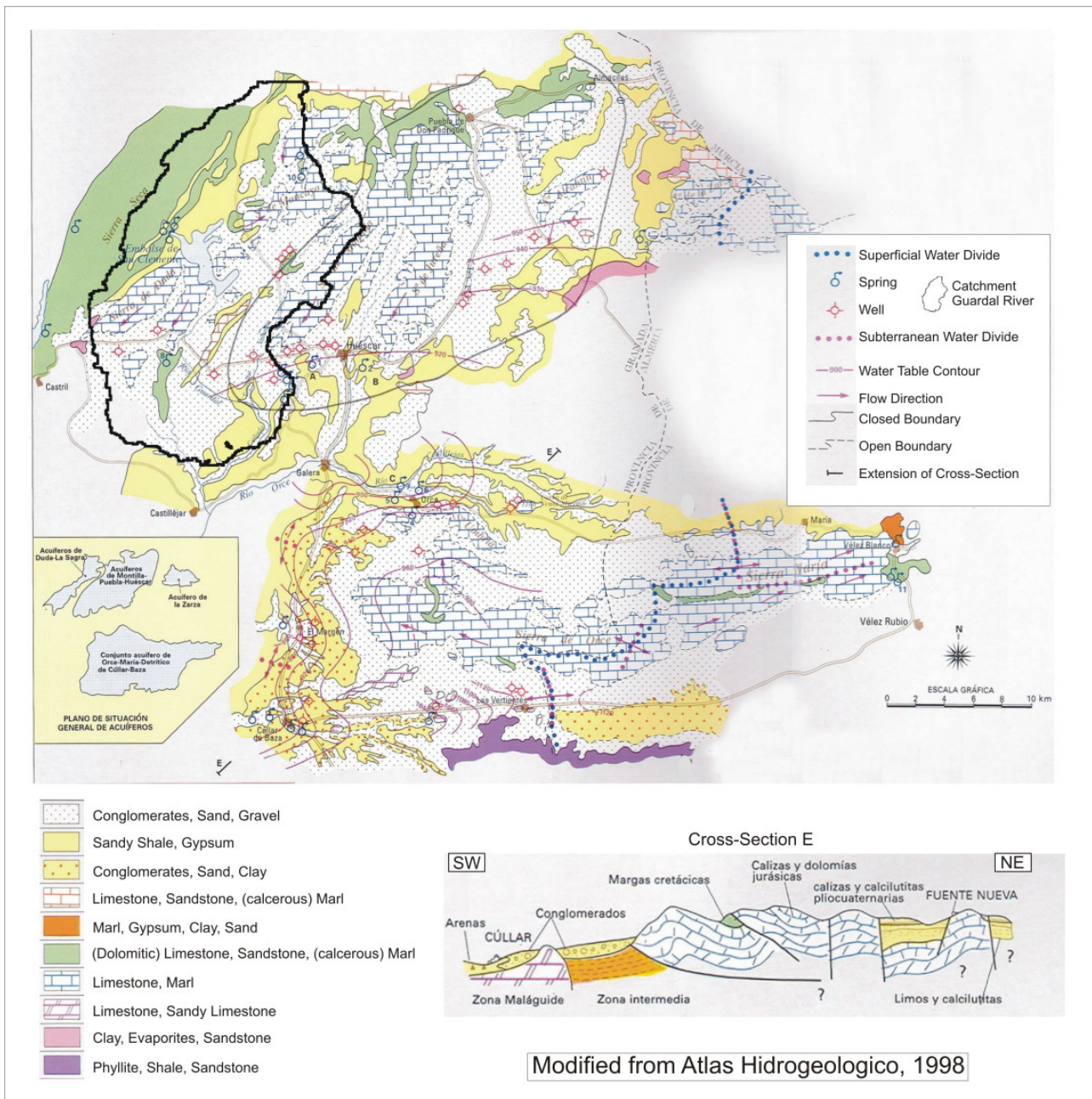


Figure 1.6: Overview map of the Upper Guadiana Menor shows the geological and hydrogeological setting. The study area is in the NW corner where the Guardal River Catchment is indicated. A schematic geological cross-section displays the transition zone of the S mountains and the basin with horst and graben structures where faults establish possible pathways for groundwater to the surface (e.g. thermal springs). The empty areas are the central parts of the basin where the sediments are impermeable.

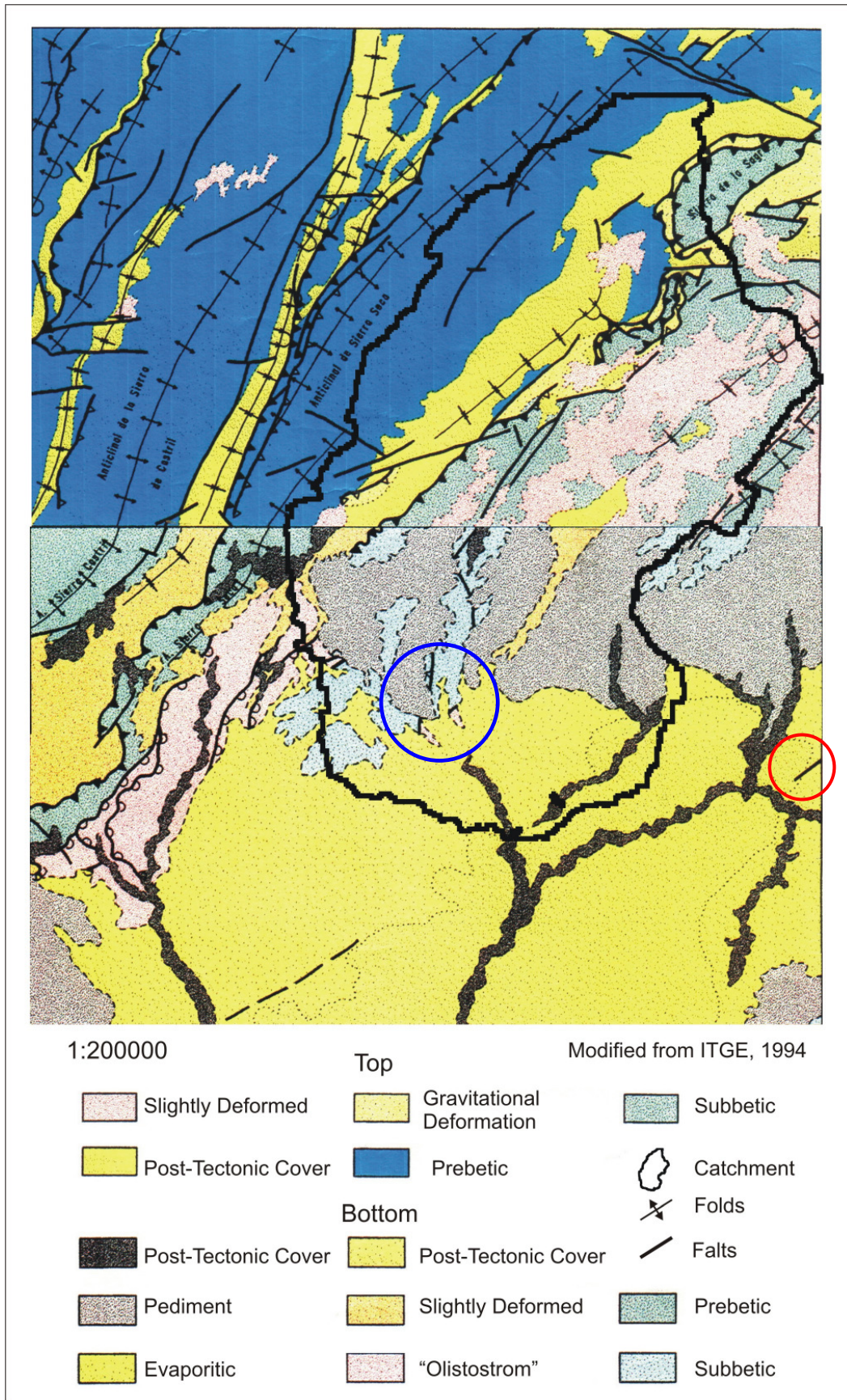


Figure 1.7: Simplified structural map of the study area. Indicated are the Guardal River sampling site (blue) and Fuencaliente (red) where the water is highly mineralized. Modified from ITGE, 1994.

The structural map of the study area (Figure 1.7) shows the SW-NE directed faulting and folding and displays the concurrence of faults and two sampling sites (Guardal River SP-GM-016 and Fuencaliente SP-GM-007).

1.4. Geomorphology

The regions morphology is designed by folding, faulting, erosion in the elevated areas and deposition in the basin during the geological past. The altitude in the study area ranges from ca. 750 masl in the Guardal river valley to 2383 masl at the summit

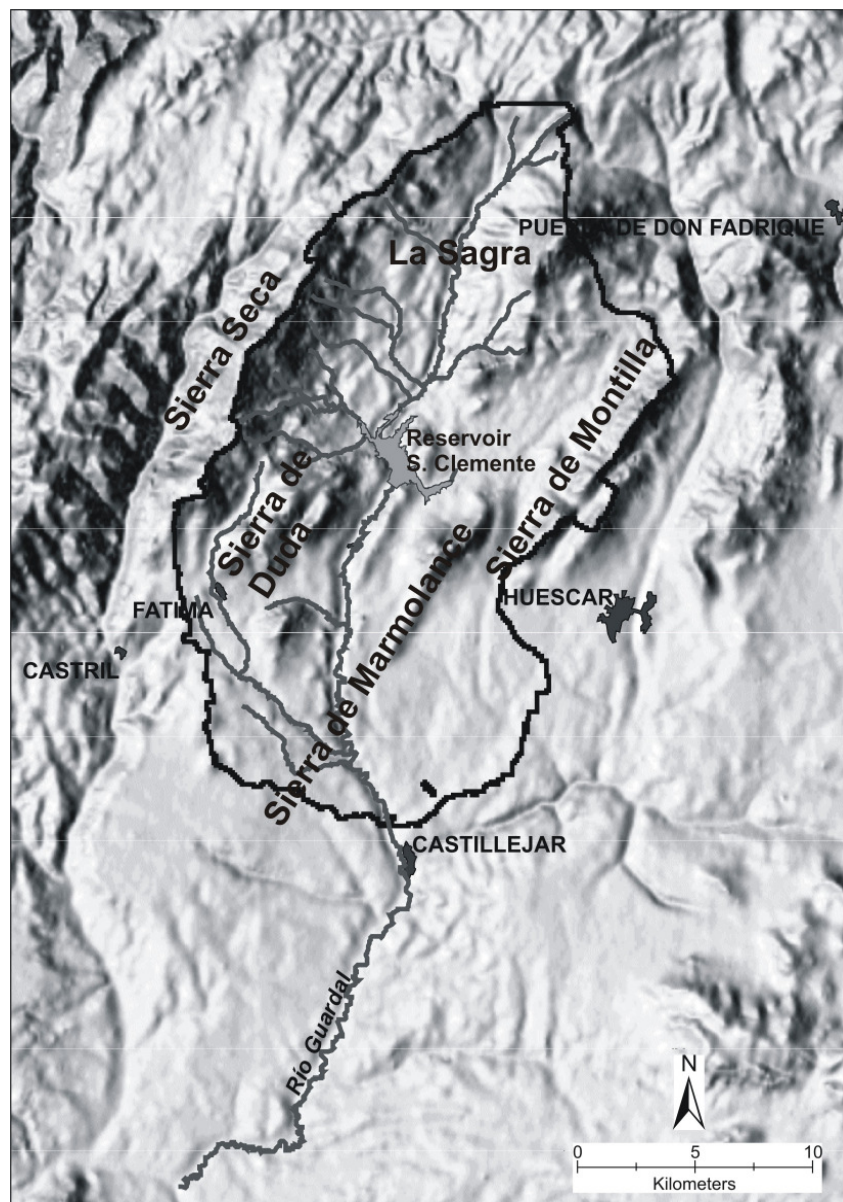


Figure 1.8: Contour map of the study area with the main morphologic features of the transition zone from the mountainous northern part to the southwards open basin, the Guardal River and catchment. Generated with ESRI ArcMap 8.3; data source: Mapa Digital de Andalucía 1:100.000, 1999.

of the La Sagra Mountain. The Duda-La Sagra area is dominated by a series of NE-SW aligned parallel shallow mountain ranges, from E to W: Sierra Seca, Sierra de Duda, Sierra Marmolance and Sierra Bermeja/Montilla (Figure 1.8). Sierra Seca consists mainly of Cretaceous carbonates and represents an antiform structure with isoclinal flanks and altitudes of 1000 - 2100 masl. The Sierra Bermeja/Montilla represents a anticlinal structure built up of Jurassic Carbonates (1100 -1600 masl) with a high degree of karstification (MEMORIAS No. 929, IGME). Between the two, the course of the Guardal River and two smaller elevations are located. The Sierra de Duda on the western bank and the Sierra de Marmolance on the eastern bank. The Sierra de Duda and the solitary La Sagra peak form an alignment of Jurassic limestone and dolomite. Opening to the south of the study area is a Neogene intermontane basin with altitudes of around 900 masl at the borders of the study area. The dimensions of the investigation area are about 20 km from east to west and 30 km north to south. The course of the Guardal and associated Rivers (partly ebbed during summer) within the area is about 30 km, while the actual distance from its origin in the Sierra Seca to where it leaves the work scope is about 20 km of permanent current. The Guardal River is a tributary to the Guadiana Menor which it joins some 20 km further downstream and about 100 km downstream from Castillejar it merges with the Gaudalquivir River.

1.5. Hydrogeology

1.5.1. Hydrogeology Aquifer Duda-La Sagra

The aquifers in the study area are locally different. While the aquifers in the sierras consist mainly of hard rock, the basin aquifers are composed of unconsolidated (detritic) material. The first are Cretaceous and Jurassic limestones and dolomitic limestones, and the second Miocene to Quaternary detritic deposits. The material of the carbonate terrains is fissured, faulted and object to chemical dissolution and represents important karst aquifers. The detritic material has relatively high intergranular porosity and is therefore a good aquifer. These two types are developed within the study area in roughly equal proportions. For an overview of the following descriptions refer to Figure 1.5.

1.5.1.1. Carbonate terrains

Sierra Seca – This mountain range represents a water divide between the Castril River to the west and the Guardal River catchment to its east. Its anticlinal structure consists mainly of Cretaceous material with limestone and dolomitic limestone layers with thickness between 100 - 400 meters interbedded with marl. The main groundwater flow for the eastern face of this hydrogeological unit is the origin of the Guardal River, the Natividad valley with Fte. De la Natividad, Fte. Enmedio and Fte. Alta. The latter is a tapped spring which is supplying drinking water for households as far as Castillejar through a pipeline. IGME 2005 reports a discharge of 450 l/s for the three and states a potential discharge of 2000 m³ p.a.

Sierra Duda – This hydrogeological unit comprises Jurassic limestone and dolomitic limestone that represents the occidental margin of the Subbetic synclinal structure and that extent NE parallel to Sierra Seca to La Sagra Mountain. There are no springs of important discharge, a few small ones with less than 5 l/ are located in the Village of Duda on the west bank of the river. IGME 2005 suggests that the main groundwater flow occurs as river bed exfiltration and beneath the waterline of the reservoir, which covers widely the former course of the Guardal River. Statements of the potential discharge of this unit are 575 m³ p.a. plus an additional 125 m³ p.a. from the perched aquifer of Sierra La Sagra which belongs to this unit. The main discharge occurs in Cueva del Agua with 30 – 50 l/s.

Sierra Montilla – This unit of Lower Jurassic limestone and dolomitic limestone extends NE as far as Puebla de Don Fadrique and is fragmented into several sierras of which Sierra Montilla north of Huescar has groundwater runoff discharging in a few basinal springs in detritic deposits in which this unit merges towards SE. These springs are Man. Fuencaliente with a discharge of 350-500 l/s and Man. Parpacen with discharge of 100-200 l/s near Huescar. IGME reports that wells indicate a hydraulic gradient of the groundwater table of 0.25 – 0.3 % directed SE towards Fuencaliente with coefficients of hydraulic conductivity of approximately 10⁻² to 5*10⁻³ m/s for limestone and 2*10⁻³ m/s for dolomitic limestone.

1.5.1.2. Pliocene/Quaternary basin deposits

Detritic aquifer Huescar-Puebla – This hydrogeological unit at the northern border of the Guadix-Baza Depression extends to NE in direction to Puebla de Don Fadrique and represents an open boundary to the adjacent carbonate aquifers. In the Huescar region the deposits comprise conglomerates, sand and clay of thickness between 100 and 150 m with coefficients of hydraulic conductivity around 10^{-4} m/s (sand). Facies changes from conglomerate to sand are observed. There the two main springs discharge, the aforementioned Fuencaliente and Parpacen. These are considered to have lateral influx from the carbonate terrain upstream. The potential discharge of this unit is reported as 2100 m³ p.a. (IGME 2005).

1.6. Agriculture, Land-use, Soils

The mountainous areas are forested mostly with pines, ample areas of the slopes are farmed with almond plantations and wherever suitable, vegetable horticulture is present and overhead irrigation is applied. The water supply is provided by the San Clemente Reservoir and numerous pumping wells that range from high-capacity pumping wells with automated power-sets to smaller (often unreported) wells with solar units or diesel engines. It can be supposed that in the past decades the extraction quantity increased significantly because the depth to water table in the basin increased observably. This is confirmed by the information of local residents stating that old dug wells ran dry within few years time.

Vast areas are grassland used by sheep farms. A detailed insight with agricultural facts for the Huescar-Puebla area is given in a report provided by the Administration of Andalusia at http://www.juntadeandalucia.es/agriculturaypesca/portal/www/portal/com/bin/portal/DGPAgraria/Estudios_Prospectiva/Estudios_Informes/innovacion2/huescaroca.pdf.

The soils in the area are described as entisols associated with the carbonate sierras and transition zones between the mountains and the basin as well as inceptisols associated with the Quaternary deposits (IGME, 2005).

1.7. Climate, Meteorology

1.7.1. Climate, Temperature, Precipitation, Groundwater recharge

The Huescar region is in a semi-arid Mediterranean Climate zone with annual Precipitation of 250-500 mm, a hot and dry summer period and a moderate cold winter. The mean annual temperatures (2000 – 2006) in the area range from 12.9°C to 15.4°C at selected meteorological stations and show a maximum during the months June, July and August (Fig 1.9) and precipitation values range between 320

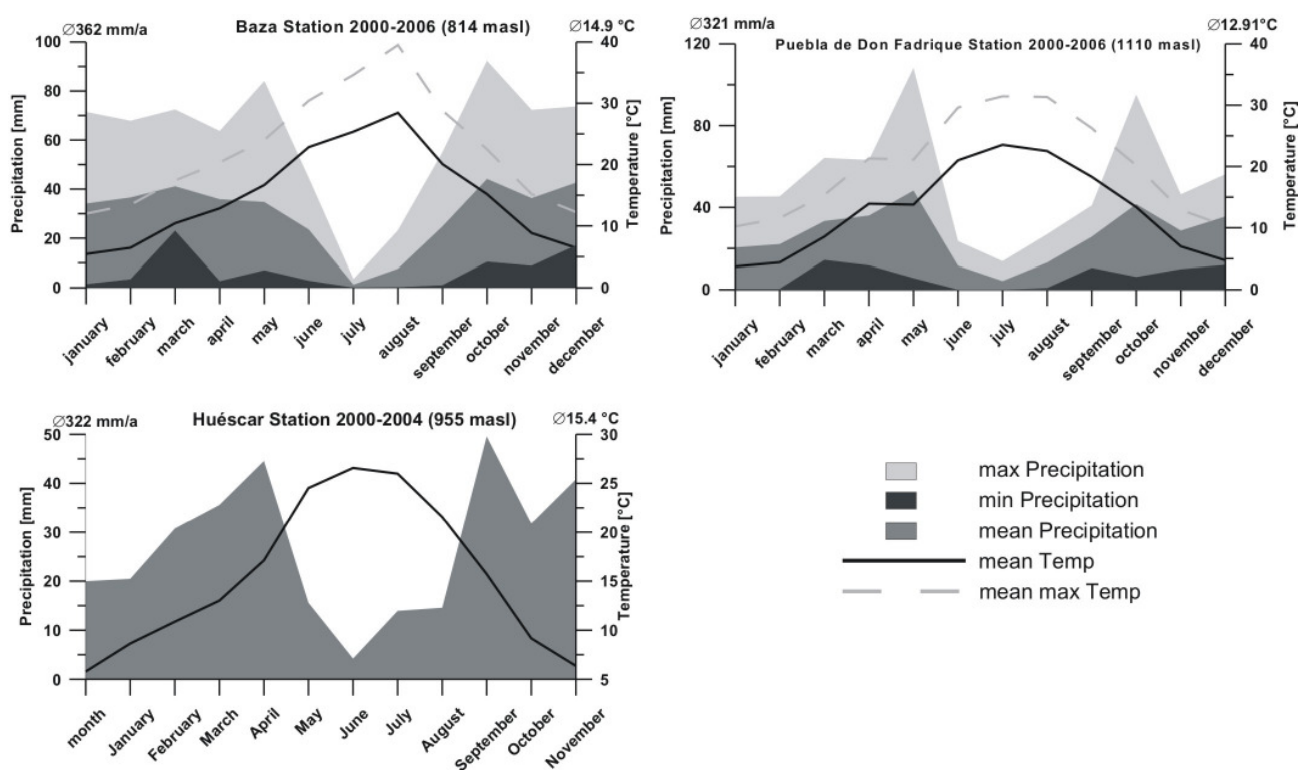


Figure 1.9: Mean annual temperature and precipitation values for the years 2000 – 2006 for the meteorological stations in Baza (X: 520628; Y: 4157712), Puebla de Don Fadrique (X: 554482; Y: 4192456) and 2000 – 2004 in Huéscar (X: 539946; Y: 4184099)[Data: www.juntadeandalucia.es, 5/9/2006].

Table 1.1: Mean annual temperature T and precipitation P for the Baza station (data: Junta de Andalucía, 5/9/2006).

	2005	1971-2000	deviation
T [°C]	14.25	14.1	0.15
P [mm]	237.1	372.8	-135.7

and 360 mm/y with maximum peaks in October and May followed by November. The meteorological stations are located in (Huescar) or close to the study area distributed in the basin (Huescar, Baza) or further up the plateau (Puebla de Don Fadrique), but, however, do not cover the topography developed in the area. The elevations range from mountain ranges (Sierras) with forests and peaks of up to 2381 masl which are snow covered in winter with low temperatures and high wind speed to a plateau-like scant basin , agriculturally used where possible, with moderate temperatures without snow events and only few rains often during storms. For the station within the boundaries of the study area data only from 2000 to 2004 is at hand. The data from the Baza station shows deviations from the mean annual values of the time period from 1971 to 2000 (CONSEJERÍA DE MEDIO AMBIENTE, JUNTA DE ANDALUCIA) during that time (Table 1.1).

The mean annual temperature 2005 is close to the normal values but the precipitation shows significant deviation from the long term average.

1.7.2. Evapotranspiration, hydrological balance

Evaporation is the process of liquid water being converted to water vapor and removed from the evaporating surface. Water evaporates from a variety of surfaces, such as lakes, rivers, soils and wet vegetation (FAO 56, 1998). Transpiration consists of the vaporization of liquid water contained in plant tissues and the vapor removal to the atmosphere. Solar radiation, air temperature, air humidity and wind speed are climatological parameters governing the evaporation and transpiration process. Evapotranspiration (ET) describes all parameters of physical evaporation and physiologically controlled transpiration of vegetation. Only if the amount of precipitation exceeds the amount of potential evapotranspiration, i.e. in case of a positive hydrological or climatic water balance, groundwater recharge is significant. Figure 1.8 a) shows a negative climatic water balance for the Baza station during 7 months for mean monthly values (data used: monthly mean maximum) from 2000 to

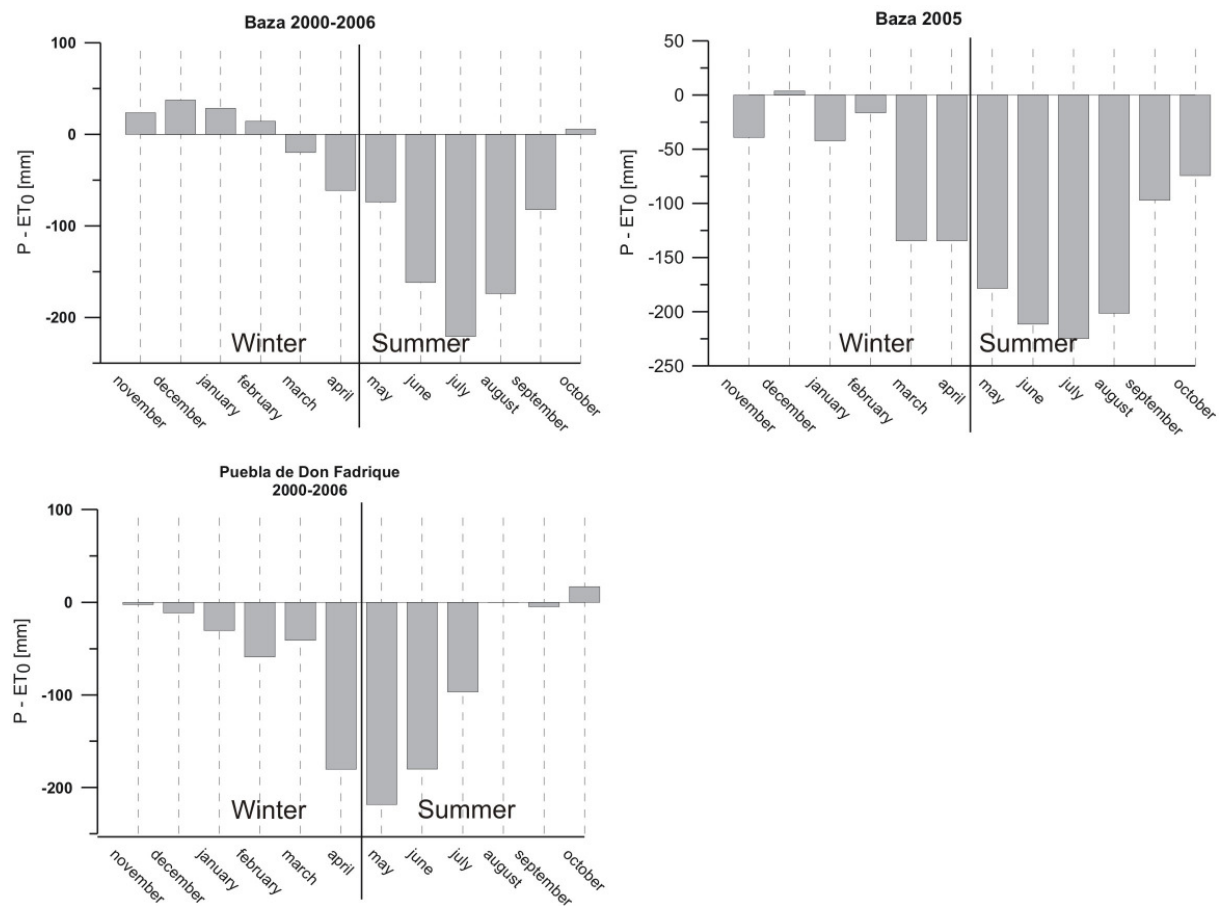


Figure 1.10: Climatic water balance for Baza station: mean monthly values 2000-2006 (left) and hydrological year (2005) of field campaigns (right) and for 2000-2006 at Puebla de Don Fadrique station.

2006. In comparison to the average values, the hydrological year 2004/05 (Figure 1.10) shows a negative budget in 11 months, strengthening the fact, that this particular year has been the driest in decades.

A similar result can be observed for the years 2000-2006 at the Puebla station (Figure 1.10), where the evapotranspiration exceeds the precipitation during 10 months (data used: monthly maximum mean precipitation)

The modeling of groundwater recharge potential included calculation of actual evapotranspiration from climate data (see methods chapter) and consequentially led to negative values for the hydrological year 2005 (Baza station: -1.48 mm; Puebla station: -3.3 mm) but positive mean values for the years 2000-2006 (14.62 mm and 13.91 mm respectively).

1.8. Hydrology

1.8.1. Principle river and San Clemente Reservoir

The main river is the Guardal River which runs north to south through the study area for a length of about 50 km. It has permanent current throughout the whole year. The total discharge of the Guardal catchment can not be quantified for the time of the field



Figure 1.11: Extraction tower and dam of San Clemente Reservoir (Height of tower: ca. 30m).

work but is reported to be at a mean value of 3100 m³ p.a. with a maximum of 6100 m³ p.a. in the hydrological year 1947 and a minimum value of 1100 m³ p.a. in 1957 (IGME, 2005). But since the hydrological year 2005 in which the field work took place is the driest in a time period of 60 years the total discharge should well be below average values.

The Guardal River catchment is influenced by the San Clemente Dam and Reservoir, construction finished in 1989. It was designed for a capacity of 12000 m³ for the purpose of distributing water for irrigation of 8823 hectares of agriculturally used land

surface in Huescar, Orce and Cullar. The total height of the dam is 84 m. A canal runs from the eastern end of the dam to Huescar.

The name San Clemente derives from the former village in the Guardal valley now beneath the reservoir water level. In dry years with little amount of rain input, especially in summer, it is difficult to regulate the amount needed to keep the river at its “natural” flux and to meet the necessary requirements for irrigation systems. Additionally, it remains unclear how the raising of the water level and the infiltration through the ground now under water influences the water budget. Figure 1.11 gives an impression of the dimension of the reservoir facilities compared to the available amount of water (Picture taken in September 2005). However, a total discharge of the Guardal River for the catchment considered in this work is reported as roughly 3100 m³ p.a. (IGME, 2005).

2. Stable Isotopes

Stable isotope studies are useful tools helping to comprehend the hydrological cycle. Variations of the stable isotopes of Hydrogen (H) and Oxygen (O), the two components building up water, provide important information on the genesis of waters. Evaporation, condensation and other processes change the isotopic composition of water. Meteoric waters retain their distinct isotopic signature (ratio of heavy to light isotope) until they mix with waters of different compositions or there are reactions with minerals or fluids. With this helpful, natural “tool” groundwater recharge, residence time or groundwater provenances can be traced and estimated. An introductory compendium of environmental isotopes in hydrology gives CLARK & FRITZ (1997).

2.1. Isotope fractionation

Isotopes are atoms of the same element that have different numbers of neutrons, which also makes differences in the masses of the isotopes. Stable isotope compositions are reported as δ values in units of parts per thousand (‰) relative to a standard of known composition and are in this work reported as ‰ deviation from VSMOW (Vienna – Standard Mean Ocean Water), an equivalent to SMOW (Standard Mean Ocean Water), a hypothetical water introduced by CRAIG (1961). δ Values are calculated by:

$$\delta_{\text{sample}} (\text{‰}) = \left(\frac{R_{\text{sample}} - R_{\text{reference}}}{R_{\text{reference}}} \right) \times 1000 \quad (2.1)$$

R is defined as the ratio of the heavier isotope to the lighter isotope, e.g.

$$R_{\frac{^{18}\text{O}}{^{16}\text{O}}} = \frac{^{18}\text{O}}{^{16}\text{O}}$$

The variations in isotopic composition are controlled by fractionation during equilibrium or unidirectional kinetic isotope exchange reactions.

2.1.1. Equilibrium fractionation

During a phase transition reaction, e.g. evaporation (equilibrium exchange reaction), the individual isotopes react differently due to differences in chemical and physical properties (KENDALL ET. AL., 1998). The fractionation between two substances *A* and *B* can be expressed by the fractionation factor α :

$$\alpha_{A-B} = \frac{R_A}{R_B} \quad \text{e.g. } \alpha_{\text{liquid-vapor}} = \frac{R_{\text{liquid}}}{R_{\text{vapor}}} \quad (2.2)$$

where R = the ratio of the heavy isotope to the lighter isotope (i.e. D/H, $^{18}\text{O}/^{16}\text{O}$) in the compounds *A* and *B*. The fractionation factor ($\alpha_{\text{l-v}}$) for the water liquid-vapor phase transition is 1.0098 and 1.084 at 20°C and 1.0117 and 1.111 at 0°C for ^{18}O and D respectively. For $\alpha_{\text{l-v}}$ larger than 1, the first phase (liquid) is “heavier” than the second one (vapour). The fractionation factor α and the δ values are related by:

$$\alpha_{A-B} = \frac{(\delta_A + 1000)}{(\delta_B + 1000)} \quad (2.3)$$

The isotopic difference in these two compounds can be expressed by the enrichment factor ϵ in ‰-notation:

$$\epsilon_{A-B} = (\alpha_{A-B} - 1) \times 1000 \quad (2.4)$$

2.1.2. Non-equilibrium (kinetic) fractionation

Isotopic effects can be unidirectional if reaction products become physically isolated from the reactants, e.g. evaporation of water from the sea surface and partial withdrawal of the vapor by wind. Kinetic fractionation is initialized by the differences in bond energies of the isotopes, and the reaction rates depend on parameters like surface temperature, salinity and relative humidity (KENDALL ET. AL., 1998). Bonds between lighter isotopes are broken more easily than the equivalent ones of the heavier isotopes; the lighter isotopes react faster and become concentrated in the product while the residual reactant becomes enriched in the remaining heavy isotopes. A fractionation factor is defined by:

$$\alpha = \frac{R_p}{R_s} \quad (2.5)$$

where R_p and R_s are the ratios of the heavy to light isotope in the product and substrate (reactant) respectively. Thus, an enrichment factor can be defined by:

$$\epsilon_{p-s} = (\alpha - 1) * 10^3 \quad (2.6)$$

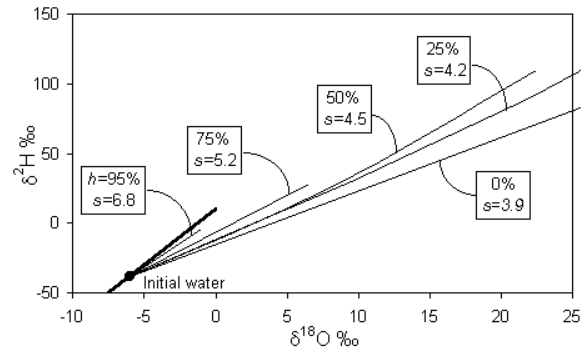


Figure 2.1: Isotopic enrichment in evaporating water and the effect of humidity (h). Slopes (s) are approximations of each curve near the GMWL (heavy line) (from CLARK AND FRITZ, 1997).

The isotopic composition of the evaporated moisture for either ^{18}O or ^2H can be expressed as:

$$\delta_E = \frac{(\alpha^* \delta_w - h \delta_a - \epsilon)}{\left[\frac{(1-h) + \Delta\epsilon}{10^3} \right]} \approx \frac{(\delta_w - h \delta_a - \epsilon)}{(1-h)} \quad (2.7)$$

where $\epsilon = \epsilon^* + \Delta\epsilon$, $\epsilon^* = (1 - \alpha^*) * 10^3$, $(\alpha^* = 1/\alpha) < 1$. The variable $\Delta\epsilon$ is an additional diffusive isotope fractionation which results from the different diffusivities of the water molecules in the liquid-air boundary layer. δ_w and δ_a are the isotopic compositions of the surface water and the atmospheric moisture (vapor) respectively, and h is the relative humidity. CRAIG AND GORDON, 1965, describe this model in detail. The deviation from the GWML through evaporative enrichment is shown by GONFIANTINI, 1986 for different relative humidity (Figure 2.1)

2.1.3. Rayleigh fractionation and Meteoric Water lines

Rayleigh fractionation expresses the exponential relation that describes the partitioning of isotopes between two reservoirs as one reservoir decreases in size. A system where the material removed from one reservoir accumulates in a second reservoir while isotopic equilibrium is maintained throughout the process is referred

to as a “closed” system (GAT & GONFIANTINI, 1981), e.g. the condensation of vapor to droplets in a cloud. This can be considered an equilibrium fractionation. Evaporation of water is regarded as an “open” system process, where the vapor is isolated and continuously removed with a constant fractionation factor α_{l-v} depending on temperature. This is an example of kinetic fractionation. Air masses are altered in their isotopic composition along their trajectories across continents by rainout events (condensation processes). This evolution is described as a Rayleigh process (DANSGAARD, 1964) and the reactant continuously becomes depleted in heavy isotopes with respect to the product. Isotopic compositions of precipitation correlate on a global scale. The data from rain and surface water samples from all over the world form a linear band in $\delta^{18}\text{O}$ versus δD plots with a regression line described by

$$\delta\text{D} = 8 \delta^{18}\text{O} + 10 \quad (\text{CRAIG, 1961}) \quad (2.8)$$

the Global Meteoric Water Line (GMWL). The majority of the meteorological stations are in immediate proximity to oceans though. The GMWL is actually a best-fit line to many local and regional meteoric water lines that differ from it due to varying geographic and climatic settings. It has a slope $s = 8$ which is approximately the value of the ratio of the equilibrium fractionation factors for H and O isotopes at 25-30°C. The GMWL has a y-intercept (or deuterium-excess) value of 10 rather than 0, which would be the composition of ocean water, the main water supply for vapor masses, because of the $\approx 10\%$ kinetic enrichment in D of vapor evaporating from the ocean at an average humidity of 85%. The deuterium-excess provides a measure of non-equilibrium effects and is defined by:

$$d - excess = \delta^2\text{H} - 8 * \delta^{18}\text{O} \quad (\text{DANSGAARD, 1964}) \quad (2.9)$$

Evaporation under high temperature and low humidity results in higher d-values (JOUZEL AND MERLIVAT, 1984). Rain of Mediterranean origin shows d-excess values of up to +15‰ while Atlantic precipitation is characterized by d-values of about +10‰. The Western Mediterranean Meteoric Water Line (WMMWL) is equal in slope to the GMWL but differs in deuterium intercept and is defined by:

$$\delta\text{D} = 8 \delta^{18}\text{O} + 13.7 \quad (\text{VANDENSCHRICK ET. AL., 2002}) \quad (2.10)$$

2.2. Isotope effects

The stable isotopic composition of precipitation is dominantly controlled by temperature due to the temperature dependency of the fractionation factor α between liquid and vapor. Geographic and temporal variations are observable in the isotopic composition of meteoric waters. These variations are called isotope effects (KENDALL ET. AL., 1998).

The alteration of isotope compositions signifies a change of the ratio of the heavy isotope with respect to the light isotope. These changes will in the following be reported as either enrichment or depletion with respect to the heavier isotope. Isotopically enriched therefore signifies a smaller amount of lighter and a larger amount of heavier isotope species relative to e.g. VSMOV.

temperature effect – the fractionation between liquid and vapor increases with decreasing temperature, precipitation becomes isotopically depleted

continental effect – meteoric water is more depleted farther from the source of the water vapor (ocean). Fractionation removes the heavier isotopes from the vapor mass through condensation; this recurrent rainout of the heavier isotopes leaves the remaining vapor mass more and more depleted on its trajectory inland

elevation effect – meteoric water is more depleted at higher elevations. Continuous

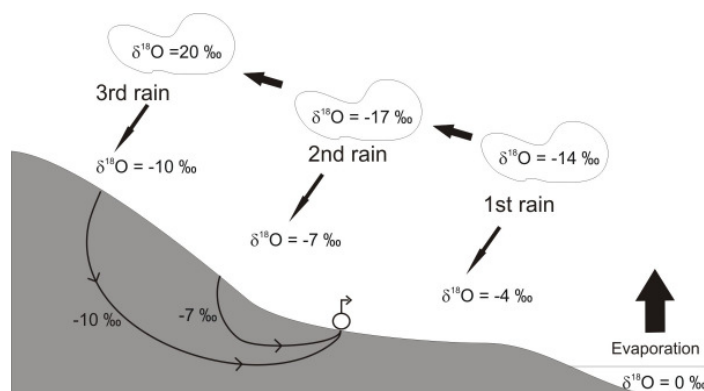


Figure 2.2: Elevation effect and groundwater mixing for spring water (modified after www.iaea.org).

cooling of air masses for lower temperatures at higher altitudes causes condensation with progressive depletion of the rain (Figure 2.2). This orographic effect is a combination of temperature effect and rain-out process. A good correlation of $\delta^{18}\text{O}$ has been reported for Sierra de Gador by VALLEJOS ET AL. (1997)

latitude effect – this effect is caused by increased fractionation at cooler temperatures of condensation prevalent in higher latitudes and lesser amounts of more enriched evapotranspired vapor being available in the air mass system. DANSGAARD (1964) reports a latitudinal gradient for mean δ values of 5.6 ‰ and 0.7‰ for D and ^{18}O respectively.

amount effect – small rain events generally show a isotope signal more enriched in heavy isotopes than larger events. During larger rainstorms, the air below cloud base may become more saturated which reduces the evaporative loss of the raindrops on the way to the ground.

2.3. Previous stable isotope studies

In a combined isotopic study of D and ^{18}O , VANDENSCHRICK ET. AL. (2002) relate the isotopic composition of surface and groundwater sampled in Sierra de Gador, located west of Almería, southern Spain, along an altitudinal gradient from the recharge zone in the mountains to the coastal plain, to precipitation of Mediterranean and Atlantic origin. Isotope signals of precipitation samples from Gibraltar (Atlantic influence) and from Barcelona (Mediterranean influence) show characteristic differences in deuterium excess (GNIP data, IAEA/WMO, 2001) which made it possible to detect end member compositions in the aquifer. VANDENSCHRICK ET. AL. (2002) report that the samples taken display in a $\delta \text{D} - \delta ^{18}\text{O}$ diagram on a mixing line connecting a pole of Mediterranean waters to a pole of Atlantic waters. The Atlantic signature predominates in the shallow groundwater of the karstic aquifer while the Mediterranean signature mainly shows in the deep groundwater in the coastal plain. The authors conclude that according to meteorological data the Mediterranean signature of deep groundwater could be due to past extreme rainfall events during which connectivity between recharge and reservoir exists, while at the same time the Atlantic signature of recent winter rains dominates in shallow groundwater.

The doctoral thesis from GARRIDO (2003) discusses the general composition of stable isotopes ($\delta^{18}\text{O}$, $\delta^2\text{H}$) of the vapor in the atmosphere and the precipitation in the

Granada province. The author determines the average δ -values in precipitation for Granada ($\delta^{18}\text{O} = -5.7 \text{ ‰}$; $\delta\text{D} = -37 \text{ ‰}$ vs. VSMOW). Analyses of the d-excess in precipitation verify that the major part of rain bearing air masses for the Granada Region has as its origin the Atlantic ocean (d-excess $\sim 10 \text{ ‰}$). Furthermore the author shows that isotope compositions of atmospheric water vapor show altitude gradients for the Sierra Nevada between -0.2 and -1.3 ‰ (for $\delta^{18}\text{O}/100\text{m}$) and -1 and -9 ‰ (for $\delta\text{D}/100\text{m}$).

3. Methods

3.1. Sampling Strategy and Sampling Network

According to the object of this combined study of hydrogeochemical (major and minor ions) and isotope data, it was essential to develop a grid of water sampling points in different types of water sources. Since in the study region several individual, possibly interconnected aquifers are developed rather than one large one (Figure 1.3), a good spatial distribution of sampling sites is important to cover the area of the aquifer(s) in a representative way (Figure 3.1). The sampled points include springs of important discharge, a few small springs, river sites, wells and a local reservoir (Table 3.1). Since the groundwater of the basin was assumed to be relatively constant in terms of temporal variations in its chemical and isotopical composition, a network of accessible wells was sampled once or twice (in May and October) in order to detect spatial differences in isotope end-member compositions. Surface waters (springs, rivers etc.) often show temporal variations and were sampled at least monthly (Table 3.2) along with rain samples from different altitudes as they occurred in order to calculate local δ -value vs. altitude relations. The quantity and the abundance of individual precipitation samples was insufficient for proceeding with the latter though. A few other sites were visited and sampled that are within the Guadiana Menor catchment, but not within the immediate investigation area.

Table 3.1: Site types

Type	Amount
Spring	14
River	4
Wells	11
Reservoir	1

Table 3.2: Data of sampling sites

#	site ID	Name	Type	Samp led	East UTM	North UTM	Altitude masl	Discharge l/s	Depth to water table m
1	SP-GM-001	Manantial de la Natividad	spring	9x	528577	4194100	1083	<50	-
2	SP-GM-002	Manantial de Parpacen	spring	8x	537982	4184411	921	<100	-
3	SP-GM-007	Fuencaliente	spring	9x	542145	4184085	916	<100	-
4	SP-GM-013	Fuente Alta	spring	9x	527700	4194175	1137	<50	-
5	SP-GM-014	Reservoir San Clemente	reservoir	7x	530937	4190510	1037	-	-
6	SP-GM-015	Barranco Natividad	river	8x	528577	4194100	1083	-	-
7	SP-GM-016	Rio Gaurdal/Los Ruices	river	7x	529035	4184550	867	-	-
8	SP-GM-017	Fuentecillas	spring	7x	537083	4203250	1434	<5	-
9	SP-GM-018	Rio Raigadas/Puente Animas	river	2x	532163	4194162	1069	-	-
10	SP-GM-019	Rio Raigadas/Puente San José	river	7x	534445	4201324	1249	-	-
11	SP-GM-020	Fuente Montilla	spring	7x	537816	4204628	1466	<50	-
12	SP-GM-021	Fuente Carrillo	spring	2x	537439	4203155	1464	<5	-
13	SP-GM-022	Cueva del Agua	spring	1x	537842	4197651	1499	<50	-
14	SP-GM-023	Fuente Tornajo	spring	2x	529110	4187630	930	<5	-
15	SP-GM-024	Fuente de Oliva	spring	1x	529215	4187772	930	<5	-
16	SP-GM-025	Cortijo de Penalba	spring	1x	529035	4187430	937	<5	-
17	SP-GM-026	Fuente Felin Grande	spring	7x	527013	4178294	892	<50	-
18	SP-GM-027	Sondeo Felin	well	2x	525171	4181082	926	-	-
19	SP-GM-031	Fuente de Ortiz	spring	1x	523958	4180996	1141	<5	-
20	SP-GM-036	Fuente de la Piedra	spring	1x	534333	4192501	1115	<5	-
21	SP-GM-050	Cjo. Mazagorda	well	1x	535952	4190772	1092	-	2.5
22	SP-GM-051	Cjo. Corcoles	well	1x	538115	4190064	1145	-	-
23	SP-GM-052	Zabar	well	1x	535491	4191638	1096	-	-
24	SP-GM-053	Rambla Valentin	well	1x	534965	4184572	961	-	-
25	SP-GM-054	Cantera Ferrer 1	well	1x	530730	4182703	962	-	-
26	SP-GM-055	Cantera Ferrer 2	well	1x	531053	4183447	1050	-	-
27	SP-GM-056	Cjo. Los Jaros	well	1x	525428	4185356	1048	-	-
28	SP-GM-057	Castro-Cubo	well	1x	523304	4184997	1092	-	-
30	SP-GM-059	Artesian	well	1x	533152	4182802	923	-	0
31	SP-GM-060	FAO well	well	1x	536469	4185133	934	-	41
32	SP-GM-061	Sondeo Diablo	well	1x	525171	4181082	926	-	39

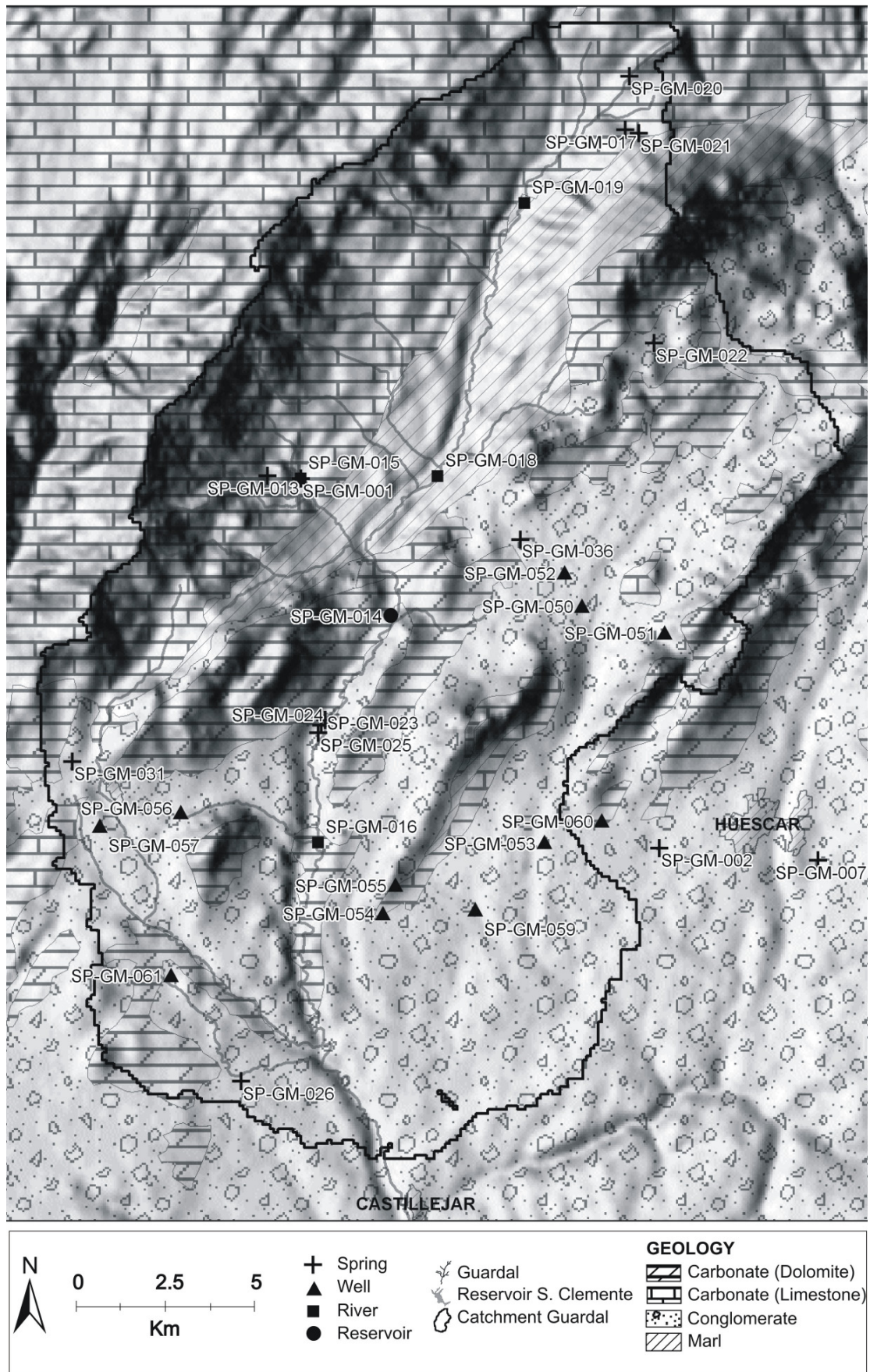


Figure 3.1: Sampling Network

3.2. Sampling Methods

Water samples were taken from February to October 2005 and stored in precleaned polypropylene bottles (50 ml) with airtight caps. Each sample included three separate bottles, one each for major (Ca^{2+} , Mg^{2+} , Na^{+} , K^{+} , Cl^{-} , SO_4^{2-} , NO_3^{-}) and selected minor ion analysis (Fe^{2+} , Mn^{2+} , Sr^{2+}) as well as for stable isotope analysis ($\delta^{18}\text{O}$, δD). The samples for cation measurements were acidified to pH 2 with ultra pure HNO_3 . EC and water temperature were measured on site. EC is the measurement of the total dissolved salts based on current flow. EC, measured in $\mu\text{S}/\text{cm}$ or mS/cm , is the reciprocal value of electrical resistivity (HÖLTING, 1995). The pH was measured on site with a hand-held pH/mV meter frequently calibrated using two standard buffers (Table 3.2). The pH was accidentally measured with a pH probe without temperature which led to a systematic error. The values were double checked afterwards together with Prof. Pekdeger and the error (2. decimal place) was considered negligible.

Table 3.3: Methods and devices of sampled parameters.

Parameter (effective range)	Method	device/quick determination test
Temperature 0 to 100 °C	electrometric Log	Multiline P4 (WTW Inc.); Temperature probe integrated in pH probe SenTIX 41
pH-value (pH 1 to pH 13)	potentiometric Log with automatic temperature compensation	Multiline P4 + pH probe SenTIX 41 (WTW Inc.)
Spec. conductivity (10 to 10 ⁶ $\mu\text{S}/\text{cm}$)	electrometric Log with automatic temperature compensation (25 °C)	Multiline P4 + cond probe TetraCon 325 (WTW Inc.)
Oxygen saturation (1 – 100%)	polarographic Log	Multiline P4 + oxygen probe CellOx 325 + calibrate vessel OxiCal-SI (WTW Inc.)
Redox potential (-200 to 1000 mV)	potentiometric Log (Ag/AgCl-reference electrode)	Multiline P4 (WTW Inc.) + Eh probe Pt 4805 (Ingold Inc.)
Carbon species	in situ log, titration with 0,1 N HCl to pH 4,3 respectively with 0,1 N NaOH to pH 8,2 / colorimetric	Bulb pipette (100 ml) field burette, pH meter, beaker <i>OR VISOCOLOR® HE</i> test kit
NO_2^{-} (0,005 to 0,1 mg/l)	in situ log: colorimetric	Quick test: Aquaquant 1.4408 (Merck Inc.)
NH_4^{+} (0,05 to 0,8 mg/l)	in situ log: colorimetric	Quick test: Aquaquant 1.4400.001 (Merck Inc.)

The sampling routine differed depending on the sampling site. Rivers and the reservoir were sampled near the surface from the same location on the bank each

time and were filtered on site with 0.45 µm acetate cellulose filters. Springs were sampled as close to the source as possible, depending on accessibility, and not filtered. Groundwater was sampled in different ways, depending on the type of well. Some of the pumping wells were in operation and the sample was taken from a tap on the piping or outlet (SP-GM-051,-052,-053,-054,-055), some pumps were started exclusively for sampling after they had been out of operation for some time and the sample was taken directly from the outlet (SP-GM-056,-057). In one case the sampling was executed by the use of a plastic ladle device (from IGME) from right below the water table (SP-GM-050).

The groundwater sampling above was carried out on September 15 and 16 2005 by F. F. Chacon from IGME and the author. Because of the fact, that some of the wells were not listed or attended, no information about the assembly of the wells and pumps was available. The pumping wells that were started by the proprietor in order to take samples were not running long enough for the field parameters to stabilize or in order for the sampling routine to be done completely. The alkalinity (HCO_3^-) was then measured either on site by a VISOCOLOR[®] quick-test or later by titration from an extra sample taken. Since the determination of the HCO_3^- is time-consuming with setting up the titration equipment, on some sampling days, an extra bottle of sample was taken at each sampling point, and the measurements were done later altogether in order to work off as many sampling points as possible.

On September 22 and 23 2005 a sampling campaign was accompanied and supervised by Prof. Dr. A. Pekdeger and Dr. C. Kohfahl (FUB) and three wells were sampled. One of the wells is artesian (SP-GM-059) and the other two (SP-GM-060,-061) were pumped with a MP1 immersion pump connected with plastic piping and hooked up to a gasoline current generator. The depth to water in the wells was determined with an electrical plummet and the pump was lowered accordingly. The outlet of the pump was attached to a “flow-through cell” where the field parameters were measured and about twice the static water volume of the well was pumped with a rate of approximately 4 l/s until the parameters were stable before the samples were taken. The samples were stored refrigerated and shipped in several loads to the FUB and then distributed to the laboratories for analysis.

3.3. Analysis

3.3.1. Ions

Major ion analysis (Ca^{2+} , Mg^{2+} , Na^+ , K^+ , Cl^- , SO_4^{2-} , NO_3^-) and selected minor ion analysis (Fe^{2+} , Mn^{2+} , Sr^{2+}) was operated at the Hydrogeology Laboratory for AMS and ICP measurement at the FUB. Precision and analytical methods are listed in Table 3.4.

Table 3.4: Analytical methods hydrogeochemistry.

Ions	Method	device	Detection limit
Na^+	Flame photometer	Eppendorf Elex 6361r	1,0 [mg/l]
K^+	Flame photometer	Eppendorf Elex 6361r	0,1 [mg/l]
Al^{3+}	ICP	Leemans	0,5 [mg/l]
Mg^{2+}	AAS	Perkin Elmer 5000	0,05 [mg/l]
Ca^{2+}	AAS	Perkin Elmer 5000	0,05 [mg/l]
Li^+	AAS	Perkin Elmer 5000	0,05 [mg/l]
Sr^{2+}	ICP	Leemans	0,05 [mg/l]
Mn^{2+}	AAS	Perkin Elmer 5000	0,05 [mg/l]
Fe^{2+}	AAS	Perkin Elmer 5000	0,1 [mg/l]
Br^-	DEV (1986)	Titration	0,01 [mg/l]
Cl^-	photometric	Technicon Autoanalyser	1,0 [mg/l]
SO_4^{2-}	photometric	Technicon Autoanalyser	0,05 [mg/l]
NO_3^-	photometric	Technicon Autoanalyser	0,05 [mg/l]

3.3.2. Stable Isotopes

Oxygen and Hydrogen isotope ratios ($\delta^{18}\text{O}$, δD) were measured at the AWI Isotope Laboratory in Potsdam by Dr. H. Meyer with Finnigan MAT Delta-S mass spectrometers using the equilibrium method (MEYER ET. AL., 2000). Aliquots of ca. 5ml of sample are filled into reaction vessels and are equilibrated with carbon dioxide at a constant temperature well below room temperature to avoid evaporation. The reaction vessel is then evacuated by pumping and the reaction gas fed into the mass spectrometer. This technique has been improved to fully automated procedures and both species can be measured in one run. The precision of measurement is approx. 0.1‰ for $\delta^{18}\text{O}$ and 0.8‰ for δD . At the AWI laboratory, own standards are used which are calibrated in reference the VSMOW standard.

3.4. Climatology, evapotranspiration, groundwater recharge

The daily evapotranspiration data used in this work is taken from the data sheets available at the Administration of Andalusia website at www.juntadeandalucia.es (5/9/2006) for selected stations, but no information about the methods used could be obtained. The FAO-Penman-Monteith-method is recommended as a standard method for determining ET_0 . This method closely approximates grass ET_0 at the location evaluated, is physically based, and explicitly incorporates both physiological and aerodynamic parameters. Detailed information is given in FAO IRRIGATION AND DRAINAGE PAPER 56, 1998.

Actual evapotranspiration can roughly be calculated for annual mean values with the equation 3.1 by Turc (GRAY, 1970), however leaving parameters like soil moisture, soil moisture capacity, humidity and other climatic factors out of consideration:

$$ET_A = P / [0.9 + (P/J)^2]^{0.5} \quad (3.1)$$

where P = mean annual precipitation [mm]; T = mean annual temperature [$^{\circ}\text{C}$]; $J = 300 + 25 \cdot T + 0.05 \cdot T^3$

Considering the fact, that this and other formulas might not be representative for semiarid climates, that a number of parameters important for other equations were not available and to the due to the semi-empirical character of the equations, groundwater recharge potential was modeled for two stations for the hydrological year 2005 disregarding the fact, that this was the driest year in decades recorded. Groundwater recharge was computed with the general equation 3.2

$$P = ET_A + R + GWR \quad (3.2)$$

where P = precipitation; R = runoff; GWR = groundwater recharge

It was not possible to quantify surface runoff, so that it was simplified by pooling together runoff with GWR for modeling causes. The determination of GWR by the use of the chloride balance method seemed inappropriate for the possible alteration of the low concentrations through the agricultural use of parts of the basin (e.g. fertilization).

3.5. Catchment, Digital Elevation Model (DEM)

The catchment area was calculated with Arc Hydro Tools Extension (version 1.1 Beta 3, May 2003; ESRI) for ArcGIS and verified by flow path modeling based on a digital elevation model. The DEM was generated from the Mapa Digital de Adalucia. The elevation data was exported as an ASCII text file and then interpolated to a grid file by the kriging method with Surfer 7.0. The grid file was converted to an elevation tagged-image-file (tiff) with Global Mapper 6.

3.6. Hydrochemistry

3.6.1. Reliability check

In order to create a classification of the sampled water into groups of similar geochemical characteristics by the use of graphical and statistical methods, first a reliability check of the sample data was made to assure the validity of the analysis data. The accuracy of the ion analysis can be estimated from the electro neutrality (EN) condition according to equation 3.3 since the sum of positive and negative charges (cations and anions) in the water must be equal (APPELO, 1999).

$$\text{Electroneutrality } [\%] = \frac{\sum \text{cations } [meq/l] - \sum \text{anions } [meq/l]}{\sum \text{cations } [meq/l] + \sum \text{anions } [meq/l]} \times 100 \quad (3.3)$$

Figure 3.3 shows that 4 out of 80 samples measured are exceeding the 5% tolerance; they were excluded from further calculations after repeated analysis with unchanged results

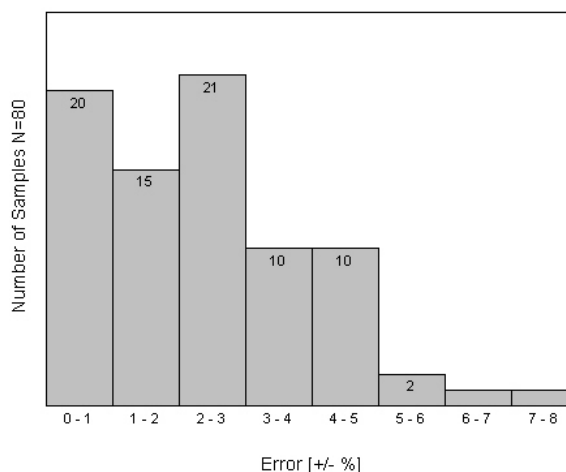


Figure 3.2: Electro neutrality vs. number of samples.

4. Results and Discussion

4.1. Hydrochemistry

The accuracy of analysis can be estimated by comparing calculated with measured electrical conductivities (EC). EC is closely related to the ions in the water (Figure 4.2), and at 25°C the EC divided by 100 gives a very good estimate of the sum of cations or anions (in meq/l) of an average $\text{Ca}(\text{HCO}_3)_2$ freshwater containing some NaCl according to equation 4.2 (APPELO, 1999)

$$\sum \text{cations} = \sum \text{anions} (\text{meq/l}) = \frac{\text{EC}}{100} (\mu\text{S/cm}) \quad (4.2)$$

Figure 4.1 shows the correlation between EC and dissolved amount of salts in solution. The best fit to the regression line is between 300 and 800 $\mu\text{S/cm}$. The EC-values measured in field range from 312 to 1788 $\mu\text{S/cm}$ for springs, from 300 to 369 for the reservoir, 360 to 2160 for rivers and 538 to 1503 for groundwater samples.

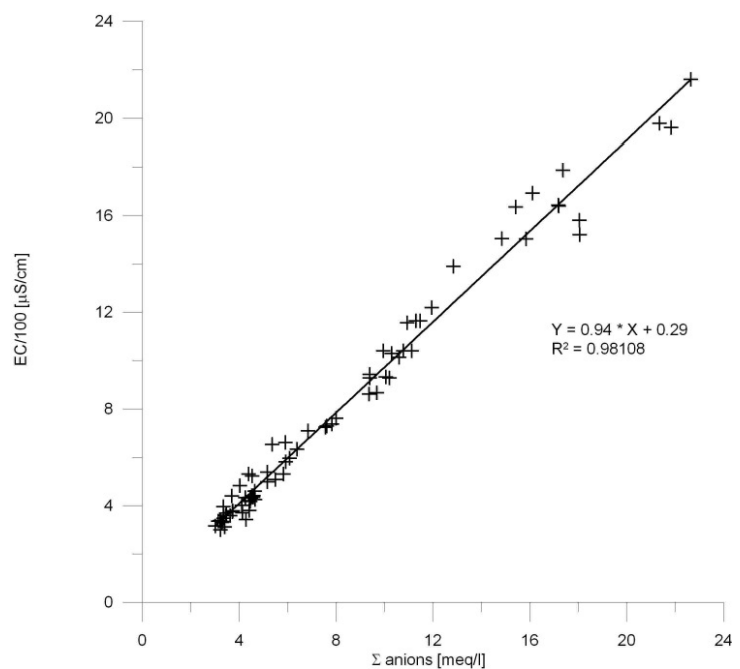
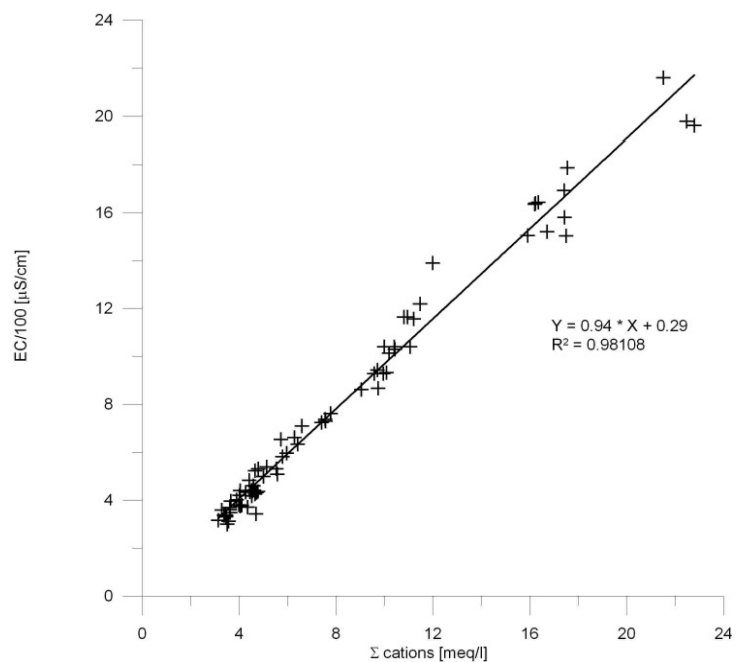
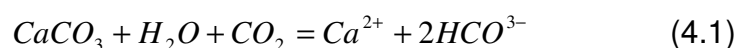


Figure 4.1: Linear correlations of EC and sum of cations (top) and anions (bottom) of measured samples.

4.1.1. Concepts

4.1.1.1. Carbonate Dissolution

The chemistry of waters in carboniferous aquifers is dominated by the dissolution and precipitation of carbonates according to equation 4.1 (DREVER, 1997)



thus depending on the presence of CO_2 . Rainwater is in equilibrium with atmospheric CO_2 which has a partial pressure (P_{CO_2}) of $10^{-3.5}$ atm. Soil gases contain much more CO_2 due to respiration and decay of organic matter. The CO_2 content in rainwater percolating through soil typically increases to an equivalent P_{CO_2} of around 10^{-2} . This additional CO_2 increases the amount of CaCO_3 the water can dissolve. Hence, the Ca^{2+} concentration in the water depends on the initial CO_2 concentration and on the extent to which the CO_2 in the water can be supplemented by exchange with a gas phase. If there is no CO_2 gas replenishment it is referred to as a closed system and the amount of calcite that can be dissolved by the water is limited to the initial amount of CO_2 . If the system is open to CO_2 , the P_{CO_2} in the water will remain constant and the consumed CO_2 for dissolution will be replaced by CO_2 from the gas phase. Nearly all samples are in a relatively narrow pH-range of 7.1 to 8.6, where according to FREEZE AND CHERRY (1997) the dissolved inorganic carbon almost entirely exists as HCO_3^- species and open-system conditions are suggested to dominate.

4.1.1.2. Saturation Index

In a system without input and output all chemical reactions will proceed towards an equilibrium state with stable concentrations of all solutes (FITTS, 2002). These processes are determined by thermodynamic principles. E.g. a chemical reaction 4.2



where A and B are the reactants and E and F the products with a , b , e , f as the proportion factors.

Their equilibrium concentrations are related to a thermodynamic factor K by

$$K = \frac{[E]^e [F]^f}{[A]^a [B]^b} \quad (4.3)$$

The terms on the right hand side of equation 4.3 are ion activities and the products called ion activity product (IAP). If $IAP=K$ the reaction is in equilibrium.

The equilibrium constant or solubility product for a mineral-solute is K_{so} and relating to eq 4.3 with the product aA^*bB as solid phase (activity = 1 in equilibrium) defined by

$$K_{so} = [E]^e [F]^f \quad (4.4)$$

When the $IAP < K_{so}$ for a given mineral, the solution is undersaturated and capable of dissolving more of the mineral and in the opposite case the mineral might precipitate from solution. When $IAP = K_{so}$ the solution is at equilibrium with the mineral phase.

The saturation index (SI) is a measure of how close a water-mineral system is to equilibrium.

$$SI = \log(IAP / K_{so}) \quad (4.5)$$

A sample is considered being saturated with respect to a certain mineral phase if its SI, expressed in logarithmic form, is in the range -0.1 to +0.1 (DREVER, 1997). More dissolution will occur if the initial water has low concentrations of the dissolution product than if it has high concentrations. Solubility products $[\log(K_{so})]$ as listed by FITTS (2002) are -8.48 for calcite and -17.1 for dolomite which shows that dolomite dissolves much slower than calcite which is a reason for the fact karstification is hardly found in dolomitic rocks.

Conditions of disequilibrium (super- and undersaturation) are common in carbonate aquifers and in field situations, unlike under laboratory conditions, weeks or months of residence time can be necessary for dissolution to proceed to equilibration with respect to calcite and dolomite. The solubility is the controlling factor of the concentrations of Ca^{2+} , Mg^{2+} and HCO_3^- in the water. The average $Ca^{2+}:Mg^{2+}$ ratio of 3.4 suggests prevailing calcite dissolution with occurring dolomite dissolution. Alterations in the molal ratio of Ca^{2+}/Mg^{2+} above and below one in a terrain with calcite and dolomite can be caused by their sequential distribution, simultaneous or incongruent dissolution, CO_2 partial pressures or temperatures (FREEZE AND CHERRY, 1997).

4.1.2. Classification

The data of 76 samples was processed in AquaChem 4.0 and 5.0 and classified into groups of similar geochemical properties. A piper diagram of all samples shows this classification according to their mineralization taking into consideration the location of the sampling sites (Figure 4.2; Overview map: Figure 4.7).

Three different groups of water types can be distinguished and especially the spring samples allow a distinction with regard to their location in the higher altitudes (Sierra) and the basin. Group 1 members which are mostly the sierra springs are normal earth alkaline waters with predominant hydrogen carbonate and electric conductivities (EC) of 300 – 600 $\mu\text{S}/\text{cm}$ while the Group 2 samples show earth alkaline waters with prevailing sulfate and hydrogen carbonate as well as some chloride and EC of 800 – 1400 $\mu\text{S}/\text{cm}$. The sites in this group are situated in the basin. However, 3 wells also located in the basin show compositions similar to the

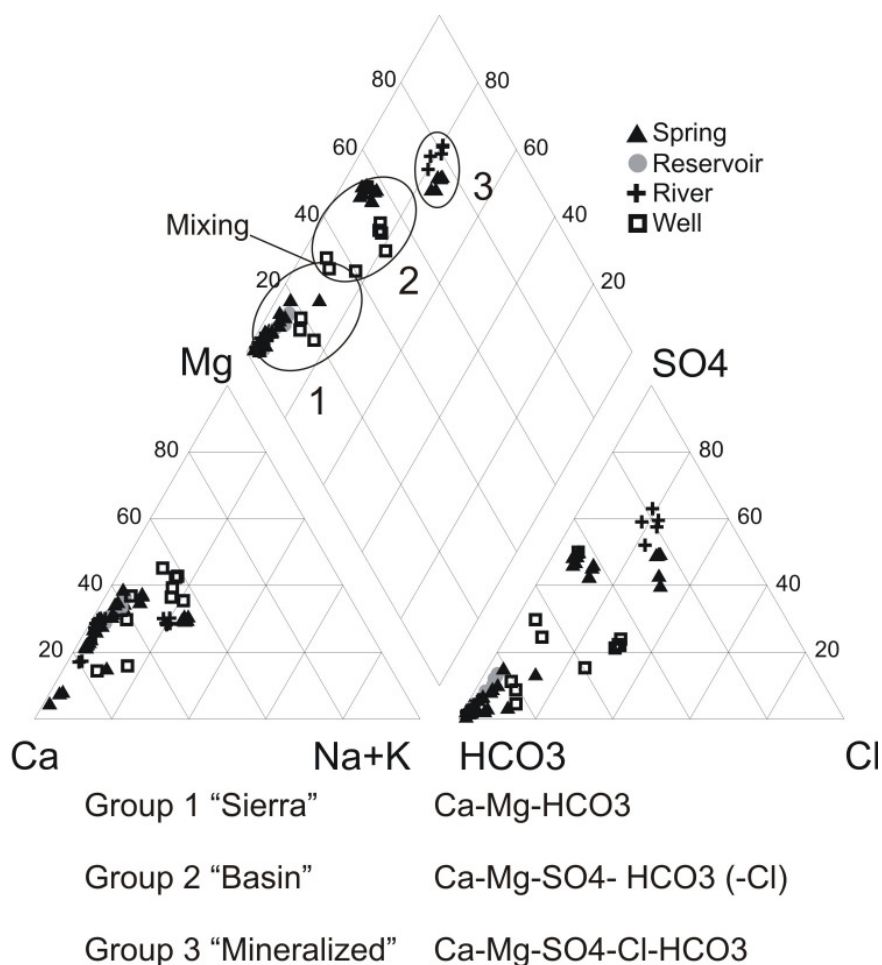


Figure 4.2: Piper diagram of all samples.

second group with EC between 710 and 930 $\mu\text{S}/\text{cm}$, except that hydrogen carbonate dominates the sulfate, similar to Group 1.

The third group consists of two sites with the highest EC of 1500 - 2100 $\mu\text{S}/\text{cm}$ which are a basin spring and a river downstream from the reservoir with earth alkali water with increased alkalis and sulfate as well as chloride and some hydrogen carbonate.

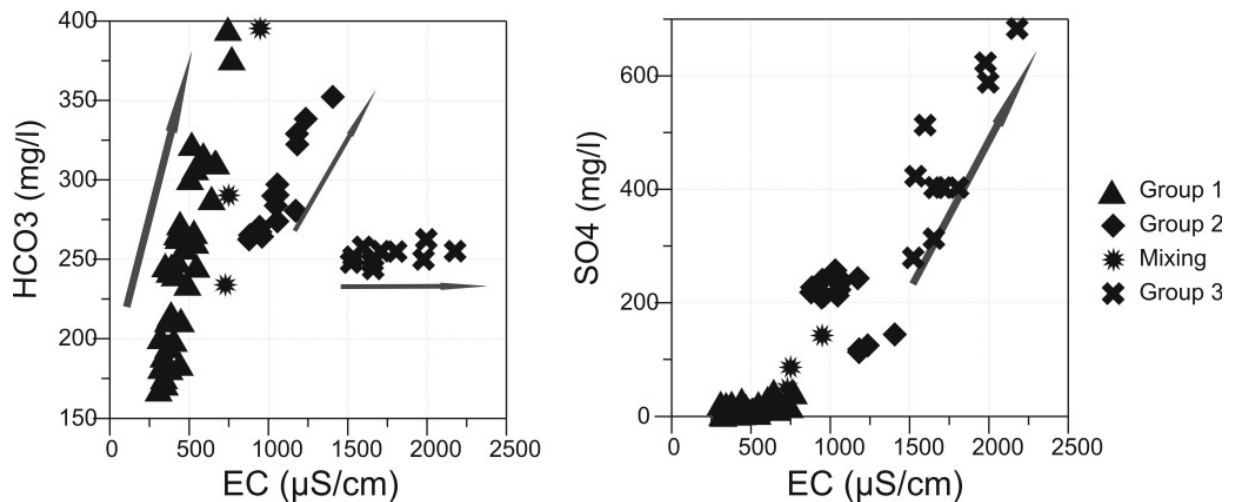


Figure 4.3: Correlation of carbonate (left) and sulfate (right) dissolution of the 3 groups.

Figure 4.3 displays the evolution of dissolution for the different groups and shows that Groups 1 and 2 are mainly subject to carbonate dissolution while Group 3 is dominated by sulfate dissolution.

For measured field data and analysis results refer to Appendix Tables 5-8.

4.1.2.1. Group 1

This group of Ca-Mg-HCO₃ type water combines 17 sites with similar geochemical characteristics. These sites contain a group of typical mountain springs with mean discharge of 25 l/s located in Cretaceous and Paleogene carbonates (Natividad, Fte. Alta, Fte. Montilla, Cueva del Agua,) with pH values of 7-8 and EC between 300 and 450 $\mu\text{S}/\text{cm}$, some small springs (Fte. Carrillo, Fte. Tornajo, Fte. Oliva, Fte. Penalba, Fte. de Ortiz, Fte. de la Piedra) with discharge of < 0.5 l/s located in Jurassic carbonates or bordering Quaternary conglomerates with pH of ca. 7.5 and EC between 350 and 600 $\mu\text{S}/\text{cm}$. SP-GM-023, -024, -025 are all situated in the village of

Table 4.1: Summary of Group 1 physical parameters and saturation indices (SI).

n= 45	Min	Max	Average
T [°C]	8.00	21.60	12.87
pH	7.09	9.16	-
EC [µS/cm]	300.00	761.00	448.13
SI Calcite	-0.40	1.47	-
SI Dolomite	-1.26	1.77	-
SI Anhydrite	-3.79	-2.22	-
SI Gypsum	-3.53	-1.97	-

Duda on the western bank of the Guardal river, which forms a steep canyon through Jurassic limestone and dolomite and the adjacent conglomerates. The reservoir San Clemente (SP-GM-014) also belongs to this group of water types, since during

summer, it is fed primarily by the discharge of the aforementioned Natividad and Montilla valleys and is located partly in Neogene marls and Jurassic and Cretaceous carbonates. The samples were taken near the surface and show pH of 8.2 – 8.6 and EC between 300 and 370 µS/cm. This group also comprehends another surface water site; the Raigadas River (SP-GM-019) which drains the northern part of the catchment but during the summer months seeps away and runs dry before contributing superficially to the reservoir. The pH values for this site range from 8 to 8.6 and EC from 360 to 440 µS/cm. Three wells also belong to this group (SP-GM-051, -052, -055). The first two are located in Quaternary conglomerates and no information about depth and screening could be obtained, but it can be assumed, that they reach into the carbonate (limestone and dolomite) aquifer. The latter of the wells (SP-GM-055) is used for cooling of rock saws in a limestone quarry. Again, no data of well assembly could be obtained. Table 4.1 shows a summary of field parameters and saturation indices calculated with AquaChem (Version 4.0.264 with PHREEQC applet, default settings used). The maximum SI-value for Calcite of 1.47 has to be considered as an error because a supersaturation of this magnitude (logarithmic value) would definitely result in carbonate precipitation. This is not the case. The accordant spring (SP-GM-020) shows barely supersaturated values in all of the other samples.

All samples of this group show undersaturation with respect to gypsum and anhydrite.

4.1.2.2. Group 2

Comprised in this group of Ca-Mg-SO₄-HCO₃ type waters are two springs and two wells all located in the basin in the southern part of the catchment area. The site Parpacen (SP-GM-002) is a spring where the water emerges through the ground to form a pool while Felin Grande (SP-GM-026) is a tapped spring only accessible by a storage facility. The FAO site (SP-GM-060) is a well that was sampled from 41 m below casing top by pumping. The other sites (SP-GM-028, -029, -030) are actually the same well (SP-GM-061) but pulled up with a sampling ladle from 40, 90 and 150 m respectively. The site was then sampled at a different time by pumping from 46 m below casing top. A concentration vs. constituents (Schoeller) plot of these samples where water of the same type is displayed as parallel lines (Figure 4.4) shows the increased SO₄-concentration compared to Group 1 as described. SP-GM-002 and -060 have nearly the same composition. This fact supports the assumption that these two sites are fed from the same aquifer since they are located close together. SP-GM-060 is an old FAO monitoring well with casing reaching down as far as 82 m below ground which is screened between 42 and 82 m below ground (IGME). The stratigraphic column states limestone belonging to a partly dolomitic carbonate formation. The Parpacen spring (SP-GM-002), which in October 2005 had a discharge of 25 l/s (IGME) while it notably became less during summer, shows variations from supersaturated with respect to both calcite and dolomite in the summer months to undersaturated in autumn and spring. These variations might be because of the fact that the spring is discharging in quaternary cover consisting of

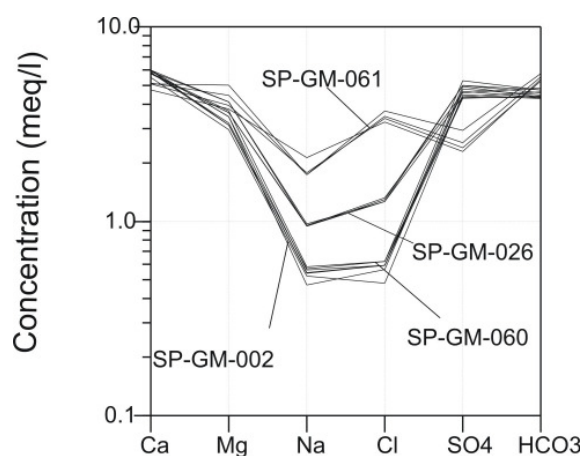


Figure 4.4: Concentration [meq/l] vs. constituents plot of Group 2 members.

conglomerates, sand and clay where the SI could be altered through precipitation while the groundwater emerges through that material and that residence times differ seasonally. The source of Fte. Felin Grande (SP-GM-026) could not be located exactly but discharges in either Neogene fluvial conglomerates and carbonate deposits or quaternary conglomerates in the intermediate presence of dolomitic

carbonates, and shows SI that indicate supersaturation to both calcite and dolomite. The average molal ratio of $\text{Ca}^{2+}/\text{Mg}^{2+}$ of 1.5 is typical for the dissolution of dolomite with the presence of calcite (FREEZE AND CHERRY, 1997).

Three wells (SP-GM-053, -054, -056) are located in the transition zone between the sierras and the basin and show chemical compositions which appear to be a mixture of Group 1 and 2 type waters (Figure 4.2 "Mixing"). The Rambla Valentin well (SP-GM-053) is an industrial well for irrigation that was unattended and in operation when the sample was taken from a tap on the piping. No construction information about the well was available but since it was operating for several hours, the parameters should have been stable. Unstable parameters present a problem for analysis, e.g. in case of SP-GM-56, a private well for irrigation with a diesel pump that had not been

in operation for a few days and was started exclusively for sampling for a few minutes. SP-GM-054 is yet another pumping well for rockwork purposes in a stone quarry adjacent to the aforementioned. These samples show variations in the SI (Table 4.2) from under- to supersaturation.

Table 4.2: Summary of Group 2 physical parameters and saturation indices.

n= 3	Min	Max	Average
T [°C]	15.50	17.50	16.57
pH	7.10	7.64	-
EC [µS/cm]	710.00	929.00	789.67
SI Calcite	-0.13	0.38	-
SI Dolomite	-0.57	0.59	-
SI Anhydrite	-2.09	-1.63	-
SI Gypsum	-1.85	-1.38	-

4.1.2.3. Group 3

This group includes two sites of relatively high mineralized water, the Fuencaliente spring (SP-GM-007) near Huescar and the Río Guardal (SP-GM-016) in a transition area between the Sierra and the basin about 2 km downstream from the reservoir San Clemente with discharge of 65 l/s (October 2005, IGME) and 80-100 l/s respectively. The first is a "slightly" thermal spring in Quaternary conglomerates with temperatures of around 19 °C with EC between 1500-1800 µS/cm and pH of around 7.3. The samples were taken from water emerging from the sand in a little stream next to the public swimming pool. The water of this site has relatively high concentrations of the related ions, especially in SO_4^- . The second stated site is the

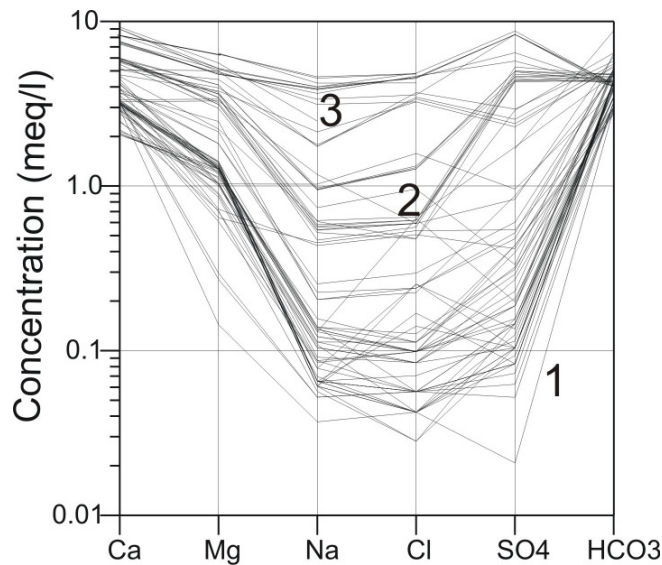


Figure 4.5: Concentration [meq/l] vs. constituents plot of all Group 1-3.

main river which drains the catchment area at a regulating gate built by the Guadalquivir Hydrologic Confederation. A Schoeller plot of the samples shows the exceptionally high concentration of all constituents especially of the river in comparison to the other two groups (Figure 4.5). Rock-source deduction modeling in AquaChem 4.0 for this group suggests Gypsum dissolution as a possible reason for the increased SO_4^- concentration. In case of Fuencaliente it could be reasonable to say, that it is probably fed by deeper groundwater with long flow paths and residence times dissolving Tertiary evaporites that have been described (IGME, 2005) in the region. This deep groundwater comes up to the surface along fractures and faults (structural map, Figure 1.7).

4.1.3. Discussion and conceptual model

The distinction between the three main groups (Figure 4.5) into Ca-Mg- HCO_3 type Sierra water (Group 1), Ca-Mg- SO_4 type basin water (Group 3) and Ca-Mg- SO_4 - HCO_3 type water (Group 2) suggests that the latter is a product of groundwater mixing between the first two groups in the transition zone between the mountains and the intermontane basin. It can be assumed, that the mountain-borne hydrogen carbonate water recharges a shallow aquifer while the sulfate bearing groundwater comes from a deeper aquifer in the basin (Figure 4.6). The sites with the most mineralized water concur with faults in the Subbetic and Quaternary Units (Figure

1.7). This suggests that the described transition zone which represents the boundary of the intermontane basin possibly offers flow paths for the (deeper) basin sulfate groundwater to the shallow aquifers. The sites nearest to the fault zones show the highest concentrations due to the low dilution of the emerging deep groundwater with the shallow groundwater (Figure 4.13).

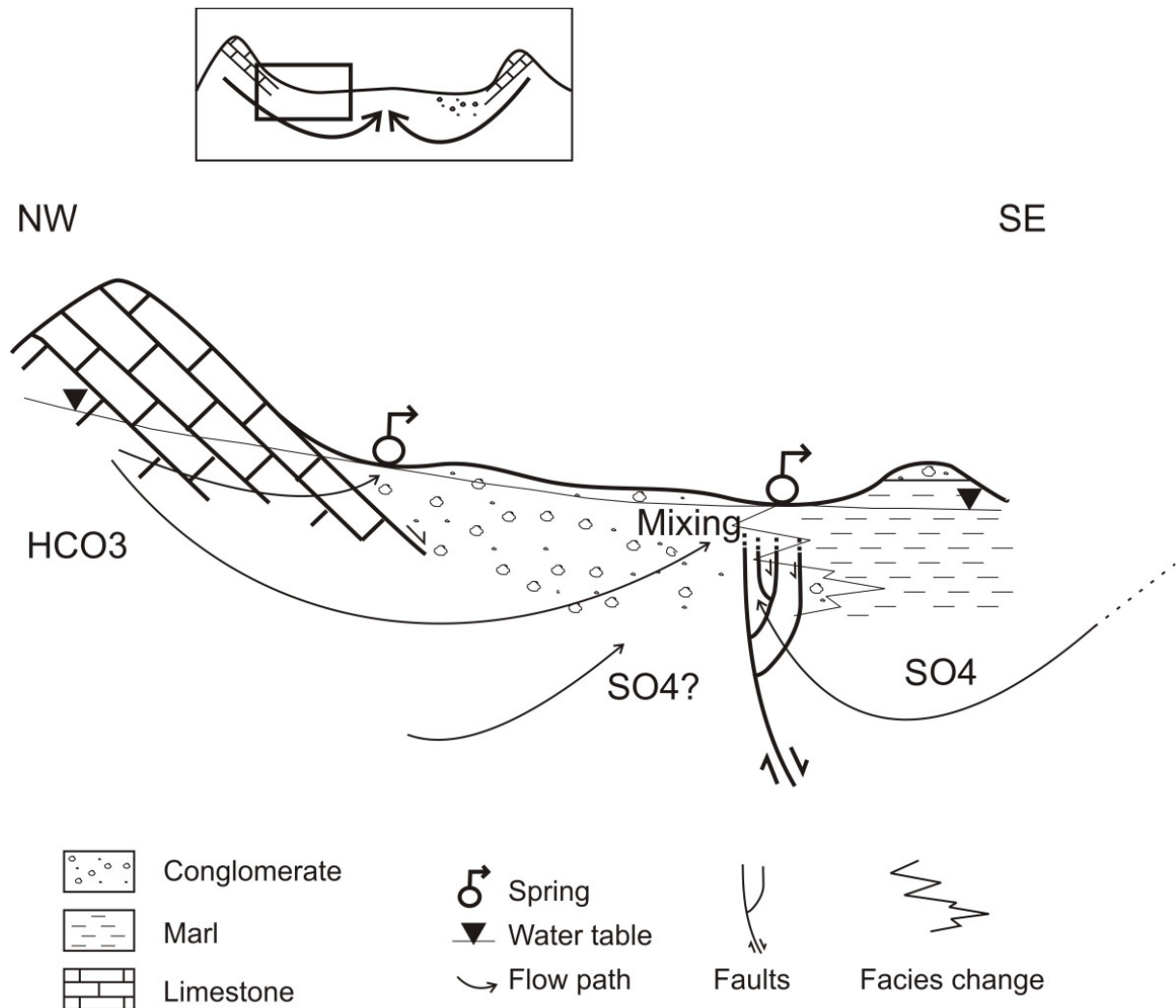


Figure 4.6: Schematic cross-section of the mountain-intramontane basin transition zone with flow paths of shallow groundwater from recharge areas in the elevated regions and of groundwater from the basin along tectonic faults to a mixing zone of the two (scetch not to scale).

The distribution of calcium/magnesium ratios of the sampled sites allows no clear distinction of spatial patterns (Figure 4.7). This is caused by the variety of site types like superficial water, springs and wells. Processes like dedolomitisation through sulfate waters or dissolution of carbonate bearing conglomerates in the basin locally influence the molal ratios. A spring in carbonatic Quaternary material might have a

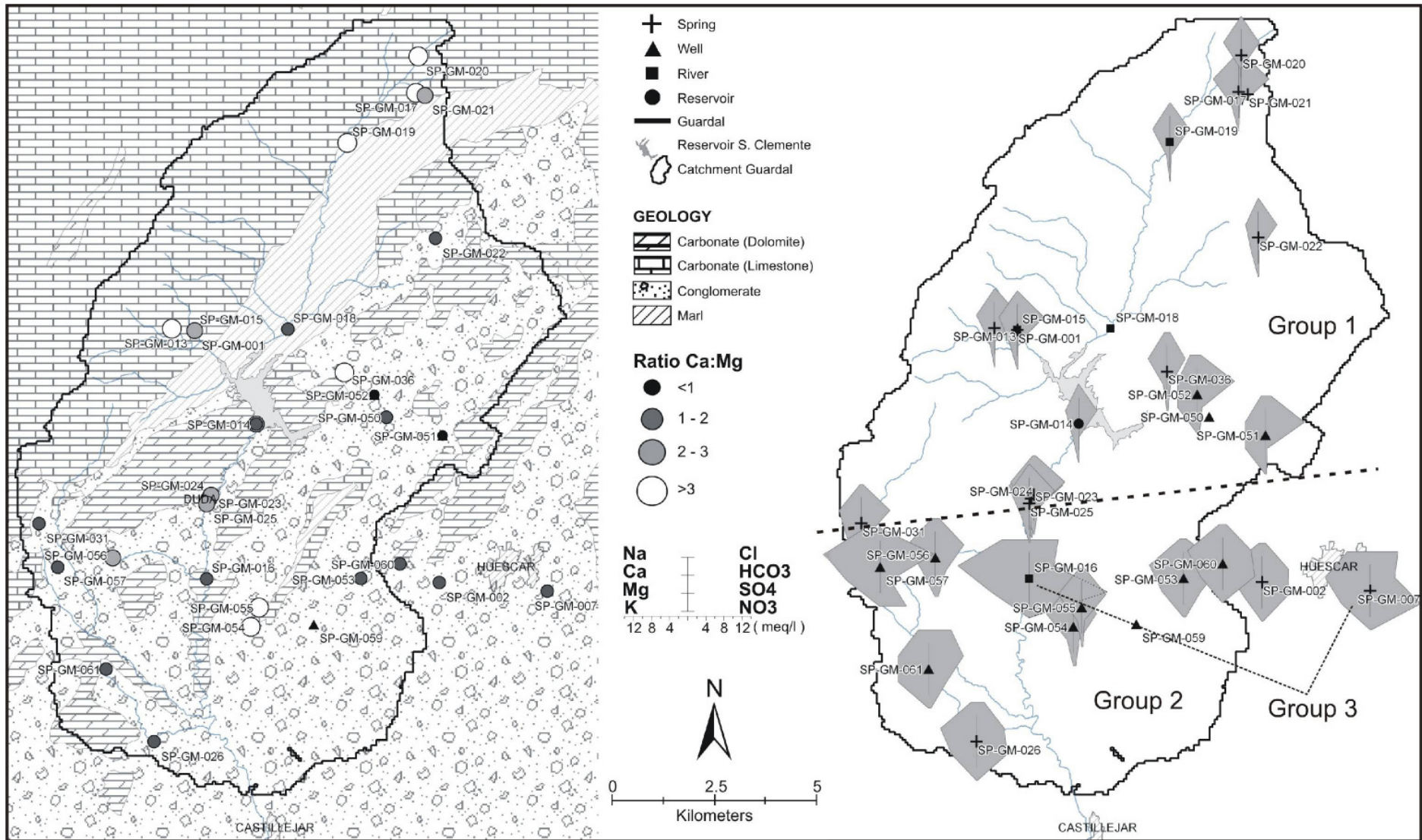


Figure 4.7: Simplified geological maps with overview of the spatial distribution of Ca-Mg ratio (left) and the major chemical constituents presented as Stiff-Diagrams (right) where the spatial distribution of the three groups is indicated.

Ca/Mg ratio larger than 3 while an adjacent well has a ratio of less than 1 simply because of the fact that the well reaches into the dolomitic foot wall and also draws groundwater from there.

Stiff diagrams are convenient to display variations of chemical compositions of single samples by geometry. The variations of e.g. chloride concentration can be seen by the shape of the tip of a Stiff diagram. A map with characteristic Stiff diagrams for each sampling site shows the location of the described groups and illustrates the distinction between sierras and basin (Figure 4.7).

The positive trend in saturation indices observed for some Group 1 springs in the assumed recharge area in the sierras combined with the observation that these springs have declining discharge from February to October leads to the conclusion that the residence times or flow paths are longer during the dry summer months

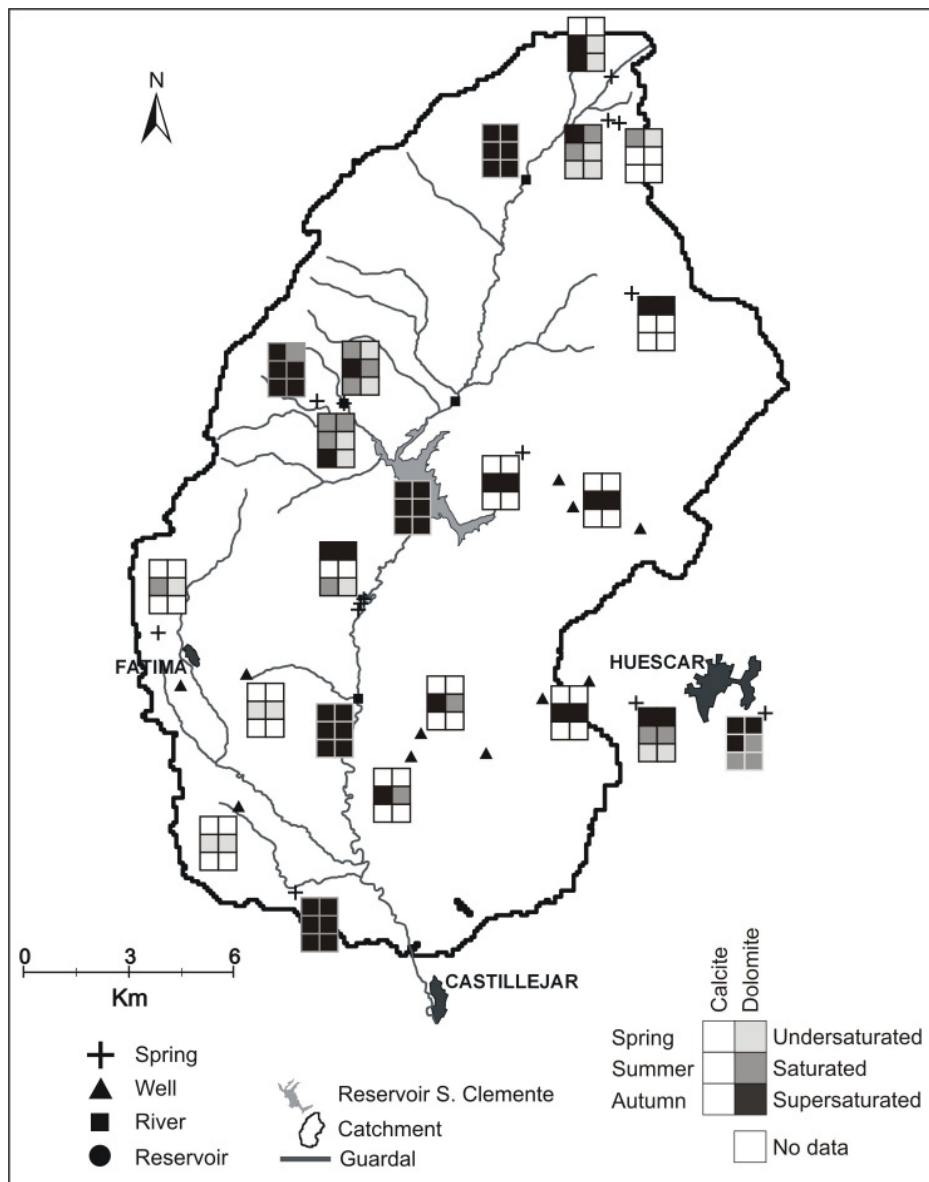


Figure 4.8: Development of saturation indices (calcite & dolomite) from spring to autumn 2005 for the study area.

4.2. Stable Isotopes

4.2.1. Precipitation, GNIP

Concerning the hydrological cycle of natural waters, the input factor for groundwater recharge is precipitation. As for isotope studies in natural waters long term observations are essential to understand patterns and variations in processes determining them. The same processes are influential to the isotopic composition of groundwater and in order to detect similar patterns it is necessary to study precipitation. The IAEA (International Atomic Energy Agency) runs a database of isotope analyses from meteorological stations all over the world; GNIP (Global Network of Isotopes in Precipitation). Isotopic data for two stations in Spain (Barcelona and Gibraltar) is presented in their meteorological context in two diagrams (Figure 4.14).

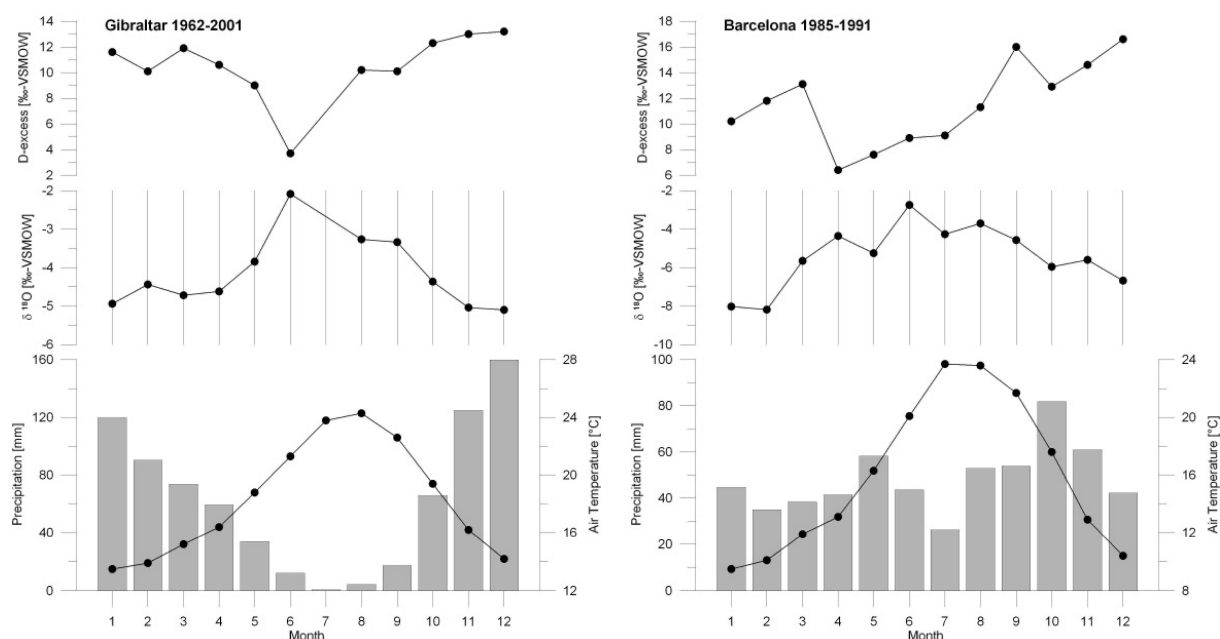


Figure 4.9: Mean weighted monthly values for $\delta^{18}\text{O}$ (middle) and d-excess (top), both in ‰ vs. VSMOW and with individual scales, are plotted with meteorological data for Gibraltar (left, 1962-2001) and Barcelona (right, 1985-1991). The lower diagram displays mean monthly precipitation in mm (bars, left ordinate) and temperature in °C (lines, right ordinate) Data: GNIP, IAEA, 27/10/2006.

Due to its geographical position, Gibraltar is expected to have climatic influences from both the Atlantic Ocean and the Mediterranean while in Barcelona the latter should prevail. VANDENSCHRICK ET. AL. (2002) observe both Atlantic and

Mediterranean isotope signals in groundwater in Sierra de Gador at the SE margin of Spain, which suggests these influences are also given for the study area.

The first observation from Figure 4.9 is that the weather pattern is different in the two cities. Gibraltar shows a seasonal variation in precipitation with rain season from October to April and a dry season from May to September with a mean annual amount of 761.8 mm while the precipitation is distributed more uniformly in Barcelona a less mean annual amount of 597.3 mm. The temperature course is similar for both stations with slightly lower mean monthly temperatures in Barcelona. Mean annual temperatures are 18.3 °C for Gibraltar and 15.9 °C for Barcelona. The mean weighted monthly values for $\delta^{18}\text{O}$ range between -2 and -5 ‰ and -2 and -8 ‰ for Gibraltar and Barcelona respectively while the d-excess ranges from 3.7 to 13.2 ‰ and 6.4 to 16.6 ‰. The Gibraltar station shows a mean weighted d-excess value of 10.5 ‰ and Barcelona 11.5 ‰. The differences for the two stations are caused by various isotope effects presented in the methods chapter.

The $\delta^{18}\text{O}$ values correlate with the temperature course with low values in the colder months and higher values during summer. This signifies a seasonal variation of $\delta^{18}\text{O}$

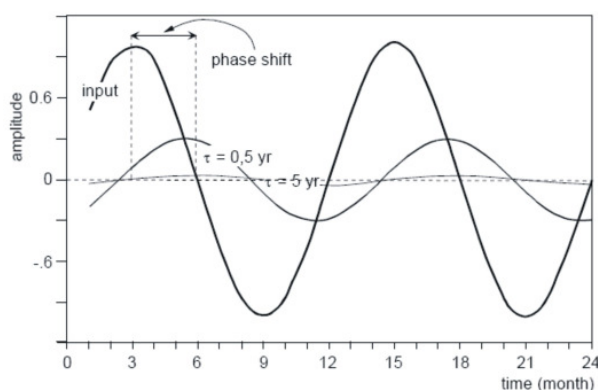


Figure 4.10: The amplitude of the seasonal variation of the ^{18}O values of precipitation can be observed in groundwater (exponential model by STICHLER AND HERRMANN, 1983. source: IAEA B, 2000).

in precipitation with depleted (light) isotope signals in winter and enriched (heavy) isotope signals during summer.

The temperature related seasonal isotopic trend in precipitation can be approximated by a sine curve that can be retraced in young groundwater. The temperature coefficient of the ^{18}O value for continental precipitation is 0.7 ‰ per °C or less (IAEA B, 2000). The response signal (discharge) is

damped and phase-shifted compared to the input signal (rain) depending on the residence time of the water in the host-rock and attenuation by reservoir effects (Figure 4.10). If, for example a karst aquifer system is recharged by a large catchment area where a relatively large amount of precipitation with different isotopic compositions is accumulated and the mean residence time is long, e.g. in a karst

cave system that behaves like a natural reservoir, the variations can be attenuated by mixing. An ideal mechanism to detect seasonal variation in groundwater would be a spring with short reaction time between input and response signal with a small catchment area.

4.2.2. Stable Isotopes ($\delta^{18}\text{O}$, δD)

An overview of $\delta^{18}\text{O}$ and δD relations of all sampled sites shows the general distributions and variations (Figure 4.11). The samples are classified according to their type in springs (14) and sub-groups by their geographic situation in “Sierra Sagra”, “Sierra Secca” and “Basin”, surface water (4 river, 1 reservoir) and wells (11). Each of these different groups that are plotted in the diagram has different characteristic isotope signals.

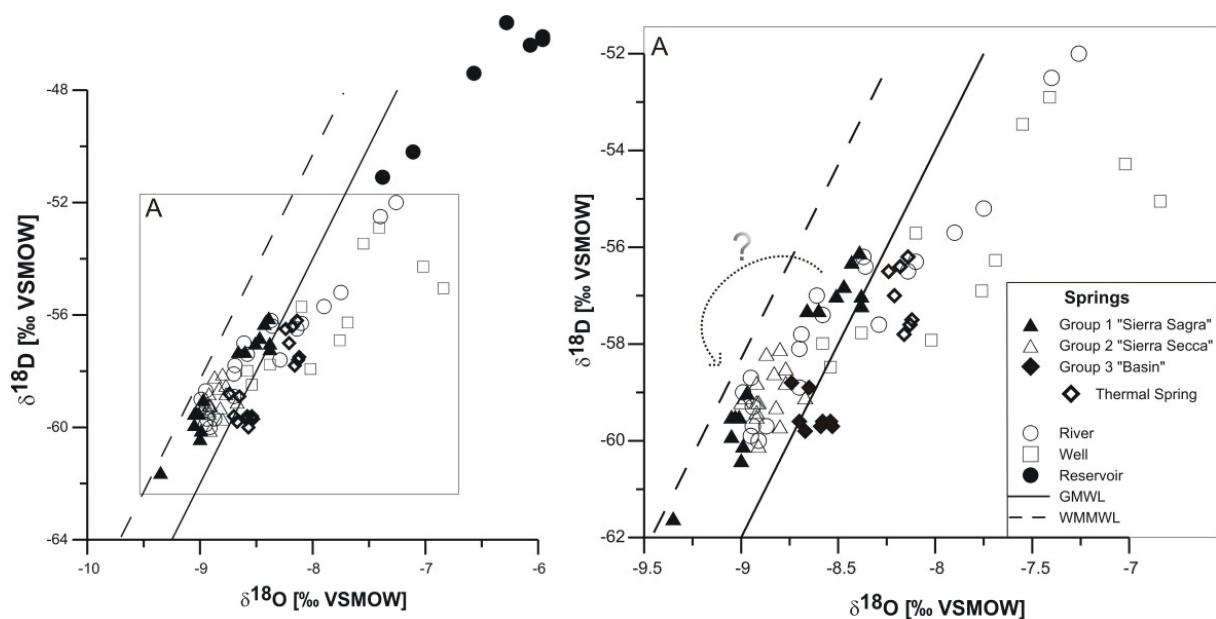


Figure 4.11: Overview of $\delta^{18}\text{O}$ and δD values of all samples ($n=48$) with GWML and WMMWL reference and magnified section (A) of the plot for better identification. Some of the members of spring Group 1 “Sierra Sagra” (solid triangles) are assumed to be affected by “secondary” evaporation and are possibly located closer to the rest of this group as indicated by the arrow (for explanation see description of group section below).

Spring samples show variations in $\delta^{18}\text{O}$ from -6.8‰ to -9.35‰ and δD from -51.2‰ to -61.6‰ (all δ -values are per mill values in reference to VSMOW if not stated otherwise) with a d-excess up to 13‰ . A few springs are possibly altered due to evaporation in interception tanks (see section below), and their probable position in the plot is suggested by the dotted arrow in the figure. The slightly thermal spring

(Fuencaliente, Huescar, ØEC: 1621 µS/cm, ØT: 19°C (IGME)) has δ -values of -8.24 to -8.12 for ^{18}O and -57.8 to -56.2 for D.

Samples taken from surface water including the reservoir show variations in $\delta^{18}\text{O}$ from -5.96 to -8.99 and δD from -45.6 to -60.0

Samples from wells show variations from -6.84 to -8.58 in $\delta^{18}\text{O}$ and from -51.9 to -57.9 in δD .

The fact that the isotope signals of the mountain springs plot between the GMWL and the WMMWL, some closer to the GMWL which represents the signals in precipitation derived from oceans (Atlantic) and some closer to the WMMWL (Mediterranean) suggests that the local precipitation is influenced by both origins of vapor masses. Mediterranean originated air masses have a d - excess of up to 15 ‰ caused by low relative humidity and high temperatures during primary evaporation while air masses from the Atlantic show values of around 10 ‰. The most depleted signal is from a single sample from Cueva del Agua which discharges a small catchment and shows that the preceding rain event was of Mediterranean origin. The basin springs are shifted on the ^{18}O axis towards less negative values due to geothermal water-rock interaction in case of Fuencaliente (slightly thermal). The surface water follows an evaporation trend with spring water as one end member and reservoir water as the other. Some of the groundwater reflects this evaporative trend, while some of the sampled sites show enriched isotope signals that can not be derived from evaporation or local geological settings and are considered to be due to mixing effects. The next sections further describe the individual groups and try to elaborate their details. For location of sampling sites see figure 3.1.

The study area's topography is an elevated plain with surrounding mountains with differences in altitude of approx. 1400 m which are 5 m elevation gain per 100 m distance. The most elevated spring (Cueva del Agua, SP-GM-022) at 1499 masl, has a limited recharge area since it is located on the slope of a secluded solitary peak, the highest point in the area with 2340 masl. It is snow covered in winter and has patches until as late as May, and shows the most depleted isotope signal of all samples (-9.35 and -61.6 for $\delta^{18}\text{O}$ and δD respectively). This site was sampled only once due to poor accessibility.

4.2.2.1. Springs

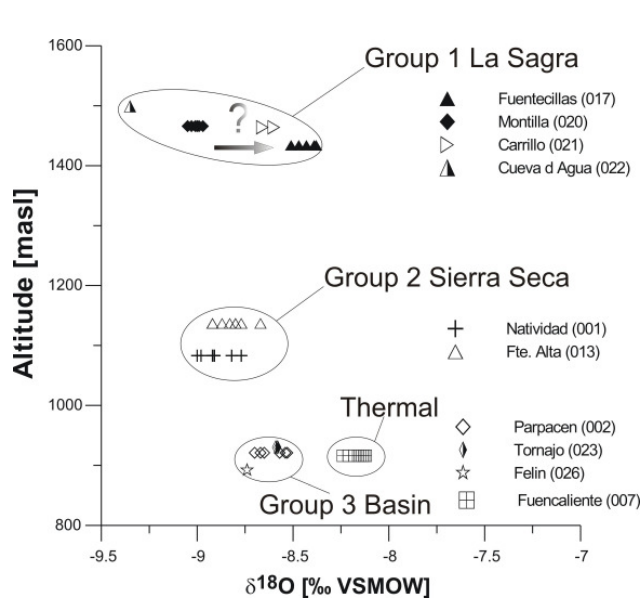


Figure 4.12: Overview of $\delta^{18}\text{O}$ and δD values of all samples ($n=48$) with GWML and WMMWL reference and magnified section (A) of the plot for better identification. Some of the members of spring Group 1 “Sierra Sagra” (solid triangles) are assumed to be affected by “secondary” evaporation and are possibly located closer to the rest of this group as indicated by the arrow (for explanation see description of group section below).

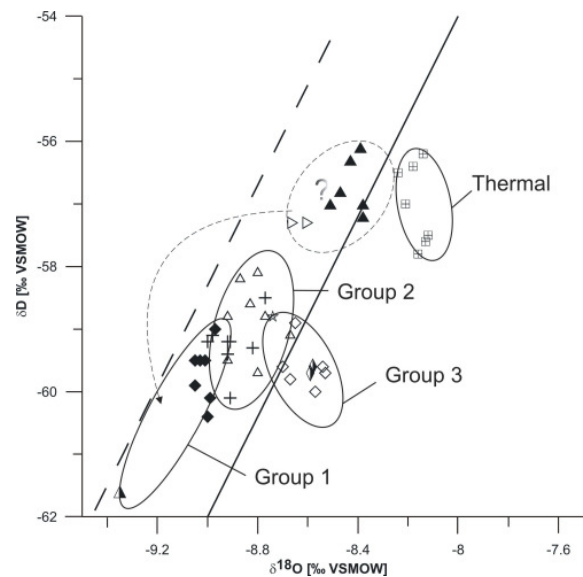


Figure 4.13: $\delta^{18}\text{O}$ and δD -correlation of sampled springs in reference to the Global and Western Mediterranean MWL.

The two figures (4.12, 4.13) above show the largest group of sampled sites, the springs. A $\delta^{18}\text{O}$ vs. altitude plot (Figure 4.12) shows a classification of the sites according to their altitude which corresponds well with their geographic situation in the working area (Figure 3.1). Due to these differences in orographic conditions like exposure to wind etc. a realistic calculation of altitude- $\delta^{18}\text{O}$ relations was not possible.

4.2.2.1.1. Group 1 “Sierra de la Sagra” (SP-GM-017; -020; -021; -022)

This group of springs is located between 1434 and 1499 masl in the northern part of the study area. The δ -values range from -8.38 to -9.35 in ^{18}O and -56.1 to -61.6 in D. With decreasing elevation the isotope signals show enriched values in both $\delta^{18}\text{O}$ and δD . Nevertheless, the variation of $\delta^{18}\text{O}$ indicates possible additional alteration of the isotope signals. SP-GM-017 and -021 are springs where the exact origin of the water could not be determined. The sites are regulated springs with storage tanks of unknown size. The samples were taken from the outlets of these tanks in which the stored water was probably subject to evaporation. Only two samples from SP-GM-021 were taken before the spring ran dry during summer. This “secondary” evaporation might be the reason for the rather scattered signals. SP-GM-022 is a karst spring on the slope of the solitary La Sagra Mountain that represents a perched aquifer which is recharged by winter precipitation and snowmelt and is located in a

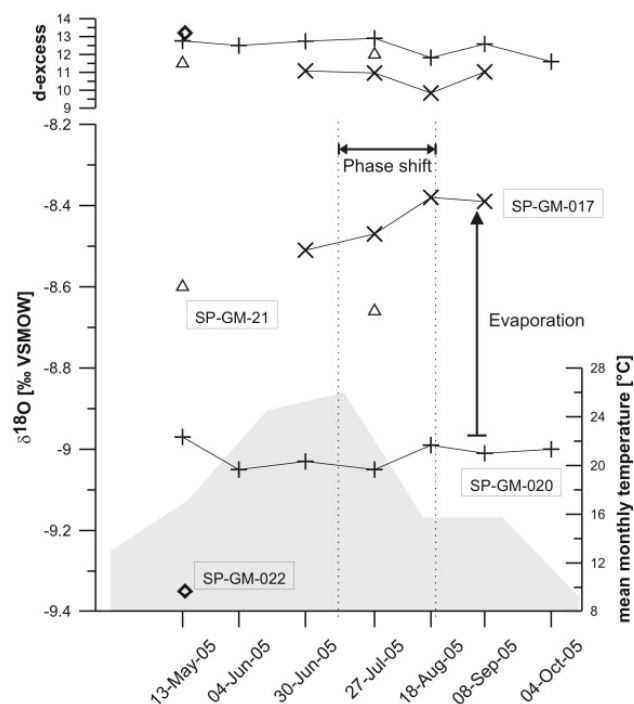


Figure 4.14: Temporal variations of $\delta^{18}\text{O}$ and d-excess of Group 1 springs with mean monthly temperatures 2005 Huescar. The dotted lines indicate a phase shift between the input (summer precipitation) and the response signal (enriched isotope compositions). (clima data: www.juntadeandalucia.es, 5/9/2006)

cave and therefore a site unsusceptible to evaporation. The two signals (SP-GM-017 & -021) should plot closer to SP-GM-020 & -022 (Figure 4.12 and 4.13). SP-GM-020 has a discharge of approximately 10 l/s while SP-GM-017 & -021 are small springs with a discharge of < 1 l/s. Figure 4.14 shows $\delta^{18}\text{O}$ - values of Group 1 members and two time series show variations in the isotope signals with depleted values in winter and enriched values in summer, according to isotopically light (depleted) winter rainfall and heavy (enriched) summer rain. These variations are well above the standard deviations of the analysis

of 0.02 ‰ for $\delta^{18}\text{O}$ and 0.3‰ for δD , but are within a small range, especially SP-GM-020, so that they might be standard deviations of the mean isotopic composition in the aquifer. But the isotope signals show an increase in $\delta^{18}\text{O}$ combined with a decrease in d-excess in August which is also observed in the long-term measurements from Gibraltar for June (Figure 4.9). The highest temperatures in 2005 were recorded for July and a shift towards enriched values can be observed for August which might signify a mean residence time of about two months. However, a phase shift of 14 months would obviously not be visible in this model. The vertical shift in d-excess and $\delta^{18}\text{O}$ values might be another indication for secondary evaporation effects as supposed. With progressing evaporation the δ -values will increase towards enriched values (eq 2.6). Hence, the d-excess will decrease. The springs are located close together on the same slope of the sierra and the parallel course of the isotope ratios reflects the similar climatic and orographic conditions.

Group 2 “ Sierra Seca” (SP-GM-001; -013)

These two springs are located on the eastern face of Sierra Seca at elevations of 1083 masl and 1137 masl respectively. The δ -values range from -9 to -8.67 and -60.1 to -58.1 for ^{18}O and D respectively. Both sampling sites are karst springs inside caves and the samples were taken from pools close to where the water emerges, so that no alteration of the isotope signals should occur through evaporation. These springs exhibit less variation compared to Group 1 members which indicates less

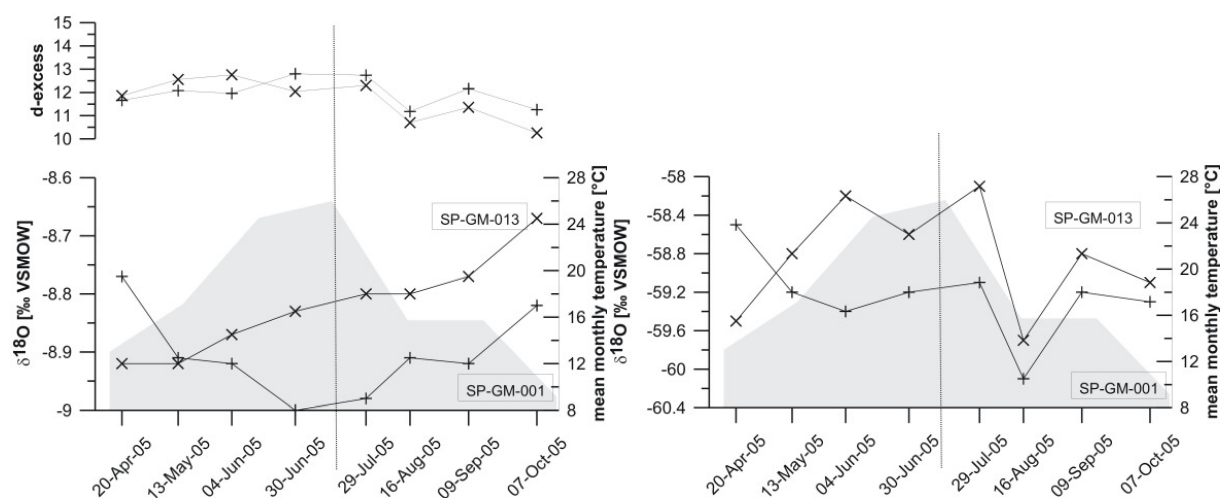


Figure 4.15: Temporal variations of $\delta^{18}\text{O}$ (left) and δD (right) with mean monthly temperatures 2005 (Huescar, www.juntadeandalucia.es, 2006).

altitude differences in the catchment area.

Time series at the two sites show that the seasonal variations for both $\delta^{18}\text{O}$ and δD correlate with each other to some extent from the beginning of July on (Figure 4.15). The δ -values show a depletion peak in August for D which can not be observed in ^{18}O . This incongruent course can not be explained by seasonal variations. Depleted values which are typical for winter precipitation should occur for both isotopes. And with an expected phase shift of two to three months they should occur in spring not in summer.

Man. de la Natividad shows an increase of $\delta^{18}\text{O}$ with a coeval decrease in d-excess similar to the one described for Group 1. The increasing $\delta^{18}\text{O}$ values over time can not be explained by evaporation because the δ -D values do not affirm this trend. The generally scattered distribution of the samples in this group (Figure 4.13) leads to the conclusion that the associated catchments comprise various factors that determine isotopic composition of recharge waters, e.g. different altitudes and slope exposure. The parallel course of the d-excess roughly shows the same magnitude, an indicator for the Mediterranean as the vapor source for the precipitation masses.

4.2.2.1.3. Group 3 “Guardal Basin” (SP-GM-002; -023; -026)

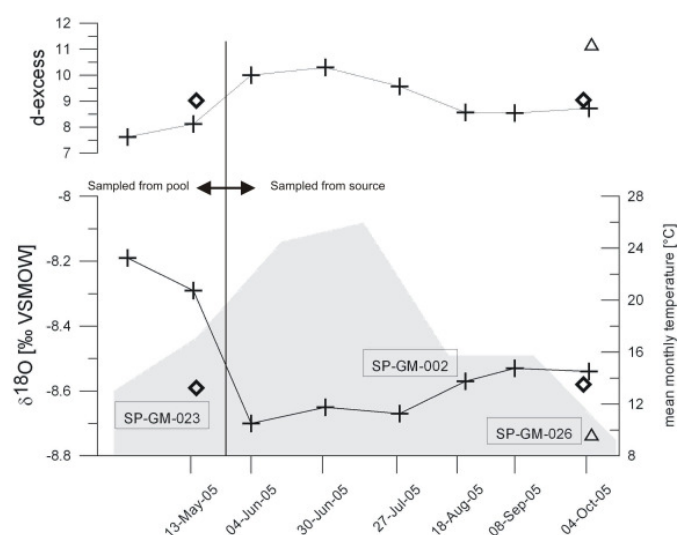


Figure 4.16: Group 3 values and temporal variations of $\delta^{18}\text{O}$ and d-excess with mean monthly temperatures 2005 (Huescar, www.juntadeandalucia.es 5/9/2006). Line indicates change of sampling location for SP-GM-002.

These sites are springs in the basin and the valley of the Guardal River between 892 and 937 masl. The δ -values range from -8.79 to -8.19 and from -60 to -57.9 for ^{18}O and D respectively. The data collected for the only spring in the SW part of the study area (SP-GM-026) is applicable for temporal variation interpretation, for the same problem with alteration by evaporative enrichment in a storage tank. Only during the last

sampling campaign a sample from streaming water could be taken so that generating a time series for that particular spring was not possible. Group 3 member compositions (Figure 4.16) however do not show the seasonal variations as described earlier for reasons of attenuation through a larger catchment and longer residence time. The first two samples were taken from the surface of a natural pool fed by the spring. And from the third sampling on a spot was chosen where the water emerges through the soil. The water at the pool surface is evaporating which can be seen by the shift on the $\delta^{18}\text{O}$ towards enriched values.

The d-excess values differ from the other groups. D-excess values lower than 10 ‰ have possible reasons e.g. in secondary evaporation processes that rain droplets are exposed to beneath cloud base especially during small rain events in warm months (IAEA A, 2000). This implies that the basin springs are also influenced by groundwater recharge that occurs through direct infiltration of precipitation in the basin. As shown in the hydrochemistry chapter the basin springs are subject to groundwater mixing with deep groundwater so that variations through lateral influx are likely.

4.2.2.1.4. “Group” 4 “Thermal” (SP-GM-007)

The only (slightly) thermal spring in the study area shows no significant seasonal variations. As mentioned above, the basin springs discharge not only groundwater from the shallow carbonate aquifers like Group 1 and 2 members but are located in a transition zone where the carbonate terrain “communicates” with the detritic aquifers of the intermontane depression. The catchment of this depression is much larger and seasonal variations are likely to be attenuated by mixing processes. Thermal springs are often associated with tectonic faults that produce gateways for deep groundwater with relatively long mean residence times to the surface. The Spanish name Fuencaliente translates to hot spring and with the temperature deviating little from 20 °C, it will be considered as thermal water. A $\delta^{18}\text{O}$ enrichment related to water-rock interaction with the calcareous rock present in the area is observable. Figure 4.18 shows various processes capable of shifting the δ -values for both ^{18}O and D: evaporation displaces both; $\delta^{18}\text{O}$ is enriched by isotopic exchange with limestone; δD by silicate hydration (IAEA B, 2000).

A remarkable thing though is the fact that this spring plots relatively close to the GMWL which is another indication for lateral mixing processes.

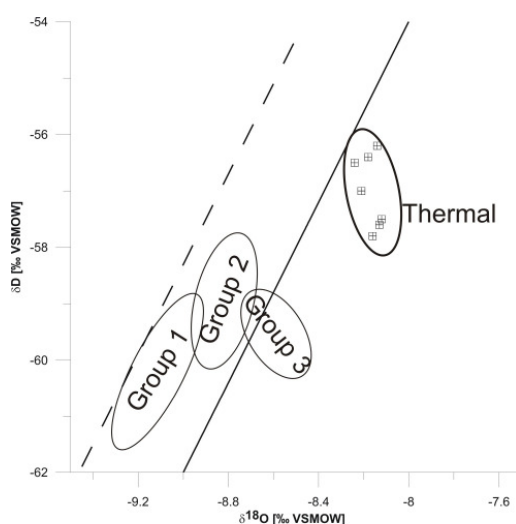


Figure 4.17: $\delta^{18}\text{O}$ vs. δD plot of the previously described groups of springs and the slightly thermal spring which is shifted on both axes.

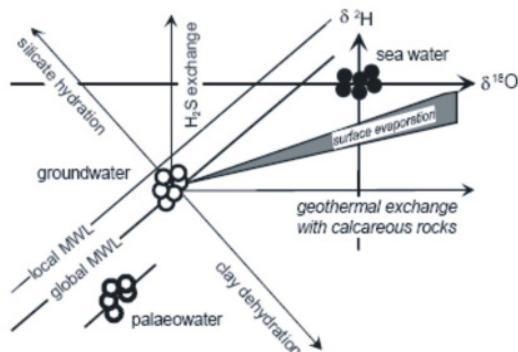


Figure 4.18: Different processes that shift the δ -values for ^{18}O and D away from the MWL. Local MWL corresponds to Mediterranean Water Line (Source: IAEA, 2006).

4.2.2.2. Surface water

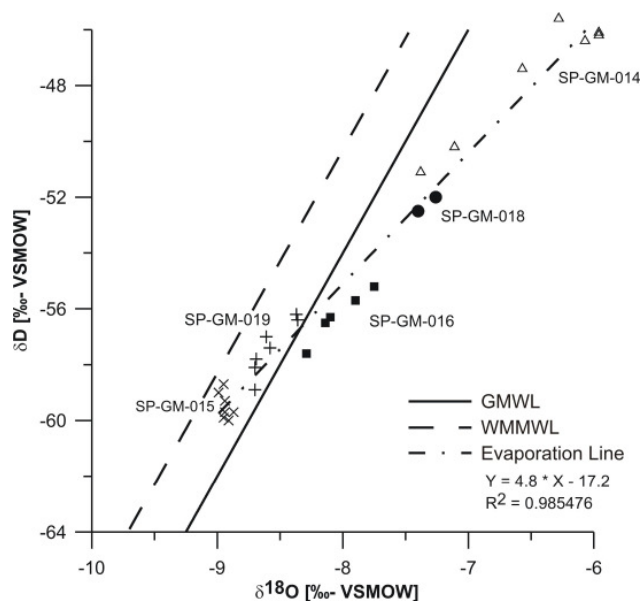


Figure 4.19: $\delta^{18}\text{O}$ and δD -correlation of sampled surface water in reference to the global and western Mediterranean MWL.

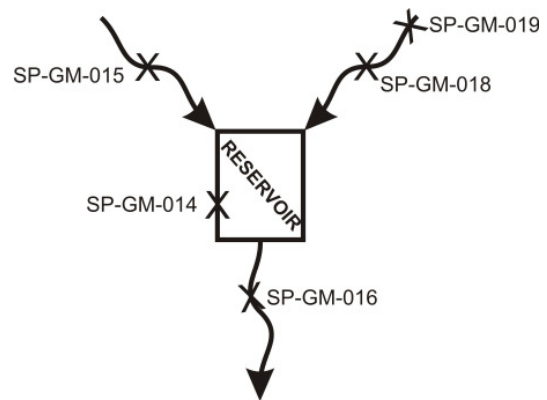


Figure 4.20: Location of river sampling sites upstream and downstream from the reservoir.

The δ -values of ^{18}O and D show variations from -8.99 to -5.96 and -60 to -45.6 respectively.

The surface water samples show a regression line with the slope of 4.8 (Figure 4.19) between the fresh water and the accumulated reservoir water as end members. The slope of evaporative enrichment less than 5 is typical for evaporation from open surfaces.

The most enriched δ -values are from the Reservoir (SP-GM-014). The samples were taken from the surface and even though no vertical stratification was expected the signal is probably more enriched than the average value for the reservoir.

SP-GM-015 plots between the Global and Western Mediterranean MWL close to the Sierra Seca springs since it is the origin of the Guardal River.

SP-GM-019 is a site in the Guardal/Raigadas headwaters and the signals plot between the MWL due to proximate influence of the contributing springs. Following the course further downstream the site SP-GM-018 is situated immediately upstream the reservoir. The river is at this point exposed to evaporation and as a result the

isotope signal plots below the GMWL. This site was sampled twice before the river in this section ran dry during summer.

The site SP-GM-016 about two km downstream the reservoir plots close to the GMWL and shows a slight evaporation trend.

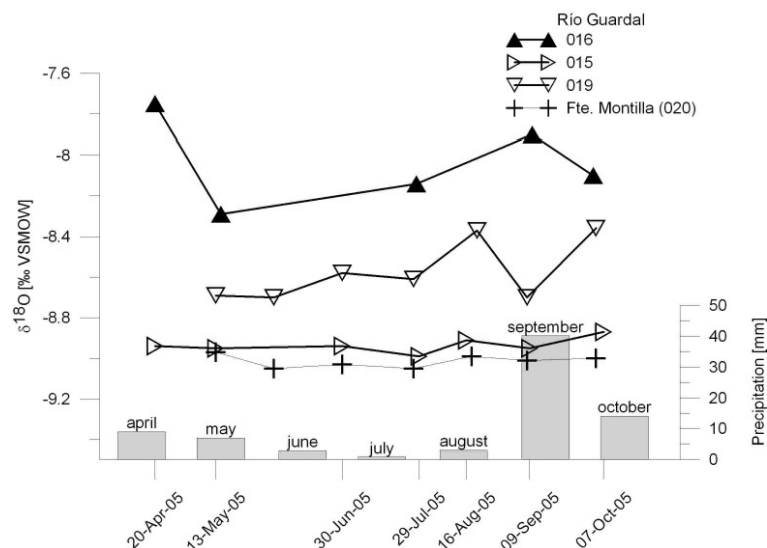


Figure 4.21: Temporal variations of $\delta^{18}\text{O}$ of all river sites compared to a contributing spring with the monthly precipitation 2005 (grey bars) to visualize rain amounts.

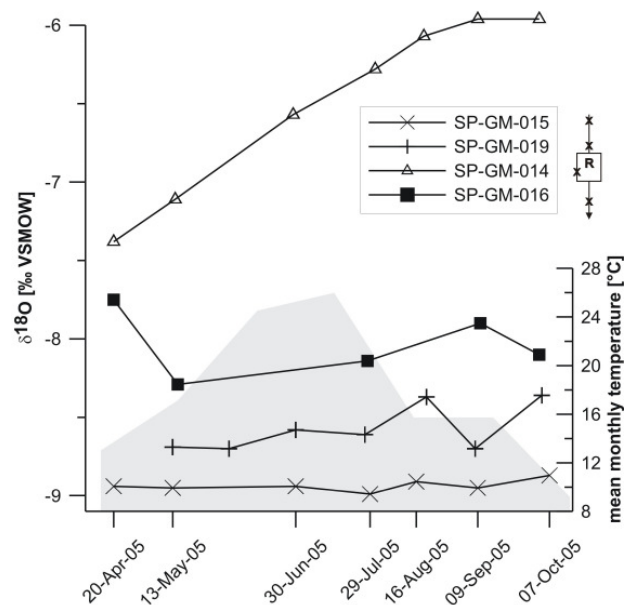
A time series of all the river sites except SP-GM-018 was plotted to detect possible correlations as the water proceeds along the course of the river (Figure 4.21).

The time series of SP-GM-015 shows variations similar to the Natividad valley springs. This site is close to the source of the Guardal River, a spring adjacent to Man. de la

Natividad.

The δ -values for ^{18}O for the river sites are enriched and the magnitude of the variations exceed the one of the springs. The course of SP-GM-019 shows strong variations with a depletion peak in September. The reason for this could be mixing processes with superficial runoff from the slopes of the surrounding sierras. A correlation with the rain events at the beginning of September (Figure 4.21) seems likely because a river responds faster to changes in isotope compositions in precipitation. This indicates that these rainstorms that produced a large amount of precipitation in a short time had isotope signatures more depleted and therefore characteristic for autumn/winter. It also implies that an amount effect and an altitude effect could have disadvantaged isotopic enrichment. In other words an intense rain in the mountains is not exposed to evaporation to the same degree as a lighter rain in the basin where the droplets encounter higher temperatures and larger distances from cloud base to the ground.

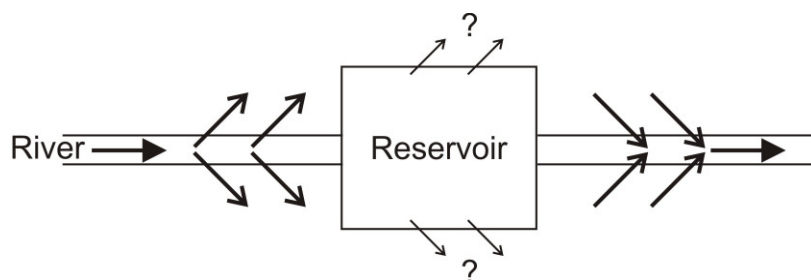
SP-GM-016, a site about two km downstream from the reservoir shows variations of larger magnitude with generally more enriched $\delta^{18}\text{O}$ values. In a similar plot of $\delta^{18}\text{O}$ vs. time like above, completed with the data for the reservoir it becomes obvious that SP-GM-016 is shifted toward enriched $\delta^{18}\text{O}$ values for the fact that the river in this section is downstream the reservoir (Figure 4.22). But the influence of the



reservoir does not seem to attenuate completely the seasonal variation in isotopic composition of the river water.

Two possible causes seem reasonable. The first is that the reservoir is stratified in contrary to the assumption that the water is not deep enough for a stratification to develop and vertically mixed by the outlet flow. The outtake of reservoir water into the river is located close to the bottom and a vertical stratification could cause that the bottom of the water column is not affected by evaporative enrichment to the same degree as to near the surface.

Secondly, as described in the hydrochemistry chapter, the Duda-La Sagra aquifer is discharging a large quantity of its exploitable amount under water into the river along its course. The fact that the upstream site SP-GM-018 runs dry during summer implies that the Guardal head water is subject to losing river conditions while the lower course is developed as gaining river (Figure 4.23). The reservoir loses water to the aquifer because the water level is raised above the groundwater table through the dam.



4.2.2.3. Wells

From all the well samples taken only three could be sampled according to the proper procedures described in the methods section. The fact that the well assembly details for most of the wells are unknown makes isotope interpretation and interrelationships difficult to some extent. The FAO well SP-GM-060 has a depth of 80 m. Table 3.2 gives an overview of the known depth of water table below ground for the sampled wells and Figure 3.1 displays the spatial distribution of the sites.

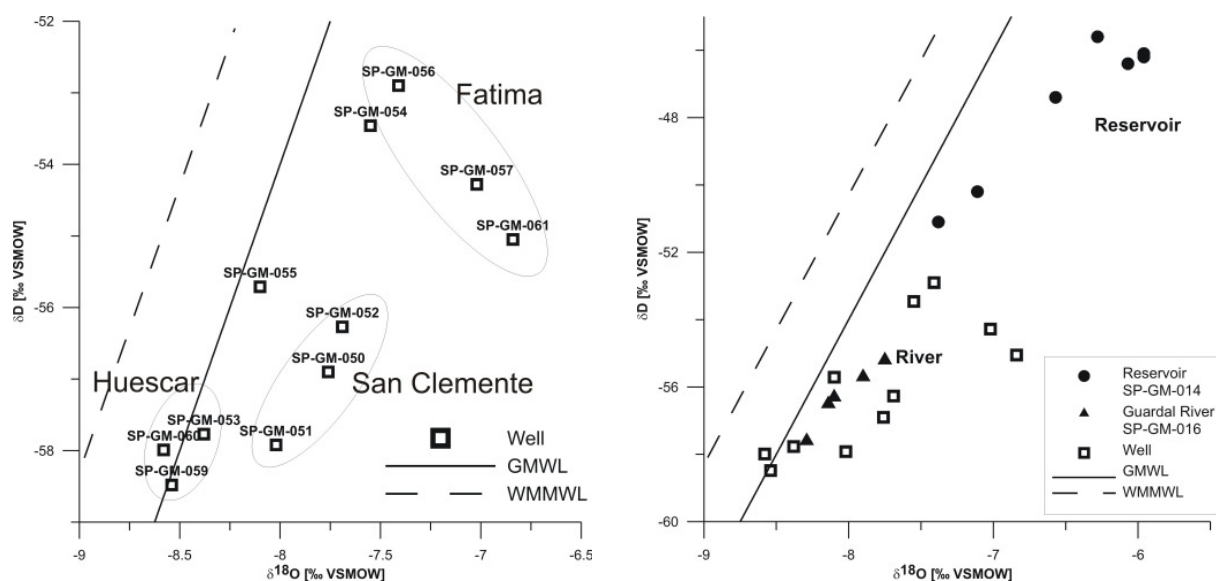


Figure 4.24: $\delta^{18}\text{O}$ vs. δD plot of the sampled wells with MWL as reference (left) and with river and reservoir to visualize the evaporation trend in the study area (right).

The δ -values range from -8.58 to -6.84 ‰ for ^{18}O and -57.9 to -51.9 ‰ for D and are widely scattered (Figure 4.16; 4.27). If compared with the spatial distribution of the sites (Figure 4.24) three groups can be distinguished (Figure 4.24).

4.2.2.3.1. Group Huescar

This group comprises three wells, a FAO observation well (SP-GM-060), a large automatic pumping well (SP-GM-053) and an artesian well (SP-GM-059). The fact that the latter is an artesian well considering the proximity to the Parpacen spring (SP-GM-002) suggests that these wells and the spring are fed by the same aquifer which is affirmed by the hydrochemical analysis (Ca-Mg-SO₄-HCO₃ type waters.) The

FAO well has a depth of 80 m and the enrichment of the δ - values of this group compared to the Basin Springs (Group 3 “Guardal Basin”) allows the assumption that the mixing of the shallow groundwater from the sierras is observable within this range but gets less with increasing depth where the deeper basinal groundwater prevails. The isotope composition of the deeper groundwater of the wells shows enrichment of ^{18}O compared to the shallow sierra water likely due to water-rock-interaction and mixing effects with groundwater possibly of geothermal origin.

4.2.2.3.2. Group San Clemente

This group is represented by a private well (SP-GM-050), a solar powered pumping well (SP-GM-051) and an agricultural pumping well which was constructed recently before sampling (SP-GM-052). These wells are located in a flat plain between the surrounding sierras east of the Reservoir and it can be assumed that they are not deeper than the wells in the first group for the fact that the SP-GM-050 has a depth of water table below surface of about 2 meters. The δ -values for D are within the range of values observed in spring water but show enrichment in ^{18}O . Without knowledge of construction details of the wells it is difficult to explain the development of such isotopic compositions usually associated with water-rock interactions of geothermal waters in a context of hydrogen carbonate water in a carbonate domain (sierras). A possible answer would be mixing with geothermal water emerging along tectonic pathways. The groundwater head 2 meters below ground allows the assumption that evaporation might have a certain influence on the indicated enriched isotope signatures.

4.2.2.3.3. Group Fatima

This group includes three sites (SP-GM-56, -057, -061) that are located west of the Guardal River near the town of Fatima. These wells are similar to the previously described wells with depths of less than 100 m and water table at around 40 m below surface. SP-GM-061 is the southernmost well that is located furthest away from the sierras in the basin and since it was sampled according to the appropriate

procedures it should show unambiguous results. It is in fact the most distant from the MWL (Figure 16) together with SP-GM-057 which is an indicator for mixing with groundwater with enriched isotope composition due to e.g. geothermal water-rock-interaction.

An enrichment related to evaporation as described for the surface water can also be observed in the wells. The sites SP-GM-054, -055 and -056 display the evaporation line of the river and reservoir samples (Figure 4.19; 4.24).

4.2.2.3.4. Conclusions

The individual groups show isotopic compositions that are distinct from each other with values as described in the Groups section. This clarifies that the springs, rivers and wells have clearly different catchment areas despite the fact that they are located relatively close together.

The sites with the most depleted isotopic composition that lie closest to the GMWL are located on the east of the Guardal River in the basin towards Huescar while the sites with the most enriched δ -values are situated west of the river towards the basin near the village of Fatima. A third group of sites is located east of the San Clemente reservoir and shows enrichment in $\delta^{18}\text{O}$.

The correlation of SP-GM-54 and -055, pumping wells used for rinsing rock saws at a local stone quarry is delicate since they are situated closely together between the first two groups described but show δ - values that are along the typical evaporation trend described earlier in this chapter.

5. Outlook

This work gives a basic idea of the flow processes of parts of the Guadiana Menor catchment area in the Guadix-Baza basin and an example of a sampling network in the mountain-basin transition zone. In order to understand flow patterns and recharge processes in a better way it is necessary to expand the study area to gain comprehensive insights. A first step would be to gather more data contributing to a larger scale flow pattern. Essential objectives are discharge and runoff measurements as well as time series measurements of the isotopic compositions of precipitation. In order to detect recharge areas it is important to gain information about local isotope-altitude relations. A rain sampling network could be installed preferably along a well accessible mountain slope with a steep gradient covering as much elevation as possible where individual rain events could be sampled at different altitudes.

7. References

- ALLEN RG, PEREIRA LS, RAES D, SMITH M (1998). Crop evapotranspiration - Guidelines for computing crop water requirements. FAO Irrigation and drainage paper 56.
- ALONSO-ZARZA, AM; BRAGA,JC; MUNOZ, A. (2002). The Geology of Spain, 13 Tertiary The Geological Society London, Cardiff. 649 p
- APPELO CAJ, POSTMA D (1993). Geochemistry, Groundwater and Pollution. Balkema, Rotterdam, Brookfield, 552 pp.
- AZAÑÓN JM, GALINDO-ZALDIVAR J, GARCIA-DUENAS V, JABALOY A (2002). The Geology of Spain. Alpine Tectonics II: Betic Cordillera and the Balearic Islands Gibbons, Wes, Moreno. The Geological Society London, Cardiff. 649 p
- CRAIG H (1961). Isotopic variations in meteoric waters. *Science* 133, 1702-1703.
- CRAIG H & GORDON L (1965). Deuterium and oxygen-18 in the ocean and the marine atmosphere. In: *Stable Isotopes in Oceanographic Studies and Paleotemperatures*, Tongiorgi E (Ed). 130 pp.
- DANSGAARD W (1964). Stable isotopes in precipitation. *Tellus* 16, 436-468.
- DREVER J (1997). *The Geochemistry of Natural Waters*. Prentice Hall, New Jersey 436 pp
- FITTS C (2002). *Groundwater Science*. Academic Press, Imprint of Elsevier, London. 450 pp.
- FLÜGEL E (2004). *Microfacies of Carbonate Rocks*, Har/Cdr. Springer, Berlin, 976 pp
- FREEZE RA & CHERRY JA (1979). *Ground Water*. Prentice Hall, New Jersey. 604 pp
- GAT JR & GONFIANTINI R (1981). Stable isotope hydrology. Deuterium and oxygen-18 in the water cycle. International Atomic Energy Agency. Vienna, Technical Reports Series 210, 347 pp.
- GARRIDO JR (2003). *Composicion Isotopica del vapor de agua atmosferico en el sureste de la Peninsula Iberica*, Departamento de ciencias de la tierra y quimica ambiental, PhD Thesis, 418.
- GIBBONS W & MORENO MT (2002). *The geology of Spain*. Geological Society. London, 649 pp.
- GONFIANTINI R (1986). Environmental isotopes in lake studies. In: *Handbook of environmental isotope geochemistry. The terrestrial environment*, Fritz B & Fontes Ch (Eds.). Vol. 2. Elsevier, Amsterdam, 113-168.
- GUTIÉRREZ-ELORZA M; GARCÍA-RUIZ JM; GOY JL (2002) *The Geology of Spain*, 14 Quaternary The Geological Society London, Cardiff. 649 p
- HOEFS J (1997). *Stable Isotope Geochemistry*. Springer, Berlin, Heidelberg, New York, 201 pp.
- HÖLTING B (1996). *Hydrogeologie*. Enke, Stuttgart, 441 pp.
- IAEA A (2000).: GAT JR, Mook WG, Meijer HA *Environmental Isotopes in the Hydrological Cycle. Principles and Applications Volume II: Atmospheric water*. www.iaea.org.
- IAEA B (2000). *Environmental Isotopes*. In: *The Hydrological Cycle Principles and Applications Volume IV: Groundwater*, GEYH M (Ed.). www.iaea.org.
- ITGE (unpublished). *Mapa Geologico de España – San Clemente 22-37: 929*. 1:50 000. Madrid.
- ITGE (unpublished). *Mapa Geologico de España – Huéscar 22-37: 950*. 1:50 000. Madrid.

- JOUZEL J & MERLIVAT L (1984). Deuterium and oxygen 18 in precipitation: Modeling of the isotopic effects during snow formation. *J. of Geophys. Res.* 89 (D7), 11749-11758.
- JUNTA DE ANDALUCÍA (2005). Modelo digital del terreno de Andalucía. Relieve y Orografía. DVD-ROM.
- KENDALL C & McDONNELL J (1998). *Isotope Tracers in Catchment Hydrology*. Elsevier Science, Amsterdam. 870 pp
- MAPA DIGITAL DE ANDALUCÍA 1:100.000 (1999). Sevilla: Consejería de obras publicas y transportes, Instituto de cartografía de Andalucía, CD-ROM.
- MATTHEB G (2003). *Allgemeine Hydrogeologie – Grundwasserhaushalt*. Lehrbuch der Hydrogeologie Band 1. Gebr. Bornträger, Berlin-Stuttgart, 575 pp.
- MEYER H, SCHÖNICKE L, WAND U, HUBBERTEN H-W, FRIDRICHSEN H (2000). Isotope Studies Of Hydrogen and Oxygen in Ground Ice. Experiences With The Equilibration Technique. *Isotopes Environ. Health Stud.* 36P, 133-149.
- MCCLAY K (1992), *The Mapping of Geological Structures*. Geological Society of London Handbook, London, 160 pp
- SORIA LM, FERNÁNDEZ J, VISERAS C (1999). Late Miocene stratigraphy and palaeogeographic evolution of the intramontane Guadix Basin (Central Betic Cordillera, Spain): Implications for an Atlantic–Mediterranean connection; *Palaeogeography, Palaeoclimatology, Palaeoecology* 151 (4), 255-266.
- VANDENSCHRIK G, VAN WESEMAEL B, FROT E, PULIDO-BOSCH A, MOLINA L, STIÉVENARD M, SOUCHEZ R (2002). Using stable isotope analysis (d D–d 18O) to characterise the regional hydrology of the Sierra de Gador, south east Spain, *J. of Hydrol.* 265, 43–55.
- VALLEJOS A, PULIDO-BOSCH A, MARTIN-ROSALES W, CALVACHE ML (1997). Contribution of environmental isotopes to the understanding of complex hydrologic systems. A case study: Sierra de Gador, SE Spain. *Earth Surf. Proc. Landf.* 22, 1157–1168.

Appendix

Appendix Table 1 Meteorological stations used for climatic statistics with coordinates, time period of recording and mean annual values for temperature and precipitation

station ID	station	X	Y	Z	years	source	Ø temperature	Ø precipitation
1	Baza	520628	4157712	814	2000-2006	www.juntadeandalucia.es	14.92	361.90
2	Puebla de Don Fadrique	554482	4192456	1110	2000-2006	www.juntadeandalucia.es	12.91	320.60
5071E	Huéscar ICONA	539946	4184099	955	2000-2004	www.juntadeandalucia.es	15.40	322.00

Appendix Table 2 Climatic data used for climatic balance and GWR and runoff calculation for meteorological station in Baza

	Ø temperature	Ø max temperature	Ø precipitation	Ø min precipitation	Ø max precipitation	Ø Eto	p max-Eto
	°C	°C	mm	mm	mm	mm	mm
january	5.46	12.00	34.00	1.4	71.4	42.99	28.41
february	6.48	13.48	36.50	3.4	67.8	53.57	14.24
march	10.45	17.42	41.07	23.00	72.40	92.28	-19.88
april	12.87	20.36	35.80	2.60	63.60	124.87	-61.27
may	16.67	24.00	34.67	7.00	84.00	157.93	-73.93
june	22.84	30.43	23.43	2.80	44.40	206.22	-161.82
july	25.35	34.63	1.20	0.00	3.40	224.20	-220.80
august	28.44	39.51	7.60	0.20	23.20	197.16	-173.96
september	20.07	28.81	24.80	1.00	55.00	137.24	-82.24
october	15.17	22.47	44.07	10.40	92.20	86.54	5.66
november	8.84	15.17	36.23	8.80	72.20	48.60	23.60
december	6.44	12.26	42.53	17.20	73.60	36.19	37.41
Ø year	14.92	22.54	361.90	77.80	723.20	1407.77	-684.57
						ETA (Turc)	347.28
						GWR + runoff	14.62

Appendix Table 3 Climatic data used for climatic balance and GWR and runoff calculation for meteorological station in Puebla de Don Fadrique

	$\bar{\varnothing}$ temperature	$\bar{\varnothing}$ max temperature	$\bar{\varnothing}$ precipitation	$\bar{\varnothing}$ min precipitation	$\bar{\varnothing}$ max precipitation	$\bar{\varnothing}$ Eto	p max-Eto
	°C	°C	mm	mm	mm	mm	mm
january	3.73	10.22	20.50	0.4	45.2	47.59	-2.39
february	4.41	11.59	22.03	0.4	45.4	56.91	-11.51
march	8.58	15.37	33.33	14.4	64.2	94.64	-30.44
april	13.93	21.30	35.97	11.8	63.2	122.03	-58.83
may	13.77	21.11	48.20	5.6	108.2	149.19	-40.99
june	21.00	29.61	11.60	0	23.6	203.82	-180.22
july	23.54	31.43	4.23	0	13.8	232.39	-218.59
august	22.51	31.33	13.13	0.8	27	207.17	-180.17
september	18.30	26.22	25.77	10.6	41	137.69	-96.69
october	13.39	20.17	41.60	6.2	95.2	95.30	-0.09
november	6.99	12.91	28.70	10	46.4	51.13	-4.73
december	4.74	10.33	35.53	12	56.2	39.32	16.88
$\bar{\varnothing}$ year	12.91	20.13	320.60	72.20	629.40	1437.18	-807.78
						ETA (Turc)	306.69
						GWR+ runoff	13.91

Appendix Table 4 Mean monthly values of precipitation and temperature for meteorological station in Huescar

	$\bar{\varnothing}$ temperature	$\bar{\varnothing}$ precipitation
	°C	mm
january	5.8	20.02
february	8.6	20.48
march	10.9	30.76
april	13.0	35.60
may	17.1	44.58
june	24.5	15.62
july	26.6	4.22
august	26.0	13.96
september	21.6	14.60
october	15.7	49.58
november	9.2	31.78
december	6.4	40.80
$\bar{\varnothing}$ year	15.44	322.00

Appendix Table 5 Description of the sampled sites with name, ID, location and coordinates

site	site ID	village	town	type	Altitude m	East UTM km	North UTM km
Manantial de la Natividad	SP-GM-001	San Clemente	Huéscar	spring	1083	528577	4194100
Manatíal de Parpacén	SP-GM-002		Huéscar	spring	921	537982	4184411
Fuencaliente	SP-GM-007		Huéscar	spring	916	542145	4184085
Fuente Alta	SP-GM-013	San Clemente	Huéscar	spring	1137	527700	4194175
Embalse de San Clemente	SP-GM-014	San Clemente	Huéscar	reservoir	1037	530937	4190510
Barranco de la Natividad	SP-GM-015	San Clemente	Huéscar	river	1083	528577	4194100
Río Guardal	SP-GM-016		Huéscar	river	867	529035	4184550
Fuentecillas	SP-GM-017	Cortijos Nuevos	Puebla D.Fadrique	spring	1434	537083	4203250
Río Raigadas/Puente de las Ánimas	SP-GM-018		Puebla D.Fadrique	river	1069	532163	4194162
Río Raigadas/Puente Cjo. San José	SP-GM-019		Puebla D.Fadrique	river	1249	534445	4201324
Fuente de Montilla	SP-GM-020		Puebla D.Fadrique	spring	1466	537182	4204656
Fuente Carrillo	SP-GM-021	Cortijos Nuevos	Puebla D.Fadrique	spring	1464	537439	4203155
Cueva del Agua	SP-GM-022		Puebla D.Fadrique	spring	1499	537842	4197651
Fuente Tornajo	SP-GM-023	Duda	Huéscar	spring	930	529119	4187630
Fuente de Oliva	SP-GM-024	Duda	Huéscar	spring	930	529215	4187772
Cortijo de Penalba	SP-GM-025	Duda	Huéscar	spring	937	529035	4187430
Fuente Felin Grande	SP-GM-026	Santa Catalina	Castilléjar	spring	892	527013	4178294
Fuente de Ortiz	SP-GM-031	Fátima	Castril	spring	1141	522583	4186679
Fuente de la Piedra	SP-GM-036	San Clemente	Huéscar	spring	1115	534333	4192501
Cjo. Mazagorda	SP-GM-050	San Clemente	Huéscar	well	1092	535952	4190772
Cjo. Corcoles	SP-GM-051	San Clemente	Huéscar	well	1145	538115	4190064
Zabar	SP-GM-052	San Clemente	Huéscar	well	1096	535491	4191638
Rambla Valentin	SP-GM-053		Huéscar	well	961	534965	4184572
Cantera Ferrer	SP-GM-054		Huéscar	well	962	530730	4182703
Cantera Ferrer	SP-GM-055		Huéscar	well	1050	531053	4183447
Cjo. Los Jaros	SP-GM-056	Fátima	Castril	well	1048	525428	4185356
private well	SP-GM-057	Cortijosillos	Huéscar	well	1092	523304	4184997
Cjo. Mazachica	SP-GM-058	San Clemente	Huéscar	well		535930	4190455
artesian well	SP-GM-059		Huéscar	well	923	533152	4182802
well FAO	SP-GM-060		Huéscar	well	934	536469	4185133
Sondeo Diablo	SP-GM-061	Santa Catalina	Castillejar	well	926	525171	4181082

Appendix Table 6 Summary of chemical analysis and field parameter results of samples used for hydrochemical examination

sample ID	sample date	analysis results [mg/l]								field measurements				
		Ca ⁺²	Mg ⁺²	Na ⁺	K ⁺	Cl ⁻	SO ₄ ⁻²	HCO ₃ ⁻	NO ₃ ⁻	wT °C	EC µS/cm	pH	EH mV	O ₂ mg/l
SP-GM-001-050223	23-Feb-05	65	16	1.4	0.5	9	5	263.1	3.4	12.0	425			
SP-GM-001-050331	31-Mar-05	55	13.5	2.6	0.9	4	14	248.0	1.8	12.0	420	7.4		
SP-GM-001-050420	20-Apr-05	65	15.5	1.4	0.5	1.5	6	265.8	4	10.0	441	7.7		
SP-GM-001-050513	13-May-05	62	16.3	1.5	1.1	1.5	5	266.1	5.5	10.1	441	7.5		7.6
SP-GM-001-050604	4-Jun-05	63	16	1.4	0.5	1	5	268.7	4	10.2	437	7.7		
SP-GM-001-050909	9-Sep-05	63	17	1.5	1	2	4	271.8	3	10.3	435	7.7		12.57
SP-GM-001-051007	7-Oct-05	66	16.9	1.5	0.6	2	4	260.3	3	12.3	531	7.3	137	12.4
SP-GM-002-050223	23-Feb-05	110	36	12	1.1	17	215	261.4	11.7	16.9	862			
SP-GM-002-050420	20-Apr-05	120	38	12.5	1.1	21	224	264.0	10	18.6	867	8.1		
SP-GM-002-050514	14-May-05	117	39	13.1	1.5	22	209	263.2	10.5	17.6	943	8.2		14.54
SP-GM-002-050604	4-Jun-05	117	38	12.4	1.1	21	206	269.2	10	14.2	928	7.3		
SP-GM-002-050908	8-Sep-05	120	42	12.9	1.2	21	237	266.1	14	15.4	933	7.2		3.77
SP-GM-002-051005	5-Oct-05	120	42	10.8	1	20	230	272.7	12	17.8	1040	7.0	200	4.36
SP-GM-007-050224	24-Feb-05	146	59	84	1.8	165	276	246.9	25	19.6	1505			
SP-GM-007-050421	21-Apr-05	148	58	90	2.2	162	310	247.0	22	16.4	1635	7.7		
SP-GM-007-050515	15-May-05	152	58	89	2	162	400	243.0	18.5	16.5	1643	7.3		5.17
SP-GM-007-050604	4-Jun-05	150	58	88.5	2	162	400	247.0	15.5	16.5	1640	7.3	171	
SP-GM-007-050908	8-Sep-05	150	62	92	1.9	172	420	250.6	22	20.0	1520	7.3		7.53
SP-GM-007-051005	5-Oct-05	165	63	92	2.1	160	400	253.8	23	20.6	1788	7.2		
SP-GM-013-050331	31-Mar-05	67	15.2	1.5	0.6	5	5	245.3	5	12.8	342	7.6		
SP-GM-013-050420	20-Apr-05	50	8.6	1.3	0.5	1	7	210.8	3.5	12.8	359	7.8		
SP-GM-013-050513	13-May-05	59	10.4	1.6	0.6	1.5	7.5	239.6	3	12.3	401	8.0		7.19
SP-GM-013-050604	4-Jun-05	60	10.8	1.8	0.7	9	6.5	245.0	4.5	10.5	380	8.3	262	
SP-GM-013-050909	9-Sep-05	64	12.5	2	0.9	2	7	241.8	2.5	13.0	370	8.2		8.81
SP-GM-013-051007	7-Oct-05	65	12.8	1.8	1.2	2	7	233.7	3.5	10.9	482	7.9		11.58
SP-GM-014-050514	14-May-05	49	12.5	2.6	0.9	3	13	183.2	3.5	15.5	348	8.3	187	8.05
SP-GM-014-050629	29-Jun-05	44	12.6	2.5	0.9	1.5	4.5	182.9	3	19.2	336	8.5	146	7.15
SP-GM-014-050731	31-Jul-05	42	13.8	3.6	1.5	4	15.5	171.0	1	20.3	338	8.6		
SP-GM-014-050819	19-Aug-05	41	15	3.1	1.3	3.5	19	175.1	0.5	19.6	334	8.5	140	7.61
SP-GM-014-050909	9-Sep-05	41	15.4	3.1	1.5	3.5	21	167.4	0	21.6	300	8.6		10.02
SP-GM-014-051003	3-Oct-05	43	15.5	3.2	1.7	4	21	180.6	0.5	18.0	369	8.2	180	11.45
SP-GM-015-050420	20-Apr-05	64	14.8	1.5	0.9	1.5	5	265.5	2	12.1	417	7.7		
SP-GM-015-050513	13-May-05	63	15.4	1.4	0.5	6	4	265.8	3	10.3	441	7.5		7.65
SP-GM-015-050729	29-Jul-05	61	15.8	1.4	0.7	1.5	4	265.1	3.5	10.4	434	7.6		
SP-GM-015-050816	16-Aug-05	63	17	3.2	0.7	2	4	265.9	3.5	10.3	432	7.5	196	8.79
SP-GM-015-050909	9-Sep-05	65	17.2	1.5	1	2	3.5	268.8	4	10.5	436	7.5		12.04
SP-GM-015-051007	7-Oct-05	64	16.5	1.5	0.5	2.5	5.5	266.3	3.5	12.5	523	7.6	190	12.9
SP-GM-016-050420	20-Apr-05	228	77	106	2.2	171	585	261.5	4.5	18.9	1978	8.0		
SP-GM-016-050515	15-May-05	236	77	104	2.2	170	620	248.7	3	19.2	1961	8.0	240	6.63
SP-GM-016-050728	28-Jul-05	180	60	77.5	2.2	127	400	253.9	3.5	15.9	1693	8.1		
SP-GM-016-050910	10-Sep-05	180	63	72	2.2	115	510	256.6	0	15.6	1580	8.2		10.25
SP-GM-016-051003	3-Oct-05	215	78	97	2.2	150	680	254.1	6	16.4	2160	7.7		
SP-GM-017-050421	21-Apr-05	83	15.5	3	0.5	3.5	9	321.6	1.5	10.0	508	7.6		
SP-GM-017-050513	13-May-05	84	14.3	3	0.5	22.5	9.5	306.4	3	8.5	530	7.3		5.32
SP-GM-017-051004	4-Oct-05	86	15.5	2.8	0.3	3.5	11	310.0	2	9.3	654	7.1	-38	
SP-GM-019-050604	4-Jun-05	58	7.4	1.95	0.9	3.5	7	194.6	4	15.0	360	8.4	142	
SP-GM-019-050820	20-Aug-05	58	12.2	2.4	1	3	9	213.9	0	16.5	375	8.4	153	8.56
SP-GM-019-050908	8-Sep-05	65	8.5	2	2.4	3.5	7.5	215.1	0.5	13.3	379	8.6		9.05
SP-GM-019-051004	4-Oct-05	60	11	2.4	1	3	10	210.8	0	12.7	440	8.0	189	
SP-GM-020-050604	4-Jun-05	59	1.75	0.85	0.3	1.5	1	181.4	1.5	8.3	316	8.1	159	
SP-GM-020-050908	8-Sep-05	64	3.3	1.2	1.4	2	3	200.0	3.5	8.5	312	9.2		9.5

SP-GM-020-051004	4-Oct-05	65	3.6	1.2	2.4	2	2.5	198.4	3	8.3	396	7.8		
SP-GM-021-050513	13-May-05	71	15.8	2.8	0.7	3.5	9	300.2	2	8.8	498	7.3		6.2
SP-GM-022-050514	14-May-05	42	14.6	2.1	1.7	3	5	188.5	3.5	8.0	331	8.1	270	7.77
SP-GM-023-050515	15-May-05	74	22	5.2	1.1	8.5	23	315.0	8	13.5	582	7.6	226	6.07
SP-GM-023-051003	3-Oct-05	78	26	4.7	0.8	8.5	25	310.0	9.5	16.8	662	7.3	200	
SP-GM-024-050515	15-May-05	77	22	5.85	0.8	10.5	29	312.1	9.5	13.7	596	7.6	270	6.96
SP-GM-025-050515	15-May-05	63	15.5	3.2	0.5	4.5	15	256.5	4	12.7	460	7.5	250	8.15
SP-GM-026-050515	15-May-05	115	44	22	1.5	47	220	296.0	5	15.5	1040	7.7	295	6.26
SP-GM-026-050603	3-Jun-05	115	44	21.8	2.5	45	210	282.7	5	15.5	1030	7.7	222	7.05
SP-GM-026-050910	10-Sep-05	118	50	21.8	1.7	46	240	289.5	9	16.0	1041	7.9		7.4
SP-GM-026-051005	5-Oct-05	120	50	22.4	2.6	45	240	279.5	9	15.7	1156	7.4	191	
SP-GM-028-050603	3-Jun-05	103	54	40	3.2	123	122	337.2	29	14.3	1219	7.4	207	1.86
SP-GM-029-050603	3-Jun-05	102	48	41	2.8	120	115	321.3	29	14.7	1165	7.4	190	1.65
SP-GM-030-050603	3-Jun-05	95	46	49	3.7	115	110	327.8	27	15.0	1164	7.4	203	1.72
SP-GM-031-050708	8-Jul-05	74	30	4.7	0.6	8	42	287.6	40	13.2	634	7.4		6.29
SP-GM-036-050729	29-Jul-05	63	7.8	10.4	0.6	19	26	183.3	13	13.3	433	8.3	180	
SP-GM-050-050915	15-Sep-05	52	25	61	2.9	31.5	37	332.3	33	18.1	724	7.1		4.45
SP-GM-051-050915	15-Sep-05	67	41	17	1.6	34	16	394.0	11	14.5	737	7.5		6.27
SP-GM-052-050915	15-Sep-05	65	40	27	1.1	21	40	375.6	32	17.2	761	7.4		9.52
SP-GM-053-050915	15-Sep-05	113	44	14	1.2	17	139	394.0	29	17.5	929	7.4		10.15
SP-GM-054-050915	15-Sep-05	90	12.5	23.6	0.9	56	46	232.8	33	16.7	710	7.6		10.92
SP-GM-055-050915	15-Sep-05	79	8.8	10	0.7	18	20	245.2	17.5	17.4	538	7.6		10.32
SP-GM-056-050916	16-Sep-05	93	27	14.2	1.8	23	83	289.2	35	15.5	730	7.1		
SP-GM-057-050916	16-Sep-05	185	68	57	4.1	0	81	538.2	340	15.6	1503	6.8		
SP-GM-060-050922	22-Sep-05	116	45	13.4	2.3	22	254	288.9	2	19.1	1014	7.3	130	
SP-GM-061-050923	23-Sep-05	102	61	40	2.7	131	141	351.1	31	16.4	1389	7.0	179	

Appendix Table 7 Electrical balance and saturation indices of samples used for hydrochemical examination

sample ID	cations	anions	balance	electr. balance	SI calcite	SI dolomite	SI aragonite	SI Gypsum
	meq/l			%				
SP-GM-001-050223	4.66	4.66	0.00	0.02	-0.33	-1.10	-0.48	-2.88
SP-GM-001-050331	4.01	4.43	-0.05	5.02	0.02	-0.41	-0.13	-2.48
SP-GM-001-050420	4.62	4.52	0.01	1.04	0.29	0.09	0.14	-2.79
SP-GM-001-050513	4.55	4.53	0.00	0.26	0.12	-0.22	-0.04	-2.89
SP-GM-001-050604	4.56	4.53	0.00	0.28	0.35	0.22	0.19	-2.88
SP-GM-001-050909	4.66	4.57	0.01	0.93	0.34	0.24	0.19	-2.98
SP-GM-001-051007	4.79	4.39	0.04	4.38	-0.02	-0.47	-0.17	-2.97
SP-GM-002-050223	9.05	9.37	-0.02	1.74	-0.14	-0.53	-0.29	-1.20
SP-GM-002-050420	9.74	9.69	0.00	0.27	0.98	1.73	0.83	-1.17
SP-GM-002-050514	9.71	9.40	0.02	1.63	1.11	1.99	0.96	-1.20
SP-GM-002-050604	9.58	9.40	0.01	0.99	0.18	0.07	0.03	-1.19
SP-GM-002-050908	10.09	10.05	0.00	0.18	0.09	-0.06	-0.06	-1.14
SP-GM-002-051005	10.00	9.95	0.00	0.20	-0.05	-0.31	-0.20	-1.16
SP-GM-007-050224	15.91	14.85	0.03	3.46	-0.05	-0.22	-0.20	-1.07
SP-GM-007-050421	16.20	15.43	0.02	2.46	0.61	1.05	0.46	-1.02
SP-GM-007-050515	16.35	17.18	-0.02	2.46	0.20	0.22	0.05	-0.91
SP-GM-007-050604	16.23	17.20	-0.03	2.88	0.20	0.23	0.05	-0.92
SP-GM-007-050908	16.72	18.06	-0.04	3.87	0.20	0.30	0.06	-0.92
SP-GM-007-051005	17.55	17.37	0.01	0.53	0.18	0.23	0.03	-0.90
SP-GM-013-050331	4.70	4.28	0.05	4.59	0.29	0.10	0.13	-2.87
SP-GM-013-050420	3.29	3.63	-0.05	4.99	0.33	0.08	0.18	-2.80
SP-GM-013-050513	3.90	4.11	-0.03	2.63	0.61	0.62	0.45	-2.72

SP-GM-013-050604	4.00	4.42	-0.05	5.00	0.82	1.04	0.67	-2.78
SP-GM-013-050909	4.35	4.14	0.02	2.45	0.79	1.06	0.64	-2.73
SP-GM-013-051007	4.43	4.03	0.05	4.70	0.46	0.34	0.30	-2.72
SP-GM-014-050514	3.63	3.37	0.04	3.72	0.73	1.08	0.58	-2.56
SP-GM-014-050629	3.38	3.13	0.04	3.79	0.94	1.62	0.79	-3.06
SP-GM-014-050731	3.44	3.21	0.04	3.51	0.98	1.76	0.83	-2.55
SP-GM-014-050819	3.47	3.33	0.02	2.05	0.86	1.56	0.71	-2.48
SP-GM-014-050909	3.51	3.24	0.04	4.00	1.00	1.88	0.85	-2.44
SP-GM-014-051003	3.62	3.47	0.02	2.14	0.60	1.02	0.45	-2.41
SP-GM-015-050420	4.52	4.46	0.01	0.66	0.37	0.26	0.22	-2.88
SP-GM-015-050513	4.51	4.59	-0.01	0.92	0.14	-0.21	-0.02	-2.98
SP-GM-015-050729	4.45	4.46	0.00	0.15	0.19	-0.09	0.03	-2.99
SP-GM-015-050816	4.72	4.49	0.03	2.59	0.16	-0.13	0.00	-2.98
SP-GM-015-050909	4.77	4.53	0.03	2.62	0.19	-0.08	0.03	-3.03
SP-GM-015-051007	4.65	4.54	0.01	1.25	0.24	0.05	0.08	-2.85
SP-GM-016-050420	22.48	21.36	0.03	2.55	1.09	1.99	0.95	-0.67
SP-GM-016-050515	22.79	21.83	0.02	2.15	1.07	1.92	0.92	-0.64
SP-GM-016-050728	17.43	16.11	0.04	3.91	1.05	1.84	0.90	-0.85
SP-GM-016-050910	17.44	18.05	-0.02	1.73	1.15	2.06	1.00	-0.77
SP-GM-016-051003	21.52	22.65	-0.03	2.54	0.66	1.12	0.51	-0.63
SP-GM-017-050421	5.58	5.50	0.01	0.78	0.41	0.22	0.26	-2.55
SP-GM-017-050513	5.53	5.83	-0.03	2.60	0.08	-0.52	-0.08	-2.51
SP-GM-017-051004	5.72	5.36	0.03	3.25	-0.10	-0.85	-0.26	-2.44
SP-GM-019-050604	3.62	3.45	0.02	2.47	0.91	1.14	0.76	-2.75
SP-GM-019-050820	4.05	3.72	0.04	4.16	0.96	1.47	0.81	-2.66
SP-GM-019-050908	4.11	3.73	0.05	4.75	1.14	1.59	0.99	-2.69
SP-GM-019-051004	4.05	3.69	0.05	4.56	0.58	0.59	0.42	-2.59
SP-GM-020-050604	3.14	3.01	0.02	2.06	0.55	-0.34	0.39	-3.54
SP-GM-020-050908	3.56	3.40	0.02	2.32	1.54	1.91	1.39	-3.09
SP-GM-020-051004	3.66	3.36	0.04	4.36	0.30	-0.56	0.15	-3.12
SP-GM-021-050513	5.01	5.16	-0.02	1.52	-0.01	-0.58	-0.17	-2.59
SP-GM-022-050514	3.45	3.29	0.02	2.44	0.35	0.32	0.19	-3.00
SP-GM-023-050515	5.79	5.93	-0.01	1.23	0.37	0.39	0.22	-2.21
SP-GM-023-051003	6.29	5.92	0.03	3.07	0.13	0.02	-0.02	-2.17
SP-GM-024-050515	5.96	6.09	-0.01	1.10	0.43	0.50	0.28	-2.10
SP-GM-025-050515	4.59	4.64	-0.01	0.53	0.15	-0.13	0.00	-2.42
SP-GM-026-050515	10.41	10.78	-0.02	1.74	0.60	1.01	0.45	-1.19
SP-GM-026-050603	10.43	10.30	0.01	0.61	0.53	0.86	0.38	-1.21
SP-GM-026-050910	11.06	11.13	0.00	0.32	0.77	1.39	0.62	-1.16
SP-GM-026-051005	11.21	10.94	0.01	1.21	0.26	0.36	0.11	-1.15
SP-GM-028-050603	11.47	11.96	-0.02	2.09	0.27	0.46	0.12	-1.49
SP-GM-029-050603	10.95	11.47	-0.02	2.32	0.24	0.35	0.09	-1.51
SP-GM-030-050603	10.81	11.30	-0.02	2.22	0.27	0.44	0.12	-1.55
SP-GM-031-050708	6.42	6.39	0.00	0.25	0.09	-0.04	-0.06	-1.98
SP-GM-036-050729	4.27	4.25	0.00	0.19	0.77	0.81	0.61	-2.17
SP-GM-050-050915	7.41	7.56	-0.01	1.02	-0.22	-0.50	-0.37	-2.19
SP-GM-051-050915	7.55	7.84	-0.02	1.89	0.30	0.59	0.15	-2.46
SP-GM-052-050915	7.79	8.01	-0.01	1.40	0.20	0.43	0.05	-2.09
SP-GM-053-050915	9.96	10.20	-0.01	1.23	0.46	0.75	0.31	-1.39
SP-GM-054-050915	6.59	6.85	-0.02	1.90	0.42	0.23	0.27	-1.85
SP-GM-055-050915	5.14	5.17	0.00	0.32	0.40	0.09	0.25	-2.23
SP-GM-056-050916	7.56	7.61	0.00	0.34	-0.05	-0.41	-0.20	-1.62
SP-GM-057-050916	17.50	15.85	0.05	4.94	0.05	-0.10	-0.10	-1.55
SP-GM-060-050922	10.19	10.61	-0.02	2.03	0.25	0.36	0.10	-1.14
SP-GM-061-050923	11.99	12.84	-0.03	3.43	-0.04	-0.08	-0.19	-1.45

Appendix Table 8 Main field parameters, saturation indices and Ca/ Mg ratio of Group 1 members

sample ID	sample date	T °C	pH	EC µS/cm	SI calcite	SI dolomite	SI aragonite	SI Gypsum	ratio Ca/Mg
SP-GM-001-050223	23-Feb-05	12.0		425	-0.33	-1.10	-0.48	-2.88	2.44
SP-GM-001-050331	31-Mar-05	12.0	7.4	420	0.02	-0.41	-0.13	-2.48	2.44
SP-GM-001-050420	20-Apr-05	10.0	7.7	441	0.29	0.09	0.14	-2.79	2.52
SP-GM-001-050513	13-May-05	10.1	7.5	441	0.12	-0.22	-0.04	-2.89	2.28
SP-GM-001-050604	4-Jun-05	10.2	7.7	437	0.35	0.22	0.19	-2.88	2.36
SP-GM-001-050909	9-Sep-05	10.3	7.7	435	0.34	0.24	0.19	-2.98	2.22
SP-GM-001-051007	7-Oct-05	12.3	7.3	531	-0.02	-0.47	-0.17	-2.97	2.34
SP-GM-013-050331	31-Mar-05	12.8	7.6	342	0.29	0.10	0.13	-2.87	2.64
SP-GM-013-050420	20-Apr-05	12.8	7.8	359	0.33	0.08	0.18	-2.80	3.49
SP-GM-013-050513	13-May-05	12.3	8.0	401	0.61	0.62	0.45	-2.72	3.40
SP-GM-013-050604	4-Jun-05	10.5	8.3	380	0.82	1.04	0.67	-2.78	3.33
SP-GM-013-050909	9-Sep-05	13.0	8.2	370	0.79	1.06	0.64	-2.73	3.07
SP-GM-013-051007	7-Oct-05	10.9	7.9	482	0.46	0.34	0.30	-2.72	3.05
SP-GM-014-050514	14-May-05	15.5	8.3	348	0.73	1.08	0.58	-2.56	2.35
SP-GM-014-050629	29-Jun-05	19.2	8.5	336	0.94	1.62	0.79	-3.06	2.10
SP-GM-014-050731	31-Jul-05	20.3	8.6	338	0.98	1.76	0.83	-2.55	1.83
SP-GM-014-050819	19-Aug-05	19.6	8.5	334	0.86	1.56	0.71	-2.48	1.64
SP-GM-014-050909	9-Sep-05	21.6	8.6	300	1.00	1.88	0.85	-2.44	1.60
SP-GM-014-051003	3-Oct-05	18.0	8.2	369	0.60	1.02	0.45	-2.41	1.66
SP-GM-015-050420	20-Apr-05	12.1	7.7	417	0.37	0.26	0.22	-2.88	2.59
SP-GM-015-050513	13-May-05	10.3	7.5	441	0.14	-0.21	-0.02	-2.98	2.45
SP-GM-015-050729	29-Jul-05	10.4	7.6	434	0.19	-0.09	0.03	-2.99	2.32
SP-GM-015-050816	16-Aug-05	10.3	7.5	432	0.16	-0.13	0.00	-2.98	2.22
SP-GM-015-050909	9-Sep-05	10.5	7.5	436	0.19	-0.08	0.03	-3.03	2.27
SP-GM-015-051007	7-Oct-05	12.5	7.6	523	0.24	0.05	0.08	-2.85	2.33
SP-GM-017-050421	21-Apr-05	10.0	7.6	508	0.41	0.22	0.26	-2.55	3.21
SP-GM-017-050513	13-May-05	8.5	7.3	530	0.08	-0.52	-0.08	-2.51	3.52
SP-GM-017-051004	4-Oct-05	9.3	7.1	654	-0.10	-0.85	-0.26	-2.44	3.33
SP-GM-019-050604	4-Jun-05	15.0	8.4	360	0.91	1.14	0.76	-2.75	4.70
SP-GM-019-050820	20-Aug-05	16.5	8.4	375	0.96	1.47	0.81	-2.66	2.85
SP-GM-019-050908	8-Sep-05	13.3	8.6	379	1.14	1.59	0.99	-2.69	4.59
SP-GM-019-051004	4-Oct-05	12.7	8.0	440	0.58	0.59	0.42	-2.59	3.27
SP-GM-020-050604	4-Jun-05	8.3	8.1	316	0.55	-0.34	0.39	-3.54	20.23
SP-GM-020-050908	8-Sep-05	8.5	9.2	312	1.54	1.91	1.39	-3.09	11.64
SP-GM-020-051004	4-Oct-05	8.3	7.8	396	0.30	-0.56	0.15	-3.12	10.83
SP-GM-021-050513	13-May-05	8.8	7.3	498	-0.01	-0.58	-0.17	-2.59	2.70
SP-GM-022-050514	14-May-05	8.0	8.1	331	0.35	0.32	0.19	-3.00	1.73
SP-GM-023-050515	15-May-05	13.5	7.6	582	0.37	0.39	0.22	-2.21	2.02
SP-GM-023-051003	3-Oct-05	16.8	7.3	662	0.13	0.02	-0.02	-2.17	1.80
SP-GM-024-050515	15-May-05	13.7	7.6	596	0.43	0.50	0.28	-2.10	2.10
SP-GM-025-050515	15-May-05	12.7	7.5	460	0.15	-0.13	0.00	-2.42	2.44
SP-GM-031-050708	8-Jul-05	13.2	7.4	634	0.09	-0.04	-0.06	-1.98	1.48
SP-GM-036-050729	29-Jul-05	13.3	8.3	433	0.77	0.81	0.61	-2.17	4.85
SP-GM-051-050915	15-Sep-05	14.5	7.5	737	0.30	0.59	0.15	-2.46	0.98
SP-GM-052-050915	15-Sep-05	17.2	7.4	761	0.20	0.43	0.05	-2.09	0.98
SP-GM-055-050915	15-Sep-05	17.4	7.6	538	0.40	0.09	0.25	-2.23	5.39
MIN		8.0	7.1	300	-0.33	-1.10	-0.48	-3.54	0.98
MAX		21.6	9.2	761	1.54	1.91	1.39	-1.98	20.23
AVERAGE		12.8	7.8	449	0.43	0.38	0.28	-2.68	3.38

Appendix Table 9 Main field parameters, saturation indices and Ca/ Mg ratio of Group 2 members

sample ID	sample date	T °C	pH	EC µS/cm	SI calcite	SI dolomite	SI aragonite	SI Gypsum	ratio Ca/Mg
SP-GM-002-050223	23-Feb-05	16.9		862	-0.14	-0.53	-0.29	-1.20	1.83
SP-GM-002-050420	20-Apr-05	18.6	8.1	867	0.98	1.73	0.83	-1.17	1.89
SP-GM-002-050514	14-May-05	17.6	8.2	943	1.11	1.99	0.96	-1.20	1.80
SP-GM-002-050604	4-Jun-05	14.2	7.3	928	0.18	0.07	0.03	-1.19	1.85
SP-GM-002-050908	8-Sep-05	15.4	7.2	933	0.09	-0.06	-0.06	-1.14	1.71
SP-GM-002-051005	5-Oct-05	17.8	7.0	1040	-0.05	-0.31	-0.20	-1.16	1.71
SP-GM-026-050515	15-May-05	15.5	7.7	1040	0.60	1.01	0.45	-1.19	1.57
SP-GM-026-050603	3-Jun-05	15.5	7.7	1030	0.53	0.86	0.38	-1.21	1.57
SP-GM-026-050910	10-Sep-05	16.0	7.9	1041	0.77	1.39	0.62	-1.16	1.42
SP-GM-026-051005	5-Oct-05	15.7	7.4	1156	0.26	0.36	0.11	-1.15	1.44
SP-GM-028-050603	3-Jun-05	14.3	7.4	1219	0.27	0.46	0.12	-1.49	1.14
SP-GM-029-050603	3-Jun-05	14.7	7.4	1165	0.24	0.35	0.09	-1.51	1.28
SP-GM-030-050603	3-Jun-05	15.0	7.4	1164	0.27	0.44	0.12	-1.55	1.24
SP-GM-060-050922	22-Sep-05	19.1	7.3	1014	0.25	0.36	0.10	-1.14	1.55
SP-GM-061-050923	23-Sep-05	16.4	7.0	1389	-0.04	-0.08	-0.19	-1.45	1.00
MIN		14.2	7.0	862	-0.14	-0.53	-0.29	-1.55	1.00
MAX		19.1	8.2	1389	1.11	1.99	0.96	-1.14	1.89
AVERAGE		16.2	7.5	1053	0.35	0.54	0.20	-1.26	1.53

Appendix Table 10 Main field parameters, saturation indices and Ca/ Mg ratio of "Mixing" Group members

sample ID	sample date	T °C	pH	EC µS/cm	SI calcite	SI dolomite	SI aragonite	SI Gypsum	ratio Ca/Mg
SP-GM-053-050915	15-Sep-05	17.5	7.4	929	0.46	0.75	0.31	-1.39	1.54
SP-GM-054-050915	15-Sep-05	16.7	7.6	710	0.42	0.23	0.27	-1.85	4.32
SP-GM-056-050916	16-Sep-05	15.5	7.1	730	-0.05	-0.41	-0.20	-1.62	2.07
MIN		15.5	7.1	710	-0.05	-0.41	-0.20	-1.85	1.54
MAX		17.5	7.6	929	0.46	0.75	0.31	-1.39	4.32
AVERAGE		16.6	7.4	790	0.28	0.19	0.13	-1.62	2.64

Appendix Table 11 Main field parameters, saturation indices and Ca/ Mg ratio of Group 3 members

sample ID	sample date	T °C	pH	EC µS/cm	SI calcite	SI dolomite	SI aragonite	SI Gypsum	ratio Ca/Mg
SP-GM-053-050915	15-Sep-05	17.5	7.4	929	0.46	0.75	0.31	-1.39	1.54
SP-GM-054-050915	15-Sep-05	16.7	7.6	710	0.42	0.23	0.27	-1.85	4.32
SP-GM-056-050916	16-Sep-05	15.5	7.1	730	-0.05	-0.41	-0.20	-1.62	2.07
SP-GM-007-050224	24-Feb-05	19.6		1505	-0.05	-0.22	-0.20	-1.07	1.48
SP-GM-007-050421	21-Apr-05	16.4	7.7	1635	0.61	1.05	0.46	-1.02	1.53
SP-GM-007-050515	15-May-05	16.5	7.3	1643	0.20	0.22	0.05	-0.91	1.57
SP-GM-007-050604	4-Jun-05	16.5	7.3	1640	0.20	0.23	0.05	-0.92	1.55
SP-GM-007-050908	8-Sep-05	20.0	7.3	1520	0.20	0.30	0.06	-0.92	1.45
SP-GM-007-051005	5-Oct-05	20.6	7.2	1788	0.18	0.23	0.03	-0.90	1.57
SP-GM-016-050420	20-Apr-05	18.9	8.0	1978	1.09	1.99	0.95	-0.67	1.78
SP-GM-016-050515	15-May-05	19.2	8.0	1961	1.07	1.92	0.92	-0.64	1.84
SP-GM-016-050728	28-Jul-05	15.9	8.1	1693	1.05	1.84	0.90	-0.85	1.80
SP-GM-016-050910	10-Sep-05	15.6	8.2	1580	1.15	2.06	1.00	-0.77	1.71
SP-GM-016-051003	3-Oct-05	16.4	7.7	2160	0.66	1.12	0.51	-0.63	1.65
MIN		15.5	7.1	710	-0.05	-0.41	-0.20	-1.85	1.45
MAX		20.6	8.2	2160	1.15	2.06	1.00	-0.63	4.32
AVERAGE		17.5	7.6	1534	0.51	0.81	0.36	-1.01	1.85

Appendix Table 12 Name and location of springs sampled for isotope examination and results of analysis

Site	site ID	East UTM	North UTM	Altitude (m)	sample ID	date	d ¹⁸ O (‰)	d ¹⁸ O (‰) error	dD (‰)	dD (‰) error	d-excess
Manantial de la Natividad	SP-GM-001	528577	4194100	1083	SP-GM-001-050420	20-Apr-05	-8.77	0.01	-58.5	0.2	11.66
					SP-GM-001-050513	13-Mai-05	-8.91	0.01	-59.2	0.2	12.08
					SP-GM-001-050604	04-Jun-05	-8.92	0.02	-59.4	0.2	11.96
					SP-GM-001-050630	30-Jun-05	-9	0.02	-59.2	0.4	12.8
					SP-GM-001-050729	29-Jul-05	-8.98	0.03	-59.1	0.2	12.74
					SP-GM-001-050816	16-Aug-05	-8.91	0.01	-60.1	0.4	11.18
					SP-GM-001-050909	09-Sep-05	-8.92	0.03	-59.2	0.5	12.16
					SP-GM-001-051007	07-Okt-05	-8.82	0.01	-59.3	0.5	11.26
Manatial de Parpacén	SP-GM-002	537982	4184411	921	SP-GM-002-050420	20-Apr-05	-8.19	0.03	-57.9	0.3	7.62
					SP-GM-002-050514	14-Mai-05	-8.29	0.01	-58.2	0.2	8.12
					SP-GM-002-050604	04-Jun-05	-8.7	0.02	-59.6	0.4	10
					SP-GM-002-050701	01-Jul-05	-8.65	0.02	-58.9	0.2	10.3
					SP-GM-002-050728	28-Jul-05	-8.67	0.01	-59.8	0.3	9.56
					SP-GM-002-050821	21-Aug-05	-8.57	0.03	-60	0.4	8.56
					SP-GM-002-050908	08-Sep-05	-8.53	0.01	-59.7	0.4	8.54
					SP-GM-002-051005	05-Okt-05	-8.54	0.01	-59.6	0.4	8.72
Fuentcaliente	SP-GM-007	542145	4184085	916	SP-GM-007-050604	04-Jun-05	-8.21	0.03	-57	0.3	8.68
					SP-GM-007-050701	01-Jul-05	-8.14	0.01	-56.2	0.2	8.92
					SP-GM-007-050707	07-Jul-05	-8.18	0.02	-56.4	0.3	9.04
					SP-GM-007-050728	28-Jul-05	-8.24	0.03	-56.5	0.2	9.42
					SP-GM-007-050821	21-Aug-05	-8.12	0.02	-57.5	0.4	7.46
					SP-GM-007-050908	08-Sep-05	-8.16	0.02	-57.8	0.5	7.48
					SP-GM-007-051005	05-Okt-05	-8.13	0.01	-57.6	0.2	7.44
Fuente Alta	SP-GM-013	527700	4194175	1137	SP-GM-013-050604	04-Jun-05	-8.87	0.01	-58.2	0.2	12.76
					SP-GM-013-050816	16-Aug-05	-8.8	0.01	-59.7	0.3	10.7
					SP-GM-013-050420	20-Apr-05	-8.92	0.02	-59.5	0.2	11.86
					SP-GM-013-050909	09-Sep-05	-8.77	0.02	-58.8	0.3	11.36
					SP-GM-013-051007	07-Okt-05	-8.67	0.02	-59.1	0.5	10.26
					SP-GM-013-050513	13-Mai-05	-8.92	0.02	-58.8	0.3	12.56
					SP-GM-013-050729	29-Jul-05	-8.8	0.01	-58.1	0.2	12.3
					SP-GM-013-050630	30-Jun-05	-8.83	0	-58.6	0.1	12.04
Fuentecillas	SP-GM-017	537083	4203250	1434	SP-GM-017-050630	30-Jun-05	-8.51	0.02	-57	0.3	11.08
					SP-GM-017-050727	27-Jul-05	-8.47	0.03	-56.8	0.2	10.96
					SP-GM-017-050818	18-Aug-05	-8.38	0.02	-57.2	0.4	9.84
					SP-GM-017-050908	08-Sep-05	-8.39	0.01	-56.1	0.4	11.02
Fuente de Montilla	SP-GM-020	537816	4204628	1466	SP-GM-020-050513	13-May-05	-8.97	0.01	-59	0.3	12.76
					SP-GM-020-050604	4-Jun-05	-9.05	0.02	-59.9	0.3	12.5
					SP-GM-020-050630	30-Jun-05	-9.03	0.02	-59.5	0.2	12.74
					SP-GM-020-050727	27-Jul-05	-9.05	0.01	-59.5	0.4	12.9
					SP-GM-020-050818	18-Aug-05	-8.99	0.02	-60.1	0.5	11.82
					SP-GM-020-050908	8-Sep-05	-9.01	0.01	-59.5	0.2	12.58
					SP-GM-020-051004	4-Oct-05	-9	0.01	-60.4	0.2	11.6
Fuente Carrillo	SP-GM-021	537439	4203155	1464	SP-GM-021-050513	13-Mai-05	-8.6	0.01	-57.3	0.3	11.5
Cueva del Agua	SP-GM-022	537842	4197651	1499	SP-GM-022-050514	14-Mai-05	-9.35	0.01	-61.6	0.2	13.2
Fuente Tornajo	SP-GM-023	529110	4187630	930	SP-GM-023-050515	15-Mai-05	-8.59	0.02	-59.7	0.2	9.02
					SP-GM-023-051003	03-Okt-05	-8.58	0.02	-59.6	0.2	9.04
Fuente Oliva	SP-GM-024	529215	4187772	930	SP-GM-024-050515	15-Mai-05	-8.63	0.01	-60	0.3	9.04
Cortijo Penalba	SP-GM-025	529035	4187430	937	SP-GM-025-050515	15-Mai-05	-8.79	0.02	-59.8	0.2	10.52
Fuente Ortiz	SP-GM-031	522583	4186679	1141	SP-GM-031-050708	08-Jul-05	-7.22	0.03	-52.2	0.1	5.56
FuentePiedra	SP-GM-036	534333	4192501	1115	SP-GM-036-050729	29-Jul-05	-8.2	0.02	-57.7	0.3	7.9

Appendix Table 13 Name and location of surface water sampled for isotope examination and results of analysis

Site	site ID	East UTM	North UTM	Altitude (m)	sample ID	date	d ¹⁸ O (‰)	d ¹⁸ O (‰) error	dD (‰)	dD (‰) error	d-excess
Embalse de San Clemente	SP-GM-014	530937	4190510	1037	SP-GM-014-051003	03-Okt-05	-5.96	0.03	-46.20	0.4	1.48
					SP-GM-014-050909	09-Sep-05	-5.96	0.02	-46.10	0.3	1.58
					SP-GM-014-050731	31-Jul-05	-6.28	0.01	-45.60	0.2	4.64
					SP-GM-014-050629	29-Jun-05	-6.57	0.02	-47.40	0.3	5.16
					SP-GM-014-050420	20-Apr-05	-7.38	0.02	-51.10	0.3	7.94
					SP-GM-014-050514	14-Mai-05	-7.11	0.00	-50.20	0.2	6.68
					SP-GM-014-050819	19-Aug-05	-6.07	0.01	-46.40	0.3	2.16
Barranco de la Natividad	SP-GM-015	528577	4194100	1083	SP-GM-015-050909	09-Sep-05	-8.95	0.01	-59.90	0.3	11.7
					SP-GM-015-050420	20-Apr-05	-8.94	0.01	-59.70	0.3	11.82
					SP-GM-015-050630	30-Jun-05	-8.94	0.02	-59.30	0.3	12.22
					SP-GM-015-051007	07-Okt-05	-8.87	0.01	-59.70	0.3	11.26
					SP-GM-015-050729	29-Jul-05	-8.99	0.02	-59.00	0.2	12.92
					SP-GM-015-050816	16-Aug-05	-8.91	0.02	-60.00	0.5	11.28
					SP-GM-015-050513	13-Mai-05	-8.95	0.01	-58.70	0.3	12.9
Río Guardal	SP-GM-016	529035	4184550	867	SP-GM-016-051003	03-Okt-05	-8.10	0.02	-56.30	0.4	8.5
					SP-GM-016-050910	10-Sep-05	-7.90	0.02	-55.70	0.4	7.5
					SP-GM-016-050420	20-Apr-05	-7.75	0.01	-55.20	0.3	6.8
					SP-GM-016-050515	15-Mai-05	-8.29	0.02	-57.60	0.3	8.72
					SP-GM-016-050728	28-Jul-05	-8.14	0.02	-56.50	0.2	8.62
Río Raigadas/Puente de las Ánimas	SP-GM-018	532163	4194162	1069	SP-GM-018-050630	30-Jun-05	-7.26	0.01	-52.00	0.2	6.08
					SP-GM-018-050513	13-Mai-05	-7.40	0.01	-52.50	0.3	6.7
Río Raigadas/Puente Cjo. San José	SP-GM-019	534445	4201324	1249	SP-GM-019-050727	27-Jul-05	-8.61	0.01	-57.00	0.3	11.88
					SP-GM-019-051004	04-Okt-05	-8.36	0.01	-56.40	0.2	10.48
					SP-GM-019-050513	13-Mai-05	-8.69	0.02	-57.80	0.2	11.72
					SP-GM-019-050820	20-Aug-05	-8.37	0.01	-56.20	0.1	10.76
					SP-GM-019-050604	04-Jun-05	-8.70	0.02	-58.10	0.3	11.5
					SP-GM-019-050630	30-Jun-05	-8.58	0.01	-57.40	0.2	11.24
					SP-GM-019-050908	08-Sep-05	-8.70	0.01	-58.90	0.1	10.7

Appendix Table 14 Name and location of wells sampled for isotope examination and results of analysis

Site	site ID	East UTM	North UTM	Altitude (m)	sample ID	date	d ¹⁸ O (‰)	d ¹⁸ O (‰) error	dD (‰)	dD (‰) error	d-excess
Cjo. Mazagorda	SP-GM-050	535952	4190772	1092	SP-GM-050-050915	15-Sep-05	-7.76	0.02	-56.9	0.3	5.18
Cjo. Corcoles	SP-GM-051	538115	4190064	1145	SP-GM-051-050915	15-Sep-05	-8.02	0.01	-57.92	0.3	6.24
Zabar Rambla	SP-GM-052	535491	4191638	1096	SP-GM-052-050915	15-Sep-05	-7.69	0.02	-56.27	0.4	5.25
Valentin	SP-GM-053	534965	4184572	961	SP-GM-053-050915	15-Sep-05	-8.38	0.02	-57.77	0.5	9.27
Cantera Ferrer	SP-GM-054	53073	4182703	962	SP-GM-054-050915	15-Sep-05	-7.55	0.01	-53.46	0.3	6.94
Cantera Ferrer	SP-GM-055	531053	4183447	1050	SP-GM-055-050915	15-Sep-05	-8.1	0.02	-55.71	0.2	9.09
Cjo. Los Jaros	SP-GM-056	525428	4185356	1048	SP-GM-056-050916	16-Sep-05	-7.41	0.02	-52.9	0.1	6.38
private well	SP-GM-057	523304	4184997	1092	SP-GM-057-050916	16-Sep-05	-7.02	0.01	-54.28	0.3	1.88
Artesian	SP-GM-059	533152	4182802	923	SP-GM-059-050922	22-Sep-05	-8.54	0.02	-58.48	0.6	9.84
well FAO	SP-GM-060	536469	4185133	934	SP-GM-060-050922	22-Sep-05	-8.58	0.02	-57.99	0.2	10.65
Sondeo Diablo	SP-GM-061	525171	4181082	926	SP-GM-061-050923	23-Sep-05	-6.84	0.02	-55.05	0.2	-0.33

Appendix Table 15 Methods and devices of sampled parameters

Parameter (effective range)	Method	device/quick determination test
Temperature 0 to 100 °C	electrometric Log	Multiline P4 (WTW Inc.); temperature probe integrated in pH probe SenTIX 41
pH-value (pH 1 to pH 13)	potentiometric Log with automatic temperature compensation	Multiline P4 + pH probe SenTIX 41 (WTW Inc.)
Spec. conductivity (10 to 10 ⁶ µS/cm)	electrometric Log with automatic temperature compensation (25 °C)	Multiline P4 + cond probe TetraCon 325 (WTW Inc.)
Oxygen saturation (1 – 100%)	polarographic Log	Multiline P4 + oxygen probe CellOx 325 + calibrate vessel OxiCal-SI (WTW Inc.)
Redox potential (-200 to 1000 mV)	potentiometric Log (Ag/AgCl-reference electrode)	Multiline P4 (WTW Inc.) + Eh probe Pt 4805 (Ingold Inc.)
Carbon species	in situ log, titration with 0,1 N HCl to pH 4,3 respectively with 0,1 N NaOH to pH 8,2 / colorimetric	Bulb pipette (100 ml) field burette, pH meter, beaker <i>OR VISOCOLOR® HE</i> test kit
NO ₂ ⁻ (0,005 to 0,1 mg/l)	in situ log: colorimetric	Quick test: Aquaquant 1.4408 (Merck Inc.)
NH ₄ ⁺ (0,05 to 0,8 mg/l)	in situ log: colorimetric	Quick test: Aquaquant 1.4400.001 (Merck Inc.)

Appendix Table 16 Analytical Methods Hydrogeochemistry

Ions	Method	device	Detection limit
Na ⁺	Flame photometer	Eppendorf Elex 6361r	1,0 [mg/l]
K ⁺	Flame photometer	Eppendorf Elex 6361r	0,1 [mg/l]
Al ³⁺	ICP	Leemans	0,5 [mg/l]
Mg ²⁺	AAS	Perkin Elmer 5000	0,05 [mg/l]
Ca ²⁺	AAS	Perkin Elmer 5000	0,05 [mg/l]
Li ⁺	AAS	Perkin Elmer 5000	0,05 [mg/l]
Sr ²⁺	ICP	Leemans	0,05 [mg/l]
Mn ²⁺	AAS	Perkin Elmer 5000	0,05 [mg/l]
Fe ²⁺	AAS	Perkin Elmer 5000	0,1 [mg/l]
Br ⁻	DEV (1986)	Titration	0,01 [mg/l]
Cl ⁻	photometric	Technicon Autoanalyser	1,0 [mg/l]
SO ₄ ²⁻	photometric	Technicon Autoanalyser	0,05 [mg/l]
NO ₃ ⁻	photometric	Technicon Autoanalyser	0,05 [mg/l]

Project:	Guadiana Menor, Spain	Page /
Institution / Editor:	FU Berlin, University of Granada, IGME/ Krauttter	

Sampling site:	Fuente de la Natividad	Site ID.:	SP-GM-001
Site label:	929.7.2	Map:	
Locality description: spring in a private gallery at trout farm below Ctjo. Natividad homestead			

X:	528577	Type:	spring
Y:	4194100	distance [m from source]:	4.0
Z:	1083	discharge [l/s]:	25

--

Remarks:	gallery is locked, keys obtained from the owner or sampled outside of cave where water comes out
-----------------	--

Sketch map	Site picture

Date of sampling	Temperature [°C]	pH	Conductivity [mS/cm]	Remarks
31.03.2005	12	7.44	420	
20.04.2005	10	7.65	441	
13.05.2005	10.1	7.49	441	
04.06.2005	10.2	7.71	437	
30.06.2005	10.2	7.68	434	
29.07.2005	10.4	7.71	431	sample taken from outside the cave next to path
16.08.2005	10.3	7.69	432	
09.09.2005	10.3	7.7	435	
07.10.2005	10.3	7.3	531	

Project:	Guadiana Menor, Spain	Page /
Institution / Editor:	FU Berlin, University of Granada, IGME/ Krauttter	

Sampling site:	Manantial de Parpacen	Site ID.:	SP-GM-002
Site label:		Map:	
Locality description:	a pond with a poplar grove by a dirt road outside Huescar south of the road to Castril		

X:	537982	Type:	spring
Y:	4184411	distance [m from source]:	-
Z:	921	discharge [l/s]:	25

--

Remarks:	water emerges through the ground next to the large tree on southern side of pond
-----------------	--

Sketch map	Site picture

Date of sampling	Temperature [°C]	pH	Conductivity [mS/cm]	Remarks
20.04.2005	18.6	8.08	867	samples taken from pond surface
14.05.2005	17.6	8.24	943	
04.06.2005	14.9	7.32	928	
01.07.2005	15.1	7.22	989	
28.07.2005	15.4	7.39	928	
21.08.2005	15.4	7.14	933	
08.09.2005	15.4	7.22	933	
05.10.2005	15	7.03	1040	

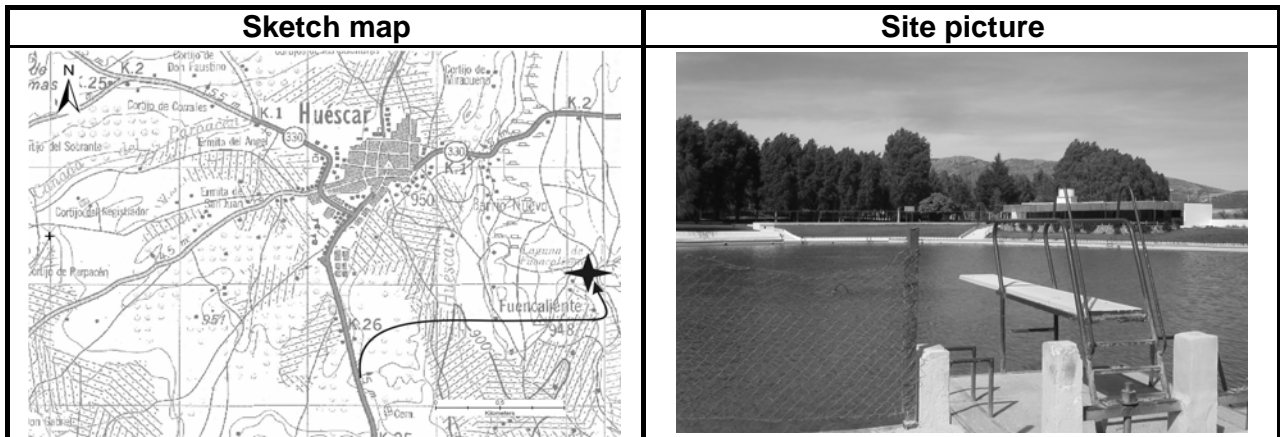
Project:	Guadiana Menor, Spain	Page /
Institution / Editor:	FU Berlin, University of Granada, IGME/ Krauttter	

Sampling site:	Fuencaliente	Site ID.:	SP-GM-007
Site label:		Map:	
Locality description:	public baths east of Huescar close to highway		

X:	542145	Type:	spring
Y:	4184085	distance [m from source]:	-
Z:	916	discharge [l/s]:	65

--

Remarks:	water emerges through the ground in the center of pool and in a small regulation channel next to the restaurant parking lot
-----------------	---



Date of sampling	Temperature [°C]	pH	Conductivity [mS/cm]	Remarks
31.03.2005	19.6	7.19	1505	
21.04.2005	16.4	7.72	1635	
15.05.2005	16.5	7.28	1643	
04.06.2005	16.5	7.32	1640	
01.07.2005	16.7	7.42	1634	
07.07.2005	18.4	7.48	1466	
28.07.2005	16.7	7.35	1641	
21.08.2005	16.5	7.22	1644	
08.09.2005	20	7.27	1520	
05.10.2005	17	7.19	1788	

Project:	Guadiana Menor, Spain	Page /
Institution / Editor:	FU Berlin, University of Granada, IGME/ Krauttter	

Sampling site:	Fuente Alta	Site ID.:	SP-GM-013
Site label:		Map:	
Locality description:	spring in a cave in Natividad valley		

X:	527700	Type:	spring
Y:	4194175	distance [m from source]:	-
Z:	1137	discharge [l/s]:	25

--

Remarks:	cave partly filled with water, below the end of the dirt road from the trout farm
-----------------	---

Sketch map	Site picture

Date of sampling	Temperature [°C]	pH	Conductivity [mS/cm]	Remarks
31.03.2005	12.8	7.62	342	
20.04.2005	12.8	7.84	359	
13.05.2005	12.3	8.01	401	
04.06.2005	10.5	8.25	380	
30.06.2005	11	8.15	382	
29.07.2005	10.5	8.16	388	
16.08.2005	11.3	7.56	401	
09.09.2005	13	8.16	370	
07.10.2005	11	7.85	482	

Project:	Guadiana Menor, Spain	Page /
Institution / Editor:	FU Berlin, University of Grana, IGME/ Krauttter	

Sampling site:	Embalse de San Clemente	Site ID.:	SP-GM-014
Site label:	Map:		
Locality description:	Reservoir		

X:	530937	Type:	reservoir
Y:	4190510	distance [m from source]:	-
Z:	1037	discharge [l/s]:	

--

Remarks:	sampled on west shore 100m from the damn across tower from the surface
-----------------	--

Sketch map	Site picture

Date of sampling	Temperature [°C]	pH	Conductivity [mS/cm]	Remarks
20.04.2005	14.2	8.13	340	
14.05.2005	15.5	8.28	348	
29.06.2005	19.2	8.5	336	
31.07.2005	20.3	8.58	338	
19.08.2005	19.6	8.46	334	
09.09.2005	21.6	8.61	300	
03.10.2005	18.9	8.18	369	

Project:	Guadiana Menor, Spain	Page /
Institution / Editor:	FU Berlin, University of Grana, IGME/ Krauttter	

Sampling site:	Barranco Natividad	Site ID.:	SP-GM-015
Site label:	Map:		
Locality description:	creek right outside Natividad cave at trout farm		

X:	537982	Type:	river
Y:	4194100	distance [m from source]:	80m
Z:	1083	discharge [l/s]:	>100

--

Remarks:	small stream about 80 m from ist source
-----------------	---

Sketch map	Site picture

Date of sampling	Temperature [°C]	pH	Conductivity [mS/cm]	Remarks
20.04.2005	12.1	7.7	417	sample taken from spring
13.05.2005	10.3	7.5	441	
04.06.2005	10.3	7.58	437	
30.06.2005	12.3	7.64	415	
29.07.2005	10.4	7.56	434	
16.08.2005	10.3	7.52	432	
09.09.2005	10.5	7.53	436	
07.10.2005	10.5	7.56	523	

Project:	Guadiana Menor, Spain	Page /
Institution / Editor:	FU Berlin, University of Granada, IGME/ Krauttter	

Sampling site:	Guardal/Los Ruices	Site ID.:	SP-GM-016
Site label:		Map:	
Locality description:	Guardal River downstream from the reservoir		

X:	537982	Type:	spring
Y:	4184411	distance [m from source]:	-
Z:	921	discharge [l/s]:	65

--

Remarks:	a small dam south of of the canyon off the Huescar-Castril road on the Los Ruices property
-----------------	--

Sketch map				Site picture
Date of sampling	Temperature [°C]	pH	Conductivity [mS/cm]	
20.04.2005	18.9	8.04	1978	
15.05.2005	19.2	8.02	1961	
29.06.2005	17.4	8.15	2110	
28.07.2005	15.9	8.1	1693	
16.08.2005	15.8	7.97	1600	
10.09.2005	15.6	8.23	1580	
03.10.2005	19.7	7.68	2160	



Project:	Guadiana Menor, Spain	Page /
Institution / Editor:	FU Berlin, University of Granada, IGME/ Krauttter	

Sampling site:	Fuentecillas	Site ID.:	SP-GM-017
Site label:	Map:		
Locality description:	trough in a bend of the Cortijos Nuevos dirt road off the Montilla road		

X:	537083	Type:	spring
Y:	4203250	distance [m from source]:	-
Z:	1434	discharge [l/s]:	<5

--

Remarks:	regulated spring, hose for water supply of the houses
-----------------	---

Sketch map	Site picture
	

Date of sampling	Temperature [°C]	pH	Conductivity [mS/cm]	Remarks
21.04.2005	10	7.6	508	
13.05.2005	8.5	7.3	530	
30.06.2005	8.8	7.42	523	
27.07.2005	10.7	7.39	503	
18.08.2005	9.2	7.23	526	
08.09.2005	9.3	7.24	527	
04.10.2005	9.3	7.09	654	

Project:	Guadiana Menor, Spain	Page /
Institution / Editor:	FU Berlin, University of Granada, IGME/ Krauttter	

Sampling site:	Raigadas/Puente Animas	Site ID.:	SP-GM-018
Site label:	Map:		
Locality description:	a pond with a poplar grove by a dirt road outside Huescar south of the road to Castril		

X:	532163	Type:	river
Y:	4194162	distance [m from source]:	-
Z:	1069	discharge [l/s]:	

--

Remarks:	little stream at the Las Animas bridge
-----------------	--

Sketch map	Site picture

Date of sampling	Temperature [°C]	pH	Conductivity [mS/cm]	Remarks
13.05.2005	16.7	8.39	574	dry
30.06.2005	19.1	8.79	481	

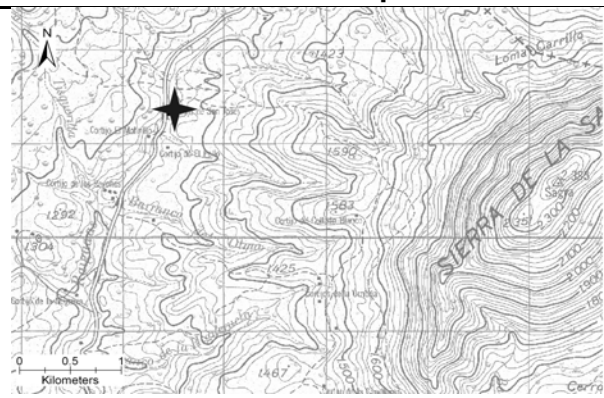

Project:	Guadiana Menor, Spain	Page /
Institution / Editor:	FU Berlin, University of Granada, IGME/ Krauttter	

Sampling site:	Raigadas/Cjo. San Jose	Site ID.:	SP-GM-019
Site label:		Map:	
Locality description:	Raigadas River near Cortijo San Jose on La Losa road		

X:	534445	Type:	river
Y:	4201324	distance [m from source]:	-
Z:	1249	discharge [l/s]:	

--

Remarks:	hole close to the road bridge near Cjo. San Jose
-----------------	--

Sketch map		Site picture	
			
Date of sampling	Temperature [°C]	pH	Conductivity [mS/cm]
13.05.2005	12.3	8.45	348
04.06.2005	15	8.38	360
30.06.2005	16.9	8.52	360
27.07.2005	16.4	8.63	357
20.08.2005	16.5	8.37	375
08.09.2005	13.3	8.57	379
04.10.2005	12.7	8.02	440

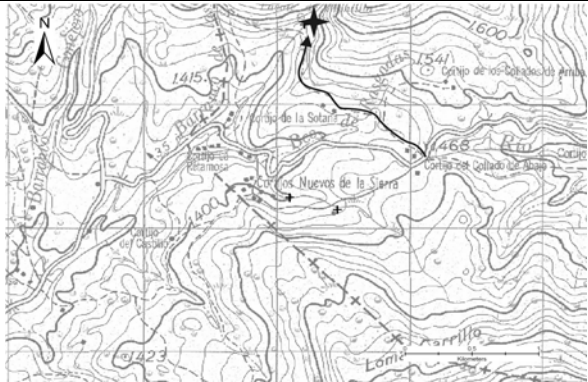

Project:	Guadiana Menor, Spain	Page /
Institution / Editor:	FU Berlin, University of Granada, IGME/ Krauttter	

Sampling site:	Fuente Montilla	Site ID.:	SP-GM-020
Site label:	Map:		
Locality description:	Montilla Spring, Montilla valley		

X:	537182	Type:	spring
Y:	4204656	distance [m from source]:	40.0
Z:	1466	discharge [l/s]:	<50

--

Remarks: track from the La Sagra road towards montilla canal accesible by car, last Km by foot. Samples taken from the creek at bottom of valley, the spring itself is grown impenetrable scrubs

Sketch map	Site picture
	

Date of sampling	Temperature [°C]	pH	Conductivity [mS/cm]	Remarks
13.05.2005	8.2	8.06	319	
04.06.2005	8.3	8.11	316	
30.06.2005	8.5	8.13	313	
27.07.2005	8.3	8.09	314	
18.08.2005	8.4	8.02	313	
08.09.2005	8.5	8.16	312	
04.10.2005	8.3	7.79	396	

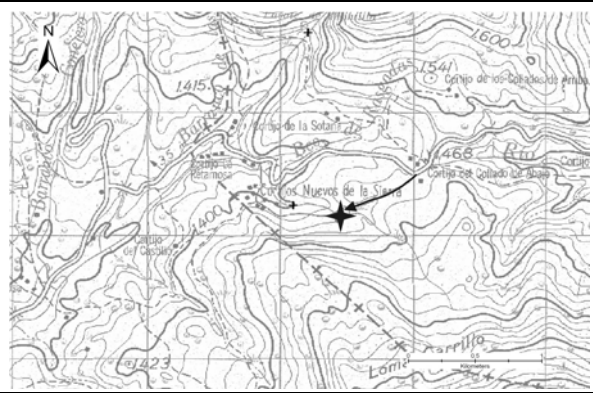

Project:	Guadiana Menor, Spain	Page /
Institution / Editor:	FU Berlin, University of Granada, IGME/ Krauttter	

Sampling site:	Fuente Carrillo	Site ID.:	SP-GM-021
Site label:		Map:	
Locality description:	Carrillo Spring, Cortijos Nuevos de la Sagra		

X:	537439	Type:	spring
Y:	4203155	distance [m from source]:	
Z:	1464	discharge [l/s]:	2

--

Remarks:	small tapped spring for water supply of Cjos. Nuevos
-----------------	--

Sketch map				Site picture					
									
<table border="1"> <thead> <tr> <th>Date of sampling</th> <th>Temperature [°C]</th> <th>pH</th> <th>Conductivity [mS/cm]</th> </tr> </thead> <tbody> <tr> <td>13.05.2005</td> <td>8.8</td> <td>7.28</td> <td>494</td> </tr> </tbody> </table>	Date of sampling	Temperature [°C]	pH		Conductivity [mS/cm]	13.05.2005	8.8	7.28	494
Date of sampling	Temperature [°C]	pH	Conductivity [mS/cm]						
13.05.2005	8.8	7.28	494						

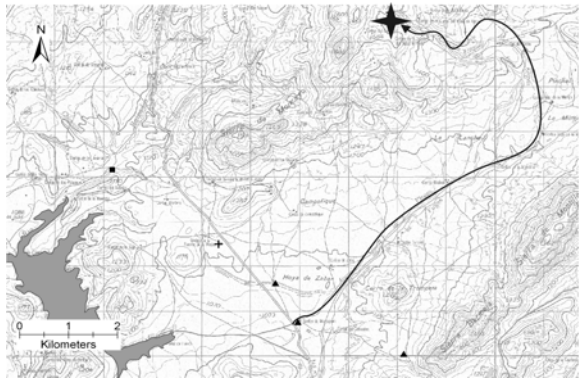

Project:	Guadiana Menor, Spain	Page /
Institution / Editor:	FU Berlin, University of Granada, IGME/ Krauttter	

Sampling site:	Cueva del Agua	Site ID.:	SP-GM-022
Site label:		Map:	
Locality description:	cave half way up eastern slope of La Sagra mountain		

X:	537842	Type:	spring
Y:	4197651	distance [m from source]:	
Z:	1499	discharge [l/s]:	

--

Remarks:	follow up the dirt road towards the mountain from Cjo. Mazagrande
-----------------	---

Sketch map				Site picture					
									
<table border="1"> <thead> <tr> <th>Date of sampling</th> <th>Temperature [°C]</th> <th>pH</th> <th>Conductivity [mS/cm]</th> </tr> </thead> <tbody> <tr> <td>14.05.2005</td> <td>8</td> <td>8.05</td> <td>331</td> </tr> </tbody> </table>	Date of sampling	Temperature [°C]	pH		Conductivity [mS/cm]	14.05.2005	8	8.05	331
Date of sampling	Temperature [°C]	pH	Conductivity [mS/cm]						
14.05.2005	8	8.05	331						

Project:	Guadiana Menor, Spain	Page /
Institution / Editor:	FU Berlin, University of Granada, IGME/ Krauttter	

Sampling site:	Fuente Tornajo	Site ID.:	SP-GM-023
Site label:		Map:	
Locality description:	tapped spring in the village of Duda		

X:	529119	Type:	spring
Y:	4187630	distance [m from source]:	
Z:	930	discharge [l/s]:	0.5

--

Remarks:	tapped spring with old sinks by old tree below the chapel
-----------------	---

Sketch map	Site picture

Date of sampling	Temperature [°C]	pH	Conductivity [mS/cm]	Remarks
15.05.2005	13.5	7.57	582	
03.10.2005	16.8	7.27	662	

Project:	Guadiana Menor, Spain	Page /
Institution / Editor:	FU Berlin, University of Granada, IGME/ Krauttter	

Sampling site:	Fuente Oliva	Site ID.:	SP-GM-024
Site label:		Map:	
Locality description:	tapped spring in the village of Duda		

X:	529215	Type:	spring
Y:	4187772	distance [m from source]:	
Z:	930	discharge [l/s]:	0.5

--

Remarks:	small storage pool for irrigation on slope below houses
-----------------	---

Sketch map	Site picture

Date of sampling	Temperature [°C]	pH	Conductivity [mS/cm]	Remarks
15.05.2005	13.7	7.62	596	

Project:	Guadiana Menor, Spain	Page /
Institution / Editor:	FU Berlin, University of Granada, IGME/ Krauttter	

Sampling site:	Fuente Penalba	Site ID.:	SP-GM-025
Site label:		Map:	
Locality description:	tapped spring in the village of Duda		

X:	529035	Type:	spring
Y:	4187430	distance [m from source]:	
Z:	937	discharge [l/s]:	0.5

--

Remarks:	small outflow of water in a field close to Cjo. De Penalba
-----------------	--

Sketch map	Site picture

Date of sampling	Temperature [°C]	pH	Conductivity [mS/cm]	Remarks
15.05.2005	12.7	7.5	460	



Project:	Guadiana Menor, Spain	Page /
Institution / Editor:	FU Berlin, University of Granada, IGME/ Krauttter	

Sampling site:	Fuente Felin Grande	Site ID.:	SP-GM-026
Site label:		Map:	
Locality description:	tapped spring near the village of Castillejar		

X:	527013	Type:	spring
Y:	4178294	distance [m from source]:	
Z:	892	discharge [l/s]:	12

--

Remarks:	regulated and stored in a small hut in a field close to Cjo. Felin
-----------------	--

Sketch map	Site picture
	

Date of sampling	Temperature [°C]	pH	Conductivity [mS/cm]	Remarks
13.05.2005	15.5	7.71	1040	water stale and no current inside small storage
03.06.2005	15.5	7.65	1030	
29.06.2005	16	7.97	1036	
28.07.2005	16.6	7.87	1040	
23.08.2005	16.5	7.77	1040	
10.09.2005	16	7.88	1041	
05.10.2005	15.7	7.37	1156	floodgate opened, current fresh water sampeled

Project:	Guadiana Menor, Spain	Page /
Institution / Editor:	FU Berlin, University of Granada, IGME/ Krauttter	

Sampling site:	Sondeo Diablo	Site ID.:	SP-GM-027
Site label:		Map:	
Locality description:	abandoned well near Almontara		

X:	525171	Type:	well
Y:	4181082	depth to water table [m]:	35.2
Z:	926	discharge [l/s]:	

--

Remarks:	sampeled with a hand ladle from diferent depths NOT PUMPED!! See SP-GM-061
-----------------	--

Sketch map	Site picture

Date of sampling	Temperature [°C]	pH	Conductivity [mS/cm]	Remarks
03.06.2005	21.1?	7.38	1130	70 m <u>SP-GM-027</u>
03.06.2005	14.3	7.37	1219	40m <u>SP-GM-028</u>
03.06.2005	14.7	7.35	1165	90m <u>SP-GM-029</u>


Project:	Guadiana Menor, Spain	Page /
Institution / Editor:	FU Berlin, University of Granada, IGME/ Krauttter	

Sampling site:	Fuente de Ortiz	Site ID.:	SP-GM-031
Site label:		Map:	
Locality description:	tapped spring near the village of Fatima		

X:	522538	Type:	spring
Y:	4186679	distance [m from source]:	
Z:	1141	discharge [l/s]:	0.5

--

Remarks:	small tapped spring with open storage pool below Cortijo
-----------------	--

Sketch map	Site picture
	

Date of sampling	Temperature [°C]	pH	Conductivity [mS/cm]	Remarks
08.07.2005	13.2	7.35	634	

Project:	Guadiana Menor, Spain	Page /
Institution / Editor:	FU Berlin, University of Granada, IGME/ Krauttter	

Sampling site:	Fuente de Piedra	Site ID.:	SP-GM-036
Site label:	Map:		
Locality description:	tapped spring near San Clemente		

X:	534333	Type:	spring
Y:	4192501	distance [m from source]:	
Z:	1115	discharge [l/s]:	0.5

--

Remarks:	small tap into a drinking trough
-----------------	----------------------------------

Sketch map	Site picture

Date of sampling	Temperature [°C]	pH	Conductivity [mS/cm]	Remarks
29.07.2005	13.3	8.26	433	

Project:	Guadiana Menor, Spain	Page /
Institution / Editor:	FU Berlin, University of Granada, IGME/ Krauttter	

Sampling site:	Sondeo Cjo. Mazagrande	Site ID.:	SP-GM-050
Site label:	Map:		
Locality description:	Farm on the Huescar- La Losa road near Turnoff to Reservoir		

X:	535952	Type:	well
Y:	4190772	depth to water table [m]:	2.5
Z:	1092	discharge [l/s]:	

--

Remarks:	sampeled with a hand ladle from ca. 2m NOT PUMPED!! Filtered
-----------------	--

Sketch map	Site picture

Date of sampling	Temperature [°C]	pH	Conductivity [mS/cm]	Remarks
15.09.2005	18.1	7.06	724	equipment UGR/IGME

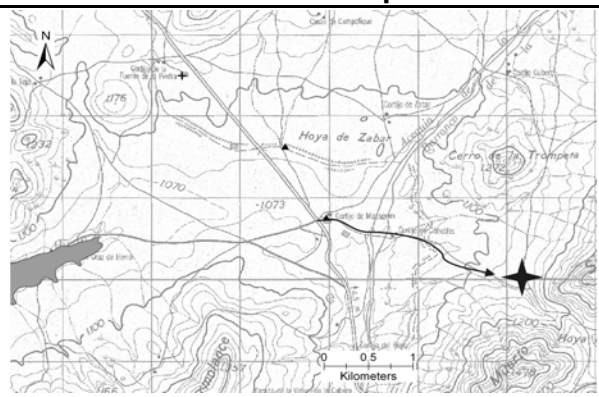
Project:	Guadiana Menor, Spain	Page /
Institution / Editor:	FU Berlin, University of Granada, IGME/ Krauttter	

Sampling site:	Sondeo Cjo. Corcoles	Site ID.:	SP-GM-050
Site label:	Map:		
Locality description:	automatic pumping well with solar unit		

X:	538115	Type:	well
Y:	4190064	depth to water table [m]:	
Z:	1145	discharge [l/s]:	

--

Remarks:	sampeled from tube at the storage basin
-----------------	---

Sketch map	Site picture
	

Date of sampling	Temperature [°C]	pH	Conductivity [mS/cm]	Remarks
15.09.2005	14.5	7.46	737	equipment UGR/IGME

Project:	Guadiana Menor, Spain	Page /
Institution / Editor:	FU Berlin, University of Granada, IGME/ Krauttter	

Sampling site:	Sondeo Cjo. Zabar	Site ID.:	SP-GM-052
Site label:	Map:		
Locality description:	off Huescar-La Losa road		

X:	535491	Type:	well
Y:	4191638	depth to water table [m]:	
Z:	1096	discharge [l/s]:	

--

Remarks:	newly constructed well running unattended sampeled from tap on piping
-----------------	---

Sketch map	Site picture

Date of sampling	Temperature [°C]	pH	Conductivity [mS/cm]	Remarks
15.09.2005	17.2	7.36	761	equipment UGR/IGME

Project:	Guadiana Menor, Spain	Page /
Institution / Editor:	FU Berlin, University of Granada, IGME/ Krauttter	

Sampling site:	Sondeo Rambla Valentin	Site ID.:	SP-GM-053
Site label:	Map:		
Locality description:	high capacity pumping well in a dry riverbed outside Huescar on road to Castril		

X:	534965	Type:	well
Y:	4184572	depth to water table [m]:	
Z:	961	discharge [l/s]:	

--

Remarks: large diesel power set powered automatic pump, can be seen and heard from distance, sampeled from tap on fixed piping

Sketch map	Site picture

Date of sampling	Temperature [°C]	pH	Conductivity [mS/cm]	Remarks
15.09.2005	17.5	7.4	929	equipment UGR/IGME

Project:	Guadiana Menor, Spain	Page /
Institution / Editor:	FU Berlin, University of Granada, IGME/ Krauttter	

Sampling site:	Cantera Atalaya 1	Site ID.:	SP-GM-054
Site label:		Map:	
Locality description:	pumping well at the lower stone quarry		

X:	530730	Type:	well
Y:	4182703	depth to water table [m]:	
Z:	962	discharge [l/s]:	

--

Remarks:	water is pumped and used for cooling rock saws
-----------------	--

Sketch map	Site picture

Date of sampling	Temperature [°C]	pH	Conductivity [mS/cm]	Remarks
15.09.2005	16.7	7.64	710	equipment UGR/IGME

Project:	Guadiana Menor, Spain	Page /
Institution / Editor:	FU Berlin, University of Granada, IGME/ Krauttter	

Sampling site:	Cantera Atalaya 2	Site ID.:	SP-GM-055
Site label:		Map:	
Locality description:	pumping well at the upper stone quarry (Ferrer)		

X:	531053	Type:	well
Y:	4183447	depth to water table [m]:	
Z:	1050	discharge [l/s]:	

--

Remarks: water is pumped into a storage basin on top of the hill and used for cooling rock saws, well at the foot of the hill, sampled from inlet into basin

Sketch map	Site picture

Date of sampling	Temperature [°C]	pH	Conductivity [mS/cm]	Remarks
15.09.2005	17.4	7.61	538	equipment UGR/IGME

Project:	Guadiana Menor, Spain	Page /
Institution / Editor:	FU Berlin, University of Granada, IGME/ Krauttter	

Sampling site:	Sondeo Cjo. De los Jaros	Site ID.:	SP-GM-056
Site label:	Map:		
Locality description:	diesel engine powered irrigation well		

X:	525428	Type:	well
Y:	4185356	depth to water table [m]:	
Z:	1048	discharge [l/s]:	

--

Remarks:	sampeled from tap on pump
-----------------	---------------------------

Sketch map	Site picture

Date of sampling	Temperature [°C]	pH	Conductivity [mS/cm]	Remarks
16.09.2005	15.5	7.1	730	started by owner for sampling

Project:	Guadiana Menor, Spain	Page /
Institution / Editor:	FU Berlin, University of Granada, IGME/ Krauttter	

Sampling site:	private well Castro-Cubo	Site ID.:	SP-GM-057
Site label:	Map:		
Locality description:	diesel engine powered irrigation well near cortijos		

X:	523304	Type:	well
Y:	4184997	depth to water table [m]:	
Z:	1092	discharge [l/s]:	

--

Remarks:	sampeled from hose on pump
-----------------	----------------------------

Sketch map	Site picture

Date of sampling	Temperature [°C]	pH	Conductivity [mS/cm]	Remarks
16.09.2005	15.6	6.75	1503	owner started pumping for sampling

Project:	Guadiana Menor, Spain	Page /
Institution / Editor:	FU Berlin, University of Granada, IGME/ Krauttter	

Sampling site:	Artesian well	Site ID.:	SP-GM-059
Site label:	Map:		
Locality description:	artesian well left open		

X:	533152	Type:	well
Y:	4182802	depth to water table [m]:	-
Z:	923	discharge [l/s]:	

--

Remarks:

Sketch map	Site picture

Date of sampling	Temperature [°C]	pH	Conductivity [mS/cm]	Remarks
22.09.2005	13.7	7.05	1003	

Project:	Guadiana Menor, Spain	Page /
Institution / Editor:	FU Berlin, University of Granada, IGME/ Krauttter	

Sampling site:	FAO well Huescar	Site ID.:	SP-GM-060
Site label:		Map:	
Locality description:	monitoring well outside Huescar		

X:	536469	Type:	well
Y:	4185133	depth to water table [m]:	40.3
Z:	975	discharge [l/s]:	

--

Remarks:	sampeled by pumping with MP1 (0.26 l/s) from 41 m
-----------------	---

Sketch map	Site picture

Date of sampling	Temperature [°C]	pH	Conductivity [mS/cm]	Remarks
22.09.2005	19	7.3	1015	

Project:	Guadiana Menor, Spain	Page /
Institution / Editor:	FU Berlin, University of Granada, IGME/ Krauttter	

Sampling site:	Sondeo Diablo	Site ID.:	SP-GM-061
Site label:		Map:	
Locality description:	abandoned well near Almontara		

X:	525171	Type:	well
Y:	4181082	depth to water table [m]:	35.2
Z:	926	discharge [l/s]:	

--

Remarks:	sampeled with MP1 from 46 m
-----------------	-----------------------------

Sketch map	Site picture

Date of sampling	Temperature [°C]	pH	Conductivity [mS/cm]	Remarks
23.09.2005	16.4	7.03	1384	

Estudio del agua subterránea del sistema acuífero
de la región de Granada (Sureste de España).
Estudio hidrogeoquímico e isotópico

Groundwater Study for the Regional Granada
Aquifer System (Southern Spain)
Hydrochemistry and Isotope Study

Structural and Sedimentological
Aspects of Basin Deposits
-Geological Mapping-

Summary

Aim of this thesis (Diplomarbeit) is the investigation of the origin and the flow pattern of groundwater which is found in an alluvial aquifer (*Vega de Granada*) at the foot of the *Sierra Nevada* (southern Spain). Open questions considering altitudes and areas of recharge from the *Vega de Granada* groundwater have been the main task. Furthermore, questions concerning lateral and subsurface groundwater flow were considered. Several hydrogeological, hydrochemical and isotope-hydrochemical methods have been applied to cope with this task.

The study area comprises vast parts of the *Granada* basin and the adjacent *Sierras* in the east. Geologically, the area can be divided into a metamorphic core (*Nevado-Filabride*), a carbonate domain (*Alpujarride*) and the sediments of the intramontaneous basin. As shown by analysis of climate data, the study area in southern Spain is considered to be semi-arid with a mediterranean climate. Due to high temperatures in summer (May-September) most of the precipitation evaporates or is transpired by plants. During winter (October - April) only little to no groundwater recharge in the *Vega de Granada* is expected to occur. The main groundwater recharge area is the *Sierra Nevada* with preferential formation of groundwater during winter.

Within this study more than 200 samples of precipitation (rain, snow), surface water (river, reservoir) and groundwater (springs, wells) over the monitoring time from February 04 to March 05 were taken and analysed. The analysis was made according to the measured hydrochemical and isotopechemical parameters and the in-field measured data.

Four hydrochemical groups can be classified according to the composition of the major constituents. Additionally, saturation indices (SI) were calculated with the software PHREEQC 2.11 in respect to calcite, dolomite, anhydrite and gypsum.

- Low mineralized samples ($EC < 100 \mu\text{S}/\text{cm}$) from precipitation and small streams (*Arroyo*) in the *Sierra Nevada* are summarized in group one.
- Water type of Ca-Mg-HCO_3^- and Mg-Ca-HCO_3 is found in the *Alpujarride* domain, where limestone gives good recharge conditions. Characteristic for this carbonate terrain with dolomite and calcite host-rocks is the changing dominance of Ca and Mg. Calculation of SI of this group show that samples are close to or in equilibrium with calcite and dolomite.
- Groundwater from the alluvial gravel and sands (*Vega de Granada*) is highly mineralized and dominated by Ca and SO_4 with high content of hydrogen. In this group oversaturation with respect to calcite and dolomite was observed.

- Thermal water (>20 °C) samples were subdivided into two groups. The first subgroup is according to their low mineralization and temperature considered to be influenced by shallow groundwater. The hydrochemical signature is similar to those in the *Alpujarride* domain but is additionally characterized by an increased content in hydrogencarbonate. The second subgroup is characterized by increased mineralization and a balanced relation of earthalkalis and alkalis at high hydrogencarbonate content. Thermal springs of this subgroup are associated with a deep-reaching fault zone between the Internal and the External Zone.

The investigation of the carbonate chemistry showed that calcite solution evolves under open-system conditions. Initial CO₂ pressures range from atmospheric derived (pCO₂ = -3) to increased CO₂ content derived from soil air (pCO₂ = -2) (p.38).

On the basis of the wide range in sampling types (rain, snow, springs, thermal springs, wells and surface water) and the time of monitoring (February 2004 – March 2005) the signatures of stable isotopes (δ¹⁸O, δD) show a diverse range, from depleted winter snow samples (δ¹⁸O = -10 ‰) to enriched and even positive (δ¹⁸O = +3 ‰) samples from small endorheic basins at altitudes >2200 masl in the *Sierra Nevada* (p.39).

Stable isotopes in rain samples were used to examine fundamental processes of rain formation, like amount-, temperature- and altitude effect. Unfortunately, the amount of rain samples was not sufficient for establishing local altitude gradients. Therefore, the pattern in precipitation was studied in samples from the IAEA-GNIP database and from 1.5 year time series from *Granada* (GARRIDO 2003). According to this datasets local altitude gradients were constructed and therefore it was possible to associate groundwater to mean recharge altitudes. Since the *Sierra Nevada* springs and the *Sierra de la Peza springs* are located on different orographic divides of the Betic Cordillera, a spatial shift in δ¹⁸O values is expected to occur. This shift is expressed by different δ¹⁸O / altitude relationship. Furthermore, it was shown that, according to the shift between the mean weighted isotope signature in rain and the mean groundwater composition, recharge will take place mainly during the winter months (p.41).

More than 70 samples taken at altitudes >2200 masl in the *Sierra Nevada* were taken and analysed. The main characteristics of local snow, snowmelt or *laguna* (small basins in the *Sierra Nevada*) samples can be described as:

- *Laguna* (n=39) samples are often enriched in δ¹⁸O following an evaporation trend which is characteristic for open water bodies. According to the low temperature (~ 5 °C) and the low humidity (~ 30 %) conditions at these altitudes, a maximum evaporative loss of 51 % in small endorheic basins was calculated.
- Snow (n=11) samples can be subdivided in fresh snow and altered snow according to their position on the MWLs. Fresh snow is depleted up to 10 ‰ in δ¹⁸O compared to snowmelt. The alteration seems to follow the MWL.

- Snowmelt samples are located near to the WMMWL following an evaporative enrichment under high humidity conditions. The slope of the regression line is characteristic for evaporation under increased equilibrium conditions during evaporation (p.49, p.58).

Within the scope of this work isotope signatures of springs were associated to average groundwater recharge altitudes. According to a changing spatial distribution in precipitation it was necessary to distinguish between the *Sierra Nevada* and the *Sierra de la Peza* groundwater recharge areas. It was recognized that the lower the spring is situated, the higher the recharge area is. Vertical discrepancy between actual altitude and estimated recharge altitude (vertical distance) was estimated between 300 – 1300 m. Local groundwater flow was visualized by three isotope cross-sections for the *Sierra Nevada* and the *Sierra de la Peza* (p.49, p.58).

Since no discharge values of rivers were available, it was not possible to calculate volume weighted river values. Samples from the *Emb.de Quentar* were taken from various depths below surface (2, 5, 10 m) and were within the precision in measurement. Therefore no further interpretation was allowed. Seasonal variations in the samples of the highest site from the *Rio Genil* were observed. This indicates the strong influence of surface run-off in the metamorphic *Nevado-Filabride* complex. Samples from the reservoir (*Emb.de Canales*) of the *Genil* and samples from the discharge of this reservoir were very similar and became progressively depleted. This trend reflects the decreasing water table of the reservoir without significant inflow. No evaporation trend was observed in samples from the *Emb.de Canales*. The influence of irrigation and other anthropogenic impacts were observed in the underflow of the *Rio Genil* by attenuated seasonal isotope signatures. The *Rio Genil* is at the inflow to the *Vega de Granada* with $\delta^{18}\text{O} = -8.3 \text{ ‰}$ one per mill lighter than at the outflow with -7.3 ‰ . The hydraulic regime in the *Vega de Granada* changes from influent (losing river) at the inflow of the *Rio Genil* to effluent (gaining river) at its outflow. Thus, the *Genil* carries at the outflow of the *Vega de Granada* the hydrochemical and the isotope signature of the groundwater. The *Rio Darro* showed at the inflow to the *Vega de Granada*, during the time of monitoring, an isotope signature which was 0.2 ‰ heavier than the signature from the *Genil*. This reflects the smaller and the lower mean altitude of the *Rio Darro* catchment area. The mean isotope signature of the *Rio Darro* at the inflow to the *Vega de Granada* was significant enriched compared to the groundwater of the *Vega de Granada*. This is interpreted as a minor influence of the *Darro* for GWR through indirect infiltration. Controversy, the mean isotope signature of the *Rio Genil* at the inflow to the *Vega de Granada* was very similar compared to the groundwater of the *Vega de Granada*. This is interpreted as a strong influence of the *Genil* for GWR through riverbed infiltration. River inflow at the northern border of the *Vega de Granada* by the *Rio Cubillas*, which drains vast parts of the *Sierra Arana*, was sampled once at three sites. A strong evaporative enrichment was observed in the sample from the reservoir of the *Cubillas* (*Emb.de Cubillas*). This enriched signature was transferred by the *Cubillas* to the *Vega de Granada* groundwater and then attenuated by mixing processes with the depleted groundwater from the east. Other river inflow signatures were not sampled and could be subject for further studies (p.53).

It is shown that the spatial distributions of stable isotopes from wells located in the south-eastern part of the *Vega de Granada* were highly depleted. Therefore, this area is considered to be influenced by lateral inflow from the adjacent *Sierras* or indirect recharge by the local rivers (*Genil, Monachil, Dilar*). In contrast, groundwater from the centre and the western part of the *Vega de Granada* is relatively enriched in both isotopes with a strong enrichment in $\delta^{18}\text{O}$ indicating evaporation losses. Maximum evaporation losses were calculated, according to the regression line of the well samples and the climatic conditions, with ~20 %. Water-Rock interaction in the *Vega de Granada* alluvial aquifer cannot be excluded and might be subject for further studies. A flow of depleted groundwater is observed south to the *Sierra Elvira* carbonate complex indicating the importance of the *Sierra Elvira* as a local groundwater recharge area. This signature was associated to GWR altitudes around 1500 masl. One of the most important springs in the *Vega de Granada* (*Manantial de la Reina*) with 12.000 l/m runoff was associated, according to the similar isotope signature with groundwater in the north, to groundwater recharge area in the *Sierra Elvira* (p.63).

The isotope signatures of thermal springs are supposed to be influenced by water-rock interactions, due to a shift from the WMMWL. In accordance to the hydrochemical classification, the thermal springs can also be divided by the isotope signatures into two subgroups. Samples which are located near to the WMMWL are supposed to be less influenced by water-rock interactions, while points which are shifted from the WMMWL represent progressively increasing water-rock interaction with the host-rocks of the aquifer under various water temperature conditions. Maximum deviations from the WMMWL are $\Delta 0.5 \text{ ‰}$ (p.66).

Acknowledgments	I
Zusammenfassung (German summary)	II - VI
Summary	VI – IX

1 INTRODUCTION

1.1 Introduction and Objectives	1
1.2 Regional Geological Setting	2
1.3 Geomorphology	4
1.4 Climate, Meteorology	5

2 BACKGROUND

2.1 Groundwater recharge	8
2.2 Hydrogeology	9
2.2.1 Alluvial aquifer Vega de Granada	9
2.2.2 Mio-/Pliocene basin deposits	11
2.2.3 Carbonate terrains (<i>Sierra de la Peza, - de Padul, - Arana, - Elvira</i>)	11
2.2.4 Metamorphic terrains (<i>Nevado-Filabride</i>)	12
2.3 Stable isotopes in hydrogeology	13
2.3.1 Isotope fractionation	13
2.3.2 The meteoric water lines	17
2.4 Previous isotope studies relevant for the study area	18

3 METHODS

3.1 Sampling Strategy	21
3.2 Sampling Campaigns	21
3.3 Analysis	24
3.3.1 Ions	24
3.3.2 Isotopes	24
3.4 Climate	24
3.4.1 Groundwater recharge potential	24
3.5 Stable Isotopes in hydrogeology	24
3.6 Digital Elevation Model (DEM)	26

4 RESULTS & DISCUSSION

4.1 Hydrochemistry	27
4.1.1 Reliability check	27
4.1.2 Classification and characterisation of water samples	29
4.1.3 Carbonate chemistry	39
4.2 Stable isotopes	41
4.2.1 Precipitation	43
4.2.1.1 Rainwater	44
4.2.1.2 Snow and snowmelt	47
4.2.2 Estimation recharge elevation	51
4.2.3 Surface water	54
4.2.3.1 <i>Rio Genil</i>	55
4.2.3.2 <i>Rio Darro</i>	56
4.2.3.3 <i>Rio Cubillas</i>	57
4.2.3.4 <i>Embalse de Quentar</i>	58
4.2.4 Springs	60
4.2.5 Wells in the <i>Vega de Granada</i>	65
4.2.6 Thermal springs	68

5 GEOLOGICAL MAPPING

5.1 Introduction and Background	71
5.2 Methods	75
5.3 Structural data.....	76
5.4 Formations.....	79
5.4.1 Alluvial	79
5.4.2 Conglomerates and Sandstones `Alhambra Formation`	79
5.4.3 Red Siltstones and Conglomerates	81
5.4.4 Sandstones and Conglomerates `Pinos Genil`	83
5.4.5 Siltstones, Sandstones and Gravel `Cenes de Lancha`	83
5.5 Profile	83
Abbreviations	86
References	87
Appendix (26 pages)	91

List of figures

• Figure 1.1 Geological sketch of Andalusia showing the threefold division of the Betic Cordillere (External Zone, Internal Zone, Flysch). The rectangle indicates the study area. (Geology simplified from IGME 2002).	2
• Figure 1.2 Geologic evolution of the Betic-Rif mountain belt (LONERGAN & WHITE 1997).	3
• Figure 1.3 Digital elevation model (DEM) of the Granada basin and the surrounding mountain ranges with the catchment area of the Rio Genil. (DEM derived from Mapa Digital Andalusia 2002).	4
• Figure 1.4 (a-c) Climate diagrams of selected stations. (Data derived from www.juntadeandalucia.es).	5
• Figure 1.5 Year to year variations from average annual of annual precipitation in the city of Granada (Data derived from IGME 2000).	6
• Figure 1.6 Isohyetal contour map of annual precipitation averages of the Granada region calculated with records of the indicated meteorological stations from various time periods (Data shown in Appendix 1, table a1.1).	7
• Figure 2.1 GWR map and extend of the Rio Genil catchment area and the tributary sub-basins.	8
• Figure 2.2 Water table trend map from 1967 (FAO-IGME 1968).	9
• Figure 2.3 Water table map from March 1994 (CASTILLO 1995).	10
• Figure 2.5: Differences in evaporation rates in relation to humidity (h) in a $\delta^{18}O$ vs. δD (‰-VSMOW) diagram for 5°C and 20°C. Showing the predominating fractionation process at values for f from 1 to 0.1. (s = slope of evaporation line, Calculated according equation 2.9).	15
• Figure 2.6: Altitude effect and mixing of groundwater in the spring water (modified after www.IAEA.org).	16
• Figure 2.7 GMWL (Global Meteoric Water Line), WMMWL (Western Mediterranean Meteoric Water Line) and LMWL (Local Meteoric Water Line) for Granada (eq. 2.11) and Sierra Nevada (eq. 2.12) with the mean groundwater signature from the alluvial aquifer (Vega de Granada).	18
• Figure 2.8 Seasonal variations of $\delta^{18}O$ in Iberian precipitation from IAEA stations based on the monthly means from 1985-1991 (Barcelona), 1988-2001 (Madrid), 1962-2001 (Gibraltar) (all data IAEA-GNIP 2004).	18
• Figure 2.9 $\delta^{18}O$ - δD diagram of IAEA-GNIP data at Gibraltar between 1961 and 2001 with regression trend line (dashed-dotted), GMWL (solid) and LMWL (dashed).	19
• Photo 1 Laguna de los Machos (X 468241 Y 4100417 Z 2919).	23
• Photo 2 Snowpatch Barr. de San Juan, Nac. Rio Genil (X 4103799 Y 467193 Z 2718).	23
• Photo 3 Laguna Mula (X 463052 Y 4101813 Z 2495).	23
• Photo 4 Laguna Aguas Verdes (X 467372 Y 4100518 Z 3059).	23
• Figure 3.1 (a-d): Trend analysis of different time periods and stations within the study area.	25
• Figure 4.1 Electrical balances vs. frequency of measured samples.	27
• Figure 4.2 Linear relation between EC and TDS of measured samples.	28
• Figure 4.3 Piper plots of all hydrochemical analysis.	30
• Figure 4.4 Piper plot and EC vs. HCO_3 scatter of group 1 members.	31
• Figure 4.5 Stiff plot of river (grey) and rain (black) samples (group 1).	31
• Figure 4.6 Piper plot and EC vs. HCO_3 scatter of group 2 samples.	33

Table of content

• Figure 4.7 Location map of group 2 members, simplified geology and stiff diagrams of spring (grey), river (light grey) and well (black). Geology simplified from IGME 2002.	34
• Figure 4.8 Piper plot and EC vs. HCO ₃ scatter of group 3 members.	35
• Figure 4.9 Location map of group 3 members, simplified geology and stiff diagrams of well (dark grey), river (light) and spring (grey) samples. Geology simplified from IGME 2002.	36
• Fig.4.10 Piper plot and EC vs. HCO ₃ scatter of group 4 members.	37
• Figure 4.11 Schoeller diagram of thermal springs (group 4).	38
• Fig.4.12 Stiff diagram of brine sample (Arr.Salado).	39
• Figure 4.13 Open and closed system trajectories for calcite dissolution of group 2 and group 3 members.	40
• Figure 4.14 Schematic overview of δD and $\delta^{18}O$ relationship of all samples with the GMWL and the WMMWL as reference.	41
• Figure 4.15 Location map of sample sites for stable isotope analysis and isotope transects I, II, III. Geology simplified from IGME 2002.	42
• Figure 4.16 Seasonal distribution of mean weighted $\delta^{18}O$ measured in precipitation at Gibraltar station (1962-2001), air temperature (right y-axis) and d-excess (‰ VS.MOW). The bars indicate mean monthly amounts of precipitation scaled to the left y-axis. IAEA–GNIP 2004.	44
• Figure 4.17 Seasonal distribution of mean weighted $\delta^{18}O$ measured in precipitation at Generalife station (Dec.1999-Nov.2002), air temperature (right y-axis) from Padul station and d-excess (‰ VS.MOW). The bars indicate mean monthly amounts of precipitation. GARRIDO 2003.	44
• Figure 4.18 Precipitation (mm) and air temperature (°C) at Padul station between 01.02.2004 and 30.04.2005, $\delta^{18}O$ (‰-VSMOW) of measured rain samples.	45
• Figure 4.19 $\delta^{18}O$ (‰-VSMOW) - δD (‰-VSMOW) diagram of rain samples.	46
• Figure 4.20 $\delta^{18}O$ - δD diagram of snowmelt samples from the Sierra Nevada with average value of Fte.Alta and Nac. Rio Darro.	47
• Figure 4.22 $\delta^{18}O$ - δD diagram of laguna samples from the Sierra Nevada. Meteoric water lines as reference.	49
• Figure 4.23 Corrected $\delta^{18}O$ (‰-VSMOW) vs. Altitude (masl) of snowmelt and laguna samples.	49
• Figure 4.24 Average $\delta^{18}O$ values of springs (squares) vs. Altitude (masl). Regression lines in spring samples calculated for the Sierra Nevada (red dashed line) and Sierra de la Peza (black dashed line). Interpolated precipitation line (red line) taken from GARRIDO 2003 is representing mean recharge altitudes. Mean weighted winter rain in the Granada basin (open square). ABL=atmospheric boundary layer.	50
• Figure 4.25 $\delta^{18}O$ with d-excess vs. time diagrams (left) and δD with Altitude (masl) vs. $\delta^{18}O$ (‰-VSMOW) diagrams (right) of Genil samples.	54
• Figure 4.26 $\delta^{18}O$ with d-excess vs. time diagrams (right) and δD (‰-VSMOW) with Altitude (masl) vs. $\delta^{18}O$ (‰-VSMOW) diagrams (left) of Darro samples.	56
• Figure 4.27 $\delta^{18}O$ vs. δD and δD (‰-VSMOW) vs. Altitude (masl) diagrams of river Cubillas samples.	57
• Figure 4.28 $\delta^{18}O$ vs. δD (‰-VSMOW) of samples from the reservoir Quentar and depth below surface (arrow indicates the range of precision in $\delta^{18}O$ measurement).	59
• Figure 4.29 $\delta^{18}O$ vs. δD (‰-VSMOW) diagram of spring samples from different Sierras in the study area.	59
• Figure 4.30 $\delta^{18}O$ (‰-VSMOW) vs. Altitude (masl) of all Sierra springs.	60

Table of content

• Figure 4.31 Isotope transect I: High altitude springs and snow samples in the Sierra Nevada. Mean recharge altitudes and precision of calculation. Black solid arrows indicate surface runoff, dotted arrows indicate flowpaths, thin line indicate water table. Altitude/distance relation is given in lower left corner.	61
• Figure 4.32 Isotope transect II: High altitude springs and river samples in the Sierra Nevada. Mean recharge altitudes and precision of calculation. Black solid arrows indicate surface runoff, dotted arrows indicate flowpaths, thin line indicate water table. Altitude – distance relation is given in lower left corner.	62
• Figure 4.33 Isotope transect III: Springs and river samples in the Sierra de la Peza. Mean recharge altitudes and precision of calculation. Black solid arrows indicate surface runoff, dotted arrows indicate flowpaths, thin line indicate water table. Altitude – distance relation is given in lower left corner.	63
• Figure 4.34 $\delta^{18}\text{O}$ vs. δD of groundwater from wells in the Vega de Granada alluvial aquifer. MWLs as reference. Numbers refer to wells documented in location map (Fig.4.15).	64
• Figure 4.35 Spatial distributions of $\delta^{18}\text{O}$ values in the alluvial aquifer Vega de Granada with mean $\delta^{18}\text{O}$ values of sampled rivers.	66
• Figure 4.36 $\delta^{18}\text{O}$ (‰-VSMOW) vs. δD (‰-VSMOW) diagram of thermal springs.	68
• Figure 4.37 Deviation in $\delta^{18}\text{O}$ (‰-VSMOW) from the WMMWL vs. water temperature ($^{\circ}\text{C}$) of thermal springs samples.	70
• Photo 5.1 Panoramic view of open gold mine near Lancha de Cenes (Mina de Oro X 450 867 Y 4 113 962 viewpoint NNE).	72
• Figure 5.2 Sketch of the geological history of the eastern border of the Granada basin and the Sierra Nevada showing the stratigraphic architecture of the corresponding conglomerate units. (modified after MARTIN & BRAGA 1997).	72
• Photo 5.3 Uninhabited cave dwelled in the unconsolidated Alhambra formation (X 450 540 Y 4 113 864).	73
Figure 5.4 (a) Sketch of the northern hillslope of the Alhambra showing the small-scale faults (saw-shaped black lines) observed in the field, as well as the main cracks (black lines) in the fence and wall. (b) Decametrescale faults affecting a palaeosol. Displacement of these faults is approximately 50 cm. (c) Three decametre-scale faults underlying the fence of the Alhambra. The fence is collapsed in relation to one of these faults. (d) Cracks in the fence of the Alhambra situated just over a metre-scale fault in the conglomerate. Note palaeosol rotated in the hanging wall of the fault. (e) Metre-scale fault in the Alhambra conglomerate. Note the fractured clast in the upper part of the fault zone (red rectangle and magnification to the right). (f) Decimetre-large fault zone with a broken and displaced clast (red rectangle and magnification to the right). Clast is approximately 5 cm long. (g) Crack in the Mohamed tower. (Azañon et al 2004).	73
• Figure 5.5 Relationship between shape and lithology (after VALLETON 1955)	74
• Figure 5.6 Recent stressfield in the Granada basin (modified after GIL 2002). Crosses indicate uplift, minus indicate subsidence. Geology simplified from IGME 2002.	76
• Photo 5.7: Red and grey conglomerates from the Alhambra formation and normal fault with strike NW – SE and dip 80° to SW (at 449 500 / 4 114 490).	77
• Figure 5.8 Rose diagram showing the dip direction of the measured faults.	77
• Photo 5.9 Small scale thrust (at 448 488 / 4 114 700) with cm scale displacement. (Hammer length 35 cm).	78
• Photo 5.10 Topographic steps in the Alhambra Formation (at 449 694/4 115 920, viewpoint to NW).	78
• Photo 5.11 1m^2 of the Alhambra formation.	80
• Photo 5.12 Sedimentological development from coarse conglomerates to soil and, divided by erosional contact, again coarse grained conglomerates. Alhambra formation(Hammer length ca. 35cm).	80
• Photo 5.13 Tractive deformation of the Alhambra formation (Hammer length ca. 35cm).	80
• Photo 5.14 Broken micaschist clast in the Alhambra formation.	80
• Figure 5.15 Relationship between lithology and shape of clasts in the Alhambra formation (after VALLETON 1955).	81

Table of content

Photo 5.16 Striaes on sedimentary surface on listric fault plains, red Sandstones formation (X 450 643; Y 4 115 537).	82
• Figure 5.17 Angular discordance and normal faults at Barr. de Teatino (at 450 794/4 115 740, viewpoint to NW).	82
• Figure 5.18 Profile Ia: Rio Darro stratigraphic and sedimentological profile (0-40 m).	84
• Figure 5.19 Profile Ib: Rio Darro stratigraphic and sedimentological profile (40-80 m).	85

List of tables

• Table 1.1 Name, ID and catchment area of Rio Genil watershed.	8
• Table 3.1 Overview of sampling campaigns in chronological order and measured parameters.	21
• Table 4.1 Summary of group 2 physical parameters and saturation indices.	32
• Table 4.2 Summary of group 3 physical parameters and saturation indices.	35
• Table 4.3 Summary of group 4 physical parameters and saturation indices.	38
• Table 4.4 Mean weighted $\delta^{18}\text{O}$ and δD values for the hydrological year, - winter and –summer at Gibraltar station (1962-2001). IAEA-GNIP 2004 data.	43
• Table 4.5 Mean weighted $\delta^{18}\text{O}$ and δD values for the hydrological year, - winter and –summer at Generalife station (Dec.1999-Nov.2002). GARRIDO 2003 data.	45
• Table 4.6 Average $\delta^{18}\text{O}$ values, maximum error and average recharge altitude for Sierra Nevada springs and Granada basin springs (cursive).	52
• Table 4.7 Average $\delta^{18}\text{O}$ values, maximum error and average recharge altitude for Sierra de la Peza springs.	52
Tab.4.8 Sites, type, date of sampling, $\delta^{18}\text{O}$, δD (‰-VSMOW), corrected values without evaporative enrichment for $\delta^{18}\text{O}$ (‰-VSMOW) in wells and observation wells and the resulting evaporative enrichment.	64
• Tab.5.1 Neogene stratigraphy with stage ages from 2004 (IUGS 2004) and stage ages from 1975 and stratigraphic ranges of formations in the mapping area.	71
• Tab.5.2 Main features of debris flows (modified after Füchtbauer 1989).	79

1 Introduction

This work is divided in two parts, the diploma thesis and the geological mapping. The work tries to collect existing data as well as it provides new data concerning hydrochemistry and hydrogeology of the aquifer systems in the study area. The main objectives of this work are:

Diploma thesis:

- Taking water samples (springs, wells, surface water and precipitation) for AAS and ICP-MS analysis as well as $\delta^{18}\text{O}$ and $\delta^2\text{H}$.
- Establishing a network of spring- and river-sites at different altitudes for frequent and single sampling.
- Using an ACCESS database to manage the hydrochemical and isotope data.
- Collect and check available data concerning hydrogeology and hydrochemistry.
- Interpretation of hydrochemical data with PHREEQC 2.11.
- Interpretation of isotope data for a better understanding of the groundwater recharge for the *Vega de Granada* aquifer.
- Use of available information of the area for generating a Digital Elevation Model (DEM).

Mapping:

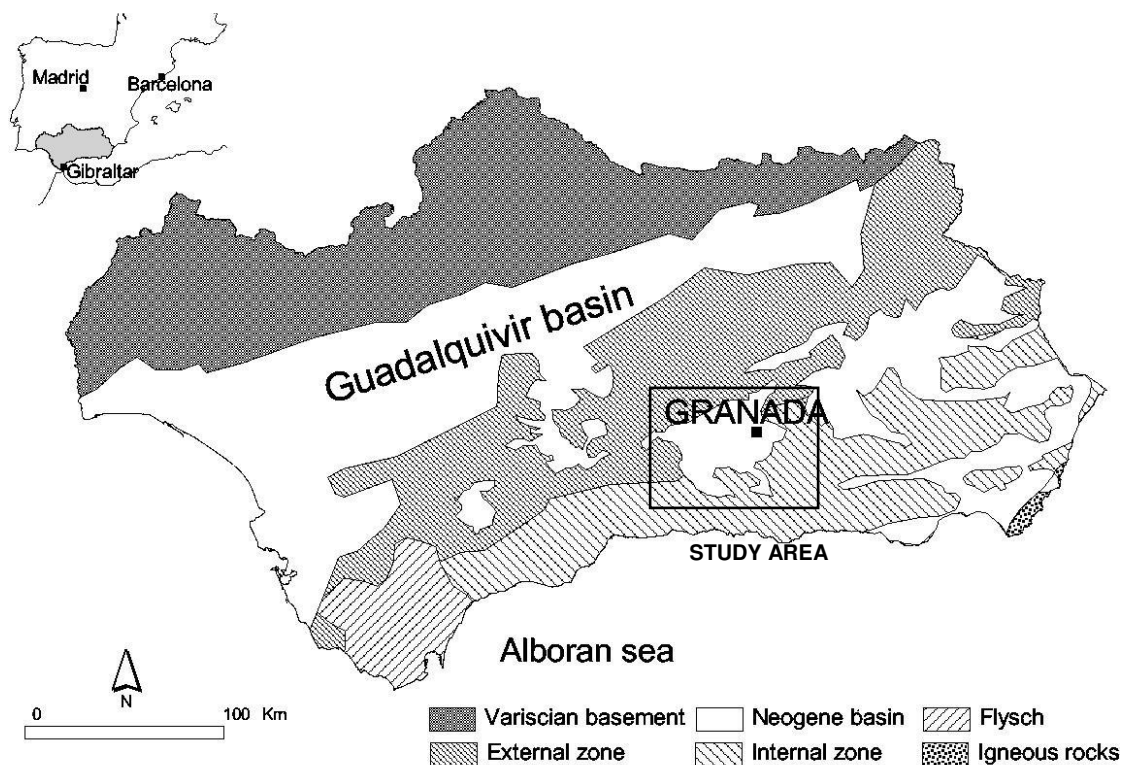
- Description of the stratigraphic sequence, geological formations and structural elements of the mapping area.
- Present a geological map of the formations in scale 1:20 000 (paper copy) generated with ArcGis 8.2.

1.2 Regional geological setting

The Betic-Rif mountain belt, located in southern Spain and northern Morocco, form an alpine orocline, which now joins at the strait of Gibraltar. This belt was developed from late Mesozoic to Cenozoic within a convergent stress regime between Africa and Iberia¹. The cordilleras are separated by the Alboran Sea, which consists of extended Neogene continental crust. The Betic-Rif orogen is, among other Mediterranean mountains, characterised by coeval shortening and extension during late stages of orogenesis. Traditionally, the rocks of the Betic-Rif orogen are divided into three zones: a) Internal Zone, b) External Zone and c) Flysch (Fig. 1.1).

The Internal Zone consists of metamorphosed Palaeozoic and Mesozoic rocks separated by several Neogene intramontane basins (e.g. the *Granada* basin). Structurally rocks of this zone were grouped, together with other metamorphosed belts, behind a north dipping subduction zone (Fig.3.2 top). From early Miocene (23-20 Ma) subduction rollback occurred in the western mediteranean and caused a counterclockwise rotation of this metamorphosed belts to their current positions (LONERGAN & WHITE 1997). The Internal Zone can be subdivided into three complexes of variable metamorphic grade. From bottom to top: (a) Nevado-Filabride, (b) Alpujarride and (c) Malaguide¹.

a) this complex crops out in large anticlinal structures that form, among others, the uppermost part of *Sierra Nevada*. It is made up of metamorphic rocks with mainly dark colours and variable lithology, which are micaschists, quartzites, gneisses, marbles, amphibolites, eclogites



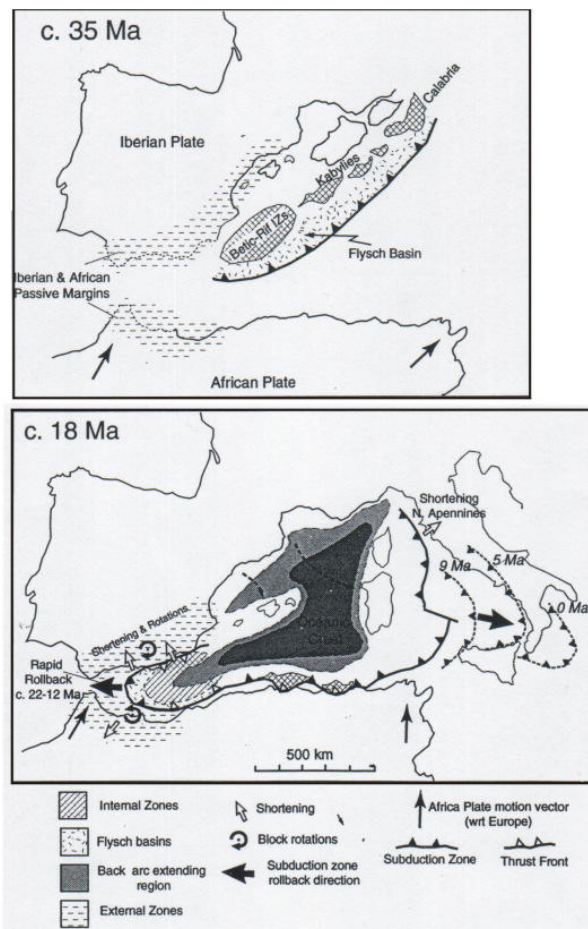
• Figure 1.1 Geological sketch of Andalusia showing the threefold division of the Betic Cordillere (External Zone, Internal Zone, Flysch). The rectangle indicates the study area. Geology simplified from IGME 2002.

¹ AZAÑON et al 2002

and serpentinites. This sequence is not good dated but associated to the Paleozoic¹ and builds the metamorphic core.

b) this complex crops out largely around the *Nevado-Filabride* and consists of metapelitic-metapsammitic formations, attributed to the Paleozoic but predominantly of calcareous and dolomitic rocks aged to middle to upper Triassic¹. The carbonatic rocks are moderate karstified¹. Most of the spring sites are located within this unit.

c) this complex consists of low-grade metamorphed carbonate and siliciclastic rocks associated to Paleozoic until Palaeogene ages¹. This unit crops out around *Malaga* and plays no important hydrogeological role in the study area.



• Figure 1.2 Geologic evolution of the Betic-Rif mountain belt (LONERGAN & WHITE 1997).

The External Zone consists of Mesozoic and Palaeogene sediments, which were deposited in a basinal- (Subbetikum) and a shelf-facies (Prebetikum) on the Iberian and the Maghrebian palaeomargin of the Thetys Ocean (Fig.1.2 top). These rocks were deformed by northwest directed thrusting and folding during early to late Miocene¹. The Flysch nappes consists of Cretaceous² to Miocene deep-water sediments in flysch-facies, now concentrated in the western parts of the Betics (around Gibraltar). The Guadalquivir basin, located to the north of the Betics, is filled with Neogene sediments and is interpreted as the Betic foreland basin¹. Further to the north the Variscian basement crops out and builds mid-range mountainous areas known as the Sierra Morena. The Internal/External Zone border is now buried under the sediments of the *Granada* basin. The *Granada* basin is an intramontane depression filled with sediments from

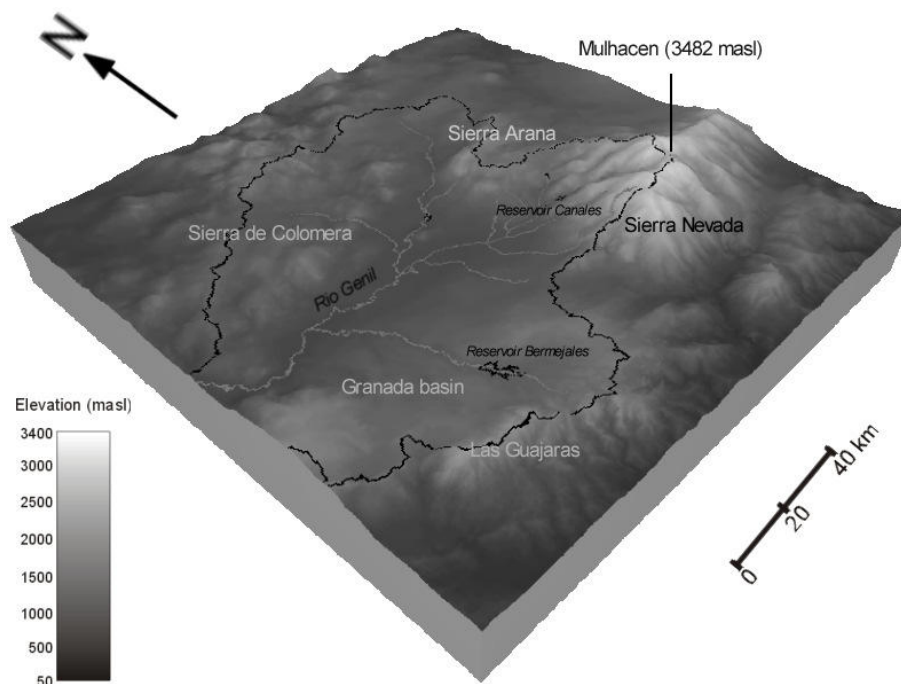
early Burdigal (lower Miocene, 20 Ma) to Quaternary¹. The sedimentary infilling is up to 2km thick. Geophysical data show that the *Granada* basin is a large half-graben structure, thickening northwards and limited by normal faults striking ENE-WSW, NW-SE and dipping to S. In early Tortonian (11.5 Ma) time the Alboran sea covered most of the Betic Cordillera and the area now called “*Granada* basin“(Fig.1.2). Sediments of this period can now be found at >1500masl near *Granada*. During the middle Tortonian (9 Ma) the sedimentary environment became more homogenous towards widespread platform calcareous sandstones and calcarenites (BRAGA et al. 1990). During the upper Tortonian (8 Ma) increasing

¹ Azañon et al 2002

geomorphodynamic took place at the eastern and north-eastern margins of the basin (e.g. DABRIO et al. 1978) and form a paleogeography similar to nowadays. Although the basin remains marine influenced and coral reef development is reported (BRAGA et al. 1990). Beginning at the Tortonian-Messinian boundary (7 Ma) the basin was gradually isolated from the sea due to uplift processes in the southern and western edges. At this time the basin was eventually dried up (Messinian salt crisis). Later a period of lacustrine sedimentation (upper Messinian, 6 Ma) took place. Since the Pliocene (5 Ma), the onshore Neogene basins (e.g. Granada basin) underwent rapid uplift, induced by continued convergence stress between Africa and Eurasia and/or slab break-off (LONERGAN & WHITE 1997) and leading later to a stage of detrital continental deposition (Pliocene and Quaternary).

1.3 Geomorphology

In general the morphology of the *Granada* region is a product of folding, faulting and erosive processes over geological time. The most dominant morphological feature is a elongated dome named *Sierra Nevada*, with altitudes from 900-3400 m above sea level (masl) and the highest mountain of the Iberian Peninsula named *El Mulhacen* (3482 masl) (Fig.1.3). To the north the *Sierra Arana* builds a shallower mountain range (with altitudes from 800-1800 masl). To the west the relative flat *Granada* basin stretches over a length from N-S ca.40km and E-W ca.55km with altitudes from 500-800 masl. The shallow mountains range *Las Guajaras* with moderate altitudes of 800-1500 masl follows in the south.



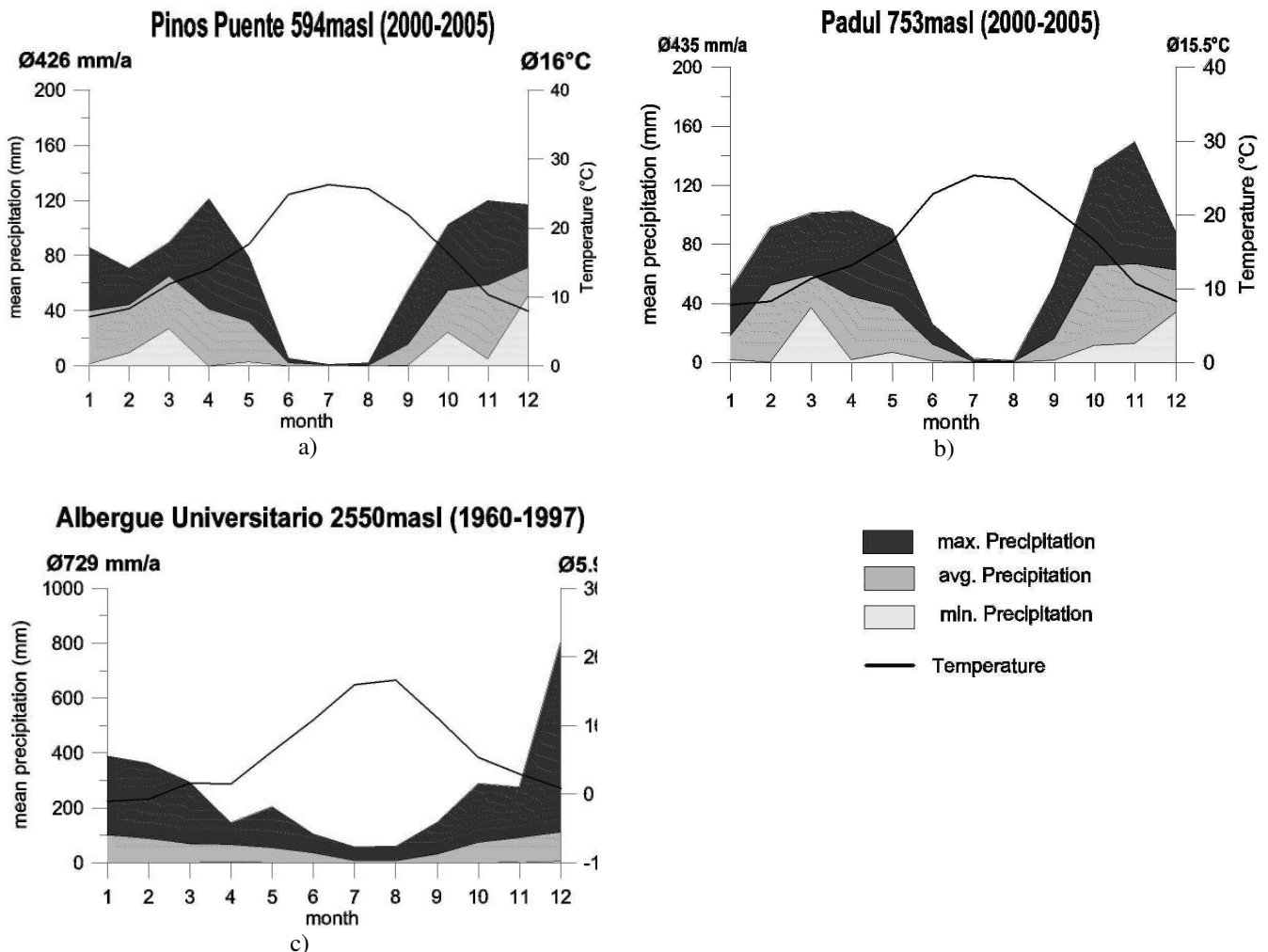
• Figure 1.3 Digital elevation model (DEM) of the *Granada* basin and the surrounding mountain ranges with the catchment area of the *Rio Genil*. (DEM derived from Mapa Digital Andalucia 2002).

From the origin of the *Rio Genil* in the *Sierra Nevada* to the end of the *Granada* basin the river courses over a length of ca. 90km. The *Rio Genil* flows into the river *Guadalquivir* and finally in the Atlantic sea. The entire catchment area of the *Rio Genil* extends largely over the study area and is printed only in parts (Fig.1.3). According to the catchment delineation, only

ca. 23% of the surface of the *Sierra Nevada* is drained by the catchment area of the *Rio Genil*. The catchment area can be subdivided into several sub basins.

1.4 Climate, Meteorology

The Granada region has a Mediterranean climate with a slight continental tendency (CASTILLO 1986) following a yearly weather pattern: dry hot season from June to October, and moderate cold wet season from November to May.

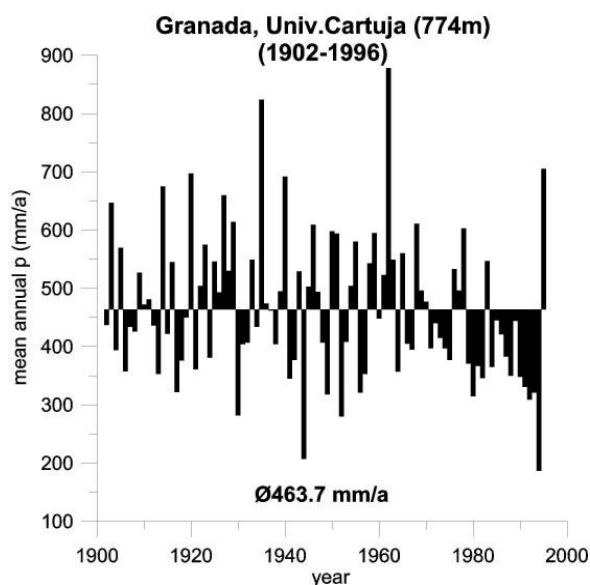


• Figure 1.4 (a-c) Climate diagrams of selected stations. (Data derived from www.juntadeandalucia.es)

The temperature course of all the meteorological stations shows a maximum from July-August and a minimum from December-January (Fig.1.4, a-c). The study area is generally characterized by strong variations in the climate. The average temperature, in the *Granada* basin lies between 15 and 16 °C, while in the high regions of the *Sierra Nevada* (*Albergue Universitario* 2550 masl) average temperatures range between 5 – 6 °C. These variations are caused by differences in elevation, spatial position and the environment around the stations. Most of the precipitation (from >20 up to more than 180 mm/month in single months) falls in few heavy rain events in rainy periods (October to March). December is the wettest month, followed by March. The driest period is around July with rainfall less than 10 mm per month, sometimes just 0-5 mm. During a 5-7 month period the potential evapotranspiration exceeds

the monthly amount of precipitation which leads to the definition of a semiarid climate in the *Granada* basin. The average decrease of air temperature with increasing altitude depends both on seasonal and regional variations. In winter, the gradients are (slightly) lower than in summer, because of frequent temperature inversion during cold season. This atmospheric boundary layer (ABL) is the bottom layer of the troposphere that is in contact with the surface of the earth. It is often turbulent and is capped by a statically stable layer of air or temperature inversion. The ABL depth (i.e., the inversion height) is variable in time and space, ranging from tens of meters in strongly statically stable situations, to several kilometres in convective conditions over deserts (STULL 1988).

More than 75% of the precipitation in the *Sierra Nevada* above 2000m falls as snow (CASTILLO 2000). Between December and March a continuous snow cover exists above 2200 masl and even in summer snow patches at shady slopes exist.

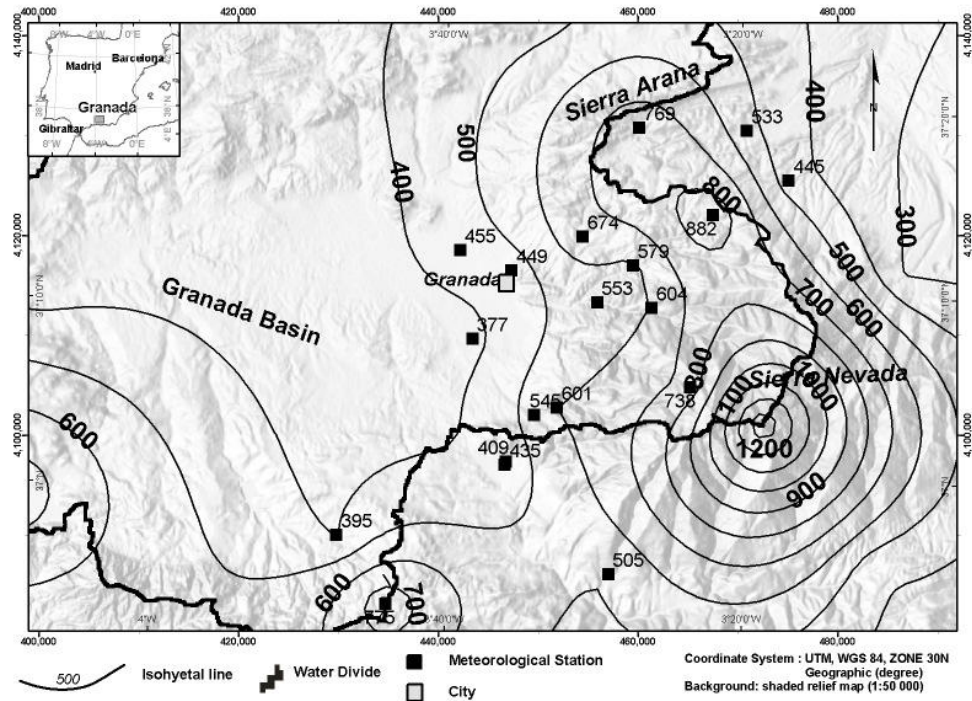


• Figure 1.5 Year to year variations from average annual of annual precipitation in the city of *Granada* (Data derived from IGME 2000).

There are considerable variations in the quantity of the annual rainfall from year to year. The average annual rainfall at *Universitario Cartuja* Meteorological Station in the city of Granada for the period 1902–1997 is 463.7 mm. The maximum recorded annual rainfall was 880 mm in the year 1962, while the minimum was 190 mm in 1994 (Fig.1.5).

The predominately weather situation in the winter months are two high pressure cells over the Azores and Russia and a low pressure cell over the British islands. This produces a circulation, bringing rain bearing air masses from the North Atlantic. In the summer months often a low pressure zone lies over the Iberian Peninsula.

In the *Granada* region, the dominant travel direction of rain bearing air masses is from the west towards the east. Rainfall increases eastwards with elevation, with the maximum rain amount at the peaks in the *Sierra Nevada* (2000-3400 masl). Further, to the east, at the lee side of the mountains, there is a decline in rainfall amounts as air masses are heated, decreasing the relative humidity and resulting in a rain shadow. The Isohyetal map (Fig. 1.6) shows annual precipitation averages of the *Granada* region during different time periods. As shown in figure 1.6 mean annual precipitation amounts in the *Sierra Arana* are in the highest region about 700 - 800 mm. Mean annual precipitation in the *Granada* basin is around 500 mm.

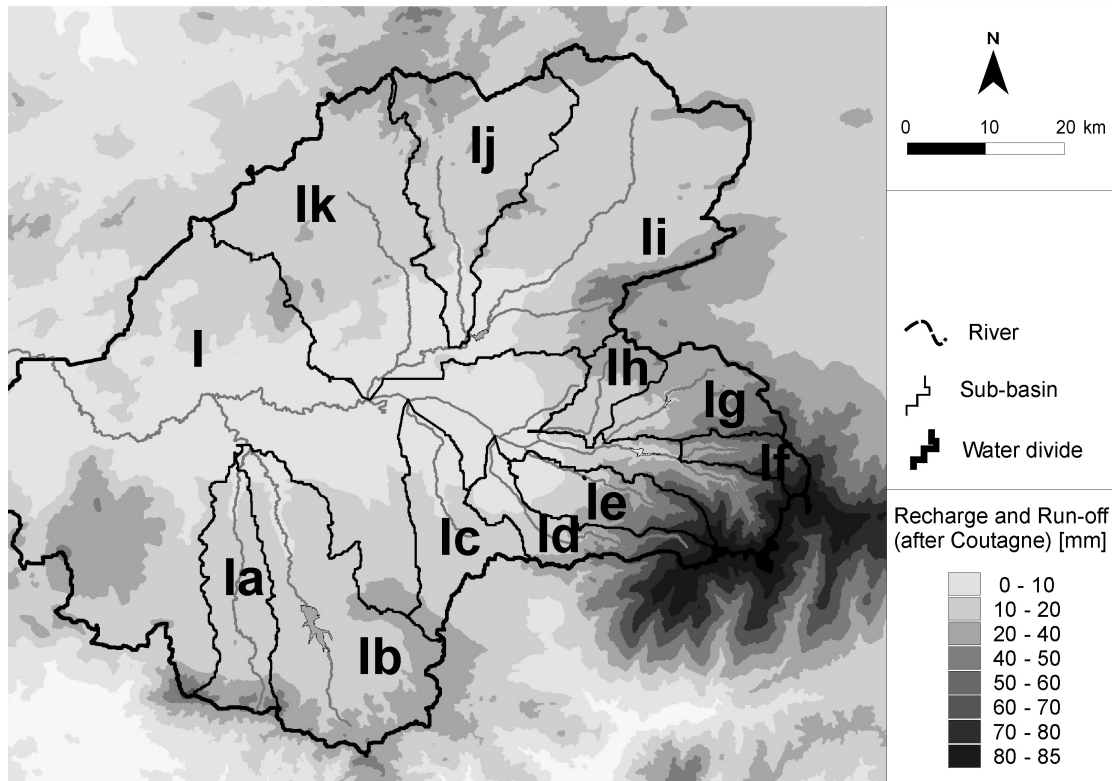


• Figure 1.6 Isohyetal contour map of annual precipitation averages of the *Granada* region calculated with records of the indicated meteorological stations from various time periods (Data shown in Appendix 1, table a1.1)

The isohyetal contour map was calculated according to data shown in appendix 1, table a1.1. Methods are explained in section 3.4.

2.1 Groundwater recharge

As expected for a semiarid area with limited precipitation groundwater recharge (GWR) in the *Granada* basin itself is very low and close connected to rainy seasons. Appendix 2 (Table a2.1 - Table a2.6) shows that the actual evapotranspiration (ETA) of 6 climate stations calculated according to Turc (GRAY 1973) and Coutagne (REMENIERAS 1974) equations (for methods see section 3.4.1). Generally Turc provides higher ETA values than Coutagne and results in negative GWR for almost all months and stations. Thus Coutagne equation is used for calculation.



• Figure 2.1 GWR map and extend of the *Rio Genil* catchment area and the tributary sub-basins.

In the basin ETA almost equalled precipitation (97-98%) and only an average of 5-10 mm/a remains for groundwater recharge. In the *Sierra Nevada* GWR is considerable higher (ca. 61.6mm/a) but due to the lack of more meteorological stations no detailed calculations are possible. Main water surplus occurs during rain periods between October to March (maximum in December 3.9 mm/month) in the basin and maximum 15.5 mm/month (January) in the *Sierra Nevada*. During the dry season around June very little to no surplus occurs at all in the basin and little in the *Sierra Nevada*. Taking into consideration the high uncertainty of

• Table 1.1 Name, ID and catchment area.

Name	ID	Area [km ²]
<i>Rio Genil</i>	I	1649.63
<i>Rio de Alhama</i>	Ia	173.73
<i>Rio Cacin</i>	Ib	403.76
<i>Arroyo del Salado</i>	Ic	167.78
<i>Rio Dilar</i>	Id	117.74
<i>Rio Monachil</i>	Ie	124.10
<i>Rio Maitena</i>	If	57.22
<i>Rio de Aguas Blancas</i>	Ig	139.82
<i>Rio Darro</i>	Ih	77.37
<i>Rio Cubillas</i>	Ii	765.5
<i>Rio de la Colomera</i>	Ij	319.27
<i>Arroyo de la Canada</i>	Ik	438.13
Σ (km²)		4434.05

the ETA calculations it is only possible to state that the groundwater recharge in the basin is very low, maybe even negative in the dry season while there maybe some minor recharge during the rain season. The main groundwater recharge is supposed to come from the *Sierra Nevada* east of the basin.

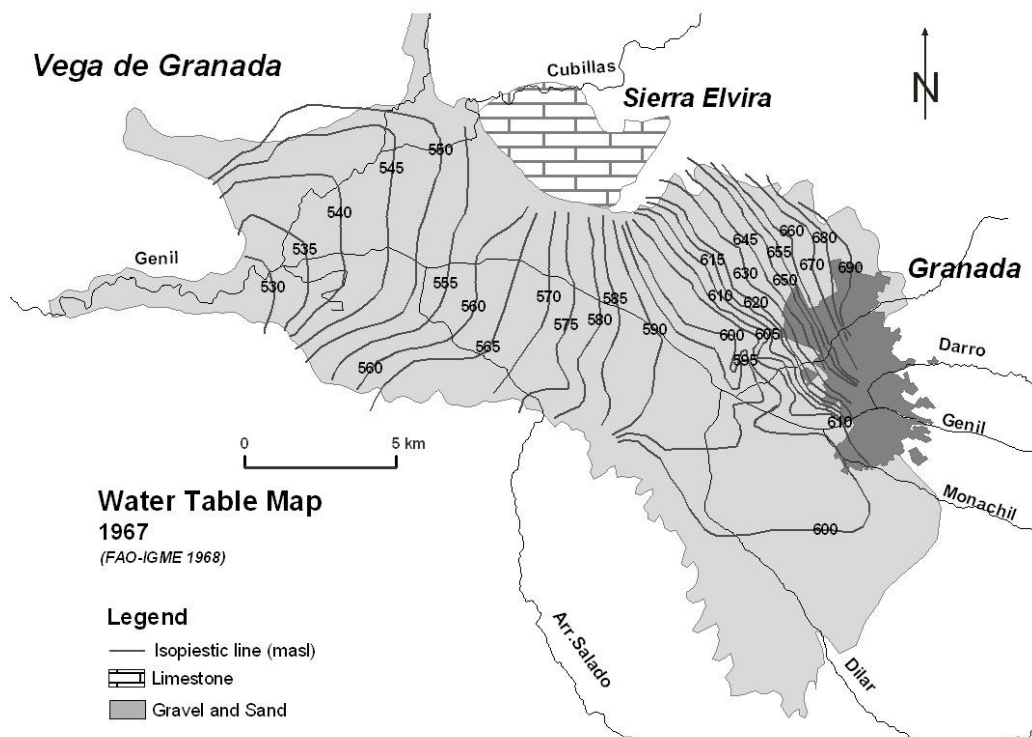
2.2 Hydrogeology

2.2.1 Alluvial aquifer (*Vega de Granada*)

Most of the previous published works is dealing with the hydrogeology of the *Vega de Granada* which is the most important aquifer. This area has been studied intensively (among others CASTILLO & FERNANDEZ-RUBIO 1985, DELGADO et. al 2002). Most of the works are about urgent problems of the aquifer like pollution by nitrates and microbiology, over exploration and vulnerability.

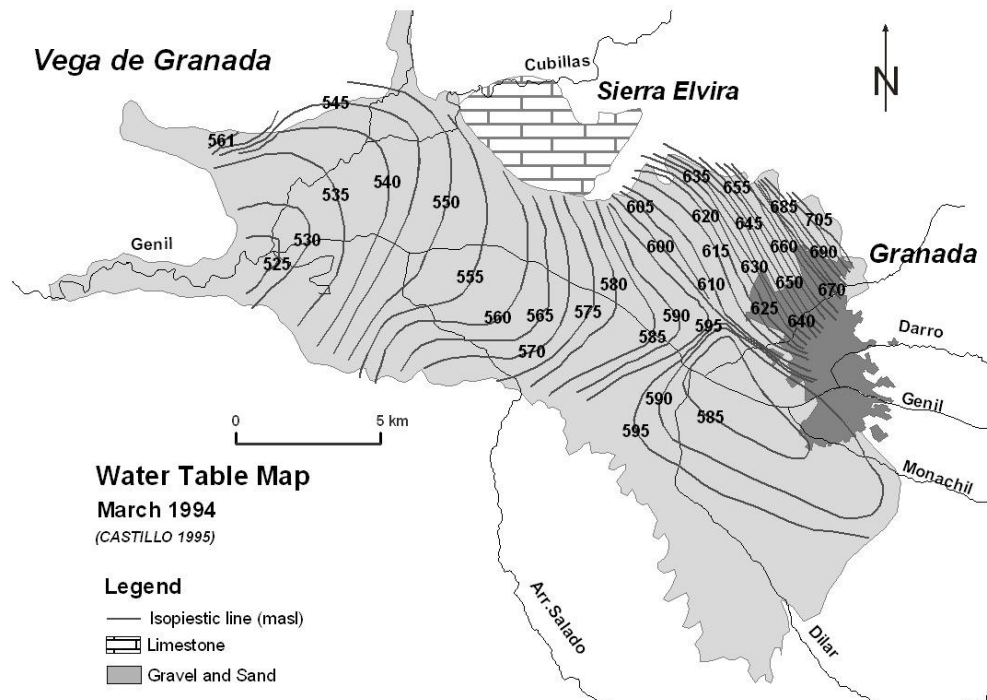
The *Vega de Granada* aquifer consists of alluvial material (Gravel, Sand, Silt, Conglomerates) deposited by the rivers *Monachil*, *Darro*, *Dilar* and, most important *Genil*. The aquifer surface occupies an area of approx. 200 km² (22 km x 8 km) and in the centre a thickness of approx. 250 m is reported.

Since prehistoric time the *Vega de Granada* is settled and humans favoured this area due to the good fertility (HAARMANN 2001). In the time of Arabian domination (8th – 15th century) an irrigation network (*Acequias*) was designed and installed which is, with minor modifications, still in use until today. The Spanish word *Vega* means cultivated land and irrigation plays an



• Figure 2.2 Water table trend map from 1967 (FAO-IGME 1968).

important role in the hydraulic balance. Nowadays in the area several plants are cultivated, like tobacco, poplar grove, cereal, corn and vegetables (CASTILLO 1993).



• Figure 2.3 Water table map from March 1994 (CASTILLO 1995).

First groundwater table surface measurement was carried out in 1967 (Fig.2.2, FAO-IGME 1968). It must be considered as a general trend map, since the period of measurement was given for a whole year (1967). This first groundwater table trend contour map represents the hydraulic regime without important anthropogenic impact on the flow system. Main hydraulic characteristics can be recognized: the isopiestic lines are relative close together in the north-eastern part of the *Vega de Granada*, due to low permeabilities of the aquifer (hydraulic gradient 1.5 %). Higher permeabilities are visible in the south-eastern part of the *Vega de Granada* (hydraulic gradient 0.2 – 0.4 %). The groundwater follows the general regional hydraulic gradients indicating an approximated E-W flow direction. The aquifer system underwent important changes in the water balance during the last century. These changes are connected to the building of the reservoirs (Reservoirs of *Quentar* 1973 and *Canales* 1988), changes in the irrigation techniques and the development in urbanisation. Changes are reflected by the groundwater table contour map from March 1994 (Fig.2.3, CASTILLO 1995). Here, in the south-eastern part a groundwater drawdown due to pumping can be observed. A decrease in the water table evolution from 1967 to 2001 is stated in IGME 5.32 2001.

Lateral limits are considered to be open boundaries to the relative low permeable deposits of the Mio-/Pliocene units in the S, E and NE. The horst structure of the *Sierra Elvira* carbonate rocks represents a potential recharge area at the central northern border of the aquifer with open boundary characteristics. General water balance considerations taken from IGME 5.32 2001 are:

Input flow:

- Direct infiltration by rainfall over permeable surface.
- Indirect infiltration by river bed recharge from the (sub-) basins (*Genil, Monachil, Dilar, Darro, Cubillas*).
- Indirect infiltration by the irrigation network (*Acequias*) losses.
- Indirect infiltration from the irrigation network.
- Lateral inflow by surface runoff from less permeable material of the *Mio-/Pliocene* unit.
- Lateral concealed inflow by the *Sierra Elvira* carbonate system.

Outflow:

- Drainage by rivers (*Genil, Cubillas*), irrigation channels (*Acequias*) and springs.
- Pumping stations for irrigation, urban and industrial demands.

Annual GWR is calculated by various authors (e.g. CASTILLO 1995, IGME 5.32 2001) and is considered to be 232 hm³/a total. A publication by CASTILLO 1995 estimates that 70 % of GWR is derived from infiltration of surface runoff water from the *Sierra Nevada*. This results in predominated high quality hydrogencarbonate water facies in the eastern and especially in the south-eastern part of the *Vega de Granada* (compare to section 4.1.2). Other parts of the aquifer are characterised by an increase in salinization (e.g. centre and southern part of the aquifer) (CASTILLO 1986).

2.2.2 Mio-/Pliocene basin deposits

This very heterogeneous unit covers most of the area of the *Granada* basin (1350 km²). The geology is divers and can be described as sedimentary sequences of an intramontane basin. These sequences include marine sediments, such as carbonates and evaporates and terrigenous sediments, such as conglomerates and sandstones. Not much data about the hydrogeological units of the Mio-/Pliocene basin sediments is available. In IGME 5.32 2001 considered to have 50 hm³/a GWR derived from rainfall on the area. Additionally, a not quantified flux of lateral and vertical groundwater flow derived from unknown origin was identified.

2.2.3 Carbonate terrains (*Sierra de la Peza, Sierra de Padul, Sierra Arana, Sierra Elvira*)

The hydrogeological unit *Sierra de la Peza* and *Sierra de Padul* consists of material from the *Alpujarride* complex which are limestone, dolomite, marble and calcareous schists. The units are moderate fissured and carstified. Within the *Sierra de la Peza* unit minor Jurassic carbonate formations of the *Subbetics* (External Zone) can be found. The carbonate terrains are considered to be unconfined aquifers with high permeabilities due to carstification. Carbonate units of the *Alpujarride* together with formations of the *Subbetics* form the northern limit of the *Sierra de Padul* unit to the *Sierra Arana* unit (IGME 5.30 2001).

Precipitation is the exclusive input for GWR and discharge takes place at the open boundaries.

In the north-eastern part of the *Sierra de la Peza* a strong discharge to the southeast, expressed as high discharge spring, in altitudes at ca. 1100 masl are observed. Important springs in this area are: *Fte.de Nivar* (1080 masl), *Fte.Grande* (1114 masl). Important springs are situated within this unit: e.g. *Nacimiento Rio Darro* situated at the boundary between the *Alpujarride* and postorogene silts (Serravielense). An N-S directed flow is estimated in the sub basin of the *Rio Darro*. No data about the piezometric evolution or exploitable water amounts of this aquifer are available (IGME 5.31 2001).

2.2.4 Metamorphic terrains (*Nevado Filabride*)

The metamorphic terrain (*Nevado Filabride*) consists of various schists (micaschists with chloritoids, garnet micaschists with andalusite) and quartzites. The schists are of low permeability, but in the *Nevado-Filabride* glaciogenic altered material is common. CASTILLO 2001 discusses the “Hydrogeologic behaviour of hard rocks affected by glacialism and periglacialism in the Sierra Nevada”. Here, high transmissivities of $1.5 - 8 * 10^{-2} \text{ days}^{-1}$ are reported.

2.3 Stable isotopes in hydrogeology

Differences in the stable isotopic signature of snow, rainfall, surface water and groundwater is used to quantify and qualify e.g. groundwater recharge, residence time or groundwater recharge provenances and is a widespread tool in hydrogeology. An introduction of the processes of stable isotopes in hydrogeological systems gives CLARK & FRITZ 1997.

2.3.1 Isotope fractionation

Isotopes are atoms of the same element with differences in their number of neutrons. All possible combinations of stable hydrogen (^1H , ^2H or D) with stable oxygen isotopes (^{16}O , ^{17}O , ^{18}O) occur in natural water, but only H_2^{18}O , HD^{16}O and the ordinary H_2^{16}O are due to their natural abundances of analytical relevance (IAEA 2000). All isotope results are reported in $\delta^{18}\text{O}$ and δD ($\delta^2\text{H}$) notation, representing per mil (‰) deviation from the Vienna Standard Mean Ocean Water (VSMOW):

$$\delta_{\text{sample}} (\text{‰}) = \left(\frac{R_{\text{sample}} - R_{\text{reference}}}{R_{\text{reference}}} \right) \cdot 1000 \quad (\text{e.g. } R_{\text{H}_2\text{O}} = \frac{\text{H}_2^{18}\text{O}}{\text{H}_2^{16}\text{O}}) \quad (\text{eq.2.1})$$

R is always defined as the ratio of the heavier to the lighter isotope. The VSMOW standard is a mixture of distilled ocean water with small amounts of ocean water (IAEA 2000). The variations of the ^{18}O and ^2H concentrations are controlled by fractionation during evaporation and condensation. This phase transition reactions can take place under equilibrium conditions or non-equilibrium (kinetic) conditions.

a) equilibrium fractionation

The variations of HD^{18}O and H_2^{18}O during fractionation are expressed by the ratios of the vapour pressures α :

$$\alpha = \frac{R_1}{R_2} \quad \text{e.g. } \alpha_{\text{water - vapour}} = \frac{R_{\text{water}}}{R_{\text{vapour}}} \quad (\text{eq.2.2})$$

α expresses the isotope ratio R_1 in the reactant phase ($R_1 = (\text{H}_2^{18}\text{O})/(\text{H}_2\text{O})$ for ^{18}O or $R_1 = (\text{HD}^{18}\text{O})/(\text{H}_2\text{O})$ for D) relative to R_2 in the product phase. At 20°C, α for $\text{H}_2^{16}\text{O}/\text{H}_2^{18}\text{O}$ is according to KAKIUCHI AND MATSUO 1979 (eq.2.4, eq.2.5) 1.0835, while α for oxygen fractionation between water and vapour at the same temperature is 1.0099. Due to the very little variations in isotopic fractionation the deviation of α from 1 is commonly used. This enrichment factor ϵ , is defined as $\epsilon (\text{‰}) = (\alpha - 1) \cdot 10^3$. ϵ represents the enrichment ($\epsilon > 0$) or the depletion ($\epsilon < 0$) of the rare isotope in the reactant with respect to the product. The relationship between α and the δ notation is then:

$$\alpha_{\text{water - vapour}} = \frac{\delta_{\text{water}} + 1000}{\delta_{\text{vapour}} + 1000} \quad (\text{CLARK \& FRITZ 1997}) \quad (\text{eq.2.3})$$

The temperature dependence of α is defined according to KAKIUCHI AND MATSUO 1979 for $\delta^{18}\text{O}$:

$$10^3 \ln \alpha = \frac{5.97 \cdot 10^6}{T^2} - \frac{32.80 \cdot 10^3}{T} + 52.22 \quad (\text{eq.2.4})$$

and for δD :

$$10^3 \ln \alpha = \frac{2.40 \cdot 10^6}{T^2} + \frac{64.55 \cdot 10^3}{T} - 168 \quad (\text{eq.2.5})$$

where T is temperature in kelvins. Vapour evaporating from ocean water, with an defined isotopic composition of 0 ‰ relative to the VSMOW scale, would be only under equilibrium conditions, depending on temperature 8 to 10 ‰ depleted in ^{18}O (T = 40 °C, $\epsilon = 8.4$ ‰; T = 20 °C, $\epsilon = 9.9$ ‰, eq.2.4;eq.2.5).

The equations 2.4 and 2.5 are useful for calculating the degree of equilibrium exchange from water with vapour. Since vapour evaporated from the ocean show enrichments of around $\epsilon = -12$ ‰ a second process, the non-equilibrium or kinetic fractionation must be considered. Isotopic fractionation between a liquid and vapour is an equilibrium process **only** when the vapour is saturated with respect to the liquid. Fractionation caused by evaporation in natural processes can be considered as a non-equilibrium process, while only weak indications of kinetic isotope effects were observed in condensation processes (DANSGAARD 1964).

b) non-equilibrium fractionation (kinetic)

Kinetic fractionation results from a “one way” physical or chemical reaction, e.g. evaporation of water with instant withdrawal of the vapour and therefore avoiding further contact to the water. Kinetic fractionation is influenced by the surface temperature, wind speed, salinity, and most important: humidity. At lower humidity, water-vapour exchange is minimized, and evaporation becomes an increasingly non-equilibrium process. This inverse kinetic isotope effect occurs most commonly in reactions involving hydrogen atoms (BIGELEISEN & WOLFSBERG 1958) and results in evaporation lines which differ in the slope to the GMWL. GONFIANTINI 1986 describes the kinetic fractionation in relation to humidity with the following equations:

$$\epsilon^{18}\text{O}_{\text{kinetic}} = 14.2 (1-h) (\times 10^3 \text{‰}) \quad (\text{eq.2.6})$$

$$\epsilon^{2}\text{H}_{\text{kinetic}} = 12.5 (1-h) (\times 10^3 \text{‰}) \quad (\text{eq.2.7})$$

where h is the humidity (100% = 1). The total fractionation between the water body and the open air is then the sum of the fractionation factor for equilibrium water-vapour exchange ($\epsilon_{\text{equilibrium}}$) and the kinetic factor ($\epsilon_{\text{kinetic}}$). For $\delta^{18}\text{O}$ according to:

$$\delta^{18}\text{O}_l - \delta^{18}\text{O}_v = \epsilon^{18}\text{O}_{\text{equilibrium}} + \epsilon^{18}\text{O}_{\text{kinetic}} = \epsilon^{18}\text{O}_{\text{total}} \quad (\text{eq.2.8})$$

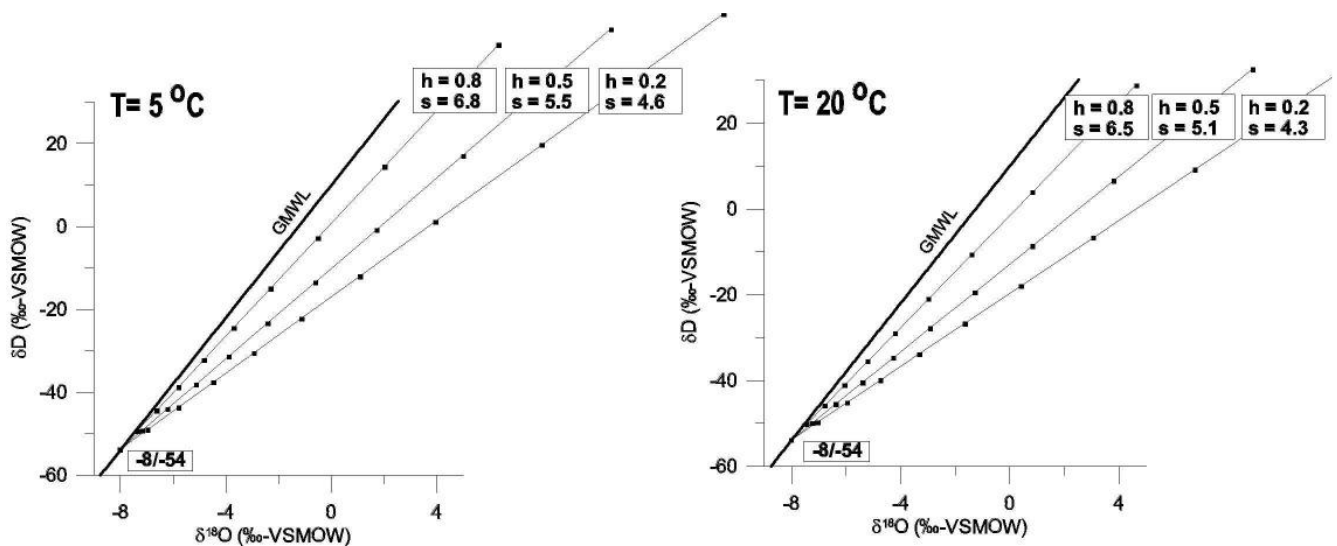
The indices l and v are for liquid and vapour, respectively. Since atmospheric water forms under about 85 % humidity a displacement of the evaporation line towards a d-excess (or intercept) is observable. If now evaporation rates are high due to high temperatures and low

relative humidity in the atmosphere at the initial formation of water vapour, a strong kinetic effect takes place and the d-excess is high (JOUZEL & MERLIVAT 1984).

Evaporation rates were calculated, according to a Rayleigh enrichment, in relation to temperature and humidity and plotted in $\delta^{18}\text{O}$ vs. δD diagrams (Fig.2.5), according to CLARK & FRITZ 1997:

$$\delta = \delta_0 + \Delta\epsilon_{\text{total}} * \ln(f) \quad (\text{eq.2.9})$$

where δ_0 is the initial value (here $\delta^{18}\text{O} = -8 \text{‰}$; $\delta\text{D} = -54 \text{‰}$) and δ is the resulting value. The resulting graphs (Fig.2.5) are useful to estimate the conditions during evaporation and the proportion of fractionation with factors f from 1 to 0.1. According to the above mentioned equations (eq.2.9) strong kinetic fractionation, due to low humidity ($h = 0.2$) and high temperatures ($T = 20 \text{ °C}$), result in more shallow slopes around 4.3. Higher humidity ($h = 0.8$) and lower temperatures ($T = 5 \text{ °C}$) results in evaporation lines which are closer to the GMWL and have slopes around 6.8.



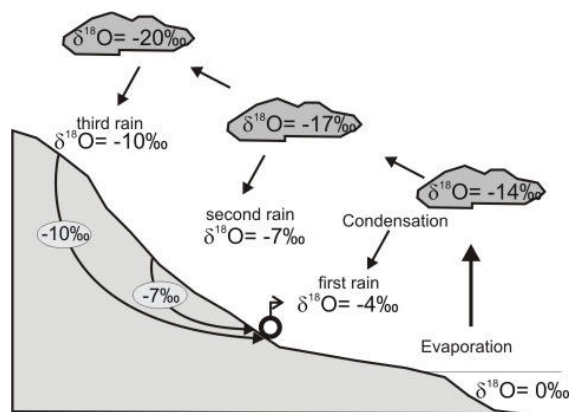
• Figure 2.5: Differences in evaporation rates in relation to humidity (h) in a $\delta^{18}\text{O}$ vs. δD (‰-VSMOW) diagram for 5 °C and 20 °C . showing the predominating exchange fractionation process at values for f from 1 to 0.1. (s = slope of evaporation line, Calculated according equation 2.9)

The strong correlation between temperature and $\delta^{18}\text{O}$ – $\delta^2\text{H}$ controls the position of precipitation on the meteoric water line. From this correlation it is possible to distinguish isotope effects due to season, altitude, amount and continentality — the basis of isotope hydrogeology.

temperature effect – with decreasing $\delta^{18}\text{O}$ values for precipitation with decreasing temperature. Temperature has the strongest effect on the isotopic composition due to the strong temperature dependence on the fractionation between vapour and liquid (CLARK & FRITZ 1997).

seasonal effect – often a seasonal change of the stable isotope ratios is observed as a result of temperature effects, different trajectories of air masses, and varying fractionation processes in the source area of atmospheric moisture, with more negative $\delta^{18}\text{O}$ values during winter (CLARK & FRITZ 1997).

altitude effect – often more depleted values of precipitation are observed at higher altitudes (Fig.2.6). This is the combined result of temperature effects and repeated rain-out.



• Figure 2.6: Altitude effect and mixing of groundwater in the spring water (modified after www.IAEA.org).

Equilibrium fractionation increases with lower temperatures, making fractionation more efficient at higher altitudes. Repeated rain-out during uplift of air masses causes a Rayleigh-type distillation process (CLARK & FRITZ 1997). The magnitude of this effect depends on local climate and topography. Gradients for the *Sierra Nevada* are between -0.2 and -1.3 ‰ ($\delta^{18}\text{O}/100\text{m}$) and -1 and -9 ‰ ($\delta\text{D}/100\text{m}$) (GARRIDO 2003).

amount effect - small amounts of rain are often enriched in heavy isotopes. No amount effect is observed in rain out events which exceed 20 mm/month (IAEA 2000). The factors that lead to a relationship between the amount of rainfall and the relative delta values are e.g.:

- with low amount of precipitation the degree of cooling below the cloud mass will be minimal. Because the below-cloud air temperature is high, there will be a significant amount of evaporation below the clouds. The light isotopes preferentially are incorporated into the vapour, leading in isotopically heavy rain (DANSGAARD1964).

2.3.2 The meteoric water lines

As shown in the previous section the forming of precipitation due to condensation can be described as an equilibrium process. Within the hydrological cycle, the ^{18}O and D stable isotopes of precipitation and fresh surface water correlate on a global scale. This linear correlation, as a best-fit line termed Global Meteoric Water Line (GMWL), is expressed as:

$$\delta^2\text{H} = 8 * \delta^{18}\text{O} + 10 \text{ (CRAIG 1961)} \quad (\text{eq.2.10})$$

This line is an average of many local or regional meteoric water lines, which vary from the global line due to different climatic and geographic parameters. Rain which condensates from water vapour at 20 °C, only under equilibrium conditions would be enriched by the factor $\epsilon^{18}\text{O} = -9.9 \text{ ‰}$ / $\epsilon \text{D} = -80 \text{ ‰}$. By calculating the ratio between $\epsilon \text{D} / \epsilon^{18}\text{O}$ we yield 8.1, which is close to the slope of the GMWL with $s=8$. The independent term of the equation 2.8 is a value for the deuterium excess (d-excess), which is therefore defined by:

$$\text{d-excess} = \delta^2\text{H} - 8 * \delta^{18}\text{O} \text{ (DANSGAARD 1964)} \quad (\text{eq.2.11})$$

Values for deuterium intercept (d-excess) range from 0 to 20 ‰ but can vary regionally due to variations in humidity, wind speed and sea surface temperature during primary evaporation (CLARK & FRITZ 1997). The d-excess is considered to be conservative and therefore useful for identifying the vapour source area. Air masses originated from the Mediterranean Sea have, due to low relative humidity and high temperatures, relative high d-excess value at about 14‰. While air masses from the Atlantic show d-excess values around 10‰. Values lower than 10 ‰ may be indicative of secondary evaporation processes, e.g. the evaporation of falling raindrops in a warm and dry atmosphere (ARAGUAS - ARAGUAS et al. 2000) which is characteristic for summer rain. The Western Mediterranean Meteoric Water Line (WMMWL) is equal in the slope but differ in the intercept to the GMWL according to:

$$\delta^2\text{H} = 8 * \delta^{18}\text{O} + 13.7 \text{ (CELLE-JENATON 2001)} \quad (\text{eq.2.12})$$

Local or regional meteoric water lines (LMWL) are presented by GARRIDO 2003 derived from rain samples for *Granada* city as:

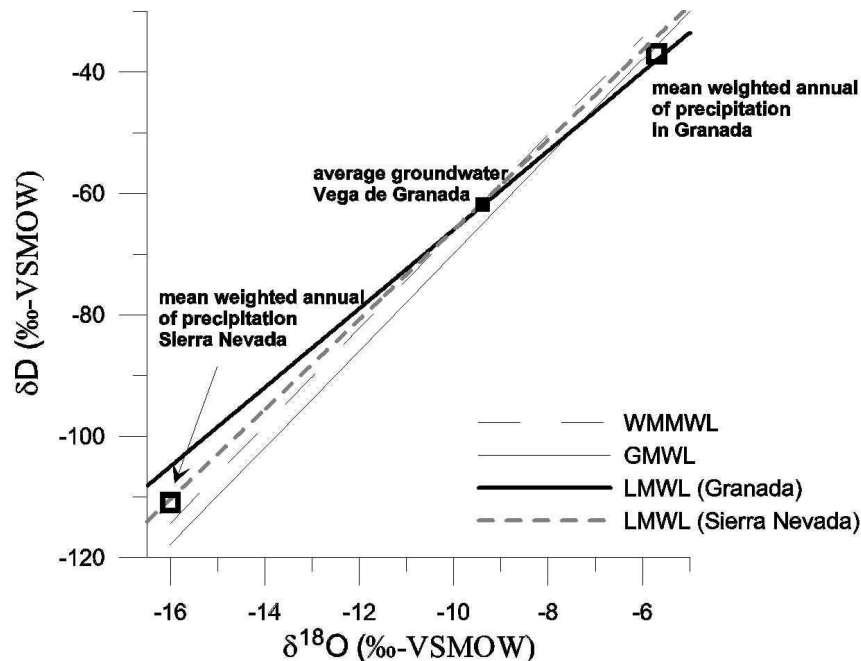
$$\delta^2\text{H} = 6.5 * \delta^{18}\text{O} - 1 \text{ (Granada)} \quad (\text{eq.2.13})$$

and for the *Sierra Nevada* derived from snow samples taken between 1200 – 2800 masl as:

$$\delta^2\text{H} = 7.4 * \delta^{18}\text{O} + 8 \text{ (Sierra Nevada)} \quad (\text{eq.2.14})$$

These equations representing the ^2H and ^{18}O relation in the study area for comparable short time periods, and are discussed in section 2.4.

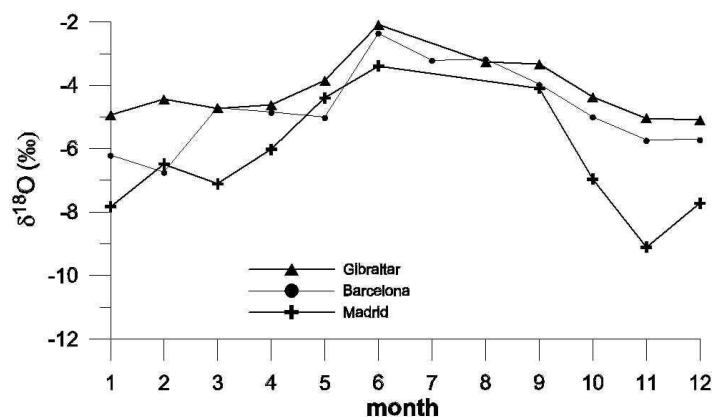
In general, groundwater values of $\delta^{18}\text{O}$ from wells in the *Vega de Granada* reflect the volume-weighted mean of recharge precipitation. The local groundwater average of well samples ($\delta^{18}\text{O}=-8.13$; $\delta\text{D}=-55.3$ (‰-VSMOW)) from the *Vega de Granada* (see section 4.2.5, table 4.7) plots on the intersection of the WMMWL with the LMWLs (eq.2.13, eq.2.14). These regression lines are considered as Local Meteoric Water Line (LMWL), but the WMMWL is a good average of these lines as indicated in Fig. 2.7.



• Figure 2.7 GMWL (Global Meteoric Water Line), WMMWL (Western Mediterranean Meteoric Water Line) and LMWL (Local Meteoric Water Line) for *Granada* (eq. 2.11) and *Sierra Nevada* (eq. 2.12) with the mean groundwater signature from the alluvial aquifer (*Vega de Granada*).

2.4 Previous isotope studies relevant for the study area

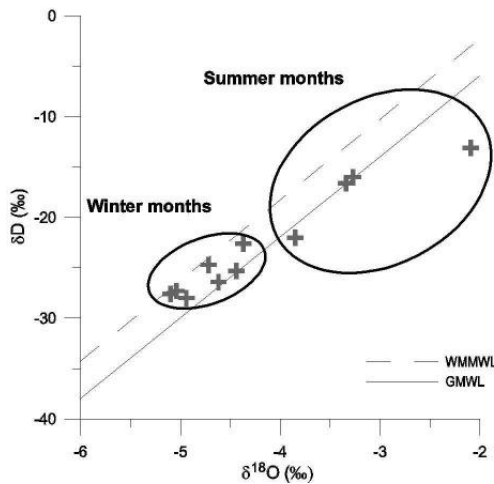
The seasonal plot of $\delta^{18}\text{O}$ from three IAEA precipitation series is plotted in Fig. 2.8 (IAEA-GNIP 2004). The Gibraltar and the Barcelona graphs are quite similar due to their position near at a shore ($\delta^{18}\text{O} \pm 3\text{‰}$), while the Madrid samples show a continental effect ($\delta^{18}\text{O} \pm 6\text{‰}$). IAEA-GNIP data from Spain and Portugal (including samples from the Azores island) is discussed in detail by BEDMAR 1994, and most striking findings are summarised here.



• Figure 2.8 Seasonal variations of $\delta^{18}\text{O}$ in Iberian precipitation from IAEA stations based on the monthly means from 1985-1991 (Barcelona), 1988-2001 (Madrid), 1962-2001 (Gibraltar) (all data IAEA-GNIP 2004).

The precipitation-weighted average of $\delta^{18}\text{O}$ at Gibraltar is -3.9‰ and the monthly average varies between -4.7 and -2.1‰ . D-excess shows the lowest values in the summer months, with variations from 4.3 (June) to 13 (November). The low d-excess for the summer data suggest high humidity conditions during primary evaporation. The regression line of $\delta^{18}\text{O}$ vs. δD in the Gibraltar samples is described as (IAEA-GNIP 2004):

$$\delta\text{D} = 6.19 * \delta^{18}\text{O} + 3 \quad (\text{eq.2.15})$$



• Figure 2.9 $\delta^{18}\text{O}$ - δD diagram of IAEA-GNIP data at Gibraltar between 1961 and 2001 with regression trend line (dashed-dotted), GMWL (solid) and LMWL (dashed).

The $\delta^{18}\text{O}$ against δD values of the Gibraltar samples plot **along** or **below** of the GMWL in the summer months and **between** the WMMWL and the GMWL in winter months (Fig.2.9). Samples of precipitation with heavier (higher) $\delta^{18}\text{O}$ and δD values tend to fall **below** the GMWL. Considering the climatic conditions at Gibraltar during the summer months (high temperatures) and the sampling method (samples from few and small rain events), this effect could be caused by evaporation in the atmosphere or during sampling.

During the hydrological summer (April – October) the highest amount of precipitation

and the most depleted $\delta^{18}\text{O}$ values are observed (Fig.2.9). For June a weighted mean value of -2.09‰ $\delta^{18}\text{O}$ was obtained. Rainfall at the beginning of the rainy season in October has a relatively light isotopic signature of $\delta^{18}\text{O}$ with a minimum weighted mean around -5.1‰ in December. At the end of the rainy season a general return to heavier (higher) $\delta^{18}\text{O}$ and lower d-excess values are observed. Due to the position of Gibraltar at the strait between Atlantic and Mediterranean Sea, it is expected that isotope signatures from precipitation show both climatic influences.

BEDMAR 1994 discusses the stable isotope composition of ca. 800 samples taken from springs and wells and ca. 900 samples from precipitation collected during the last 30 years from Spain and Portugal. In this study a local meteoric water line for the Iberian Peninsula was calculated according to $\delta^2\text{H} = (6.84 \pm 0.09)\delta^{18}\text{O} + (4.35 \pm 4.6)$. The deviations from the global meteoric water line are discussed in this paper in detail. Additionally, vapour source analyses were made to distinguish between Atlantic and Mediterranean origin. A contour map of the $\delta^{18}\text{O}$ distribution is useful to interpret local isotope data but in the *Granada* area unfortunately not the necessary precision due to the lack of a sampling network is given (e.g. no $\delta^{18}\text{O}$ vs. altitude correlation in the *Sierra Nevada* is visible). Variations of $\delta^{18}\text{O}$ - $\delta^2\text{H}$ correlation over time from groundwater and precipitation provides information about groundwater recharge processes.

The doctoral thesis from GARRIDO 2003 is about the general composition of stable isotopes ($\delta^{18}\text{O}$, $\delta^2\text{H}$) of the vapour in the atmosphere and the precipitation in the *Granada* province. This work is used to validate the mean weighted precipitation values in the study area. GARRIDO 2003 calculates here the average value in $\delta^{18}\text{O}$ for precipitation (rain) in *Granada* with -5.7‰ ($\delta\text{D} = -37\text{‰}$), while the average values snow in the *Sierra Nevada* are $\delta^{18}\text{O} = -16\text{‰}$ ($\delta\text{D} = -111\text{‰}$). Analyses of the d-excess in precipitation confirm that the major part of rain bearing air masses for the *Granada* Region is according to GARRIDO 2003 originated from the Atlantic ocean (d-excess $\sim 10\text{‰}$). The author found out that isotope composition of atmospheric water vapour show altitude gradients for the *Sierra Nevada* between -0.2 and -1.3‰ (for $\delta^{18}\text{O}/100\text{m}$) and -1 and -9‰ (for $\delta\text{D}/100\text{m}$). Since the formation of vapour in the atmosphere and the formation of rain shows similar altitude dependencies (CLARK & FRITZ 1997), it possible to adapt vapour derived gradients on recharge rain. Regression lines calculated from snow samples taken in the *Sierra Nevada* in altitudes from 1000 – 3000 (masl) vary from $\delta\text{D} = 7.1 * \delta^{18}\text{O} + 5$ in January 2003 and $\delta\text{D} = 7.4 * \delta^{18}\text{O} + 8$ in November 2001. Regression lines from precipitation taken in *Granada* city vary from $\delta\text{D} = 6.9 * \delta^{18}\text{O} + 2$ to $\delta\text{D} = 6.5 * \delta^{18}\text{O} - 1$, while regression line from the *Sierra Nevada* vary seasonal between $\delta\text{D} = 7.4 * \delta^{18}\text{O} + 8$ in January and $\delta\text{D} = 7.1 * \delta^{18}\text{O} + 5$ in March. These calculations can be considered as the local meteoric water lines (LMWL, see eq.2.13 and eq.2.14).

3 Methods

3.1 Sampling strategy

Adapted to the objectives (section 1.1), the sampling strategy of this combined study of hydrogeochemistry (major and minor ions) and stable isotope data ($\delta^{18}\text{O}$, δD) was to estimate GWR altitudes and areas for springs and wells. According to this purpose it is necessary to detect possible isotope end-members. To detect the precipitation end-members composition of isotope signatures rainwater, snow or snowmelt were sampled. Rain samples were sampled on different altitudes in order to calculate the local δ -value vs. altitude relation. Sampling strategy directed towards a dense network of springs in the assumed recharge areas (*Sierra Nevada*, *Sierra de la Peza*) to get a detailed insight on the local isotopic composition. Springs from different altitudes were chosen to detect the altitude effect in isotope signatures and selected sites were sampled frequently to discover temporal variations. The Neogene infilling of the *Granada* depression was sampled widely to get an idea of possible end member composition. Since groundwater of the *Vega de Granada* was supposed to be more or less time constant, a network of wells was sampled once in order to detect spatial differences. Observation wells and pumping wells distributed in the *Vega of Granada* should show representative isotopic signature of this important aquifer. Surface water (rivers, reservoirs etc.) and groundwater from springs show often seasonal variations and were sampled frequently. Additionally, time series at two rivers (*Rio Genil*, *Rio Darro*) were run with a sampling period of two or three weeks. Important reservoirs (*Quentar*, *Canales* and *Cubillas*) were also sampled.

3.2 Sampling campaigns

Water samples were collected for stable isotope studies ($\delta^{18}\text{O}$, δD), major (Ca^{2+} , Mg^{2+} , Na^+ , K^+ , Cl^- , SO_4^{2-} , NO_3^-) and minor ion (Fe^{2+} , Mn^{2+} , Sr^{2+}) analysis in the *Granada* region. Sites within the Neogene sediments of the *Granada* basin and the adjacent eastern mountains (*Sierra Nevada*, *Sierra Arana*, *Sierra Padul-La Peza*, *Las Guajaras*) were sampled. Site locations are shown in Figure 4.15. Sampling campaigns were carried out by the cooperation partners and by the author as listed in chronological order in Tab. 3.1. Each sampling campaign is document Ted in appendix 3 with all in field measured parameters, type of sampled site, location, operating person, laboratory analyses and the internal IGME and FUB declaration.

• Table 3.1 Overview of sampling campaigns in chronological order and measured parameters (further explanation see text)

Number of samples	Date	Parameters	Institution	sampled site types
13	Feb 04	Isotopes/Ions	FUB	springs/snow or snowmelt
4	May 04	Isotopes	UGR	springs
73	June 04 - Sept 04	Isotopes	UJA	snow or snowmelt
10	Nov 04	Isotopes	IGME	observation wells
5	Dec 04	Isotopes	IGME	rainwater
3	Feb 05	Isotopes	AWI	snow
13	Feb 05	Isotopes/Ions	FUB	wells/springs/surface water
105	Oct 04 - March 05	Isotopes/Ions	FUB	surface water/ precipitation

The first sampling campaign was carried out in February 2004 by Prof.Dr.Pekdeger (FUB) and Dr.Kohfahl (FUB). They took samples from 12 springs (*Sierra Nevada*, *Sierra La Peza-Padul*, Neogene basin). Additionally, one snow sample (*Sierra Nevada*) were taken. EC and water temperature were measured with WTW Microprocessor Conductivity Meter LF 196 device. The samples were stored in polypropylene bottles (50ml) with watertight caps. All spring samples were collected for stable isotope studies and ion analysis. For detailed information see appendix 3, tab.a3.1.

Four samples from springs were taken by Prof.Dr.Benavente (UGR) in the Neogene basin and the *Sierra Nevada* yet again. The samples were stored in polypropylene bottles (50ml), for isotopic analysis, and sealed with parafilm to avoid evaporation. EC, pH and water temperature have been measured with unknown devices (appendix 3, tab. a3.2).

During June to September 2004 snow and snowmelt samples were sampled by Dr.Hidalgo (UJA) in high regions (>2200masl) of the *Sierra Nevada*. The samples were taken from small lakes (Spanish: *laguna*), snowmelt or snow. EC and water temperature were measured in field with WTW Conductivity device. The samples were stored in polypropylene bottles (50ml), for isotopic analysis, and sealed with parafilm to avoid evaporation (see Photo 1-4). For detailed information see appendix 3, tab.a3.3. Selected sites are documented with the photos 1-4.

Ten samples of ground water from observation wells and wells in the *Vega de Granada* were drawn in November 2004 at depths right below the water table using a plastic ladle from the IGME staff. Water temperature and E.C. were measured in field with unknown devices (appendix 3, Tab. a3.4).

Five rain samples at different altitudes (670, 1310, 1500, 1550masl) were collected in December 2004 by the IGME. The samples were stored in polypropylene bottles (50ml), for isotopic analysis, and sealed with parafilm to avoid evaporation. No physical parameters were measured in field. Only isotopic analysis were made (appendix 3, tab. a3.5).

Three snow samples were collected by Dr. H. Meyer (AWI) at different altitudes. SP-GR-235 was sampled from a thin snowmelt crust at a snow patch and SP-GR-236 was sampled right below of that melt crust. The samples were stored in double density polypropylene bottles (25ml), for isotopic analysis, and sealed with parafilm to avoid evaporation. No physical parameters were measured in field. Only isotopic analysis were made (appendix 3, tab. a3.6).

13 samples were collected at the 18.2.2005 mainly in the *Vega de Granada*, with logistic support from Prof. Dr. J. Benavente, by the author. Six wells, four springs and three river samples were taken. EC and water temperature were measured in field with a WTW LF196 microprocessor conductivity meter standardised to 20 °C. The pH was measured on site with a combined In gold pH electrode and WTW pH 330/SET hand-held pH/mV meter frequently calibrated using two standard buffers (appendix 3, tab. a3.7).



• Photo 1 *Laguna de los Machos* (X 468241 Y 4100417 Z 2919)



• Photo 2 Snowpatch Barr. de San Juan Nac. Rio Genil (X 4103799 Y 467193 Z 2718).



• Photo 3 *Laguna Mula* (X 463052 Y 4101813 Z 2495).



• Photo 4 *Laguna Aguas Verdes* (X 467372 Y 4100518 Z 3059).

Surface and precipitation samples were collected between October 2004 and March 2005 by the author. Five sites at the *Rio Darro* and *Rio Genil* have been sampled every 2 to 3 weeks. Other river sites were sampled only one time. Additionally, three reservoirs (Spanish: *embalse*) were sampled (*Emb.de Quentar*, *Canales*, *Cubillas*). Reservoir and river water samples were filtered on site with 0.2 mm acetate cellulose filters. Rainwater was sampled in March 2005 at two sites (appendix 3, tab.a3.8).

Between October 2004 and March 2005 21 springs in the eastern mountains of *Granada* were sampled to establish a network and to run time series at selected springs. Nine springs were sampled three to five times. EC and water temperature were measured in field with a Multiline P4 (WTW) microprocessor conductivity meter standardised to 20°C (Tab.5.11). The pH was measured on site with a combined Ingold pH electrode and WTW pH 330/SET hand-held pH/mV meter frequently calibrated using two standard buffers. Eh and O₂ measurements sometimes took a long time and might be incorrect. It was tried to measure total alkalinity (referred to as HCO₃⁻) in field but the available time not being sufficient to do so, the

measurements were postponed to the home laboratory (kitchen) upon return. Usually HCl titration was used in the field for the determination of the HCO_3^- species. Spring water samples were not filtered. All samples were stored in precleaned polypropylene bottles (50ml). The samples for cation measurements were acidified to pH 2 with ultrapure HNO_3 , and one bottle of each sample (not acidified) was kept for anion determination. For detailed information see appendix 3, tab.a3.8 and tab.a3.9.

3.3 Analysis

3.3.1 Ions

Major ion analysis (Ca^{2+} , Mg^{2+} , Na^+ , K^+ , Cl^- , SO_4^{2-} , NO_3^-) and minor ion analysis (Fe^{2+} , Mn^{2+} , Sr^{2+}) data was conducted at the Hydrogeology Laboratory for AMS and ICP measurement at the FUB. For precision of measurement, analytical method and measurement devices see appendix 3, tab. a3.10 and tab.a3.11.

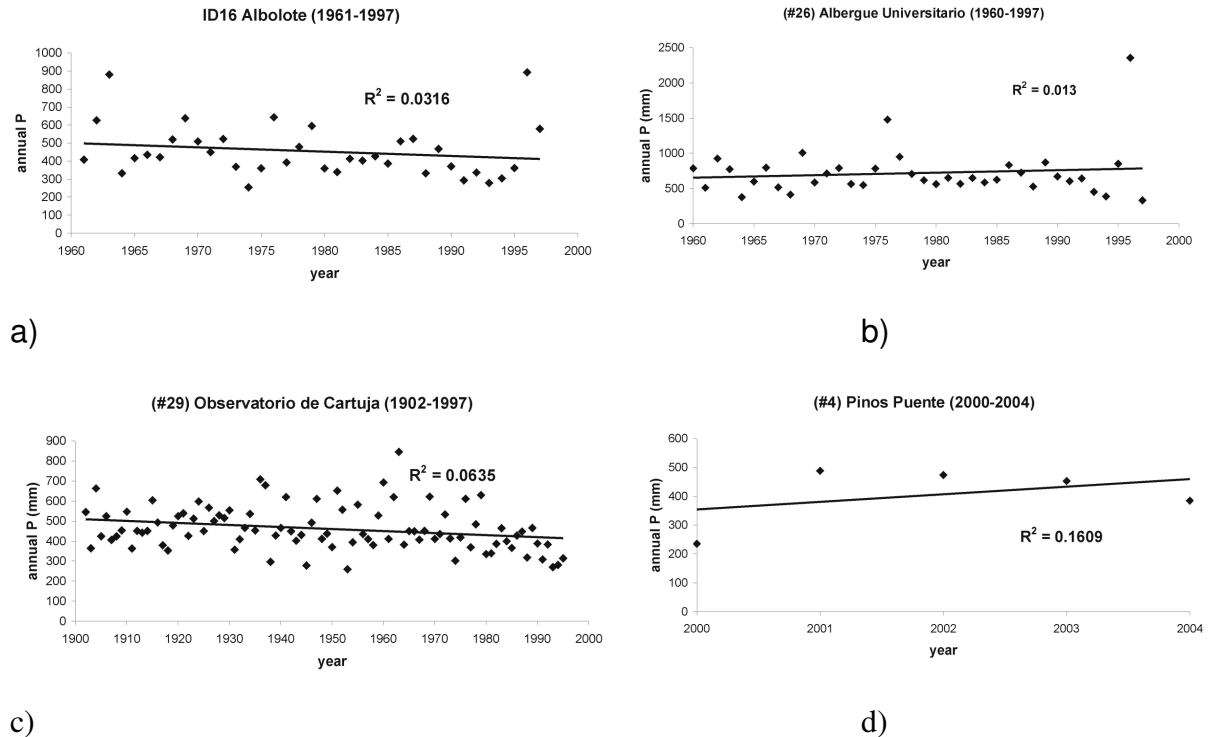
3.3.2 Stable isotopes analysis

δD and $\delta^{18}\text{O}$ were measured by the AWI (Dr. H. Meyer) mass spectrometer using the equilibrium method (MEYER et al 2003). Analyses were done on carbon dioxide that has equilibrated with the water sample at a constant temperature (18 ± 0.01 °C). Only 5 ml water were added to reaction vessels, then evacuated by pumping and connected to the mass spectrometer. This technique was improved to fully automated procedures and both species can be measured in one run. The precision of measurement is approx. 0.1 ‰ for $\delta^{18}\text{O}$ and 0.8 ‰ for $\delta^2\text{H}$, but is in most cases significant smaller. The precision in isotope measurement ranges between 0.02 ‰ and 0.09 ‰ in $\delta^{18}\text{O}$ and between 0.1 ‰ and 0.4 ‰ in δD . Each laboratory is using its own standards, which are calibrated against the VSMOW standard (appendix 3, tab.a3.10).

3.4 Climate

The calculations of the groundwater recharge are based on a database provided by the IGME and Junta de Andalucía website (www.juntadeandalucia.es). The data contains monthly and daily measurements with different time periods (oldest one 1/1902 *Observatorio Cartuja*) for 28 stations within and around the study area (appendix 3, Tab.3.14). Due to the lack of more meteorological stations in the Sierra Nevada (only one available) precipitation (P) was extrapolated according to the western slope gradient in mean annual precipitation, which is 70mm/100m (CASTILLO 2000). Thus maximum P is approximately 1330 mm/a in 3400 masl, which corresponds to the lowest estimation of previous works (e.g. CASTILLO 1985). At lower altitudes more meteorological stations are available and measured data was used to interpolate an isohyetal map. Temperature gradients for the Sierra Nevada are given by DELGADO CALVO-FLORES et.al 1989 as: T (°C) = $18.457 - 0.0061 * \text{Altitude (masl)}$. An ACCESS climate database was set up with all the above mentioned data to handle the different parameters.

To avoid mistakes, e.g. variable time periods, trend graphs were calculated. As shown in Fig3.1 (a-d) no significant trend is observable. From this data, the yearly average was calculated and an isohyetal map was calculated by using the software Surfer 7.0 with the kriging interpolation method. The variogram settings were modelled with Surfer 7.0 and applied. The map was imported to ArcView 3.2 and converted to a raster by using a linear minimum curvature (Fig.1.6).



• Figure 3.1 (a-d): Trend analysis of different time periods and stations within the study area.

3.4.1 Climatic groundwater recharge potential

Groundwater recharge (GWR) for the study area was calculated according to the general equation $P = \text{ETA} + R + \text{GWR}$ (P = precipitation, ETA = actual evapotranspiration, R = runoff). Climate information from 6 different meteorological stations in the study area was used (appendix 2, tab. a2.1 – a2.6).

Unfortunately no data about soil moisture, soil moisture changes over time and soil depths were available. Thus soil moisture storage and its change over time was not taken into account. Only one data set from stations located in the *Sierra Nevada* east of the basin (the potential recharge area) could be obtained. For that reason the climatic parameters for a “virtual” station were extrapolated.

Since it was not possible to quantify surface runoff (R), it was put together with the groundwater recharge (GWR). Actual evapotranspiration was calculated according to TURC (GRAY 1973) and COUTAGNE (REMENIERAS 1974).

TURC:
$$\text{ETA} = P / [0.9 + (P/J)^2]^{0.5} \quad J = 300 + 25 \cdot T + 0.05 \cdot T^3$$
 with P = mean annual precipitation [mm]; T = mean annual temperature [°C]

$$\text{COUTAGNE: } \text{ETA} = P - \lambda * P^2 \qquad \lambda = 1 / (0.8 + 0.14 * T)$$

with P = mean annual precipitation [m]; T = mean annual temperature [°C]
(valid for $1/8 \lambda < P \text{ [m/a]} < 1/2 \lambda$)

For calculations with more complicate equations like HAUDE or SCHROEDER & WYRNICH (MEYER & TESMER 2000) equation the necessary parameters were missing or not suitable for semiarid regions.

Generally the ETA values obtained with the TURC equation were lower, for all 13 stations leading to positive GWR. With the Coutagne equation higher amounts of GWR were calculated. It should be considered that the calculations were simplifications of natural processes and due to the semi-empirical character of the equations a deviation of about $\pm 15\text{-}20\%$ was assumed.

Using the salt balance method for the calculation of the groundwater recharge was impossible, since intensive agricultural use in the *Granada* basin and geogene salt modify chloride concentrations in the ground water.

3.5 Digital elevation map

A digital elevation map (DEM) was derived from a contour line shapefile (*Mapa Digital de Andalucia*). The shapefile was transferred to ASCII format by using a modified avenue script in ArcGis 3. With Surfer 7.0 the txt-file is converted to a 100x100m cell size grid using the kriging interpolation method with the adapted variogram settings. The software Global Mapper 6.0 was used to convert the surfer grid to USGS DEM format. Now the DEM can be used for spatial analysis (catchment delineation, climate etc.) in ArcGis 3.2. With the DEM and the ArcGis Hydro extensional tool catchment delineation calculations were made.

4 Results and Discussion

4.1 Hydrochemistry

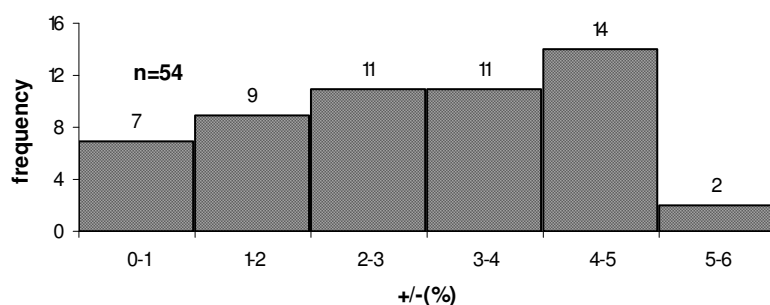
In this section graphical and statistical methods were used to classify the water samples into groups with similar geochemical characteristics. First a reliability check was made to confirm the validity of the measured sample data. Electrical balance and total dissolved solids (TDS) vs. Electrical conductivity (EC) was used to perform this reliability check.

4.1.1 Reliability check

The amount of positive ions and complexes with consideration of their valency and the amount of negative ions and complexes must be equal. The hydrochemical analysis, given in mg/l, were transformed to mmol(eq)/l [(meq/l)] and the electrical balance was calculated according to (DVWK 1992):

$$\text{balance (\%)} = \frac{\sum \text{Cations} - \sum \text{Anions}}{(\sum \text{Cations} + \sum \text{Anions}) \cdot 0.5} \cdot 100 \quad (\text{eq.4.1})$$

According to equation 4.1 analyses higher than 5% were considered as failed. Figure 4.1 shows that only two of the measured samples (n = 54) are out of the tolerance limit and therefore not used for further calculations.



• Figure 4.1 Electrical balances vs. frequency of measured samples.

TDS are the salts of calcium, sodium, potassium, magnesium, hydrogencarbonat, chlorides and sulphates, additional minor amounts if organic solvents. TDS is calculated using the equation:

$$\text{TDS (mg/l)} = \text{Ca}^{2+} + \text{Mg}^{2+} + \text{Na}^+ + \text{K}^+ + \text{SO}_4^{2-} + \text{Cl}^- + \text{NO}_3^- + \text{HCO}_3^- \quad (\text{eq.4.2})$$

The results of the calculations were shown in appendix 4, tab.a4.1. TDS values for the precipitation samples range from 7 – 16 mg/l, springs showed variations between 33 – 540 mg/l while the thermal springs had values between 2000 – 3500 mg/l. The pumping well samples values vary between 300 – 1900 mg/l. Values between 68 – 280 mg/l were calculated

for surface water in the mountains, while river samples in the *Vega de Granada* were between 910 – 9900 mg/l. The highest TDS value (9900 mg/l) was calculated from a river sample (*Arroyo de Salado*), which drains the southern part of the Granada basin.

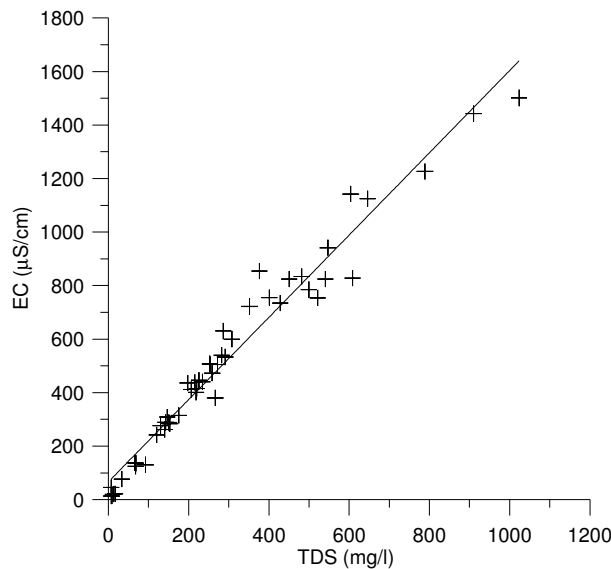
EC is the measurement of the total dissolved salts based on current flow. EC, measured in $\mu\text{S}/\text{cm}$ or mS/cm , is the reciprocal value of electrical resistivity. EC is positive proportional to the amount of total dissolved salts.

The EC measurements made in this work, ranged in the precipitation samples from 13 - 125 $\mu\text{S}/\text{cm}$. Springs showed values from 77 – 850 $\mu\text{S}/\text{cm}$, while the thermal springs had values between 750 – 3500 $\mu\text{S}/\text{cm}$. Pumping well samples vary between 820 – 1700 $\mu\text{S}/\text{cm}$. Values between 130 – 440 $\mu\text{S}/\text{cm}$ are measured for surface water in the mountains, while river samples in the *Vega de Granada* alluvial aquifer showed variations between 1500 – 15600 $\mu\text{S}/\text{cm}$.

EC and TDS are both parameters for the total dissolved amount of salts in a water solution. Therefore, they must be directly proportional to each other. Figure 4.2 shows the correlation between EC and TDS with the mathematical approximation of:

$$\text{TDS} = 0.57 \cdot \text{EC} \quad (\text{eq.4.3})$$

The best fit to the regression line is between 150 – 500 $\mu\text{S}/\text{cm}$. Low ($<150 \mu\text{S}/\text{cm}$) show minor deviation from the regression line due to high dilution.



• Figure 4.2 Linear relation between EC and TDS of measured samples.

4.1.2 Classification and characterisation of water samples

With the software Aquachem 4.0 chemical analysis were plotted in piper, stiff and schoeller diagrams to visualise general chemical characteristics. The spatial distribution of major chemical constituents, presented as stiff diagrams is shown in connection to a simplified geologic map. Additionally, saturation indices (SI) were calculated and carbonate chemistry was modelled with the software PHREEQC 2.11.

For a given reaction ($a \cdot A + b \cdot B \rightleftharpoons c \cdot C + d \cdot D$) the degree of saturation, the solubility product (K_s) of a mineral phase in aqueous solution is compared to the product of ion activities $[A]_{\text{sample}}$ and $[B]_{\text{sample}}$ (IAP) described by:

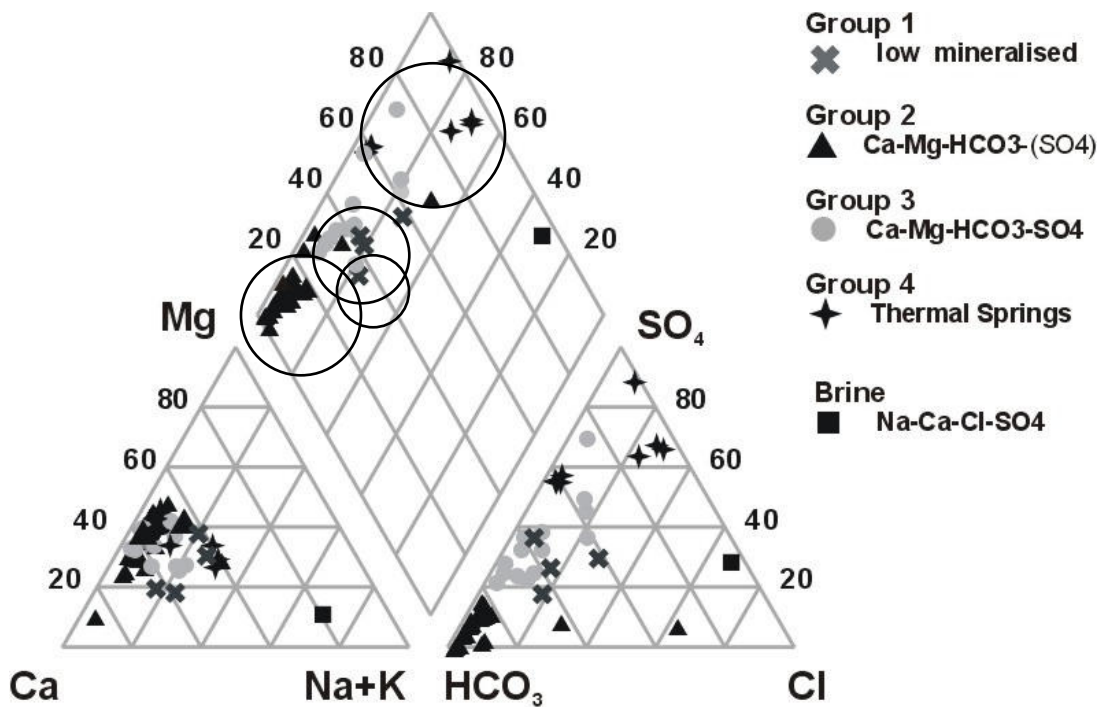
$$K_s = \frac{[C]^c \cdot [D]^d}{[A]^a \cdot [B]^b} \quad (\text{eq.4.4}) \quad \text{IAP} = [A]^a \cdot [B]^b \quad (\text{eq.4.5})$$

The ratio between the ion activity product and solubility product K_s is the saturation state with respect to a certain mineral. In general, the logarithm of the saturation state is used, according to:

$$\text{SI} = \log \frac{\text{IAP}}{K_s} \quad (\text{eq.4.6})$$

The SI is a calculation of how much a certain mineral phase has dissolved in groundwater relative to the amount it can potentially solve. Negative values indicate an undersaturation with respect to the considered mineral phase, while positive values indicate an oversaturation. Because of the logarithmic scale of the SI a value of +1 means that the sample is 10 times oversaturated. In praxis a SI of ± 0.2 (2 times over- or undersaturation) is treated to be in equilibrium with the mineral phase. Since no pH and alkalinity was determined for samples taken before September 2004, calculation of SI was made for only for spring, well and surface water samples taken between October 2004 and March 2005.

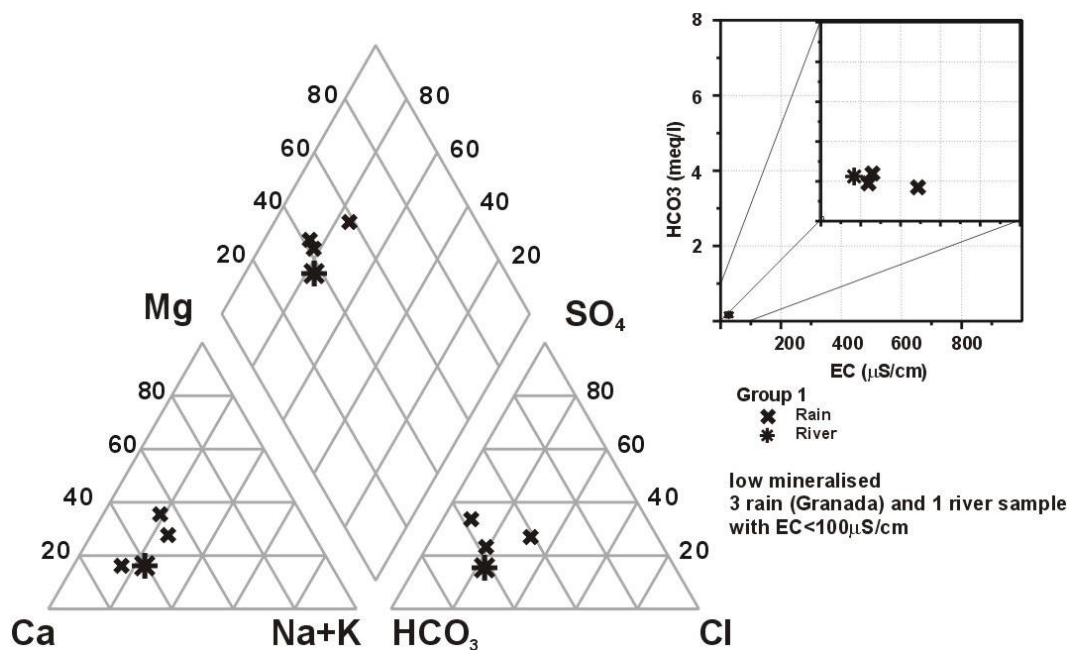
The piper plot (Fig.4.3) shows all measured samples, which were classified according to their major chemical composition. 4 main groups and one single sample (brine) can be distinguished. Most samples were classified as earth alkaline waters with prevailing bicarbonates (group 1) or prevailing sulphate (group 2). Group 3 members (thermal springs) can be subdivided into earth alkaline water with prevailing sulphate (*Fte. Urquiza*) and earth alkaline water with increased alkalis and prevailing sulphate and chlorides (baths or Spanish: *baños*). The low mineralized samples (group 4) are earth alkaline water with prevailing bicarbonates. The brine sample from the *Arroyo Salado* can be described as alkaline water with prevailing sulphate and chloride.



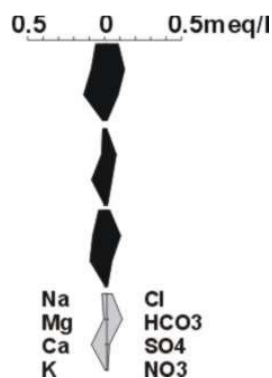
• Figure 4.3 Piper plots of all hydrochemical analysis.

Group 1 (low mineralized, $EC < 100 \mu S/cm$)

Group 1 members have electrical conductivities $< 100 \mu S/cm$. These low mineralized samples consisting of 3 rain water samples (*Granada city*) and 1 sample (*Arr. Caballo*) from a stream (ephemeral river) in the *Nevado-Filabride* metamorphic domain which was taken during snowmelt period. Due to the high dilution of these samples watertype declaration is not expressive and therefore not made. Locations are shown in fig. 4.15 together with all sites for isotope sampling. A calculation of saturation indices makes no sense for group 1 members. Stiff diagrams are constructed by plotting the 4 major anions and major cations (in meq/l) as indicated in figure 4.5. Stiff plots are used to evaluate the change in water composition as the water flows through different geological formations. First priority in precipitation samples is the study of isotope signatures.



• Figure 4.4 Piper plot and EC vs. HCO_3 scatter of group 1 members.



• Figure 4.5 Stiff plot of river (grey) and rain (black) samples (group 1).

Group 2 (Ground- and surfacewater of Ca-Mg-HCO₃-(SO₄) type)

The samples of group 2 members were taken from 15 springs located in the units of the *Alpujarride* carbonate complex, 3 sites situated (*Fte. Alta*, *Barr. de San Juan*, *Arr. Caballo*) in the *Nevado-Filabride* metamorphic complex, 5 samples (*Fte. Palmones*, *Fte. Molinos*, *Fte. de Vita*, *Rio Genil2*, *Rio Darro2*) located in the basin sediments (Mio-/Pliocene) and 1 sample (*Alhencira*) located in the *Vega de Granada* alluvial aquifer (Quaternary). Site locations and stiff diagrams are shown in connection to a simplified geological map in figure 4.7. Between the Feb.04 and subsequently taken samples no or very little variations over time were observed, therefore only one stiff diagram per site is printed.

Barr. de San Juan (Rio Genil 1), *Rio Genil 2* and *Arr. Caballo* are samples from rivers or streams and classified as Ca-Mg-HCO₃-SO₄ type. These samples are due to their low mineralization and high bicarbonate concentration also group 2 members. The well sample (*Alhencira*) represents rather the composition of the carbonate springs than wells and is therefore classified as group 2 members.

Group 2 members have electrical conductivity ranging between 77 and 854 $\mu\text{S}/\text{cm}$ and containing between 0.36 and 7.03 ($\text{Ø}3.6$) mmol/l HCO₃. All samples lie in a relative narrow pH range between 7.2 and 8.1 (Tab.4.1). Within this pH range the dissolved inorganic carbon exists almost entirely as HCO₃ species and suggests that open-system conditions dominate (FREEZE & CHERRY 1979). The scatter diagram of EC vs. HCO₃ (Fig.4.6) shows the geochemical evolution of springwater from low mineralized water (*Fte. Alta*) in the metamorphic core (*Nevado-Filabride*) to higher mineralized springwater in the *Alpujarride* carbonate complex.

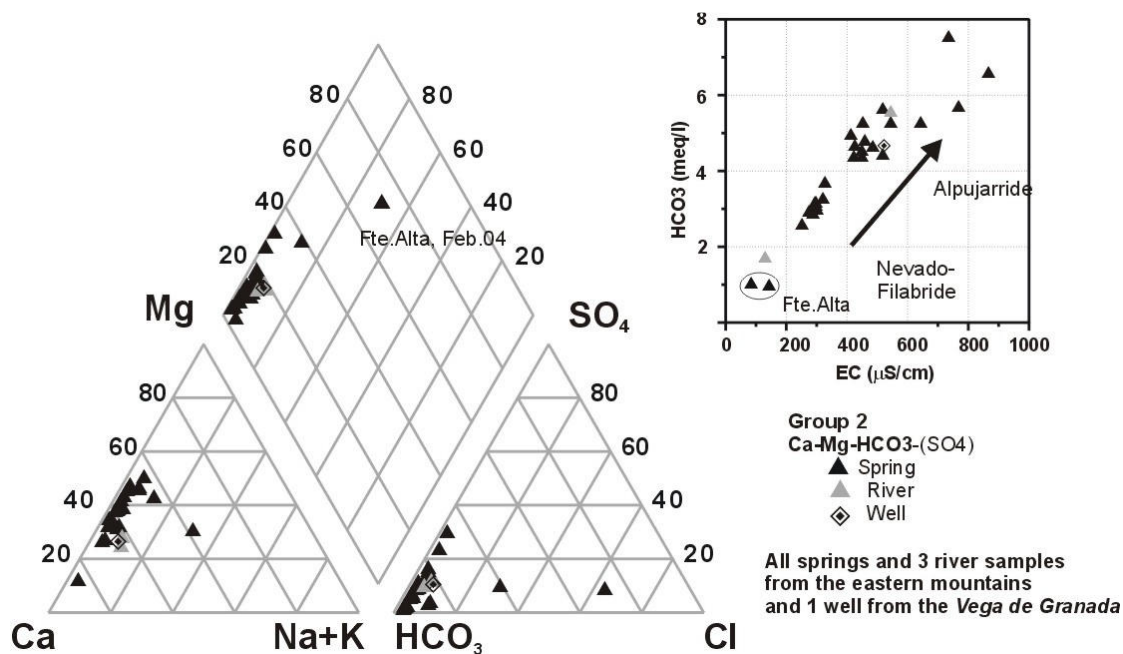
• Table 4.1 Summary of group 2 physical parameters and saturation indices.

n=33	T	pH	E.C.	SI	SI	SI	SI
				Calcite	Dolomite	Anhydrite	Gypsum
Min	6.00	7.2	125	-2.24	-4.83	-4.29	-4.03
Max	17.10	8.1	854	0.76	1.16	-1.77	-1.52
Med	11.47		417	-0.35	-0.98	-2.85	-2.59

A parameter determining differences in carbonate geochemistry of the host-rock area is the molar Ca²⁺:Mg²⁺ ratio. Geochemical modelling was made for a PHREEQC input file (appendix 4, tab. a4.2), with rainwater (taken in *Granada* city) as the initial water which was equilibrated CO₂ (log pCO₂=-2) and then equilibrated to calcite and dolomite separately and in sequence. These calculations show that dominant calcite dissolution results in a high molar Ca²⁺:Mg²⁺ ratio (far above 2), while dolomite dissolution shows a theoretically stoichiometric 1:1 relation. This finding is due to the higher solubility of calcite, which is a reason for the fact that hardly no carstification in dolomite rocks is found. However, in the study area it is more common that dolomite and calcite coexists (Fig.4.7) and this results in ratios which are around 1.4. These geochemical fingerprints can be recognized in Piper diagrams (e.g. Fig.4.6).

Cations of group 2 members are mainly composed of Ca and Mg, with a ratio between 0.9 and 7.0 with an average ratio of 2.1 (appendix 4, tab.a4.4). As indicated by calculations with PHREEQC these ratios are typical for dolomite dissolution (1.0) or dolomite dissolution in

the presence of calcite (1.4). It is obvious that springs show a positive trend in mineralization from the metamorphic core (*Nevado-Filabride*) to the carbonate domain (*Alpujarride*), reflecting the assumed flowpath from the recharge area to adjacent areas (Fig.4.6). The trend in the molar $\text{Ca}^{2+}:\text{Mg}^{2+}$ ratio develops analogous.



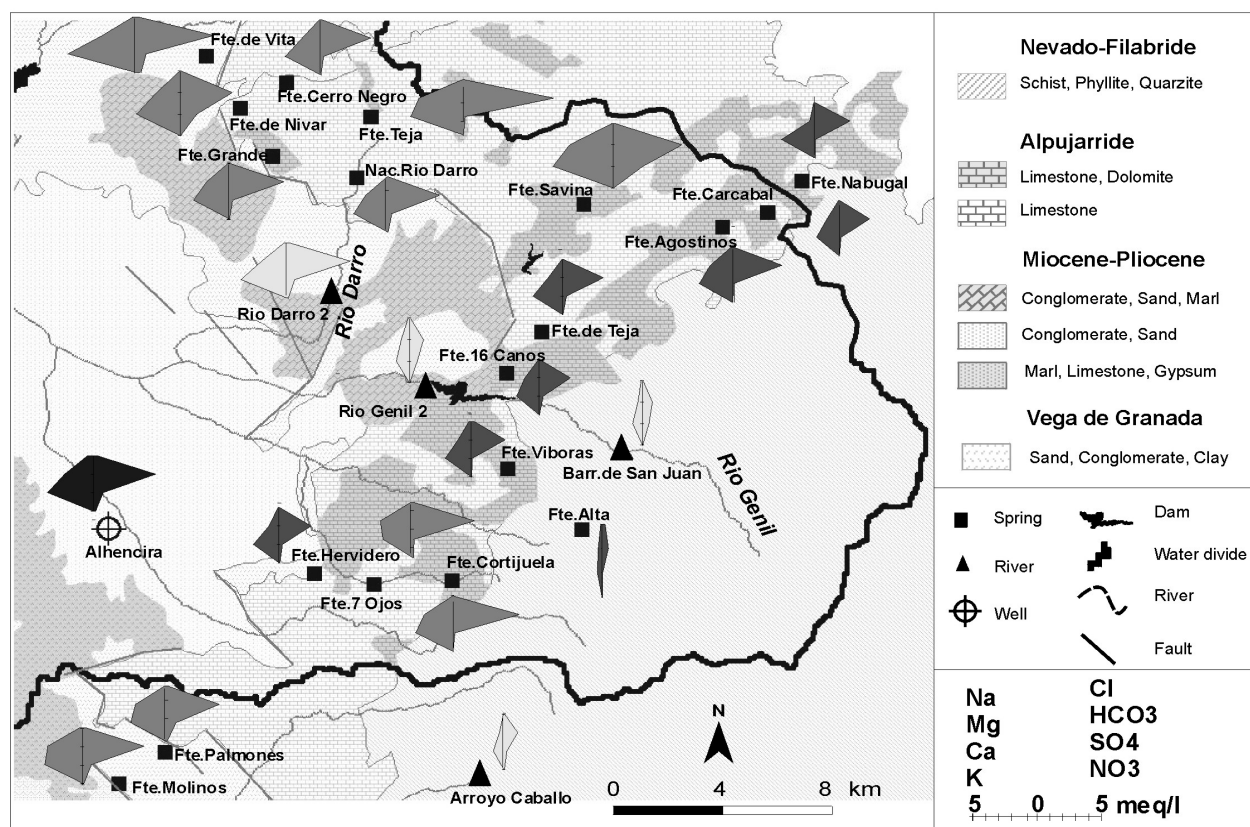
• Figure 4.6 Piper plot and EC vs. HCO₃ scatter of group 2 samples.

Unlike within group 3 sulphate concentrations are low ($\varnothing\text{SI}_{\text{CaSO}_4} = -2.59$, $\varnothing\text{SI}_{\text{CaSO}_4 \cdot 2\text{H}_2\text{O}} = -2.14$) (compare Tab.4.1 to Tab.4.2). The predominant ions are Ca, Mg and HCO₃ and the percentage of alkali elements Na and K is low. Only *Fte.Savina* shows an exceptional high content in SO₄.

Fte. Alta is located at a road to a ski resort and the February 04 (Fig.4.6) sample shows an increased content in Na and Cl. This was probably caused by contamination from road-salt during the ski season. The sample, taken in Oct.04 can be considered as less influenced by anthropogenic impacts.

Fte. Grande samples show an exceptional high content in hydrogencarbonat (ca. 260 mg/l) and a pH = 7.7 which is significant above the average. This sample is classified as HCO₃ type. As shown by the simplified geological map (Fig.4.7) the spring is situated in carbonate rocks belonging to the *Alpujarride* domain.

According to the geological map (Fig.4.7) a spatial coincidence between the distribution of calcite/dolomite host-rocks and the molar $\text{Ca}^{2+}:\text{Mg}^{2+}$ ratio around 1.4 is given in most of the cases. The geochemical calculation of saturation indices shows that almost all springs are undersaturated or close to the equilibrium with respect to dolomite and calcite.



• Figure 4.7 Location map of group 2 members, simplified geology and stiff diagrams of spring (grey), river (light grey) and well (black). Geology simplified from IGME 2002.

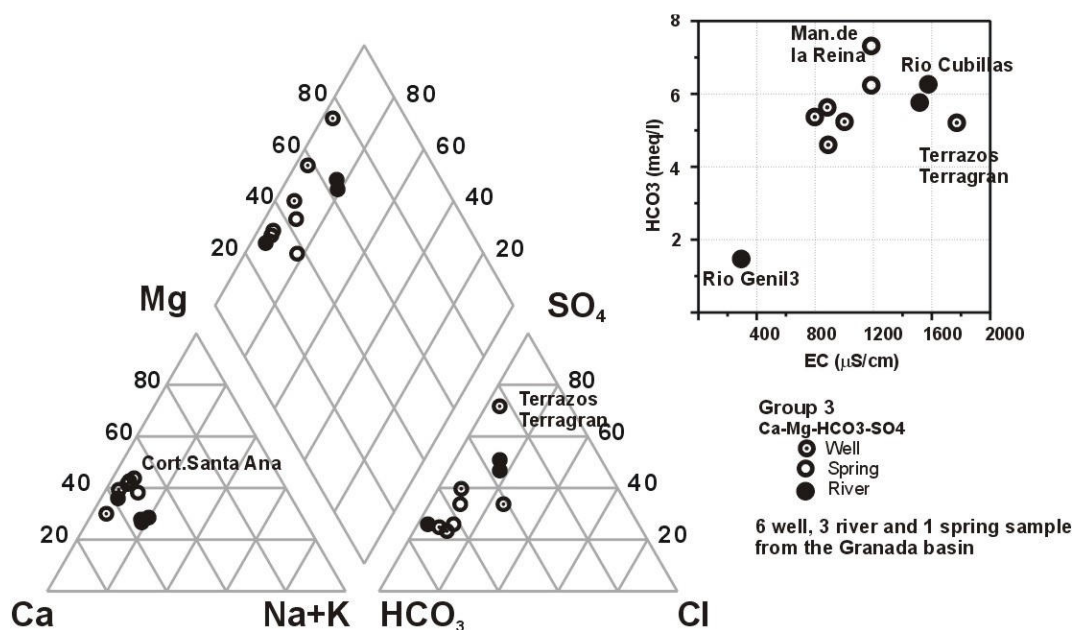
Group 3 (Ground- and surfacewater from the *Granada* basin of Ca-Mg-HCO₃-SO₄-type)

Group 3 members have electrical conductivities ranging between 380 and 1710 $\mu\text{S}/\text{cm}$ and containing between 3.45 and 7.24 HCO₃ (\varnothing 5.4 mmol/l). The high Ca concentrations of this group (61-240 mg/l) leads to an over saturation of calcite (appendix 4, tab.a4.5). The summary in tab.4.2 shows that group 3 members are over or close to the equilibrium with gypsum (SI_{CaSO₄*2H₂O} = -0.37 to 1.14), while Anhydrite is still undersaturated.

• Table 4.2 Summary of group 3 physical parameters and saturation indices.

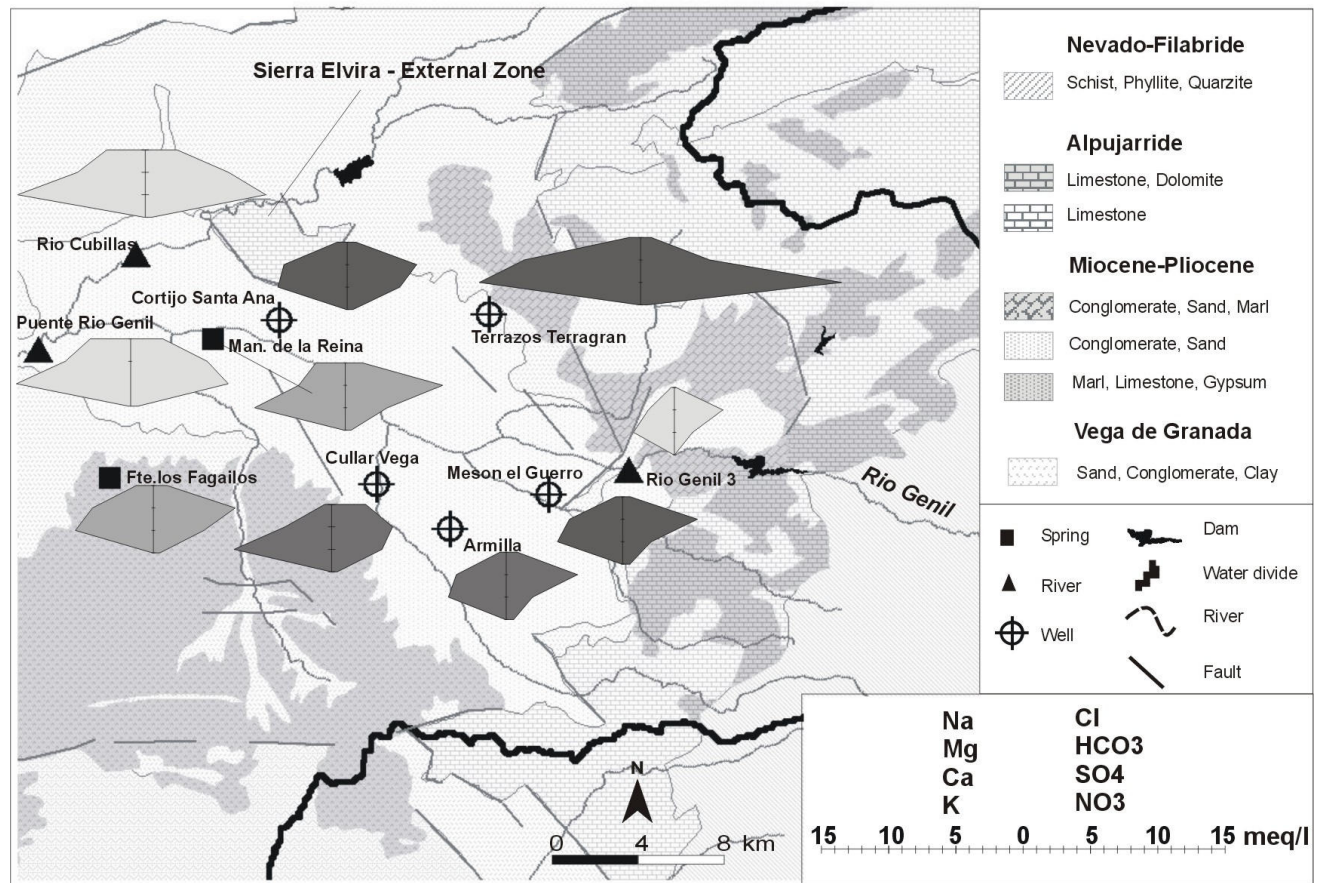
n=10	T	pH	E.C.	SI Calcite	SI Dolomite	SI Anhydrite	SI Gypsum
Min	11.57	7.03	380	0.05	-0.04	-2.07	-1.82
Max	15.78	8.10	1701	0.72	1.14	-0.82	-0.57
Med	14.1		990	0.27	0.35	-1.48	-1.23

The samples of group 3 members were taken from 5 wells, 2 surface water sites and 1 spring located in the *Vega de Granada* alluvial aquifer (Quaternary), 2 samples were taken from a spring (*Fte. los Fagailos*) and surface water site (*Rio Genil 3*) located in the basin sediments (Mio-/Pliocene) (Fig.4.9). The samples are classified as Ca-Mg-HCO₃-SO₄ water types, except for *Rio Genil 3* classified as Ca-Mg-HCO₃-Cl-SO₄ type.



• Figure 4.8 Piper plot and EC vs. HCO₃ scatter of group 3 members.

The chemical composition of the well sample (*Cortijo de Santa Ana*) shows the typical features of a carbonate influenced groundwater which is dominated by Ca, Mg, HCO₃ and minor amounts of K, Cl, and SO₄. On the basis of this chemical signature the water sample from is supposed to be influenced by water derived from the *Sierra Elvira* carbonate rocks.



• Figure 4.9 Location map of group 3 members, simplified geology and stiff diagrams of well (dark grey), river (light) and spring (grey) samples. Geology simplified from IGME 2002.

Samples from the south-eastern part of the *Vega de Granada* showing a chemical composition very similar to springwater classified as group 2, but are due to their high content in sulphate group 3 members. Approximately at *Man. de la Reina* the former influent groundwater flow regime (*Rio Genil-Vega de Granada*) becomes effluent, and the chemical composition represents the shallow groundwater chemistry.

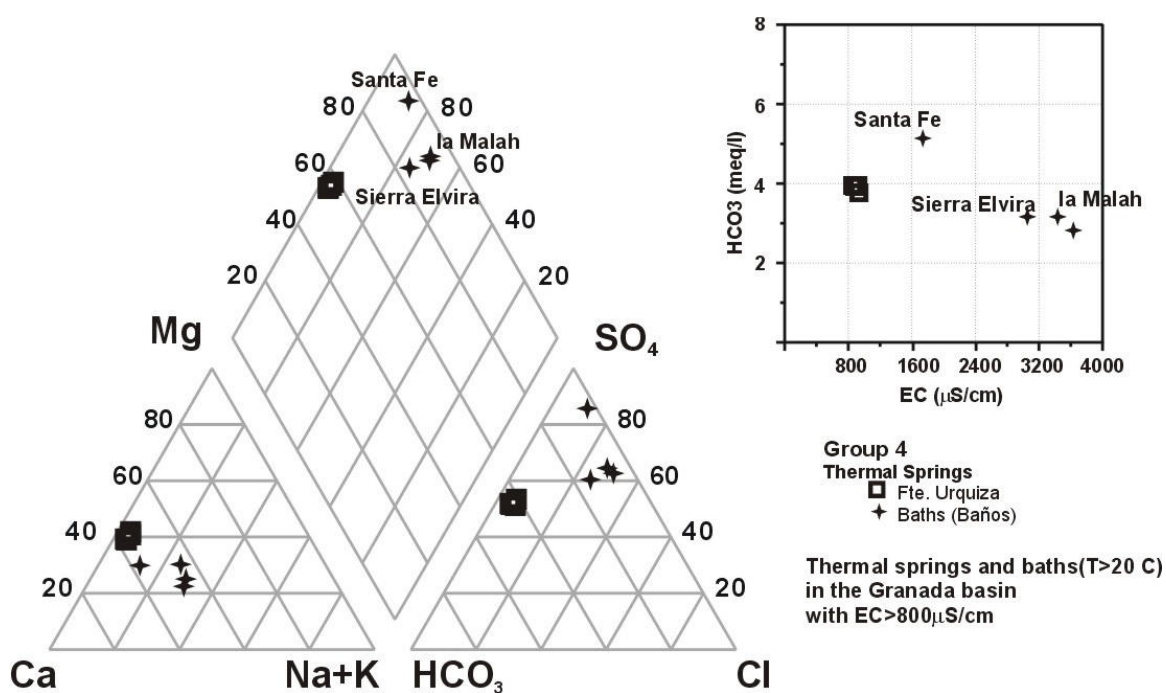
The water sample from *Terrazos Terragren* shows a very unique composition. This sample was higher mineralized than all other groundwater samples ($EC=1600\mu S/cm$). Dominant ions are Ca and SO_4 , followed by Mg and HCO_3 . This industrial well shows a very high content in $CaSO_4$ (Gypsum), which cannot be explained by local geology and is therefore probably contaminated by the industrial plant itself.

All samples have Nitrate concentrations below 50mg/l, though the *Vega de Granada* is considered to be one of the highest polluted aquifers in Andalusia. The effect of dispersion in the unsaturated zone is likely to eliminate the seasonal input of nitrate due to fertilizers. It is possible that the nitrate front which migrates slowly downwards with maybe 0.5 m/a has not yet arrived the groundwater table.

Group 4 (Thermal springs in the *Granada* basin)

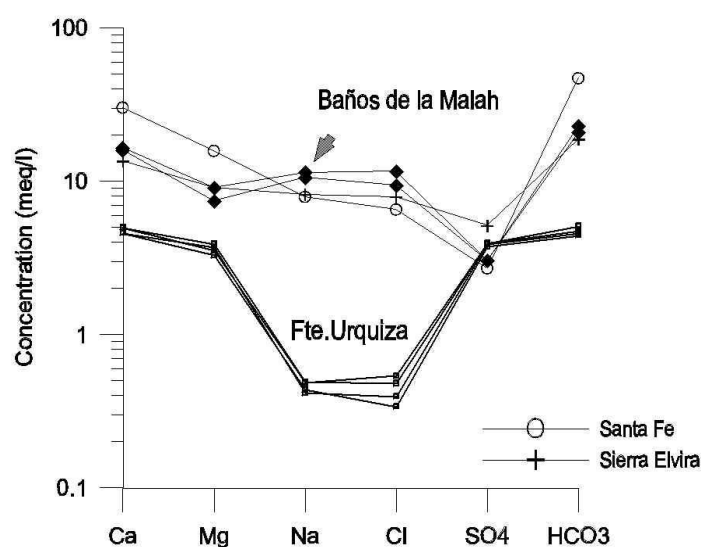
Group 4 samples have water temperatures >20 °C and are according to HÖLTING 1997 classified as thermal water. The sample sites are located in the *Vega de Granada* alluvial aquifer (Quaternary) (*Baños de Sierra Elvira*) and in the marine/terrigeneous basin sediments (Mio-/Pliocene). Locations are shown in figure 4.15. Group 4 members show two subgroups with respect to EC values and general chemical composition:

- 4a - $\bar{\varnothing}$ EC = 800 $\mu\text{S}/\text{cm}$ with prevailing sulphate (*Fte. Urquiza*)
- 4b - $\text{EC} > 2600$ $\mu\text{S}/\text{cm}$ with increased alkalis and prevailing sulphate and chlorides (*Baños de la Malah*, *Baños de Santa Fe*, *Baños de Sierra Elvira*).



Subgroup 4a samples (*Fte. Urquiza*) were taken from a double tube spring with water temperatures around 25 °C. Both tubes show a very similar chemical composition to each other and over time. *Fte. Urquiza* is used by the local population for medical purposes and classified as Ca-Mg-SO₄-HCO₃ type. The low mineralization, the low temperature and the low content in alkalis and earthalkalis indicates that this spring is more influenced by shallow groundwater derived from the eastern mountains compared to the other thermal springs (Fig.4.11). The increased sulphate ($\bar{\varnothing}$ 226 mg/l) and calcium concentration ($\bar{\varnothing}$ 100 mg/l) indicating gypsum bearing host-rocks on the flow path of this spring (e.g. Messinian evaporites). The dominant ions are Mg, Ca and HCO₃ indicating calcite bearing host-rocks on the flow path (e.g. *Alpujarride*).

Subgroup 4b samples (n=4) were taken from thermal springs termed *Baños* (baths). Samples were classified as Ca-Na-Mg-(Cl)-(SO₄) or Ca-Mg-SO₄-type. These samples are characterized by relative low pH values (7.1 – 7.3). *Baños Sierra Elvira* and *Baños Santa Fe* are located on a virtual line from the southwest of the *Granada* basin (*Alhama de Granada*) to the northeast (*Sierra Elvira*). This line coincides with the External/Internal zone boundary (see chapter 5, Fig.5.13). This fact leads to the assumption that the occurrence of thermal springs is close connected to deep reaching tectonic fault zones. *Fte.Urquiza* and *Baños de la Malah* are located on a fault system which is perpendicular to External/Internal and strikes from northeast to the southeast (compare chapter 5, Geological Mapping). This approximately NE-SW striking fault system is related to extensional tectonical motions (LOPEZ-CHICANO et al. 2001).



• Figure 4.11 Schoeller diagram of thermal springs (group 4).

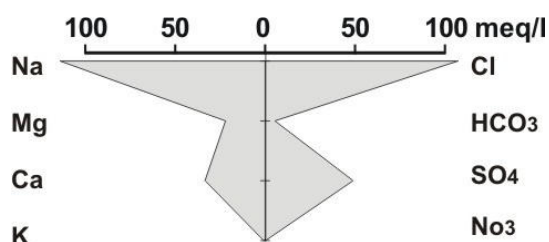
Chemical characteristics of group 4 members are visualised by a semi logarithmic plot of concentration (meq/l) vs. major constituent, termed as Schoeller diagrams. The semi logarithmic scale allows visualising a wide range of concentration and mixing effects are expressed in vertical shifts of the lines without a change in shape. Different water types will be displayed by crossing lines. The hydrochemical differences between the two subgroups are illustrated in figure 4.11.

• Table 4.3 Summary of group 4 physical parameters and saturation indices.

n=8	T	pH	E.C.	SI Calcite	SI Dolomite	SI Anhydrite	SI Gybsum
Min	21.0	7.0	754	-0.269	-0.585	-1.502	-1.273
Max	36.6	7.6	3700	0.393	0.733	-0.184	-0.023
Med	25.2		1926	0.006	-0.068	-1.046	-0.830

Single sample (Brine from the river *Arroyo Salado*)

The brine sample was taken from the river *Arroyo de Salado*, which drains an area of approx. 170 km² in the southern part of *Granada* basin (Tab.1.1). In this part of the basin marine



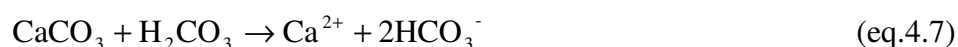
• Fig.4.12 Stiff diagram of brine sample (*Arr. Salado*).

evaporites, like gypsum and halite, are largely cropping out. The high alkali content with prevailing sulphate and chloride leads to the classification as Na-Ca-Cl-SO₄. Geochemical calculations of this high mineralized sample (EC=15 500μS/cm) shows that Ca- and Mg-Carbonate minerals are strong oversaturated (e.g. SI_{calcite}= 1.51, SI_{Dolomite} = 2.69, SI_{Aragonite}=1.35). Gypsum is saturated with SI_{CaSO₄*2H₂O} =-0.05, while Anhydrite is still undersaturated SI_{CaSO₄} = -0.31. The high Sr concentration of 14 500 ppb leads to saturation of Sr sulphate minerals (SI_{Coelestin}= 0.0). This might be explained by intense Coelestine mining in the south-eastern part of the Mio/Pliocene basin formations. Iron oxides are also highly oversaturated SI_{Fe(OH)₃}= 4, SI_{Goethite}= 9.

It is important to recognise, that the geochemical calculation of SI are based only on the analysed ions as shown in section 3.3.1 and do not account for silicate minerals.

4.1.3 Carbonate chemistry

In the study area dissolution and precipitation of carbonate minerals plays an important hydrochemical role because of the widespread distribution of calcite and dolomite host-rocks. The amount of calcium carbonate that recharge water can dissolve is controlled by temperature, pH and pCO₂ conditions in the soil zone. The higher the CO₂ concentration (expressed as carbonic acid, H₂CO₃) of the water, the lower its pH and the more aggressively the water dissolve carbonate minerals, according to:



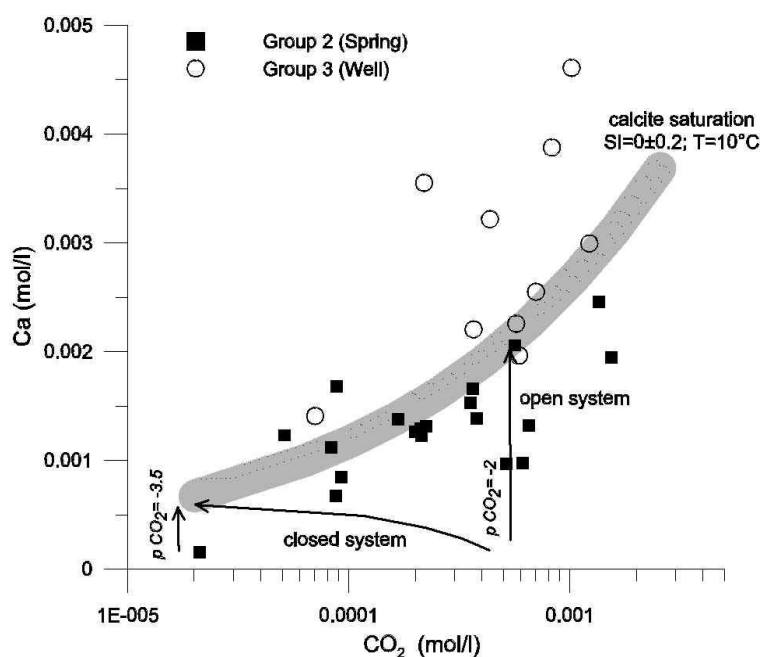
According to the equilibrium concept water from precipitation that flow through carbonate rocks dissolves calcite and dolomite to the point of saturation. As the water now encounters carbonate minerals in the saturated zone, carbonate specie H₂CO₃ is converted to HCO₃, decreasing H₂CO₃ content and partial CO₂ pressure (FREEZE AND CHERRY 1997). If this dissolution takes place in the unsaturated zone where abundant CO₂ is present this geochemical environment is termed as open-system condition (pCO₂ = const.). Controversy, closed-system conditions means that no delivery of atmospheric or soil CO₂ from the gas phase occurs, and the CO₂ will be consumed. Therefore, the equilibrium with Carbonate minerals is much sooner reached under closed-system conditions.

Calculations for calcite dissolution under closed- and open-system conditions were made with PHREEQC 2.1. The line of CaCO₃ saturation in pure water (for input file see in appendix 4, tab.a4.7) was calculated with T=10°C and pCO₂ = -2. A second input file calculates the molar

concentrations of dissolved Ca^{2+} in relation to pCO_2 under closed- and open-system conditions (input file in appendix 4, tab.a4.8). This file uses as an initial solution a rain sample from *Granada* city which was equilibrated with two CO_2 pressures representing atmospheric ($\text{pCO}_2 = -3.5$) or soil CO_2 ($\text{pCO}_2 = -2$) and equilibrated to either CaCO_3 without replenishing CO_2 (closed-system) or CaCO_3 with constant pCO_2 (open-system) conditions. By plotting the molar concentrations of dissolved Ca^{2+} in the ground water (springs, wells) against pCO_2 and then considering where the data lie relative to theoretical carbonate trajectories it should be possible to associate the samples to the assumed open or closed-system system conditions.

The semilogarithmic plot of CO_2 (mol/l) against Ca (mol/l) shows the spring samples (group 2) and well (group 3) members with consideration of possible hydrochemical evolution pattern (Fig.4.13). Vertical lines indicate open-system dissolution with different initial pCO_2 values (-2 and -3), while closed-system dissolution will evolve on curvature lines. The line of saturation ($\text{SI}=0$) with respect to calcite divides the samples taken from wells and springs. Spring samples (group 2) almost always plot below the line of saturation, indicating the geochemical evolution from recharge water in high regions with atmospheric CO_2 ($\text{pCO}_2 = -3.5$) and recharged water with increased soil development ($\text{pCO}_2 = -2$). Well samples (group 3) almost always plot above the line the saturation, indicating that still calcite dissolution takes place in the alluvial aquifer *Vega de Granada*. Most spring samples are plotting along vertical trajectories with variable initial pCO_2 content indicating open-system conditions.

It is important to recognize that the theoretical calculations are based only on calcite equilibrium and do not account for silicate weathering, complexation, cation exchange or any other biogeochemical process that may affect Ca^{2+} activities in the aquifer.



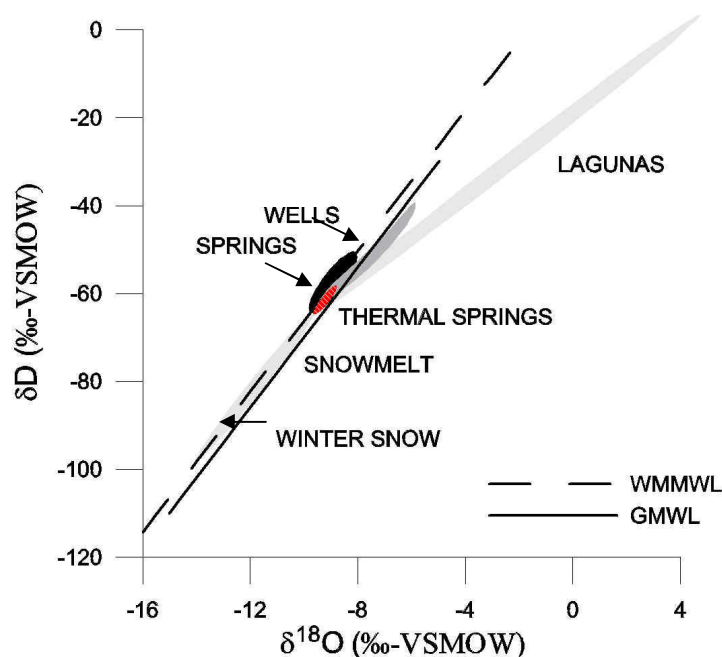
• Figure 4.13 Open and closed system trajectories for calcite dissolution of group 2 and group 3 members.

4.2 Stable isotopes of water ($\delta^{18}\text{O}$, $\delta^2\text{H}$)

In this section the signatures in the isotopic composition of water were studied in precipitation, springs, reservoirs, rivers and thermal springs in the *Granada* region. In arid and semiarid areas stable isotopes of water (^{18}O , ^2H) are important investigative tools for hydrogeological studies (VERHAGEN et al. 1991). Groundwater provenances, mechanisms of groundwater recharge (indirect, direct) and recharge conditions (altitude, degree of evaporative enrichment) can be identified by the variations in the isotopic composition. All site locations are shown in fig.4.15, for detailed information about the sampling campaigns see section 3.2.

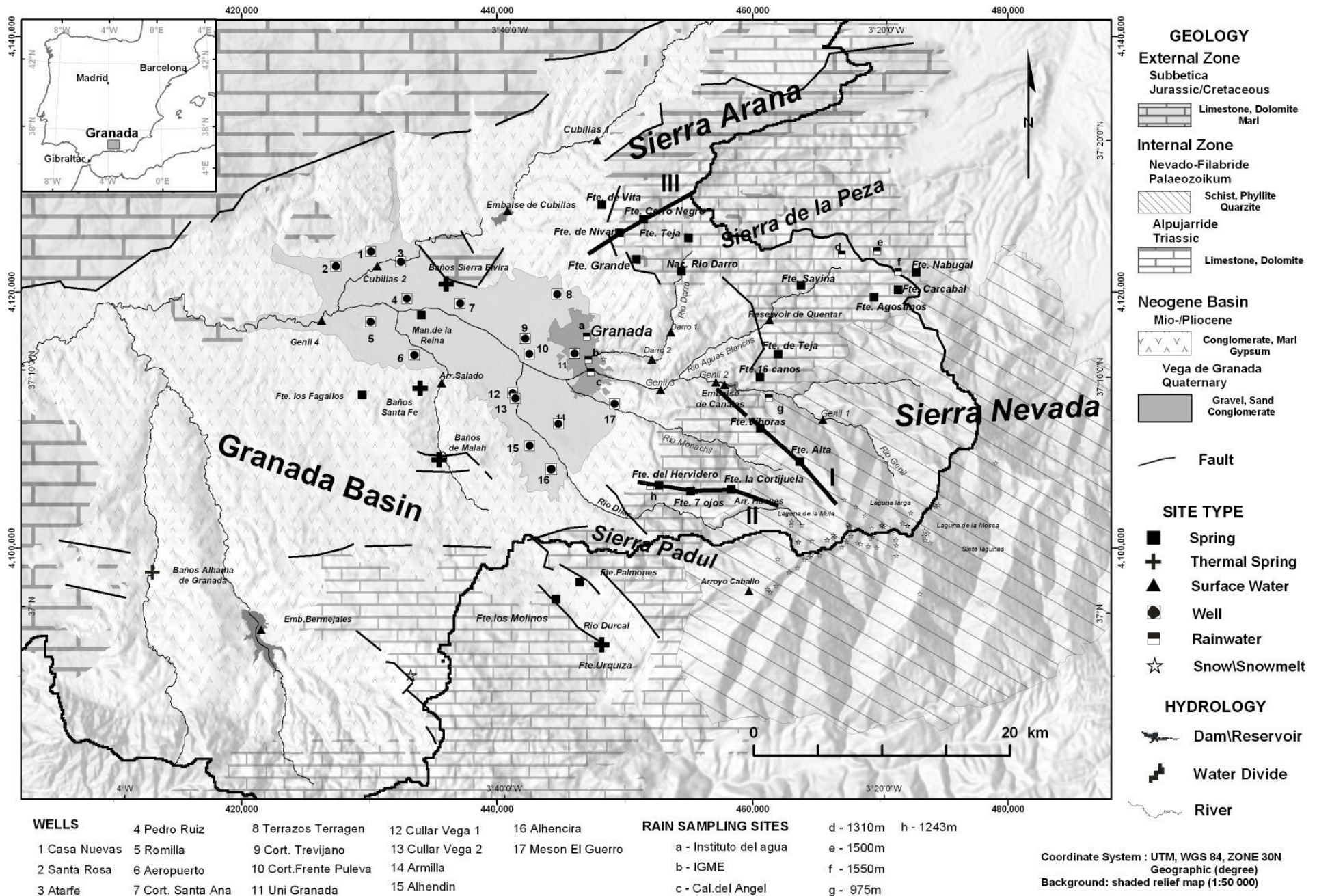
Results are presented in $\delta^{18}\text{O}$ vs. δD diagrams to visualise the isotopic characteristics. Local δ -value against altitude relationship in precipitation is constructed by data from GARRIDO 2003 and is used to calculate recharge altitudes for groundwater from springs and wells as discussed in section 2.4. Additionally, geomorphologic profiles, derived from the digital elevation model, are used to display the spatial pattern of selected springs, rivers and reservoir sites.

A schematic $\delta^{18}\text{O}$ vs. δD diagram (Fig.4.14) was plotted in order to give an overview of variations and general distribution. Because of the similar content in isotopes samples of rain and surface water are not displayed in Fig. 4.14. The samples are grouped according to their site type in rain samples (n=11), snow and snowmelt samples (n=77), spring samples (n=68), river samples (n=41), reservoir samples (n=8) and thermal spring samples (n=14). Each group shows characteristic isotopic signatures and are discussed in the following sections.



• Figure 4.14 Schematic overview of δD and $\delta^{18}\text{O}$ relationship of all samples with the GMWL and the WMMWL as reference.

Results and Discussion – Isotopes



• Figure 4.15 Location map of sample sites for stable isotope analysis and isotope transects I, II, III. Geology simplified from IGME 2002.

4.2.1 Precipitation

Precipitation is the only input source for groundwater recharge within the study area. Therefore, the understanding of the isotopic composition from rain- and snowfall is essential for hydrogeological studies. This section deals with the isotopic data provided by the GNIP (Global Network of Isotopes in Precipitation) database of the IAEA (International Atomic Energy Agency) for one station on the Iberian peninsula (*Gibraltar*) and rain samples taken from GARRIDO 2003 near *Granada (Generalife)*. These samples are presented together with few rain samples (n=11) from the *Granada* basin and samples from various altitudes in the *Sierra Nevada*. Additionally snow, snowmelt and *laguna* samples taken in the *Sierra Nevada* in altitudes >2200 masl are presented. For sampling locations see Fig.4.15.

4.2.1.1 Rainwater

Due to the position of Gibraltar at the strait between the Atlantic and the Mediterranean Sea, it is expected that isotope signatures of precipitation shows Atlantic and Mediterranean climatic influences.

The IAEA δ -values of rain are showing certain seasonal variations on the Iberian Peninsula (BEDMAR 1994) and are controlled by temperature, humidity and water vapour. Because of the higher temperature differences in winter between the source of air-vapour and the area of precipitation, more water vapour can be removed from the air masses on their trajectory, making the high altitude precipitation isotopic depleted in D and ^{18}O in winter.

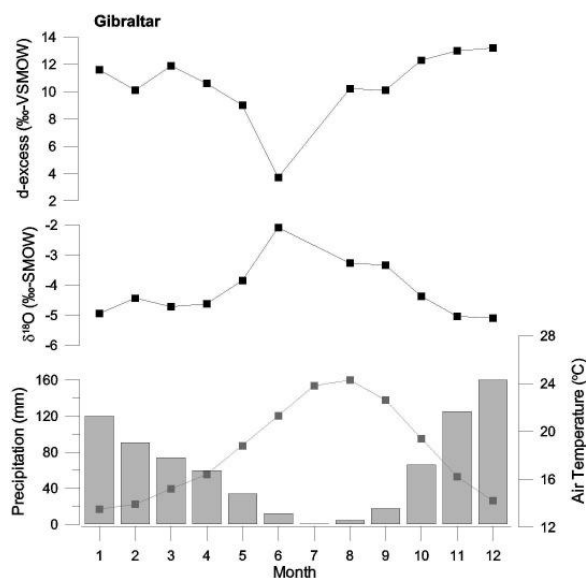
• Table 4.4 Mean weighted $\delta^{18}\text{O}$ and δD values for the hydrological year, - winter and –summer at *Gibraltar* station (1962-2001). IAEA-GNIP 2004 data.

<i>Gibraltar 5 masl</i>	mean weighted $\delta^{18}\text{O}$ (‰)	mean weighted δD (‰)
Hydrological year	-4.2	-22.7
Sommer (may-oct)	-3.9	-18.1
Winter (nov-apr)	-4.8	-26.6

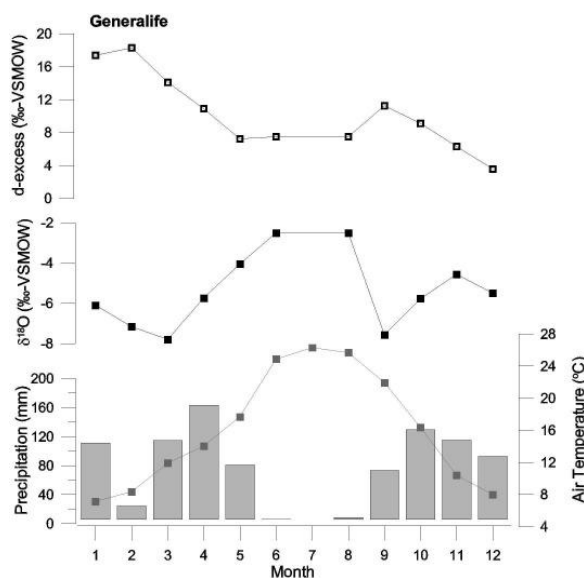
That means that in general, the δ values are higher in summer and lower in winter and averaging rain water samples from different seasons lead to false estimations of groundwater recharge. Since only winter rain-events have the climatic potential to recharge the groundwater the seasonal variation in the stable isotope compositions must be

considered. Therefore, samples are grouped in the hydrological winter (Nov.-Apr.) and the hydrological summer (May-Oct.). The mean volume weighted difference of $\delta^{18}\text{O}$ between summer and winter rain in Gibraltar is 0.9 ‰ (Table 4.4).

The seasonal distributions of the mean weighted values of $\delta^{18}\text{O}$ and d-excess of precipitation, air temperature and mean precipitation values for the IAEA-GNIP station *Gibraltar* (Fig.4.16) and for the station *Granada (Generalife)* (Fig.4.17) were plotted for each month. Samples from the station in *Generalife* represent a three-year period while samples from the station in *Gibraltar* represent a 39-year period. Therefore, the graphs from the *Generalife* station have more uncertainties, but are considered to be sufficient for the purposes of this study.



• Figure 4.16 Seasonal distribution of mean weighted $\delta^{18}\text{O}$ measured in precipitation at *Gibraltar* station (1962-2001), air temperature (right y-axis) and d-excess (‰ VS.MOW). The bars indicate mean monthly amounts of precipitation scaled to the left y-axis. IAEA–GNIP 2004



• Figure 4.17 Seasonal distribution of mean weighted $\delta^{18}\text{O}$ measured in precipitation at *Generalife* station (Dec.1999-Nov.2002), air temperature (right y-axis) from *Padul* station and d-excess (‰ VS.MOW). The bars indicate mean monthly amounts of precipitation. GARRIDO 2003

Both stations show correlation of low $\delta^{18}\text{O}$ with high monthly amounts of rainfall. During the hydrological summer (May – October) the most enriched $\delta^{18}\text{O}$ values are observed, with $\delta^{18}\text{O} = -3.9\text{‰}$ for *Gibraltar* (Tab.4.4) and $\delta^{18}\text{O} = -4.5\text{‰}$ for *Generalife* (Tab.4.5). For June both stations show weighted mean values in $\delta^{18}\text{O}$ of around -2‰ . Rainfall, at the beginning of the rainy season in October, has a relatively light isotopic signature of $\delta^{18}\text{O}$ which evolves to a weighted mean in December around -5‰ for *Gibraltar* and $\delta^{18}\text{O} = -6\text{‰}$ for *Generalife*. At the end of the rainy season (April) a general return to heavier (higher) $\delta^{18}\text{O}$ and lower d-excess values is observed in *Gibraltar* and *Generalife* samples. During the hydrological winter (November - April) the most depleted $\delta^{18}\text{O}$ values were observed, with $\delta^{18}\text{O} = -4.8\text{‰}$ for *Gibraltar* (Tab.4.4) and $\delta^{18}\text{O} = -6.1\text{‰}$ for *Generalife* (Tab.4.5). These differences are caused by continental- and altitude effects.

The mean volume weighted difference of $\delta^{18}\text{O}$ between summer and winter rain in *Generalife* is 1.6‰ (Tab.4.5).

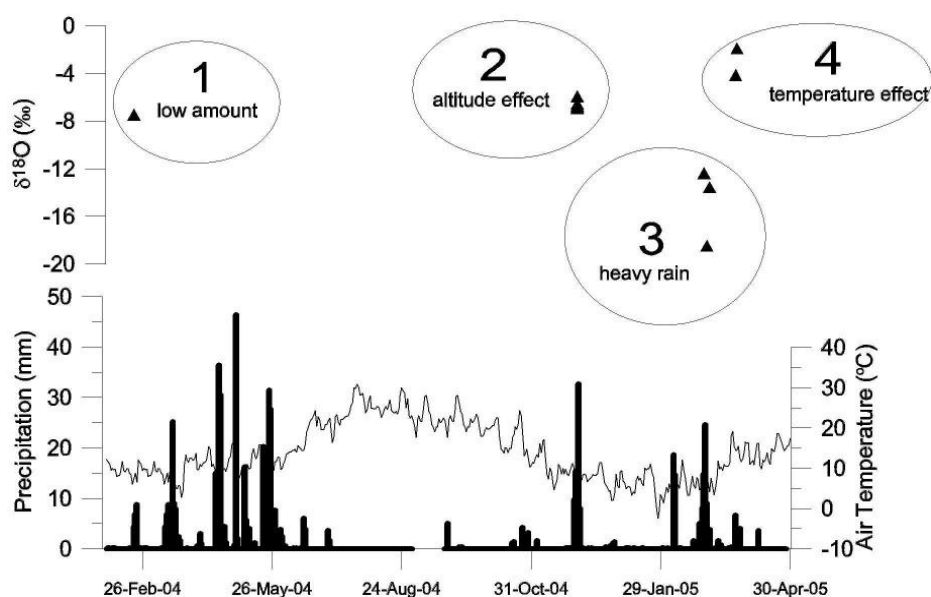
• Table 4.5 Mean weighted $\delta^{18}\text{O}$ and δD values for the hydrological year, - winter and -summer at *Generalife* station (Dec.1999-Nov.2002). GARRIDO 2003 data.

	mean weighted $\delta^{18}\text{O}$ (‰)	mean weighted δD (‰)
<i>Generalife 845 masl</i>		
Hydrological year	-5.4	-32.9
Sommer (may-oct)	-4.5	-27.4
Winter (nov-apr)	-6.1	-37.5

The distributions of $\delta^{18}\text{O}$ values of rain samples taken at various locations in the *Granada* basin and in the adjacent *Sierras* was plotted with meteorological data (air temperature ($^{\circ}\text{C}$), precipitation (mm)) from the *Padul* meteorological station for the time of monitoring from February 2004 to March 2005 (Fig.4.16) (all measured values are shown appendix 4, tab.a4.8 – tab.a4.11).

It is expected that rain samples show variation in the isotopic content due to amount, altitude and seasonality and the range in $\delta^{18}\text{O}$ between -18.6 and -2.1 ‰ is reflecting these effects. No clear correlation between altitude and δ -values can be observed in these samples. Rain samples from low amount rain events seem to tend to have enriched δ -values. Since no precise amount of the rain event is available, no exact volume weighted values can be applied. Four rain events have been sampled in four different methods ($n=11$) and are described in chronological order as:

- (1) first low amount rain event (20. – 25. February 04) with max. 8.8 mm was sampled only one time in *Granada* city ($\delta^{18}\text{O} = -7.83$ ‰, $\delta\text{D} = -59.2$ ‰, d-excess = 1.84 ‰). This rain sample seems to be affected by evaporation as it plots below of the GMWL (Fig.4.19). Furthermore, it is considered to be shifted towards more enriched values according to the amount effect.
- (2) second rain event (28.November - 6.December 04) with total amount of rainwater of 74.4 mm (max. 32.6 mm) was sampled on the 2.December cumulative on four different altitudes (670, 1310, 1500, 1550 masl). Characteristic of this event is, after a long dry period in summer, that the first rain event which falls through a dry atmosphere is altered. This alteration can be described as evaporation processes during rain fall. The rain sample taken at the lowest site (670 masl) shows the most depleted values ($\delta^{18}\text{O} = -7.08$ ‰, $\delta\text{D} = -24.3$ ‰) and rain taken at highest site (1550 masl) shows the second most depleted values ($\delta^{18}\text{O} = -6.87$ ‰, $\delta\text{D} = -29.7$ ‰). Therefore, no positive correlation can be observed between altitude and δ -values. Furthermore, the high d-excess (19.7 – 26.2‰) leads to a shift of δD above the WMMWL and cannot be explained (Fig.4.19).

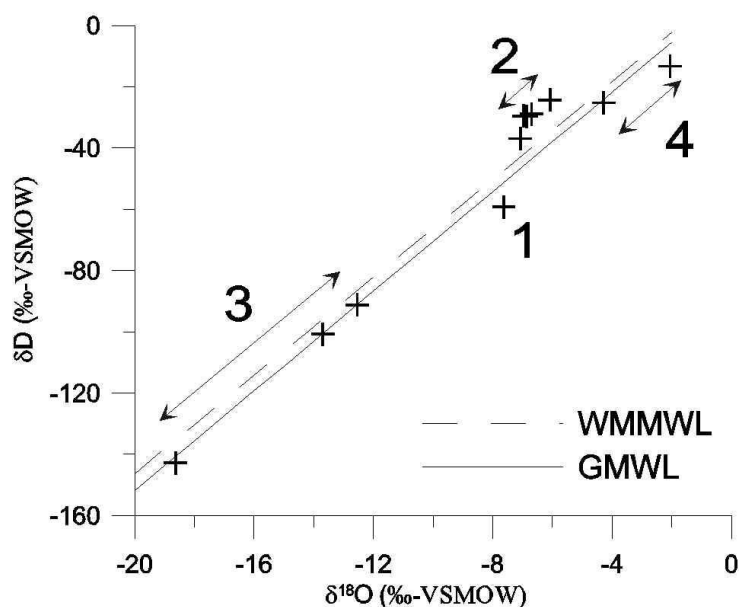


• Figure 4.18 Precipitation (mm) and air temperature ($^{\circ}\text{C}$) at *Padul* station between 01.02.2004 and 30.04.2005, $\delta^{18}\text{O}$ (‰-VSMOW) of measured rain samples.

- (3) third rain event (27. February - 5. March 05) with total amount of 63 mm (max. 24.6 mm) was sampled in *Granada* city altitudes (650 masl) in three single samples. A strong temperature correlation is observed. These samples show the most depleted δ -values and are interpreted as high amount rain event at low temperatures (reverse amount effect).
- (4) fourth rain event (23./24. March 05) with total low amount of rainwater of 6.6 mm was sampled in *Granada* city (650 masl) and in 1295 masl in two single samples. The altitude gradient in $\delta^{18}\text{O}$ is $-0.34\text{‰}/100\text{ m}$.

It is shown that local precipitation varies due to a change in altitude, temperature, season and amount. The variations in precipitation isotopes observed in the study area suggests that, in regions with highly variable microclimates and rainfall conditions, a detailed precipitation sampling network is necessary to avoid misinterpretations for temporal and spatial mean weighted precipitation.

The $\delta^{18}\text{O}$ vs. δD (‰-VSMOW) diagram shows all rain samples taken within this study. The numbers refer to the rain events introduced in the section above (Fig.4.19). Due to the lack of sufficient enough precipitation events during the time of monitoring, data from GARRIDO 2003 was used to understand local precipitation pattern.



• Figure 4.19 $\delta^{18}\text{O}$ (‰-VSMOW) - δD (‰-VSMOW) diagram of rain samples.

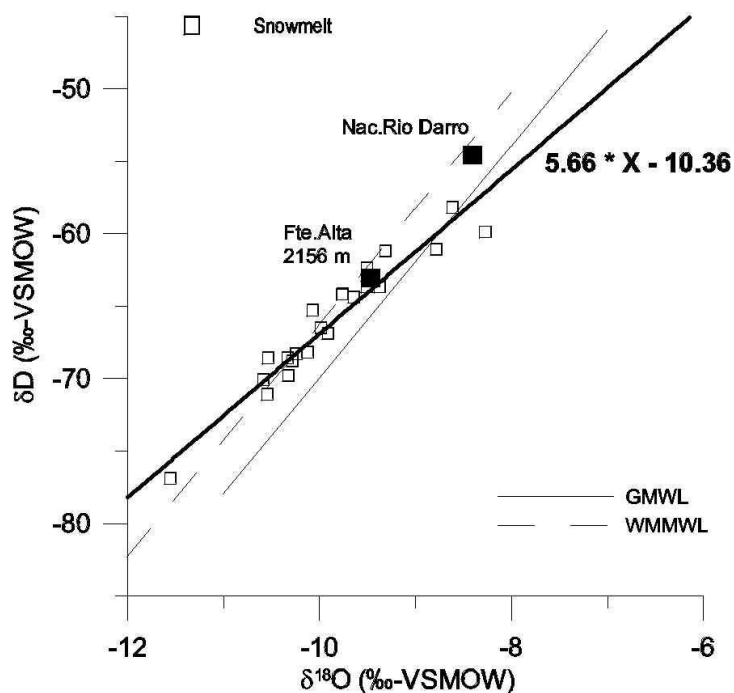
4.2.1.2 Snow and snowmelt samples

In this section more than 70 samples classified as snow, snowmelt or *laguna* (mountainous lakes in the *Sierra Nevada*) site types are presented in $\delta^{18}\text{O}$ vs. δD diagrams. The isotopic alteration of snow and the influence of this alteration on runoff and GWR were examined by many studies (e.g., MOSER & STICHLER 1974, 1980).

Snowmelt samples are often located **near** or **below** to the WMMWL. The regression line calculated with snowmelt samples is $\delta\text{D} = 5.66 * \delta^{18}\text{O} - 10.36$. Compared to the *laguna* samples, the slope of almost 6 is reflecting the increased equilibrium exchange processes, between the melt water and the vapour within the snowpack. Assuming that the average value of snowmelt samples is represented by the intersection of the regression line with the WMMWL ($\delta^{18}\text{O} = -10\text{‰}$; $\delta\text{D} = -66.3\text{‰}$), the maximum enrichment can be estimated by up to 2 ‰ in $\delta^{18}\text{O}$ (Fig.4.20).

Since signatures of melt water and fresh snow can differ, the isotope signature of fresh snow is not appropriate for the use as an end member. By determining the magnitude of alteration from snow to snowmelt in the *Sierra Nevada* it is possible to show how this alteration can influence the estimation of the importance of snowmelt as a source of groundwater recharge. Snow and snowmelt samples data show that infiltration resulting from snowmelt in the *Sierra Nevada* can be enriched in $\delta^{18}\text{O}$ and δD compared to the signature of fresh snow. The alteration in isotope signature tends to have a slope close to that of the MWL, so even highly altered samples plot near the MWL.

By comparing the signatures of snowmelt and winter rain precipitation to a local spring water signature, it is possible to calculate the proportions of snowmelt and rain in local groundwater



• Figure 4.20 $\delta^{18}\text{O}$ - δD diagram of snowmelt samples from the *Sierra Nevada* with average value of *Fte. Alta* and *Nac. Rio Darro*.

recharge. Since average snowmelt signature and average spring water signature of *Fte.Alta* ($\delta^{18}\text{O} = -9.5 \text{ ‰}$) samples is very similar, it is possible to state that *FteAlta* seems to be dominated by snowmelt derived from high altitudes in the *Sierra Nevada* (Fig.4.20).

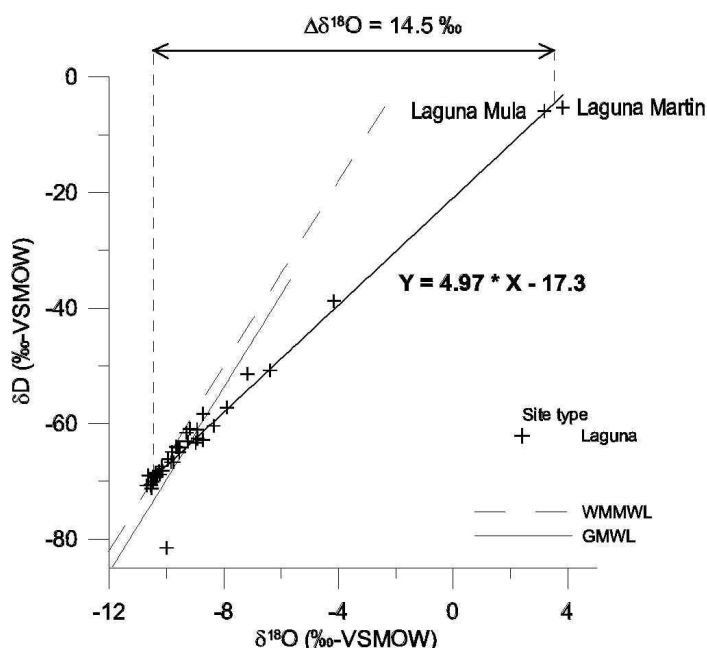
If snowmelt takes place during spring thawn due to rain, then the runoff will be a mixture of the rain and the snowmelt that has re-equilibrated with the remaining snowpack. The $\delta^{18}\text{O}$ value of the runoff will depend on the amount of rain, and the amount of melting, but will evolve towards the isotopic composition of the rain. Rain water at 2300 masl with a winter average of $\delta^{18}\text{O} = -9 \text{ ‰}$ (see Calculating recharge altitudes) and snowmelt with $\delta^{18}\text{O} = -10 \text{ ‰}$ shows that snowmelt and rain is found to be responsible for both 50% of the recharge during spring thawn. This seasonal variation can be seen in samples from *Fte. Alta*. Here the winter-sample (February $\delta^{18}\text{O} = -9.5 \text{ ‰}$) is more depleted than the summer-sample (October $\delta^{18}\text{O} = -9.4 \text{ ‰}$) and the variance of 0.1 ‰ is greater than the precision in measurement (measurement precision = 0.03 ‰). Other spring samples, e.g. *Nac.Rio Darro*, show signatures which seem to be not influenced by recharge water from snowmelt (Fig.4.20).

The *lagunas* samples show, in contrast to snowmelt samples, strong evaporative enrichment. Samples taken from *lagunas* are highly altered and even positive isotope ratios occur (e.g. *Laguna Mula* $\delta^{18}\text{O} = +3.8$). The regression line calculated with *laguna* samples is $\delta\text{D} = 4.97 * \delta^{18}\text{O} - 17.3$ ($n=39$; $r^2=0.96$). A slope of less than 5 is typical for evaporation from open water surfaces (CLARK & FRITZ 1997), such as *lagunas*. Compared to the regression-slope of the snowmelt samples, the slope of the regression-line from *laguna* samples is shallower. This reflects the increasing influence of kinetic fractionation processes (Fig.4.22).

By taking the average temperature ($\sim 5 \text{ }^\circ\text{C}$) from the meteorological station *Albergue Universitario* (see section 1.4), the slope of the regression line ($s = 4.97$) allows to approximate the relative humidity according to GONFIANTINI 1986 with around $h = 0.3$ (= 30 %). Now it is possible to determine the kinetic fractionation factors using Gonfiantini's equations (section 2.7), giving $\epsilon^{18}\text{O}_{\text{kinetic}} = -9.94 \text{ ‰}$. The total enrichment ($\epsilon_{\text{total}} = \epsilon_{\text{equilibrium}} + \epsilon_{\text{kinetic}}$) for evaporation under these conditions with the mean temperature of $5 \text{ }^\circ\text{C}$ in 2500 masl ($\epsilon_{\text{equilibrium}} = -10.8 \text{ ‰}$) is then $\epsilon_{\text{total}} = -20.74 \text{ ‰}$. The intersection of the regression line with the WMMWL is considered as the initial isotope ratio without evaporative impact ($\delta^{18}\text{O}_{\text{initial}} \sim -10.7 \text{ ‰}$). The sample taken from *Laguna Martin* shows the most enriched value and represents the maximum evaporative enrichment ($\delta^{18}\text{O}_{\text{sample}} = 3.8 \text{ ‰}$). The total enrichment of this samples can then be calculated with maximum $\Delta\delta^{18}\text{O} = \delta^{18}\text{O}_{\text{initial}} - \delta^{18}\text{O}_{\text{sample}} = 14.5 \text{ ‰}$. The fractional water loss from evaporation can then be modelled according to a Rayleigh distillation. For $\delta^{18}\text{O}$, the evaporative enrichment is up to 14.5 ‰. According to equation 2.9.:

$$\epsilon_{\text{total}}(\delta^{18}\text{O}) * \ln f = 14.5 \text{ ‰}$$

yielding a residual water fraction f of 0.49 and so a maximum evaporative loss in the sample of *Laguna Martin* of 51 %. These values must be considered as maximum evaporation losses in small endorheic basins without constant inflow, e.g. *Laguna Martin*, *Laguna de la Mula* (see photo 4).

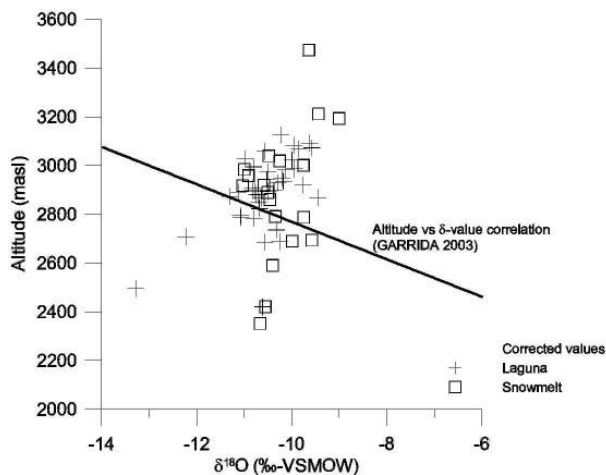


• Figure 4.22 $\delta^{18}\text{O}$ - δD diagram of *laguna* samples from the *Sierra Nevada*. Meteoric water lines as reference.

A correction of $\delta^{18}\text{O}$ from evaporative enrichment was applied, in order to establish a precipitation vs. altitude correlation. The corrected values indicate the isotopic composition without enrichment by evaporation. As the corrected value marks the intersection of the evaporation line (regression line) with the LMWL (WMMWL), it is defined by simple linear algebra according to:

$$\delta^{18}\text{O}_{\text{corrected}} = \frac{i_{\text{LMWL}} - (s_{\text{evaporation}} \times \delta^{18}\text{O}_{\text{measured}}) - \delta\text{D}_{\text{measured}}}{s_{\text{evaporation}} - s_{\text{LMWL}}} \quad (\text{eq.4.9})$$

where s corresponds to the slope of the evaporation line determined in equation above as 4.97 or s_{LMWL} with 8, and i is the intercept of the WMMWL, with $i = +13.7$ ‰. In the study area the variability of this corrected $\delta^{18}\text{O}$ in snow meltwater is assumed to reflect mainly different rain-out altitudes and seasonality. Corrected $\delta^{18}\text{O}$ values are presented in appendix 4, tab.a4.13.



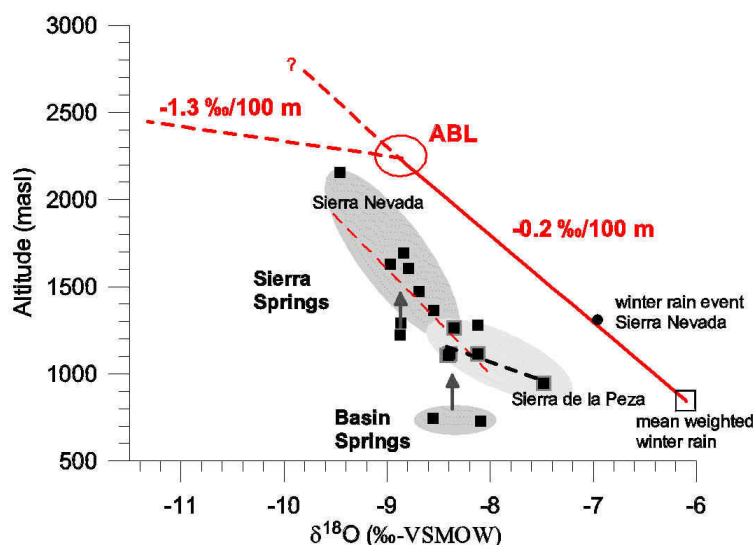
• Figure 4.23 Corrected $\delta^{18}\text{O}$ (‰-VSMOW) vs. Altitude (masl) of snowmelt and *laguna* samples.

Figure 4.23 shows the distribution of evaporative-enrichment corrected $\delta^{18}\text{O}$ -values vs. the altitude (masl). No clear correlation between altitude and $\delta^{18}\text{O}$ is observable. Considering the fact that all samples have been taken in the dry season (April-September), it indicates that these samples reflect mainly different rain events in the wet season (October-March) before and alteration processes during storage.

4.2.2 Estimation recharge altitudes

Recharge elevations for each spring and well were estimated by calculating a $\delta^{18}\text{O}$ vs. altitude relationship in precipitation. By taking the mean weighted winter value from *Generalife* (-6.1 ‰) as a end member and interpolating a gradient according to GARRIDO 2003 with -0.2 ‰/100 m for altitudes between 700 - 2200 masl. Only $\delta^{18}\text{O}$ was used for this analysis; the deuterium patterns were similar. The easy assumption in this case is that the average δ -value in groundwater represents an average elevation of recharge. By plotting $\delta^{18}\text{O}$ vs. altitude (masl) of both spring and rain sample, it is possible to estimate the recharge altitude. Therefore, the mean recharge altitude of a sample can be seen as the matching point of the intersection of a vertical line from the groundwater sample with the interpolated line of precipitation. For ground water sites that were sampled frequently, the average isotopic composition was used to determine recharge altitude.

According to the two groundwater provenances distinguished in section 4.2.4, also two groundwater recharge areas must be distinguished. Since the *Sierra Nevada* springs and the *Sierra de la Peza* springs are located on different orographic divides of the Betic Cordillera, a spatial shift in $\delta^{18}\text{O}$ values is expected to occur. This shift is expressed by different $\delta^{18}\text{O}$ / altitude relationship (Fig.4.24).



• Figure 4.24 Average $\delta^{18}\text{O}$ values of springs (squares) vs. Altitude (masl). Regression lines in spring samples calculated for the *Sierra Nevada* (red dashed line) and *Sierra de la Peza* (black dashed line). Interpolated precipitation line (red line) taken from GARRIDO 2003 is representing mean recharge altitudes. Mean weighted winter rain in the *Granada* basin (open square). ABL=atmospheric boundary layer.

The mean weighted $\delta^{18}\text{O}$ from the station *Generalife* (845 masl) within the hydrological winter 2001/02 (Nov-Apr.) seems to be a good approximation for winter rain in the *Granada* basin (see section 4.2.1.1). The $\delta^{18}\text{O}$ / Altitude gradients, taken from GARRIDO 2003 were compared with local springwater. GARRIDO 2003 divided the gradients into a low and a high altitude gradient. The separation is caused by the atmospheric boundary layer (ABL) (see section 1.4 Climate). The altitude vs. $\delta^{18}\text{O}$ gradient (-0.2 ‰/100 m, eq.4.10) is valid for 800-2200 masl. Above 2200

masl the ABL causing a stable atmospheric stratification with a temperature inversion in which temperature increases with altitude in winter. In summer the atmosphere is more turbulent and the temperature gradient is normal. Based on a best-fit linear correlation of the relationship between the interpolated $\delta^{18}\text{O}$ of precipitation vs. altitude of figure 4.24 exhibits equations, which can be used to estimate recharge altitudes according to:

<i>Sierra Nevada</i>	Equation	Altitude range	Gradient	
	Altitude (masl) = $-500 * \delta^{18}\text{O} - 2205$	800 – 2200 masl	-0.2 ‰/ 100 m	(eq.4.10)
	Altitude (masl) = $-76.9 * \delta^{18}\text{O} + 1522$	2200 – 3400 masl	-1.3 ‰/ 100 m	(eq.4.11)

According to these equations the reconstruction of groundwater recharge areas was approximated by $\delta^{18}\text{O}$ concentration of -0.2 ‰ with an increase of 100 m altitude in the *Sierra Nevada* below 2200 masl and of -1.3 ‰ / 100 m above 2200 masl for winter precipitation. GARRIDO 2003 calculated regression lines between the altitude and δ -values for $\Delta\delta^{18}\text{O} = -1.3 \text{ ‰}/100 \text{ m}$ and for $\Delta\text{D} = -9 \text{ ‰}/100 \text{ m}$ for dependencies valid for altitudes between 2200 – 3200 masl.

The actual altitude of each spring sample site was then subtracted from the precipitation derived recharge altitude. The discrepancy between actual altitude and estimated recharge altitude (vertical distance) was used to indicate sources of water. Average recharge altitudes and vertical distances for the *Sierra Nevada* and *Granada* basin springs were calculated as shown in tab.4.6. The vertical distance for the *Sierra Nevada* springs ranges between 370 and 1000 m, only basin springs have values far above 1000 m (1100; 1300 m). The basin springs (*Fte.Palmones*, *Fte.Molinos*) and the *Sierra* springs have similar $\delta^{18}\text{O}$ values (arrow in Fig.4.24). Thus the recharge altitudes must be similar. Also high vertical distance can be found in three *Sierra Nevada* springs (*Fte. de los 16 canos*, *Fte. del Hervidero*, *Fte. 7 ojos*) as indicated with the arrow in figure 4.24.

The resolution of mean recharge calculations is defined by the precision in isotope measurement and the local altitude gradient. The altitude effect of $-0.2 \text{ ‰}/100 \text{ m}$ ($-0.002 \text{ ‰}/\text{m}$ or $500 \text{ m}/\text{‰}$), with a precision of measurement of $\pm 0.1 \text{ ‰}$ on the $\delta^{18}\text{O}$ of the groundwater, leads to a maximum resolution of $500 * 0.1 = \pm 50 \text{ m}$. If the precision is higher, e.g. 0.04 ‰ , the maximum resolution for establishing recharge altitude is $500 * 0.04 = \pm 20\text{m}$. The precision in isotope measurement ranges between 0.02 ‰ and 0.09 ‰ in $\delta^{18}\text{O}$ and between 0.1 ‰ and 0.4 ‰ in δD .

• Table 4.6 Average $\delta^{18}\text{O}$ values, maximum error and average recharge altitude for *Sierra Nevada* springs and *Granada* basin springs (*cursive*).

Site	Altitude (masl)	$\delta^{18}\text{O}$ (‰)	$\delta^{18}\text{O}$ error (‰)	$\delta^{18}\text{O}$ recharge Altitude (masl)	vertical distance (m)
Fte. Alta	2156	-9.46	0.04	2522 (+/-20)	366
Fte. las Viboras	1629	-8.97	0.06	2277 (+/-30)	648
Fte. del Hervidero	1292	-8.87	0.05	2229 (+/-25)	937
Fte. la Cortijuela	1695	-8.84	0.07	2214 (+/-35)	519
Fte. de los 16 canos	1222	-8.87	0.06	2231 (+/-30)	1009
Fte. de Teja	1278	-8.12	0.03	1855 (+/-15)	577
<i>Fte. Palmones</i>	<i>745</i>	<i>-8.56</i>	<i>0.04</i>	<i>2072 (+/-20)</i>	<i>1327</i>
<i>Fte. los Molinos</i>	<i>730</i>	<i>-8.09</i>	<i>0.06</i>	<i>1841 (+/-30)</i>	<i>1111</i>
Fte. Savina	1113	-8.10	0.10	1845 (+/-50)	732
Fte. Agostinos	1362	-8.55	0.05	2070 (+/-25)	708
Fte. Carcabal	1605	-8.79	0.07	2190 (+/-35)	585
Fte. Nabugal	1471	-8.69	0.04	2140 (+/-20)	669
Fte. 7 ojos	1411	-8.97	0.02	2280 (+/-10)	869
min	730	-9.46	0.02	1841	366
max	2156	-8.09	0.10	2522	1327
average	1362	-8.68	0.05	2135	774

The groundwater flow direction from NE to SW in the *Sierra de la Peza* carbonate aquifer indicates the strong influence of the *Sierra Arana* as the recharge area for the *Sierra de la Peza* springs. Compared to the climatic conditions in the *Sierra Nevada*, the relative low decrease in temperatures with altitude in the *Sierra Arana* must produce a shallower $\delta^{18}\text{O}$ /altitude gradient. That means that rainfall at similar altitudes is in the *Sierra Arana* more depleted than in the *Sierra Nevada*. This difference in local precipitation pattern is reflected by the shallower regression between spring samples from the *Sierra de la Peza* aquifer (section 4.2.4). Since no data about isotopes in precipitation in this area is available, local gradients must be approximated according to general isotope/altitude relationship. The gradient for the *Sierra de la Peza* springs have been applied to the local geomorphology (derived from the DEM) in order to achieve reasonable recharge altitudes. Average recharge altitudes and vertical distances for the *Sierra de la Peza* spings were calculated as shown in tab.4.7.

***Sierra de la Peza* Equation** **Altitude range** **Gradient**
 Altitude (masl) = $-332 * \delta^{18}\text{O} - 1190$ 800 – 2200 masl -0.3 ‰/100 m (eq.4.12)

• Table 4.7 Average $\delta^{18}\text{O}$ values, maximum error and average recharge altitude for *Sierra de la Peza* springs.

Site	Altitude (masl)	$\delta^{18}\text{O}$ (‰)	$\delta^{18}\text{O}$ error (‰)	$\delta^{18}\text{O}$ recharge Altitude (masl)	vertical distance (m)
Fte. Grande	1114	-8.40	0.02	1597 (+/- 7)	483
Fte. de Nivar	1108	-8.41	0.04	1600 (+/-13)	492
Fte. Cerro Negro	1115	-8.12	0.08	1505 (+/-27)	390
Nac. Rio Darro	1106	-8.42	0.06	1605 (+/- 20)	499
Fte. de Vita	944	-7.48	0.04	1293 (+/-13)	349
Fte. Teja	1262	-8.35	0.02	1582 (+/-7)	320
min	944	-8.42	0.02	1293	320
max	1262	-7.48	0.08	1605	499
average	1108	-8.19	0.04	1531	422

The vertical distance for the *Sierra de la Peza* springs are low (average=422 m) and ranges between 320-499 m.

It is important to recognize that several factors may modify the above mentioned equations (eq.4.10, 4.11, 4.12). Calculations are based only on a relative small time period of monitoring of 1.5 years (eq.4.10, 4.11) or were estimated (eq.4.12). The equations should be considered as rough estimations, which can vary seasonally and spatially. As shown in section 1.4 the year to year change in precipitation is highly variable and therefore a detailed knowledge of isotopes in local precipitation is necessary. Furthermore, one could expect that $\delta^{18}\text{O}$ vs. altitude in spring samples and $\delta^{18}\text{O}$ vs. altitude in precipitation samples are parallel. This is not the case. Therefore, the above equation may overestimate recharge elevations especially in lower altitudes and the groundwater recharge altitude equation appears to be dominated by high altitude rainfall (lower $\delta^{18}\text{O}$) infiltration.

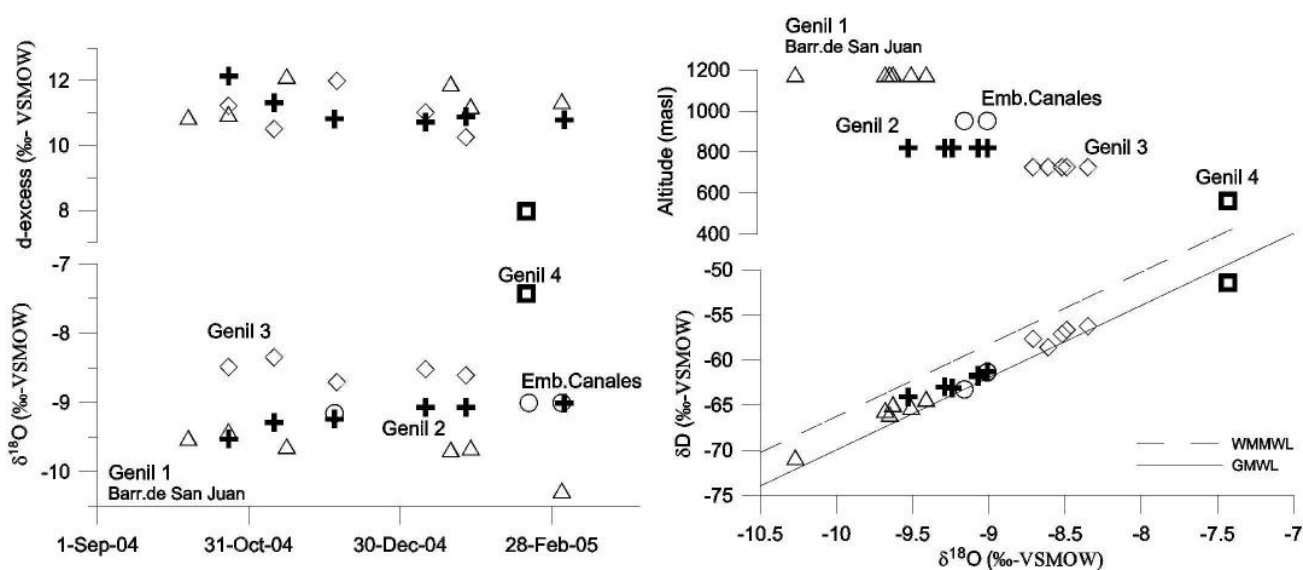
4.2.3 Surface water samples

In this section surface water samples from streams (*Arroyo*, *Barranco*), rivers (*Rio*) and reservoirs (*Embalse*) are presented. Rivers were sampled frequently on different altitudes in order to discover seasonal variations and recharge conditions in the *Rio Genil* and the *Rio Darro*. Additionally, single samples were taken from the *Rio Cubillas* and the reservoirs *Canales*, *Cubillas* and *Quentar* were sampled.

4.2.3.1 Rio Genil

The *Rio Genil* is the most important river in the study area and is considered to be a main source for indirect recharge to the alluvial aquifer *Vega de Granada*. The river sites are described from the highest point at 1180 masl (*Barr.de San Juan*) downstream to the lowest site in the *Vega de Granada* at 650 masl. D-excess and $\delta^{18}\text{O}$ (‰-VSMOW) against time is plotted in the left diagram in order to visualize seasonal effects. The right diagram shows the δD and Altitude (masl) against $\delta^{18}\text{O}$ (‰-VSMOW) diagrams of *Genil* samples in order to visualize possible evaporation processes (Fig.4.25). Site locations are shown in figure 4.15.

Seasonal variations in isotopes can be observed in the high altitude site (*Barr. de San Juan* or *Genil 1*), located in the metamorphic core *Nevado-Filabride*. Due to the low permeabilities in this terrain it is expected that surface runoff dominates the discharge. The variations in the isotopes will follow the course of a hydrograph derived from river discharge measurements. High rates of discharge are expressed as low δ - values. Therefore, samples taken between September to November (no rainfall) represent the base flow of the river, while the January sample is slightly shifted towards lighter isotopes due to snowfall and the March sample shows a strong peak towards lighter isotopes due to snow thawn. Especially the March sample represents the isotopic composition right after rainfall event.



• Figure 4.25 $\delta^{18}\text{O}$ with d-excess vs. time diagrams (left) and δD with Altitude (masl) vs. $\delta^{18}\text{O}$ (‰-VSMOW) diagrams (right) of *Genil* samples.

Following the course of the *Genil* downstream the next site is situated in the reservoir (*Emb.de Canales*) of the *Genil*. The reservoir was build between 1975 - 1989 and stretches over a length of 340 m with a maximum storage capacity of 7.248 m³ and a maximum depth of 156 m (*Ministerio de Medio Ambiente, Embalse de Canales* 2001). Samples taken from the reservoir itself and at the discharge (*Genil 2*) showing a very similar isotope composition. No samples from depth below surface were taken, since stratification within the water column was not expected and may only occur during summer, when strong sun radiation warms up the upper surface water layer. Therefore the reservoir is considered to be a well mixed water body with minor changes in the isotopic composition in relation to the water depth. Seasonal variations are attenuated in the reservoir due to fast internal mixing relative to the residence time in the reservoir. Minor to none evaporative enrichment can be observed. Nevertheless, over the time period of monitoring the isotope signature in the reservoir follows a successive trend from relative light δ -values to more positive values. This trend reflects the decreasing water table within the reservoir due to minor input flow.

Following the course of the *Genil* further downstream the next site is situated in the Mio-/Pliocene basin fillings (*Genil 3*). This site is situated after the inflow of the river *Aguas Blancas* into the *Genil*. Samples from the river *Aguas Blancas* (*Emb.de Quentar*) show a significant heavier isotopic composition with $\delta^{18}\text{O} = -7.8 \text{‰}$ and $\delta\text{D} = -52 \text{‰}$ compared to samples from site *Genil 3*. This reflects the lower altitudes where surface runoff takes place in the catchment area of the river *Aguas Blancas*. A more detailed discussion is presented in the following sections. Samples of the *Genil 3* site showing a subparallel shift along the MWLs towards heavier isotopes (max. +1‰ in $\delta^{18}\text{O}$) composition compared to upstream samples from the reservoir *Canales*. Assuming a binary mixture from water of the *Genil* with water from the *Aguas Blancas* it is possible to calculate the degree of mixture with simple algebra according to:

$$\delta_{\text{sample}} = d \cdot \delta_{\text{A}} + (1-d) \cdot \delta_{\text{B}} \quad (\text{eq.4.13})$$

where d is the degree or proportion of mixture of the mixed sample (*Genil 3*) from sample A (*Genil 2*) with sample B (*Quentar*). This leads to a calculated proportion of mixture of $d = 0.58$ and so a water surplus of 42 % by the river *Aguas Blancas* to the river *Genil*. This calculation may overestimate the influence of the river *Aguas Blancas* as it neglects other sources of water such as irrigation. However, it is obvious that the relative light isotopic composition of the *Genil* is significantly influenced by the relative heavy signature from the *Aguas Blancas* river.

The sample *Genil 4*, taken from the western part of the *Vega de Granada* shows a very strong isotopic enrichment, shifting the isotopic composition of the groundwater away from the local meteoric line along an evaporation line. This tendency could be driven by the re-use of waters mainly for irrigation purposes in combination with mixing processes with already enriched water. A more detailed discussion is presented in section 4.2.7 Wells. D-excess values provide no useful information. A trend in the δD vs. $\delta^{18}\text{O}$ from the high altitude site (*Barr.de San Juan*) downstream which courses not exactly parallel to the MWLs (Fig.4.25).

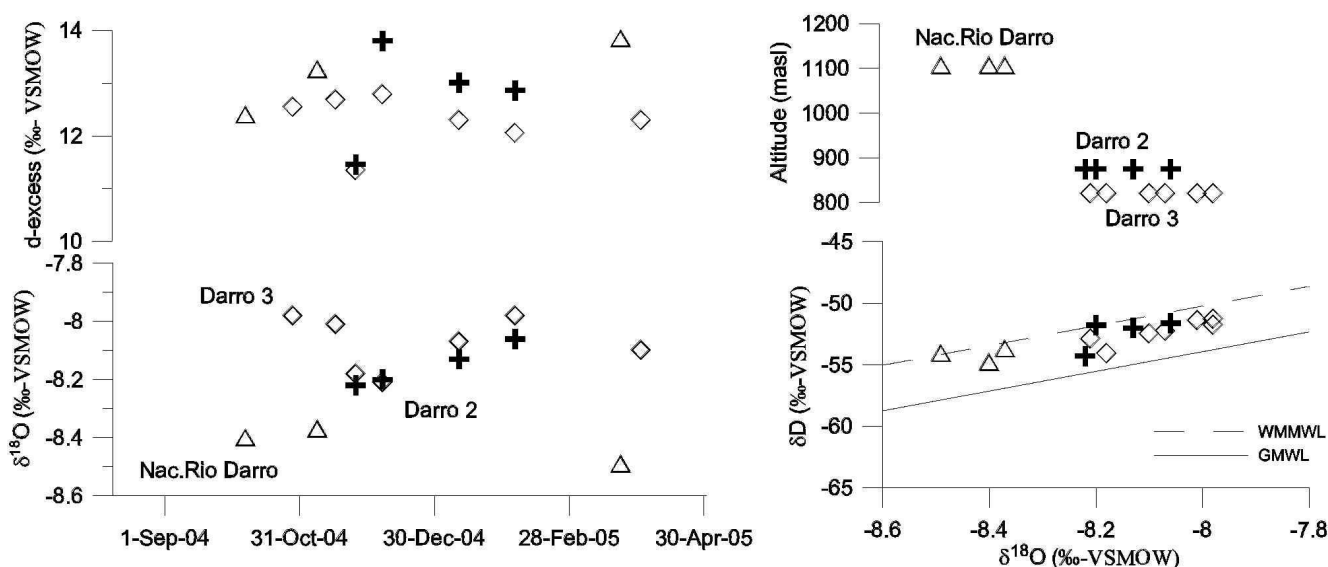
4.2.3.2 Rio Darro

The *Rio Darro* is a tributary to the *Genil* and both rivers intersect in the city of *Granada*. The sampling sites of the *Rio Darro* are described from the highest site at 1106 masl downstream to the lowest site at 820 masl. For site location see figure 4.15. D-excess and $\delta^{18}\text{O}$ (‰-VSMOW) against time is plotted in the left diagram in order to visualize seasonal effects. The right diagram shows the δD and Altitude (masl) against $\delta^{18}\text{O}$ (‰-VSMOW) in order to visualize possible evaporation processes (Fig.4.26).

Samples from the highest site (*Nacimiento Rio Darro* 1106 masl) (open triangles), showing a quite constant course of δ -values over the time of monitoring, with a maximum deviation of $\Delta 0.12$ ‰ in the $\delta^{18}\text{O}$ values between the November 04 and March 05 sample. This low deviation reflects the relative wide catchment area, where seasonal variations are attenuated by mixing processes. The isotopic most depleted sample taken in March 05 indicates the recharge water derived from precipitation probably from the winter 04/05.

Following the course of the river downstream the next site is *Darro 2* (crosses). This site is situated in the N-S stretching valley of the *Darro* at an altitude of 875 masl. Comparing *Darro 2* samples with samples from *Nac.Rio Darro* taken at the same time often a shift in $\delta^{18}\text{O}$ values to the spring is $\Delta 0.2$ ‰, which is significant above the error in measurement. Since variations in $\delta^{18}\text{O}$ ($\Delta 0.16$ ‰) are significant above the error in measurement (0.03 ‰), seasonal variations were observed.

Following the course of the *Darro* further downstream the next site (*Darro 3*) is situated in conglomeratic sediments termed as *Alhambra* formation. A typical sinusoidal course of $\delta^{18}\text{O}$ can be observed in the temporal plot of *Darro 3* samples. The fact that these seasonal variations are stronger compared to samples from *Darro 2* leads to the assumption that anthropogenic impacts (irrigation) may cause these variations.



• Figure 4.26 $\delta^{18}\text{O}$ with d-excess vs. time diagrams (right) and δD with Altitude (masl) vs. $\delta^{18}\text{O}$ (‰-VSMOW) diagrams (left) of *Darro* samples.

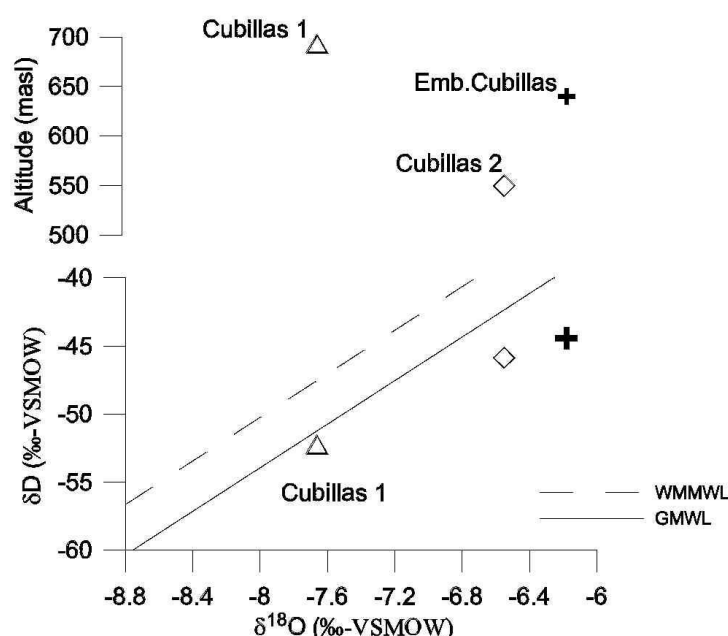
4.2.3.3 Rio Cubillas

Fig.4.27 shows all samples taken from the river *Cubillas* (*Rio Cubillas*), which is a tributary to the *Genil*. Both rivers intersect in the western part of the *Vega de Granada*, as shown in figure 4.15. Compared to river samples from the *Darro* or *Genil* the pattern of the isotopes is very different according to the large catchment area with low average elevation.

The site *Cubillas 1* is situated in the Mio-/Pliocene basin sediments in altitudes of 693 masl and exhibits the most depleted value of all *Cubillas* samples. Since *Cubillas 1* sample plots below the MWL evaporative enrichment cannot be excluded.

The sample from the reservoir (*Embalse de Cubillas*) shows strong evaporative enrichment, but cannot be quantified due to the lack of the end-member compositions. The reservoir was build between 1939 - 1963 and stretches over a length of 370 m with a maximum storage capacity of 600 000 m³ and a maximum depth of 52 m (*Ministerio de Medio Ambiente, Embalse de Cubillas 2001*).

The site *Cubillas 2* is situated in the *Vega de Granada* and is plotting between the reservoir and the *Cubillas 1* sample. In this area of the *Vega de Granada* aquifer the hydraulic behaviour is considered to be influent (gaining river). Therefore, the sample from *Cubillas 2* could be interpreted as mixing between strong enriched river water from the *Cubillas* with less enriched groundwater of the *Vega de Granada* at the north-western part of the *Vega*.

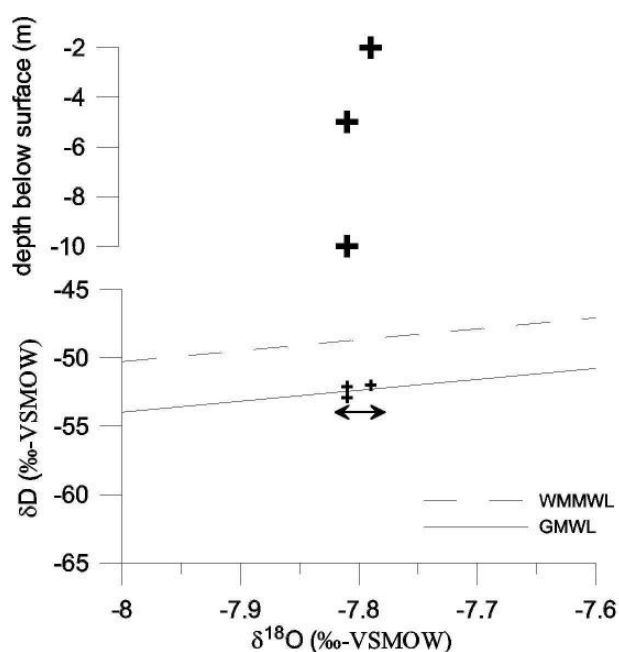


• Figure 4.27 $\delta^{18}\text{O}$ (‰-VSMOW) vs. δD (‰-VSMOW) and δD (‰-VSMOW) vs. Altitude (masl) diagrams of river Cubillas samples.

4.2.3.4 Embalse de Quentar

The reservoir (*Emb.de Quentar*) is situated near the village *Quentar*, which is situated in the north-eastern part of the study area. This reservoir is fed by the river *Aguas Blancas*, which is a tributary to the *Genil*. The catchment area of the river *Aguas Blancas* is ca. 140 km² with altitudes from 800–2300 masl (mean altitude = 2500 masl). The reservoir was build between 1971 - 1975 and stretches over a length of 200 m with a maximum storage capacity of 277 000 m³ and a maximum depth of 133m (*Ministerio de Medio Ambiente, Embalse de Quentar 2001*).

The samples were taken from three different depth below surface (-2, -5, -10 m) as shown in fig.4.28. Variations in the $\delta^{18}\text{O}$ content in relation to sample depth are within tolerance of measurement precision, thus no trend can be observed. This confirms the assumption that large water bodies like reservoirs can be, at least in winter, considered as a non stratified water column. The δ -values of these samples are located on or slightly over the GMWL. This suggests that may evaporation occurred in the reservoir, but are due to the lack of further samples not quantifiable.



• Figure 4.28 $\delta^{18}\text{O}$ (‰-VSMOW) vs. δD (‰-VSMOW) of samples from the reservoir *Quentar* and depth below surface (arrow indicates the range of precision in $\delta^{18}\text{O}$ measurement).

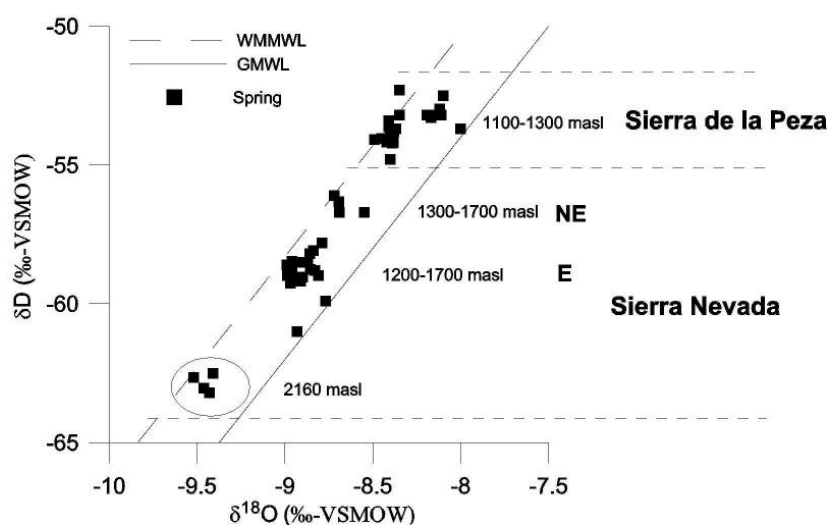
4.2.4 Springs

Groundwater derived from a spring must be considered as a mixture from different altitudes. Thus the mean $\delta^{18}\text{O}$ or δD value of each sampling location gives an approximation of the spatial and temporal mean elevation of upland recharge. The interpretation of the recharge area for groundwater also includes consideration of the geologic structure, the recharge patterns and the sample type.

According to their $\delta^{18}\text{O}$ vs. δD relationship, the spring samples show a spectrum of $\delta^{18}\text{O}$ from -9.5 to -8 (‰-VSMOW). D-excess ranges between 10 ‰ and 17 ‰ and confirms the sources of rain bearing air masses from the Atlantic (d-excess = 10 ‰) or the Mediterranean Sea (d-excess = 14 ‰). The position of the spring samples **along** the water lines is used to characterise groundwater recharge provenances. Two main groundwater provenances can be distinguished: a) *Sierra Nevada* and b) *Sierra de la Peza*. Most of the δD and $\delta^{18}\text{O}$ values plot parallel to the WMMWL, but especially in the *Sierra de la Peza* group several samples plot below of the WMMWL (Fig.4.29). This fact indicates the different climatic conditions and therefore different isotope signature as discussed in section 4.2.2, where the $\delta^{18}\text{O}$ composition of precipitation was used to estimate the source area of recharge to springs.

Sierra Nevada springs show the most depleted δ -values with -9.5 - -8.5 ‰ and can be subdivided by the spatial location in springs from the metamorphic core of the *Nevado-Filabride* and springs in the *Alpujarride* carbonate complex. Springs located in the north-eastern part of the study area in the *Sierra de la Peza* are considered to be fed by water from the *Sierra Arana* and are significant heavier (-8.5 - -8 ‰-VSMOW).

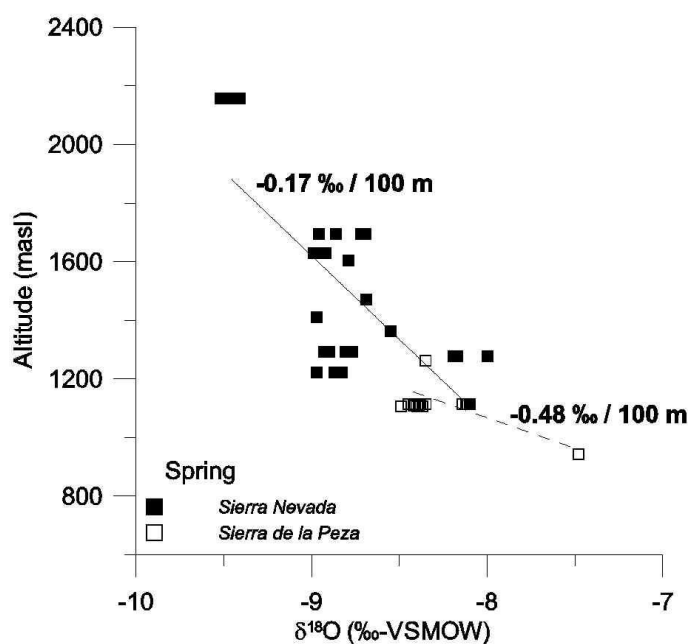
Springs, surface water and selected precipitation sites are discussed more detailed together with profiles in order to visualise the local recharge pattern.



• Figure 4.29 $\delta^{18}\text{O}$ vs. δD (‰-VSMOW) diagram of spring samples from different *Sierras* in the study area.

Because isotope partitioning at least correlates with temperature and the geomorphology in the study area shows strong temperature gradients, the composition of the groundwater isotope composition depends indirectly on altitude. By plotting the $\delta^{18}\text{O}$ value against altitude of the site it is possible to detect local altitude effects.

The regression line calculated with the average values from *Sierra Nevada* springs is defined as: $\text{Altitude (masl)} = -571.43 * \delta^{18}\text{O} - 3522.91$ ($n = 11$; $r^2 = 0.58$), thus the mean altitude gradient is $-0.17 \text{ ‰} / 100\text{m}$, which is very close to the gradients from GARRIDO 2003 with $0.2 \text{ ‰} / 100 \text{ m}$. The regression line calculated with the average values from *Sierra de la Peza* springs is defined as: $\text{Altitude (masl)} = -209.04 * \delta^{18}\text{O} - 604.81$ ($n = 6$; $r^2 = 0.58$), thus the mean altitude gradient is shallower $-0.48 \text{ ‰} / 100\text{m}$. Local $\delta^{18}\text{O}$ / altitude gradients in the literature vary from $-0.2/100 \text{ m}$ to $-0.5/100 \text{ m}$ (CLARK & FRITZ 1997). As shown in figure 4.30 springs which are located on altitudes around 1200 masl with $\delta^{18}\text{O}$ values around -9 ‰ (*Fte. Hervidero, Fte. 16 Canos, Fte. 7 Ojos*) are isotopical equal to springs located on altitudes around 1600 masl. This means that these low elevation springs are fed from the same altitudes as springs on the higher elevation. This increased flowpath should be seen in increased SI values since residence time and therefore reaction time will increase (see transect III).

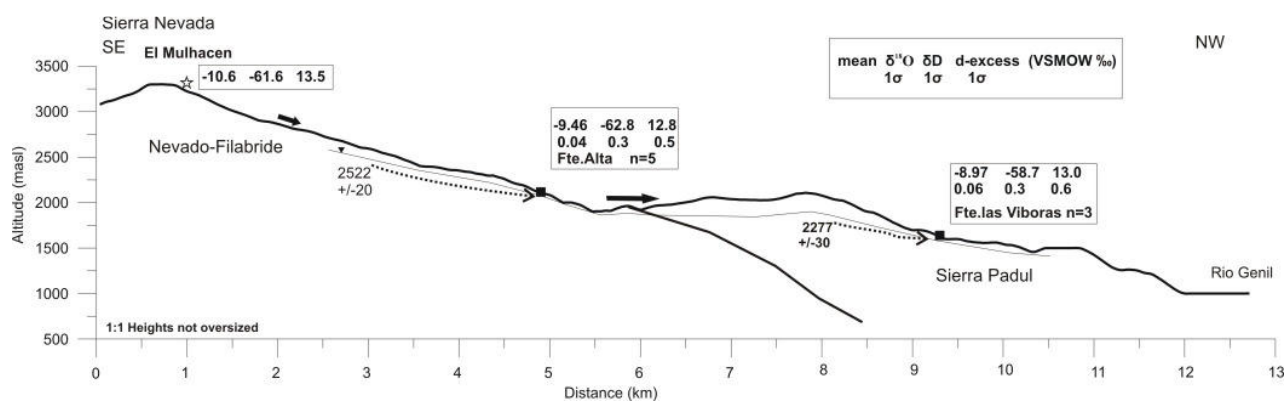


• Figure 4.30 Average $\delta^{18}\text{O}$ (‰-VSMOW) vs. Altitude (masl) of all *Sierra*

Mean recharge elevation in transect I and II (Fig.4.31; Fig.4.32) were calculated with the *Sierra Nevada* equation, valid for altitudes between 800 – 2200 masl and introduced in section 4.2.2 (tab.4.6). The rectangles in the isotope profiles for each sampling site shows the mean $\delta^{18}\text{O}$, δD and d-excess values together with the standard deviation for frequently measured sites. The water table heights are considered to be a subdued copy of the topographic relief, which was derived from the DEM. All isotope transects provide information about local flow paths.

In fig.4.31 the highest sampling site shown is a snow sample taken at the peak of *El Mulhacen* during summer. This signature is characteristic for summer snowmelt as discussed in previous section. The spring located at the highest elevation (*Fte.Alta*) exhibits the most depleted mean $\delta^{18}\text{O}$ composition (-9.5 ‰), which represents groundwater recharge provenances in the *Nevado-Filabride* metamorphic core at altitudes >2156 masl. Standard deviation of $\delta^{18}\text{O}$ and δD is low (0.04 and 0.3 respectively, equal to maximum error in measurement) and reflects that seasonal variations are attenuated. Mean recharge elevation is calculated with 2522 masl (+/-20), giving a relative low difference between real altitude and mean recharge altitude with 367 m. This relative low vertical deviation is confirmed by low run off (6 l/min) and small surface catchment area (ca.10 km²).

Fte.las Viboras located in altitudes at 1629 masl (*Alpujarride*) shows mean isotopic composition of $\delta^{18}\text{O} = -8.97$ ‰ and represents groundwater recharge provenances at the border between the *Nevado-Filabride* metamorphic core and the *Alpujarride* carbonate complex. No groundwater flow between the *Alpujarride* carbonate complex and the *Nevado-Filabride* metamorphic core can be observed and confirms the closed boundary conditions. Exchange between these units may be dominated by surface runoff.

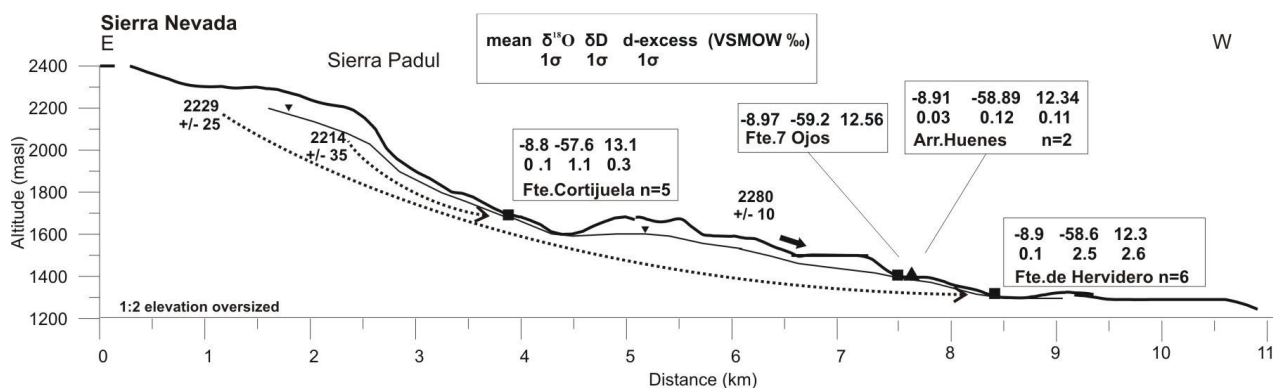


• Figure 4.31 Isotope transect I: High altitude springs and snow samples in the *Sierra Nevada*. Mean recharge altitudes and precision of calculation. Black solid arrows indicate surface runoff, dotted arrows indicate flowpaths, thin line indicate water table. Altitude/distance relation is given in lower left corner.

Fte.Cortijuela located in altitude of 1695 masl shows mean isotopic composition of $\delta^{18}\text{O} = -8.8$ and $\delta\text{D} = -57.6$ ‰ with standard deviation of 0.1 and 1.1 respectively. The relative high standard deviation is above the maximum measurement error with 0.07 and therefore seasonal variations are observed in this low runoff (0.8 l/min) and relative small catchment area spring (fig.4.32).

Fte.del Hervidero located in altitudes at 1292 masl shows mean isotopic composition of $\delta^{18}\text{O} = -8.87$ ‰. The mean composition is relative light and the mean recharge elevation is calculated with 2229 masl. The high difference between real and calculated mean recharge altitude is 937 m and the calculated undersaturation with respect to calcite and dolomite ($\text{SI}_{\text{Cc}} = -0.7$; $\text{SI}_{\text{Do}} = -1.9$) may be indicative for high flow velocities with minor dissolution of calcite host-rocks.

Fte.7 Ojos located in altitudes at 1411 masl shows isotopic composition of $\delta^{18}\text{O} = -8.97$ ‰ and $\delta\text{D} = -59.2$ ‰. This single measurement sample was taken during snowmelt period and might be misleading for calculating the mean recharge elevation since seasonal event is reflected in the *Arr. Huenes* is heavier than the *Fte.7 Ojos* sample and suggest that catchment area of the stream is smaller compared to the catchment area of the spring. No correlation between SI values and vertical deviation between real and mean recharge altitude is observed.



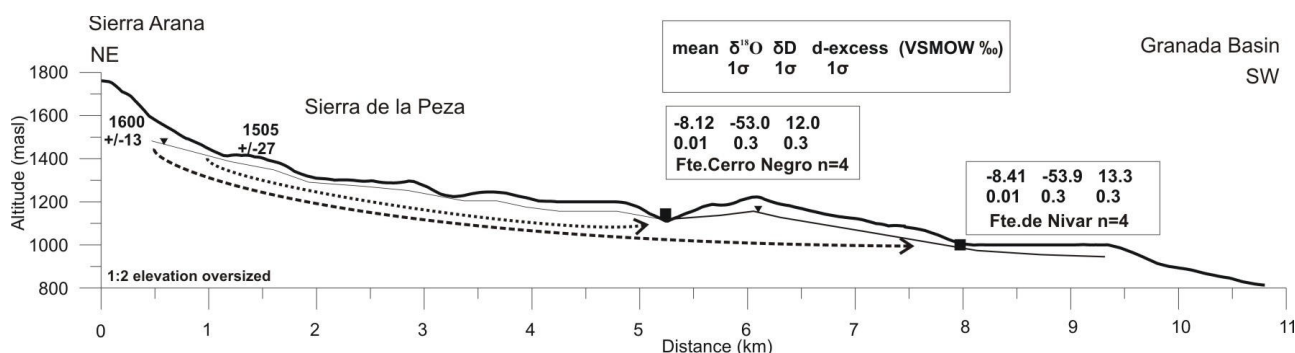
• Figure 4.32 Isotope transect II: High altitude springs and river samples in the Sierra Nevada. Mean recharge altitudes and precision of calculation. Black solid arrows indicate surface runoff, dotted arrows indicate flowpaths, thin line indicate water table. Altitude – distance relation is given in lower left corner.

Mean recharge elevation in transect III (Fig.4.33) is calculated with the *Sierra de la Peza* equation (eq.4.12) introduced in section 4.2.5. Mean recharge altitude calculations for springs located in the *Sierra de la Peza* are shown in tab.4.7.

Fte.Cerro Negro located in altitude of 1115 masl shows mean isotopic composition of $\delta^{18}\text{O} = -8.12$ and $\delta\text{D} = -53.0$ ‰ with standard deviation of 0.01 and 0.3, respectively. Mean recharge elevation is calculated with 1505 masl (+/-27), giving a relative low vertical discrepancy of 390 m. Samples from this spring are undersaturated with respect to calcite and dolomite ($\text{SI}_{\text{Cc}} = -0.34$; $\text{SI}_{\text{Do}} = -1.03$).

Fte.de Nivar located in altitude of 1108 masl shows mean isotopic composition of $\delta^{18}\text{O} = -8.41$ and $\delta\text{D} = -53.9$ ‰ with standard deviation of 0.01 and 0.3 respectively. Calculations of SI confirms the increased flowpath by increased saturation with respect to calcite and dolomite ($\text{SI}_{\text{Cc}} = -0.02$; $\text{SI}_{\text{Do}} = -0.37$). Spring samples visualised in the isotope transect III show positive correlation between SI values and vertical discrepancy between actual and recharge altitude.

It was recognized that groundwater from low altitude springs must be derived from higher altitudes compared to springs which are situated above. Therefore, the lower the spring is situated the longer the flowpath and the higher the recharge area is.



• Figure 4.33 Isotope transect III: Springs and river samples in the *Sierra de la Peza*. Mean recharge altitudes and precision of calculation. Black solid arrows indicate surface runoff, dotted arrows indicate flowpaths, thin line indicate water table. Altitude – distance relation is given in lower left corner.

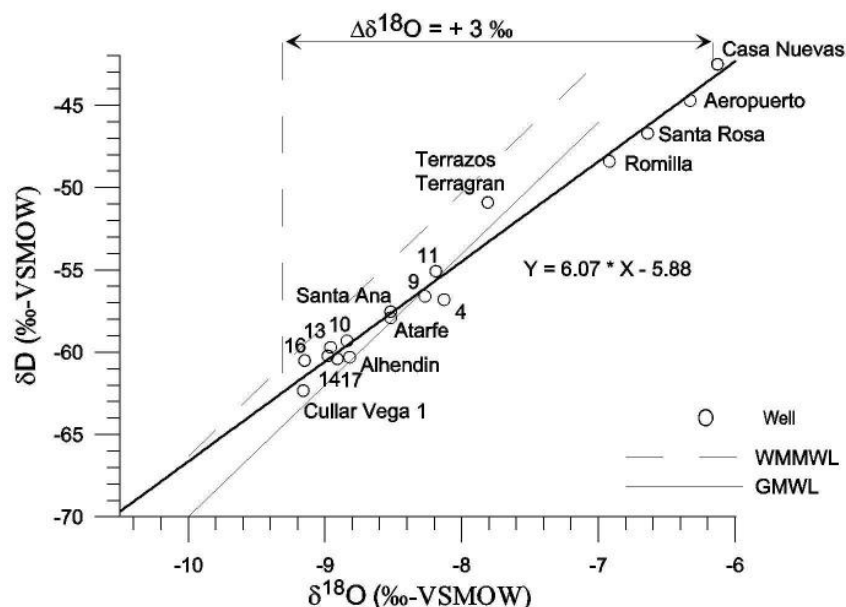
4.2.5 Wells in the *Vega de Granada*

Groundwater samples from wells in the *Vega de Granada* plot **below** of the WMMWL and show variations in $\delta^{18}\text{O}$ from -9.2‰ to -6.92‰ with a preferential enrichment in $\delta^{18}\text{O}$ indicating evaporation losses are observed (Fig.4.34). The numbers refer to wells documented in location map figure 4.15.

Samples from wells located in the **south-eastern** part of the *Vega de Granada*, at the beginning of the flowpath (e.g. *Alhencira* (16)) through the alluvial aquifer, plot near to the WMMWL. These samples are considered to be not affected by evaporation but still a displacement to the WMMWL is observed (e.g. *Cullar Vega 1*). This displacement to the WMMWL may implies minor water-rock interactions from the groundwater with the host rocks on its flowpath. Therefore, assuming attenuated seasonal effects, the mean isotopic composition of groundwater in this area can be estimated by drawing a line parallel to $\delta^{18}\text{O}$ axis until it intersects with the WMMWL. This results in local mean groundwater compositions in $\delta^{18}\text{O}$ of $\sim -9.3\text{‰}$. In contrast, groundwater from the **centre** and the **western** part of the *Vega de Granada* is relative enriched in both isotopes with a strong enrichment in $\delta^{18}\text{O}$ indicating evaporation losses. The regression line fitted to the 17 well samples is defined as:

$$\delta\text{D} = 6.07 * \delta^{18}\text{O} - 5.88 \quad (n=17, r^2=0.98) \quad (\text{eq.4.14})$$

By taking the annual average temperature ($\sim 15^\circ\text{C}$) from the *Granada* basin (see section 1.4), the slope of the regression line ($s = 6.07$) allows to approximate the relative humidity according to GONFIANTINI 1986 with around $h = 0.8$ ($=80\%$). Now it is possible to determine the kinetic fractionation factors using Gonfiantini's equations (section 2.7), giving $\epsilon^{18}\text{O}_{\text{kinetic}} = -2.84\text{‰}$. The



• Figure 4.34 $\delta^{18}\text{O}$ vs. δD in groundwater from wells in the *Vega de Granada* alluvial aquifer. MWLs as reference. Numbers refer to wells documented in location map (Fig.4.15).

total enrichment ($\epsilon_{\text{total}} = \epsilon_{\text{equilibrium}} + \epsilon_{\text{kinetic}}$) for evaporation under these conditions with the mean temperature of 15 °C in the *Granada* basin ($\epsilon_{\text{equilibrium}} = -10.3 \text{ ‰}$) is then $\epsilon_{\text{total}} = -13.14 \text{ ‰}$. The intersection of the regression line with the WMMWL is considered as the initial isotope ratio without evaporative impact ($\delta^{18}\text{O}_{\text{initial}} \sim -9.2 \text{ ‰}$). The sample taken from *Casa Nuevas* shows the most enriched value and represents the maximum evaporative enrichment ($\delta^{18}\text{O}_{\text{sample}} = -6 \text{ ‰}$). The total enrichment of this samples can then be calculated with maximum $\Delta\delta^{18}\text{O} = \delta^{18}\text{O}_{\text{initial}} - \delta^{18}\text{O}_{\text{sample}} = 3.2 \text{ ‰}$. The fractional water loss from evaporation can then be modelled according to a Rayleigh distillation. For $\delta^{18}\text{O}$, the evaporative enrichment is up to 3.2 ‰. According to equation 2.9.:

$$\epsilon_{\text{total}}(\delta^{18}\text{O}) * \ln f = 3.2 \text{ ‰}$$

yielding a residual water fraction f of 0.78 and so an maximum evaporative loss in the sample of *Casa Nuevas* of 22 %.

For identifying the source area a correction of $\delta^{18}\text{O}$ for evaporative enrichment was applied. Corrected values indicate the isotopic composition without enrichment by evaporation. As the corrected value marks the intersection of the evaporation line with the LMWL (WMMWL), it is defined by equation 4.9, where s corresponds to the slope of the evaporation line determined in equation above (eq.4.14) as 6.07, and i is the intercept of the WMMWL, with $i = +13.7 \text{ ‰}$. In the study area the variability of corrected $\delta^{18}\text{O}$ in groundwater is assumed to reflect mainly different recharge altitudes. The mean isotopic composition of corrected $\delta^{18}\text{O}$ -values is -10.16 ‰ , while uncorrected $\delta^{18}\text{O}$ -values lead to an average of -8.13 ‰ (Tab.4.8). This exceptional low mean isotopic composition of corrected δ -values leads to the assumption that either the regression line is false due to wrong measurements or other processes like water-rock interaction might shift the δ -values. Examination of this assumption might be subject to further studies.

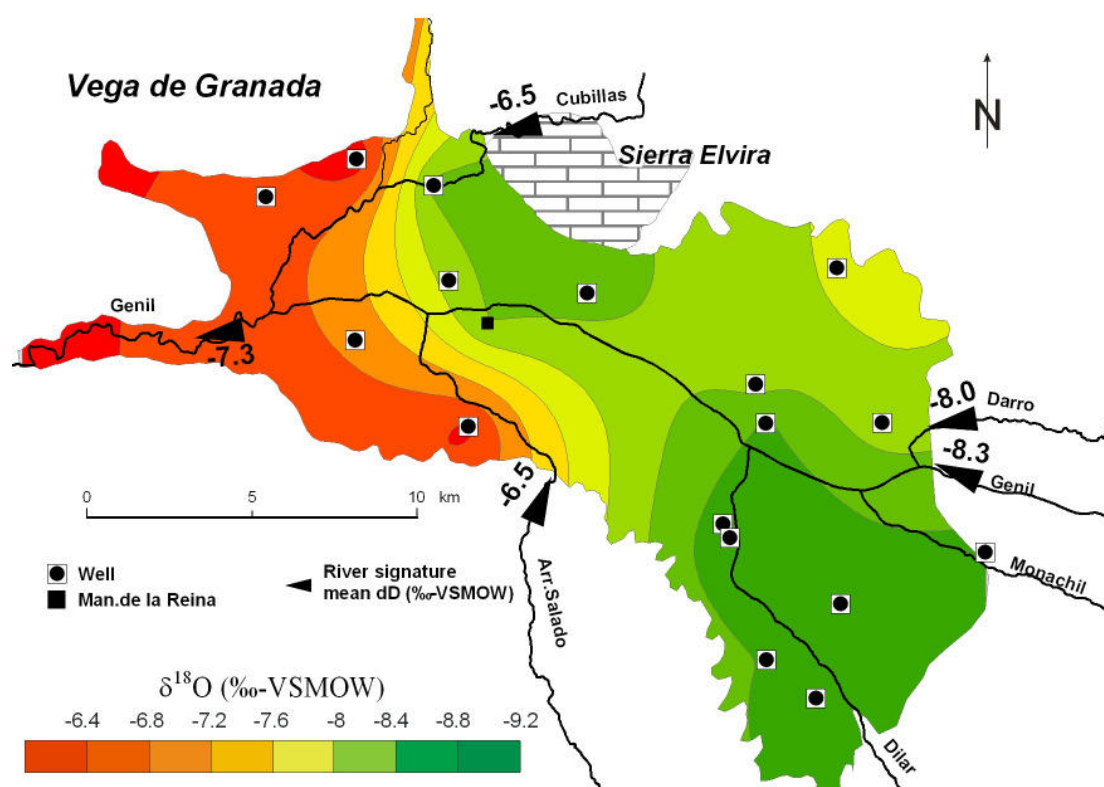
• Table 4.8 Sites, type, date of sampling, $\delta^{18}\text{O}$, δD (‰-VSMOW), corrected values without evaporative enrichment for $\delta^{18}\text{O}$ (‰-VSMOW) in wells and observation wells and the resulting evaporative enrichment.

Site name	Type	Sampling date	$\delta^{18}\text{O}$ (‰)	δD (‰)	$\delta^{18}\text{O}$ (‰) corrected	$\delta^{18}\text{O}$ (‰) enrichment
Aeropuerto	Observation well	25. Nov 04	-6.33	-44.7	-10.35	4.02
Alhencira	Well	18. Feb 05	-9.15	-60.5	-9.67	0.52
Alhendin	Observation well	08. Nov 04	-8.82	-60.3	-10.6	1.78
Armillá	Well	18. Feb 05	-8.98	-60.2	-10.06	1.08
Atarfe	Observation well	17. Nov 04	-8.52	-57.9	-10.3	1.78
Camino frente Puleva	Observation well	16. Nov 04	-8.84	-59.3	-10.02	1.18
Casa Nuevas	Well	22. Nov 04	-6.13	-42.5	-9.84	3.71
Cort. Santa Ana	Well	18. Feb 05	-8.52	-57.5	-10.11	1.59
Cort. Trevijano	Observation well	26. Nov 04	-8.27	-56.6	-10.42	2.15
Cullar Vega 1	Observation well	09. Nov 04	-8.96	-59.7	-9.85	0.89
Cullar Vega 2	Well	18. Feb 05	-9.16	-62.3	-10.58	1.42
Meson El Guerro	Well	18. Feb 05	-8.91	-60.4	-10.37	1.46
Pedro Ruiz	Observation well	12. Nov 04	-8.13	-56.8	-10.96	2.83
Romilla	Observation well	05. Nov 04	-6.92	-48.4	-10.41	3.49
Santa Rosa	Well	10. Nov 04	-6.64	-46.7	-10.41	3.77
Terrazos Terragan	Well	18. Feb 05	-7.81	-50.9	-8.91	1.1
UGR, Facultad de Ciencias	Well	09. Mrz 05	-8.19	-55.1	-9.87	1.68
	min		-9.16	-62.3	-10.96	0.52
	max		-6.13	-42.5	-8.91	4.02
	mean		-8.13	-55.28	-10.16	2.03

The spatial distribution of the measured $\delta^{18}\text{O}$ - values of groundwater from well samples and one spring sample (*Man.de la Reina*) from the *Vega de Granada* (without thermal springs) is used for interpolation with Surfer 7.0 using the kriging method, after fitting the data set to a spherical variogram. The resulting grid was converted a shapefile format and imported to ArcGis 8.3.

Figure 4.35 shows the spatial distribution of $\delta^{18}\text{O}$ values in groundwater from the *Vega de Granada* with the average δ -values of sampled rivers. Highly depleted δ -values can be found in the central **northern** and the **south-eastern** part of the *Vega de Granada* alluvial aquifer, while enriched δ -values are found in the **western** part of the *Vega de Granada*.

The *Rio Genil* is at the inflow to the *Vega de Granada* with $\delta^{18}\text{O} = -8.3$ ‰ one per mill lighter than at the outflow with -7.3 ‰. The hydraulic regime in the *Vega de Granada* changes from influent (losing river) at the inflow of the *Rio Genil* to effluent (gaining river) at its outflow. Thus, the *Genil* carries at the outflow of the *Vega de Granada* the hydrochemical and the isotope signature of the groundwater. In the **south-eastern** part of the *Vega de Granada* the most depleted values can be found in the sample from the well *Cullar Vega 1* ($\delta^{18}\text{O} = -9.12$ ‰), in the depth below surface of 110 m. In this area the under-surface depth of the wells is between 50 – 110 m and isotope stratification may be evident. Shallow groundwater is more enriched in δ -values compared to groundwater below. This fact indicated low vertical mixing of groundwater. The mean isotope signature of the *Rio Darro* at the inflow to the *Vega de Granada* was significant enriched compared to the groundwater of the *Vega de Granada*. This is interpreted as a minor influence of the *Darro* for GWR through indirect infiltration.



• Figure 4.35 Spatial distributions of $\delta^{18}\text{O}$ values in the alluvial aquifer *Vega de Granada* with mean $\delta^{18}\text{O}$ values of sampled rivers.

Controversy, the mean isotope signature of the *Rio Genil* at the inflow to the *Vega de Granada* was very similar compared to the groundwater of the *Vega de Granada*. This is interpreted as a strong influence of the *Genil* for GWR through riverbed infiltration.

The high depletion in the **south-eastern** part of the *Vega de Granada* indicates a strong groundwater flow derived from high altitudes in the *Sierra Nevada* (>2200 masl). The groundwater recharge may take place by indirect infiltration. Unfortunately, no samples were taken from the *Rio Dilar*. This river might play an important role in the recharge dynamics in the **south-eastern** part of the *Vega de Granada*.

A flow of depleted groundwater is observed south to the *Sierra Elvira* carbonate complex in the central **northern** part of the *Vega de Granada*. Groundwater in this area is in $\delta^{18}\text{O}$ around -8.4 ‰ and indicates the importance of the *Sierra Elvira* carbonate complex as a local groundwater recharge area. One of the most important springs in the *Vega de Granada* (*Manantial de la Reina*) with 12.000 l/m runoff can be associated, according to the similar isotope signature with groundwater from wells in the north (*Cort. Santa Ana, Atarfe*), to groundwater recharge area in the *Sierra Elvira*.

The **north-eastern** part of the *Vega de Granada* was sampled only at one well-site (*Terrazos Terragren*) and shows an moderate isotope signature, which is not affected by evaporation ($\delta^{18}\text{O} = -7.81$ ‰; $\delta\text{D} = -50.9$ ‰).

The river *Arr. de Salado* was sampled once at the **southern** inflow to the *Vega de Granada*. The $\delta^{18}\text{O}$ value of -6.5 ‰ ($\delta\text{D} = -48.24$ ‰) is significant lighter than the interpolated isotope distribution of the groundwater with -7.2 – -7.6 ‰. According to the $\delta^{18}\text{O}$ vs. δD distribution this sample is shifted from the WMMWL. The very unique hydrochemical composition (see section 4.1.2) of this brine

Samples from the *Rio Cubillas* at the **north-western** inflow to the *Vega de Granada* plot below of the WMMWL and show a preferential enrichment in $\delta^{18}\text{O}$ indicating evaporation losses (section 4.2.3.3). The high evaporative enrichment in the **western** part of the *Vega de Granada* could be explained by mixing processes of enriched surface water derived from the rivers (*Cubillas, Arr. Salado*) with depleted groundwater derived from eastern part of the *Vega*. The degree of this enrichment signature might be emphasized by recycling of groundwater due to irrigation use, leading to the observed evaporative enrichment signature in groundwater samples.

It is important to recognize that GWR dynamics for the *Vega de Granada* is close connected to river-groundwater interactions and a detailed sampling of this interface may be subject for further studies.

Since groundwater signature is more depleted than mean volume weighted precipitation no propriate water surplus from the *Vega* itself can be observed. Only heavy winter rain events may be able to potentially recharge the *Vega de Granada* alluvial aquifer.

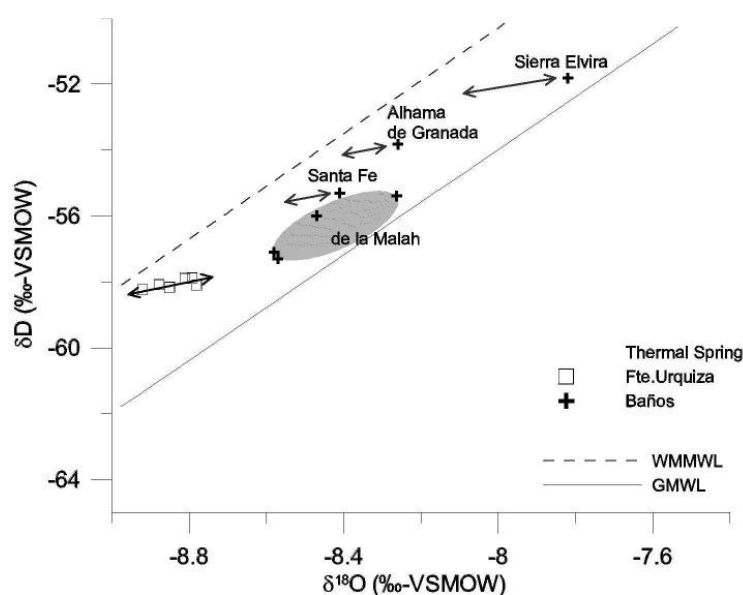
4.2.6 Thermal Springs

All thermal springs are considered to be of meteoric origin and are influenced by hydrothermal activity in the Betic Cordillera. In accordance to the hydrochemical classification (section 4.1.2), the thermal springs can also be divided by the isotope signatures in two subgroups. Samples which are located **near** to the WMMWL are supposed to be less influenced by water-rock interactions, while points which are **shifted** from the WMMWL represent progressively increasing water-rock interaction with the host-rocks of the aquifer under various water temperature conditions.

The $\delta^{18}\text{O}$ vs. δD distribution of thermal spring samples is shown in figure 4.36. The *Fte.Urquiza* samples are the most depleted of all thermal springs and are located **near** to the WMMWL with a subparallel shift to the $\delta^{18}\text{O}$ axis of $\Delta 0.3\text{‰}$. This subparallel shift could be interpreted as water-rock interaction from the thermal water with calcite host-rocks under low temperature conditions (water temperature = 22.5 °C). As expected for water-rock interaction, the δD values were not or only slightly altered and the d-excess is quite constant (around $+13\text{‰}$). The low deviation in δD values of the *Fte.Urquiza* spring samples can be explained by a wide catchment area where seasonal variations are attenuated. The samples from this double tube spring shows the most depleted δ -values with $\delta^{18}\text{O} = -8.8\text{‰}$ and can be associated to recharge altitudes from 2200-2300 masl (see section 4.2.2).

Samples from *Baños* (*Baños de la Malah*, *Baños Santa Fe*, *Baños Alhama de Granada*, *Baños Sierra Elvira*) are **shifted** from the WMMWL. Assuming a similar subparallel shift for the *Baños* samples it is possible, by calculating the matching point from the regression line with the WMMWL, to estimate the initial isotopic signature. The regression line calculated only with *Fte.Urquiza* samples may be indicative for water-rock interaction with calcite host-rocks described by:

$$\delta\text{D} = 1.88 * \delta^{18}\text{O} - 41.46 \quad (\text{eq.4.15})$$



• Figure 4.36 $\delta^{18}\text{O}$ (‰-VSMOW) vs. δD (‰-VSMOW) diagram of thermal springs.

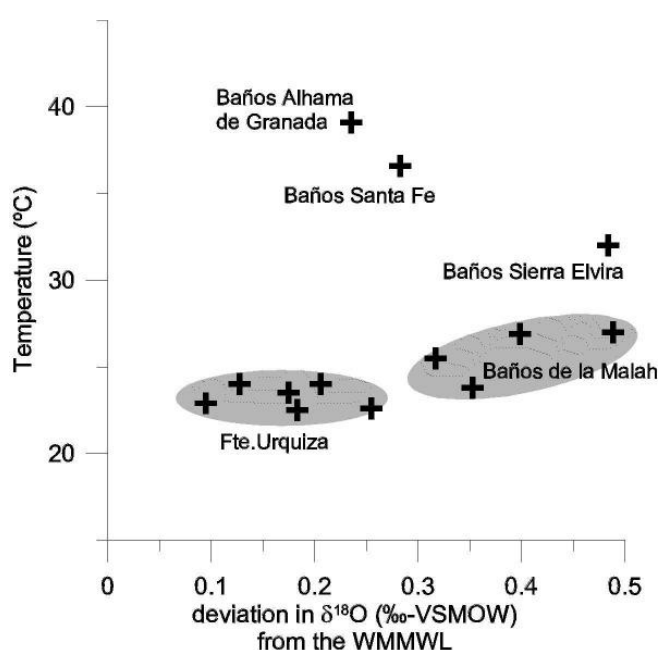
By calculating corrected $\delta^{18}\text{O}$ values and subtracting these values from the measured it is possible to plot the deviation in $\delta^{18}\text{O}$ from the WMMWL against water temperature. These corrected $\delta^{18}\text{O}$ values are considered to be representative for the initial composition of the thermal waters and therefore indicative for mean recharge elevation (Tab.4.9). Samples taken from sites called Baños are considered to be shifted subparallel to the $\delta^{18}\text{O}$ axis according to the trend in *Fte. Urquiza* samples.

• Table 4.9 Sites, Altitude (masl), date of sampling, $\delta^{18}\text{O}$, $\delta^{18}\text{O}$ error (‰) and mean recharge elevation (masl) for thermal springs.

site	Altitude (masl)	date	$\delta^{18}\text{O}$ (‰)	$\delta^{18}\text{O}$ error (‰)	$\delta^{18}\text{O}$ corrected (‰)	mean recharge Altitude (masl)
Fte. de Urquiza	650	05. Feb 04	-8.79	0.03	-9	2293 (+/-15)
Fte. de Urquiza	650	16-Oct-04	-8.81	0.03	-8.99	2291 (+/-15)
Fte. de Urquiza	650	10-Mar-05	-8.92	0.02	-9.01	2302 (+/-10)
Fte. de Urquiza left	650	05. Feb 04	-8.88	0.04	-9	2297 (+/-20)
Fte. de Urquiza left	650	16-Oct-04	-8.78	0.03	-9.03	2312 (+/-15)
Fte. de Urquiza left	650	10-Mar-05	-8.85	0.01	-9.02	2307 (+/-5)
Baños de la Malah	752	06. Feb 04	-8.26	0.02	-8.75	2170 (+/-10)
Baños de la Malah	752	16-Oct-04	-8.47	0.03	-8.79	2188 (+/-15)
Baños de la Malah	752	22. Nov 04	-8.57	0.02	-8.97	2279 (+/-10)
Baños de la Malah	752	5-Mar-05	-8.58	0.01	-8.93	2261 (+/-5)
Baños de Sierra Elvira	571	18. Feb 05	-7.82	0.02	-8.3	1946 (+/-10)
Baños Santa Fe	840	18. Feb 05	-8.41	0.02	-8.69	2141 (+/-10)
Baños Alhama de Granada	760	10-Mar-05	-8.26	0.02	-8.5	2042 (+/-10)

LOPEZ-CHICANO et al. 2001 reported of recharge areas for the *Alhama de Granada* thermal springs in the *Sierra Tejeda* located in the *Alpujarride* domain. LOPEZ-CHICANO et al. 2001 also used several geothermometers (Ab, Qz, An) for calculating equilibrium temperatures and reports of maximum water temperatures in the under surface reservoir of 110 °C. By using a normal geothermal gradient (~3 °C/100 m) it is possible to calculate the subsurface reservoir depth with ca. 3.6 km. Since the *Granada* region is expected to be a terrain with high geothermal gradients, the reservoir depth must be considered shallower.

The deviation in $\delta^{18}\text{O}$ from the WMMWL provides information about the degree of water-rock interaction. Since water-rock interaction is driven by the local carbonate content in the host-rocks on the flowpath and temperature, springs which are situated in carbonates are more deviated than springs which are located in the siliciclastic basin formations. Thermal springs which are located rather in the central part of the *Granada* basin are, despite of their high water temperatures, less deviated than springs which are located at the margins of the basin. In general, no clear correlation between deviation in $\delta^{18}\text{O}$ from the WMMWL and temperature can be observed. Only the samples from *Baños de la Malah* show a positive correlation between the water temperature and the high deviation from WMMWL. The high variance in the samples from *Baños de la Malah* may be indicative for mixing processes from deep thermal water with shallow groundwater (Fig.4.37).



• Figure 4.37 Deviation in $\delta^{18}\text{O}$ (‰-VSMOW) from the WMMWL vs. water temperature (°C) of thermal springs samples.

5 GEOLOGICAL MAPPING

5.1 Introduction

The mapping area is situated near to the town of *Granada*, in southern Spain in the province of Andalusia. The rectangular area occupies an area of approximately 24 km² (ca. 4x6 km). The corner coordinates are (UTM, WGS84, Zone 30N):

NW : 446 994 / 4 117 167

NE : 453 277 / 4 117 167

SW : 446 994 / 4 113 105

SE : 453 277 / 4 113 105


The topographic data basis maps were the “Hojas 1009; 1026 (1:50 000)” and the geological base maps were the “Mapa Geologia (IGME 1985): *Mapa Geologico-Minero de Andalusia* (1:400 000) (*Junta de Andalusia* 1985)”.

The field work was done between November 2004 and February 2005 during an `Erasmus` semester at the *Universidad de Granada* (UGR).

The highest point within the mapping area is a mountain peak in the NE corner with 1083.5 masl. From this point the elevation heights are decreasing in topographic steps to the southwest. Two main rivers are situated in the mapping area: (1) the *Rio Darro*, entering the area in the NE corner and after a sharp bend it courses E-W right in the middle of the mapping area and (2) the *Rio Genil* in the southern part. The *Rio Genil* is considered to be the approximately southern limit of the mapping area.

The mapping area is located in the Neogene fillings of the *Granada* basin. The formations in the mapping area are showing stratigraphic ranges from upper Miocene to Quaternary (Tab.5.1). The youngest formation is the alluvial deposit and river terraces of the *Rio Darro*. Most of the mapping area (70 %) is covered by the formation called “*Conglomerados de la Alhambra*” which is mainly composed of conglomerates and sand. This formation is dated as Villafranchian by using paleontological evidence (AGUIRRE 1957). Within this formation several (paleo-) soils can be found. Below of the *Alhambra* conglomerates a minor formation of red Sandstones is found. This formation is considered to be of middle Pliocene age. To the east older sequences of siltstones and conglomerates are lying under the *Alhambra* conglomerates termed as *Cenes de Lancha* formation. The oldest formation (*Pinos de Genil*) comprises of grey, calcareous siltstones and can be found in the very eastern part of the mapping area. For the stratigraphic ranges of the formations see table 5.1.

• Table 5.1 Neogene stratigraphy with stage ages from 2004 (IUGS 2004) and stage ages from 1975 and stratigraphic ranges of the formations in the mapping area.

Era Erathem	System Period	Series Epoch	Stage Age (2004)	Age Ma	Stage Age (1975)	Formations
Cenozoic	Neogene	Holocene				 Alhambra Conglomerates red Siltstones Cenes de Lancha Pinos Genil
		Pleistocene	Upper	0.0115	Oldenburgian	
			Middle	0.126	Biharian	
			Lower	0.781		
		Pliocene	Gelasian	1.806	Villafranchian	
			Piacenzian	2.588		
			Zanclean	3.600	Ruscinian	
		Miocene	Messinian	5.332		
			Tortonian	7.246	Turolian	
			Serravallian	11.608	Vallesian	
			Langhian	13.65	Maremmian	
			Burdigalian	15.97	Vindobonian	
			Aquitanian	20.43	Burdigalian	
				23.03	Aquitanian	

Aim of this work is to make a geological map, by practising field methods, interpreting the data and presenting these in the form of maps, diagrams and text. The geological map is in scale 1:20 000 and presented as paper copy at the end of this work. Prof. Dr. J. Azañon (UGR) supervised the field work and gave the initial idea, which was to get a more detailed sight on the tectonic structures. In the work “Small-scale faulting, topographic steps and seismic ruptures in the Alhambra (*Granada*, southeast Spain)” AZAÑON et al 2004, the author postulates a direct relationship between cracks in the 14th century old monument of the *Alhambra* and seismic induced ruptures in the underlying sediments. The authors are describing in this work the main faults and corresponding cracks in walls or towers in the *Alhambra* monument (AZAÑON et al 2004, Figure 5.4).

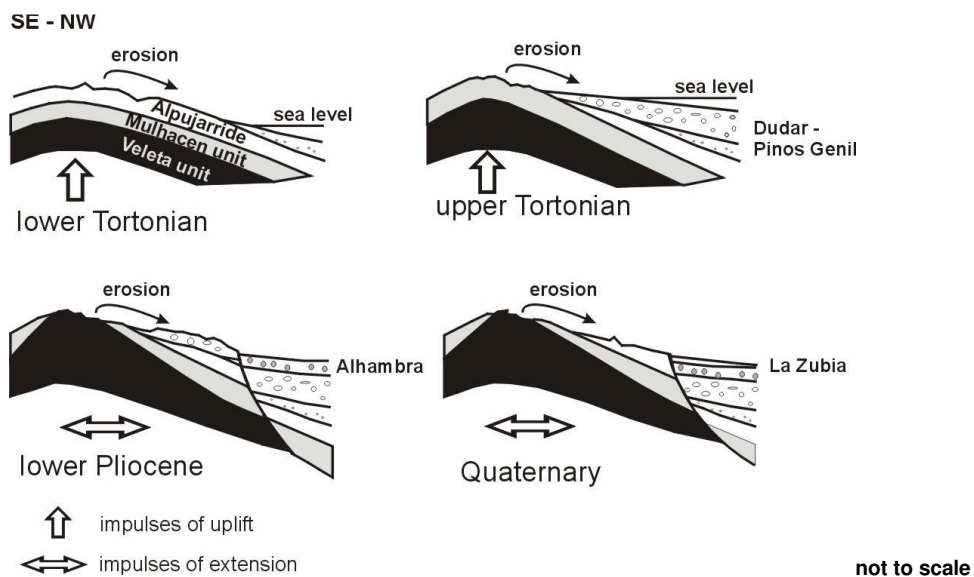
This geological mapping tries to amplify the view on the geological structures to the surrounding areas. The idea was to map the tectonic structures of the sediments around the *Alhambra* monument with the main focus on active tectonic structures and their relation to the recent stressfield. Additional, sedimentary structures and morphological features were used to determine the geological history of the mapping area. According to AZAÑON 2004 the *Alhambra* building underwent important tectonic impacts during their existence. These impacts are today visible in cracks within the walls and towers, small scale faults and cm to meter scale displacements of paleosoils. Within the mapping area several historical monuments are situated, witnessing the rich historical past of the *Alhambra* and the city of *Granada*. From the time of the Roman Empire gold mining is well documented in the *Granada* area. The Romans' gold mining technique

involved undermining entire mountains, using a method called „Ruina Montium“. By feeding vast quantities of water, along hydraulic systems and then inducing man-made landslides (MARTIN 2000). Then, slaves panned and picked up the gold. Remains of such works still can be seen in the imposing gold mine near *Cenes de Lancha* (Photo 5.1). Later, between the years 1875 and 1877 a French gold mining company runned the gold mine again and gained an average gold content of 0.5g/m^3 . They dismantled the gold-bearing conglomerate by using a powerful water stream and separated the gold by amalgamation with mercury (MARTIN 2000).



• Photo 5.1 Panoramic view of open gold mine near *Lancha de Cenes*
(*Mina de Oro* X 450 867 Y 4 113 962 viewpoint NNE).

The geological evolution of the *Granada* basin is described in chapter 1. Figure 5.2 shows the schematic geological development of the eastern border of the *Granada* basin with emphasising the corresponding conglomeratic units, like the *Alhambra* formation. The sketch in figure 5.2 makes clear that the *Alhambra* formation is derived from the *Alpujarride* and the metamorphic units (*Mulhacen*, *Veleta*) during stages of extensional tectonic motions.



• Figure 5.2 Sketch of the geological history of the eastern border of the *Granada* basin and the *Sierra Nevada* showing the stratigraphic architecture of the corresponding conglomerate units. (modified after MARTIN & BRAGA 1997).



• Photo 5.3 Uninhabited cave dwelled in the unconsolidated *Alhambra* formation.
(X 450 540 Y 4 113 864)

Several caves can be found in the mapping area. The caves were excavated in the unconsolidated rocks of the *Alhambra* formation. The *Granada* city district *Sacromonte*, in the northwestern part of the mapping area is famous for its house caves. Other caves, most of them uninhabited, are situated in the southern hillsides (photo 5.3).

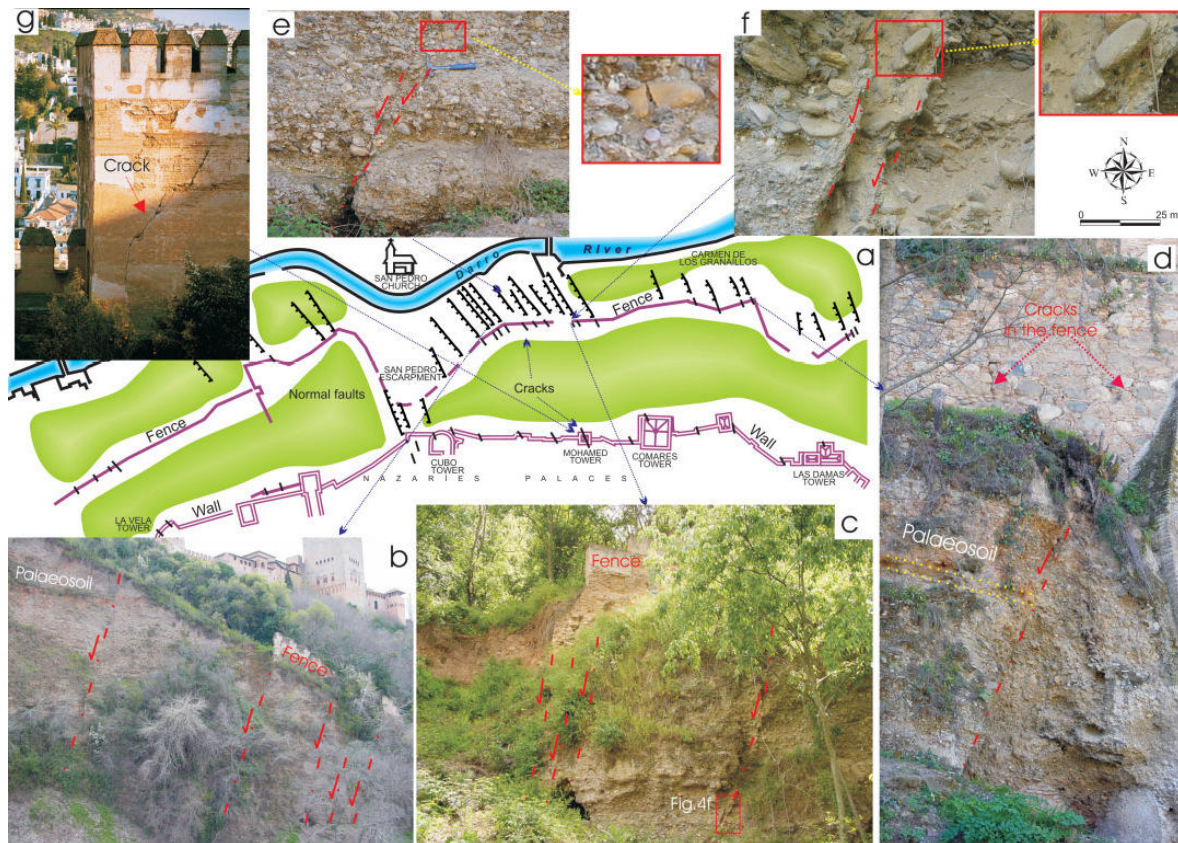


Figure 5.4 (a) Sketch of the northern hillslope of the Alhambra showing the small-scale faults (saw-shaped black lines) observed in the field, as well as the main cracks (black lines) in the fence and wall. (b) Decametrescale faults affecting a palaeosol. Displacement of these faults is approximately 50 cm. (c) Three decametre-scale faults underlying the fence of the Alhambra. The fence is collapsed in relation to one of these faults. (d) Cracks in the fence of the Alhambra situated just over a metre-scale fault in the conglomerate. Note palaeosol rotated in the hanging wall of the fault. (e) Metre-scale fault in the Alhambra conglomerate. Note the fractured clast in the upper part of the fault zone (red rectangle and magnification to the right). (f) Decimetre-large fault zone with a broken and displaced clast (red rectangle and magnification to the right). Clast is approximately 5 cm long. (g) Crack in the Mohamed tower. (AZAÑON et al 2004)

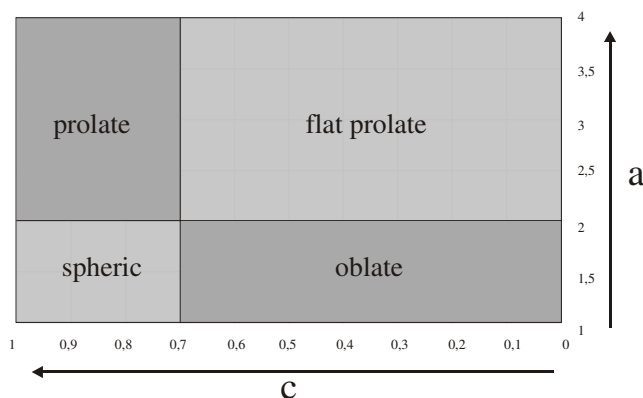
5.2 Methods

According to the aims of this work the collection of field data concerned primarily sedimentological and structural aspects. Classical methods were applied and information was recorded at outcrops within the sedimentary formations. Tools and aids used are simple, and include hammer and compass (with clinometer), 10% hydrochloric acid, hand lens, penknife, folding rule, digital camera and binocular. The main aspects of sedimentary rocks recorded in field are:

- Lithology: mineralogy/composition and colour
- Texture: grain size, grain shape, sorting and fabric
- Beds: bed thickness, contacts between beds, bed geometry
- Sedimentary structures: internal structures of beds, larger scale structures

Clasts in the conglomerates are measured within 1m^2 at selected locations using three geometric factors.

- a) max. length
- b) max. width, perpendicular to a)
- c) max. thickness, perpendicular to a) and b)



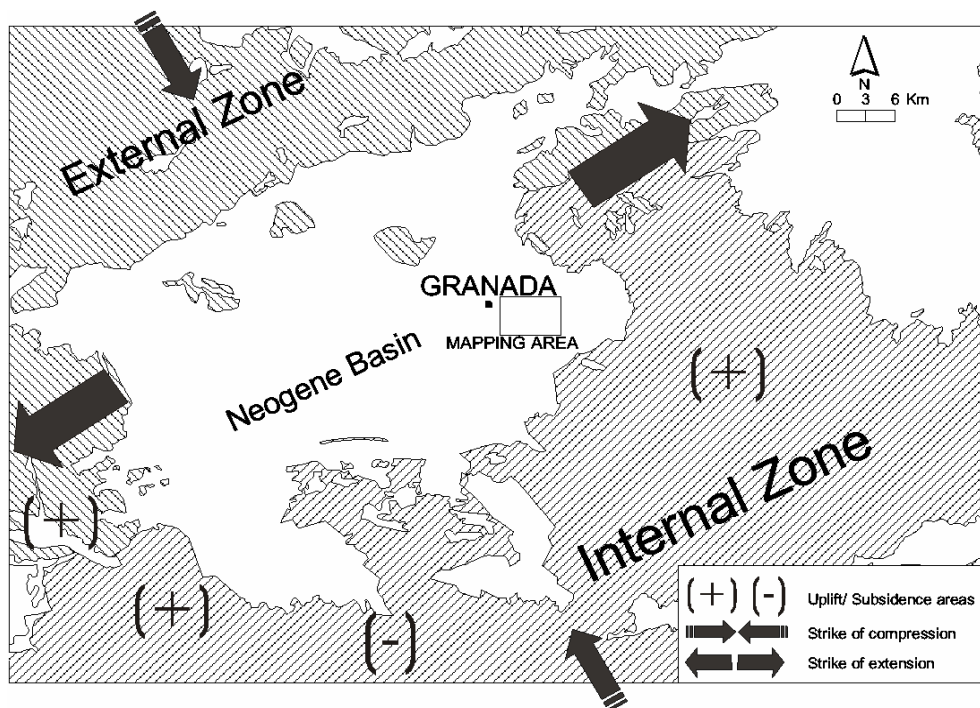
• Figure 5.5 Relationship between shape and lithology (after VALLETON 1955)

The geometric factor b was set to 1 and a and b were plotted as shown in Fig. 5.5. Further information about lithology and grade of roundness has been recorded. Derived from this data it is possible to show the relationship between lithology and shape.

Stereographic plots were done with the freeware StereoNet. Various geographical information systems (GIS) (ArcView 3.2, ArcGis 8.2) were used for generating and presenting maps.

5.3 Structural data

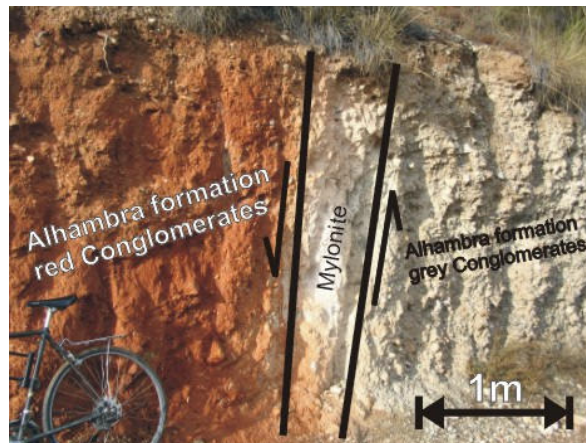
The mapping area lies in the Neogene intramontane *Granada* basin. The basin is, according to the seismographic record, one of the most seismically active zones in the whole Iberian Peninsula. Some authors try to estimate the time period in which large earthquakes will occur and SANZ DE GALDEANO et al. 2003 suggest a period of 500 years for earthquakes of magnitude 6. The recent stress field can be described as NW-SE striking compressive and a NE-SW striking extensional vector (GIL 2002) (Fig. 5.6).



• Figure 5.6 Recent stressfield in the Granada basin. Crosses indicate uplift, minus indicate subsidence (modified after GIL 2002). Geology simplified from IGME 2002.

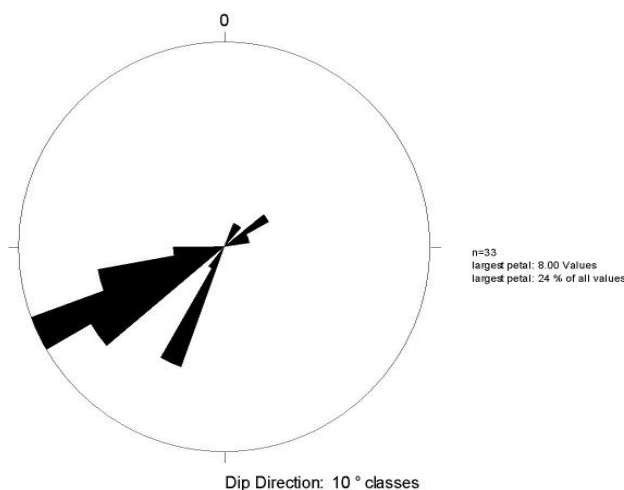
The Granada basin is affected by at least two sets of important faults. The faults of N 70E to E-W direction form the first set. They are the longest and oldest because many of them moved during the early and middle Miocene (SANZ DE GALDEANO 2003). Recent stress field of the Betic Cordillera can be described as an approximate NNW-SSE compression, combined with a near perpendicular extension (Fig.5.6). At the same time, the region was rising up (crosses), while other parts underwent subsidence (minus) (GIL 2002). The approximate NW-SE faults form the second set. These faults are also present in the eastern sector of the basin as well as in its interior, affecting areas such as *Sierra Elvira*, *Granada*, *Padul* etc. They basically move as normal faults, locally very important and, as in the previous set, moved from the late Miocene to the present. Some of them show a constant and noticeable microseismicity. The second set is considered to be very active and is made responsible for many earthquakes affecting the central and eastern sectors of the basin. The trend of the faults of its two sets facilitates the extension, generally producing small to moderate earthquakes (SANZ DE GALDEANO 2003).

Strike and dip of faults and bedding was measured in field and average values are presented in the geological map. In the mapping area a set of NW-SE orientated normal faults can be found (e.g. Photo 5.7). Most of them show dip-slip kinematics as observed in listric shear plains at *Barranco de Teatino* (section 5.4.3). Sometimes, weak strike-slip components cannot be excluded, and a wide range of displacement from cm to several m scales is observed. Most of these faults can be considered as extensional features, parallel to the slip vector between Africa and Iberia.



• Photo 5.7: Red and grey conglomerates from the Alhambra formation and normal fault with strike NW – SE and dip 80° to SW (at 449 500 / 4 114 490).

The distribution of the dip orientations of faults is shown as a rose diagram in figure 5.8. Generally, most of the faults have NW–SE orientations with dip degrees about 60–80. In the mapping area huge amounts of small-scale faults (0.4 m to 2 m length and a displacement of mm to cm) and several main faults (2 m to 5 m visible length and displacement of hectometre to kilometre) can be observed.



• Figure 5.8 Rose diagram showing the dip direction of the measured faults.

Photo 5.7 shows an important outcrop for the typical normal NW-SE faults. This fault is considered to be responsible for recent tectonic motions (AZAÑON et al 2004). Clasts at the fault zone are often reoriented parallel to the fault boundary (e.g. Photo 5.13). Sometimes broken clasts (Photo 5.14) or even fault-gauges can be observed. Small scale thrusts with cm displacement are visible in the mapping area (Photo 5.2). Reactivated faults with 2 or more Calcites crusts within the crack can be observed close

to the *Silla de Moro* (seat of the moors). The *Silla de Moro* is an ancient arabian ruin, very close

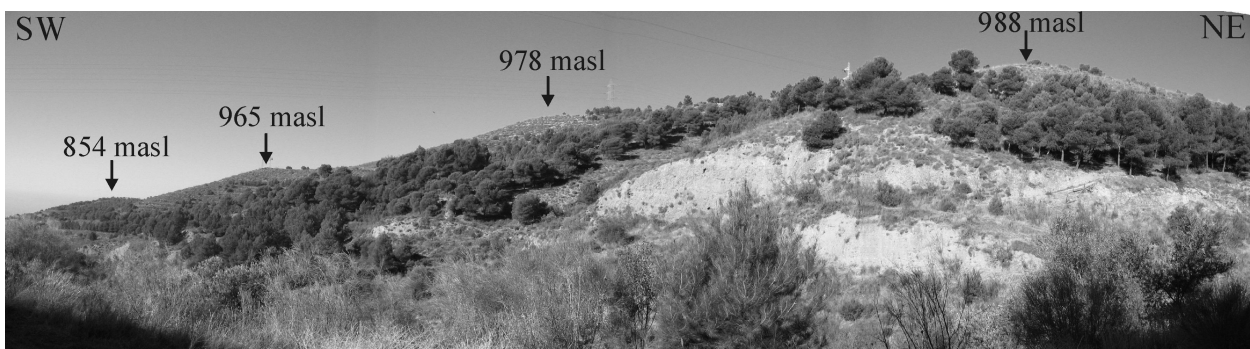
in the north to the *Alhambra* monument. Here, also NE dipping faults considered as not active were observed.

In the south of the mapping area the bedding of the *Alhambra* formation is often dipped with ca. 20 ° to SW. The dip direction is perpendicular to the second set of faults in the mapping area. Most of the faults crop out at the northern side to the *Alhambra* hill. Broken clasts or paleosoils are observed and have been used as markers to estimate displacement (Photo 5.9). In other cases striaes on fault plains were used to determine the direction of motion.



• Photo 5.9 Small scale thrust (at 448 488 / 4 114 700) with cm scale displacement. (Hammer length 35 cm).

Especially north to the *Rio Darro* topographic steps are visible separated by normal faults (Photo 5.10). One of these faults is striking NW-SE and separates the hills of *Cerro de San Miguel* and the south to the *Rio Darro* situated *Alhambra* hill. The stairway geometry of the topography is associated from AZAÑON et al 2004 to perpendicular striking normal faults dipping to the SW. The geomorphology and the geometry of the drainage network are strongly indicating the tectonic origin of these steps. The mapping area can be described as fault-bounded graben-horst structure.



• Photo 5.10 Topographic steps in the *Alhambra* Formation (at 449 694/4 115 920, viewpoint to NW)

5.4.1 Alluvial deposits Holocene

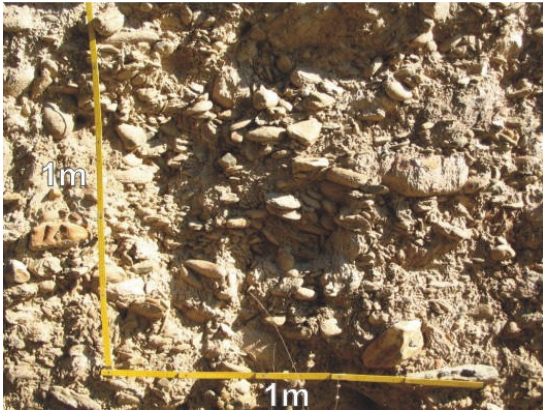
The youngest formations of the mapping area are Holocene alluvial deposits of the river *Darro*, which can be found in the centre of the mapping area, in the valley of the *Darro*. The *Rio Genil* is channelled and urbanised in the mapping area and no outcrops can be found. The level of the alluvial deposit of the *Rio Darro* is few meters above today's level. The lithology is characteristic for fluvial deposits.

5.4.2 Conglomerates and Sandstones (*Conglomerados de la Alhambra*) Plio-/Pleistocene

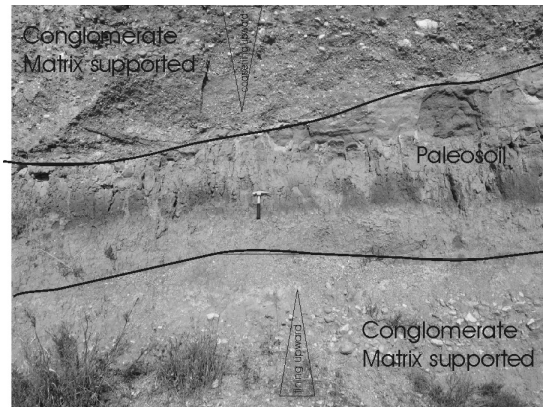
The 'Alhambra Formation' crops out largely in the eastern sector of *Granada* city. It is deposited discordant over the red Sandstone formation (5.4.3), which can be observed in *Barranco del Teatino*, or above *Cenes de Lancha* formation (5.4.4) with erosional contact. The '*Conglomerados de la Alhambra*' are stratigraphically younger than the Pleistocene sediments (MORENO et al. 1988), and have been dated as Villafranchian using paleontological evidence (AGUIRRE 1957). The Formation is considered to be a redeposit of a conglomerate of Miocene age. The origins of these sediments are connected to tectonic uplift and erosion of the surrounding *Sierras* and are interpreted as coalescent alluvial fan deposits. A geological profile taken from selected outcrops in the valley of the *Rio Darro* is used to present main sedimentological features. The profile description can be found at the end of the section. The typical features of debris flow are summarized in table 5.2.

• Tab.5.2 Main features of debris flows (modified after Füchtbauer 1989)

Name of massflow	Behaviour	Transportmechanism	Material	Sedimentary structures
Debris flow	Plastic	Particles "floating" due to Cohesion and uplift by clay minerals	Clay to Gravel	Matrix supported unsorted to weak graded may show coarse-tail or inverse grading concordent base contacts



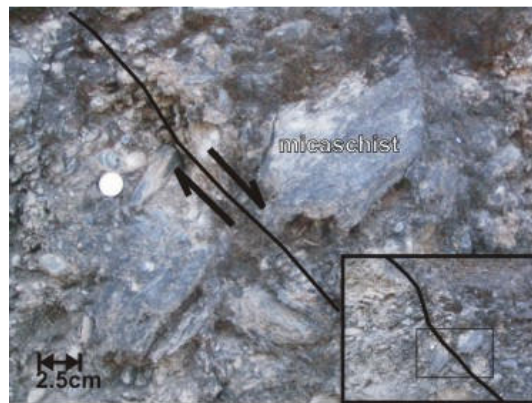
• Photo 5.11 1m² of the *Alhambra* formation.



• Photo 5.12 Sedimentological development from coarse conglomerates to soil and, divided by erosional contact, again coarse grained conglomerates. *Alhambra* formation (Hammer length ca. 35cm).



• Photo 5.13 Tractive deformation of the *Alhambra* formation (Hammer length ca. 35cm).



• Photo 5.14 Broken micaschist clast in the *Alhambra* formation.

The usual debris flow consists of grains with very wide ranges in size. The debris flow deposits, found in the mapping area consist of medium to fine grained matrix and varying proportion of matrix-supported clasts. This debris is rich in clasts of different size and lack any bedding phenomena. A debris flow event shows thickness of 2-3m and at the top reverse grading with boulders.

The clasts are in most cases matrix-supported, which can be secondary calcified. Clast supported conglomerates can also be observed, but are rare.

The distribution of quartzites, schists and carbonates within 1m² for clast analysis in the *Alhambra* formation is shown in Photo 5.11. Clast analysis was made at 5 site locations as shown in the geological map. The lithology of the clasts is very heterogeneous: e.g. various micaschists, quartzites, gneisses, gypsum, marbles, calcites, dolomites, serpentinite etc. According to the clast analysis most of the detritus is shaped like oblates, though spheroid and flat prolate figures occur.

5.4.3 Red Sandstones/Siltstones and conglomerates middle Pliocene

This formation crops out around the *Barranco de Teatino* and is tilted with angles between 40 and 45° to SW and strikes NW-SE. In *Barr. de Teatino* listric fault plains, which dip in the above conglomerates between 60 and 70° and using the sedimentary surface of the sandstones as a sheer plain, can be observed. On this sheer plains several striaes can be measured and confirm SW movements (Photo 5.16). NW-SE faults with listric geometry could be originated in crustal or shallower detachment. Angular discordance between the overlying *Alhambra* formation and the underlying red Sandstones is visible in *Barr.de Teatino*, located in the centre of the mapping area. Especially at the northern escarpment of the *Barranco* spectacular outcrops are visible (Fig.5.17).

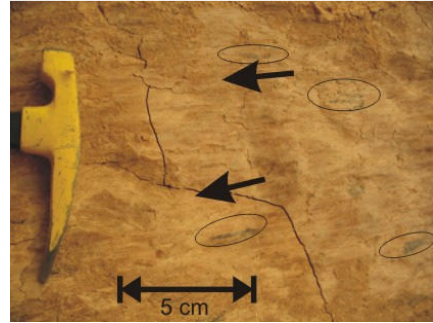
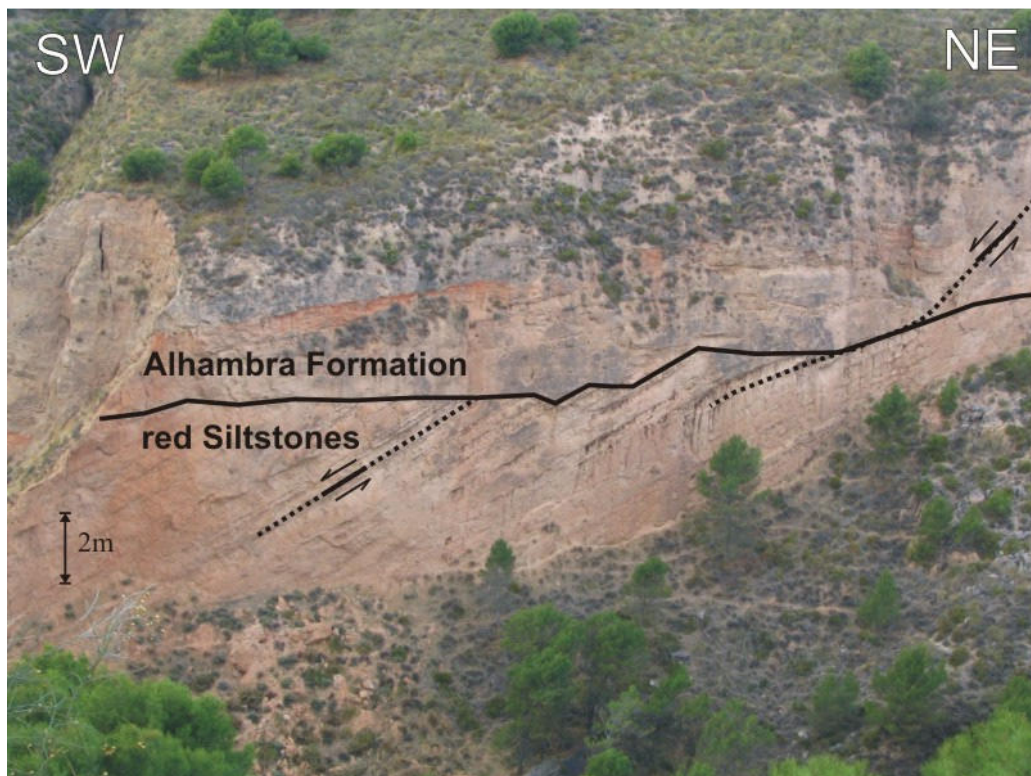


Photo 5.16 Striae on sedimentary surface on listric fault plains, red Sandstones formation (X 450 643; Y 4 115 537)



• Figure 5.17 Angular discordance and normal faults at *Barr. de Teatino* (at 450 794/4 115 740, viewpoint to NW)

5.4.4 Siltstones with micas, Sandstones and gravel (‘Cenes de Lancha’) Messinian

This formation crops out in the eastern part of the mapping area and forms gentle slopes. It is characterized by bright greyish colours. Especially the sandstones show wide cross-bedding. In this formation various fossils are being described (e.g. DABRIO et al. 1978). Within this formation landslides are very common and can be observed in the mapping area. The sedimentological facies can be described as lacustrine.

5.4.5 Conglomerates and Sandstones (‘Pinos Genil’) Tortonian

This Formation crops out in the eastern most part of the mapping area. It consists of conglomerates with mainly metamorphic (micaschists, gneisses and quartzites) and carbonatic (limestones and dolomites) clasts, which are approx. 2-15cm in diameter. The clasts are not good rounded, in opposite to the ‘*Alhambra Formation*’. The Matrix is silt/sand with high content of micas. Horizons of Sand- and Siltstones appear. Visible thickness is about 200m, though the base contact to lower formations is not cropping out in the mapping area. No evidence of marine sedimentation can be found. It is interpreted as a lacustrine environment deposit.

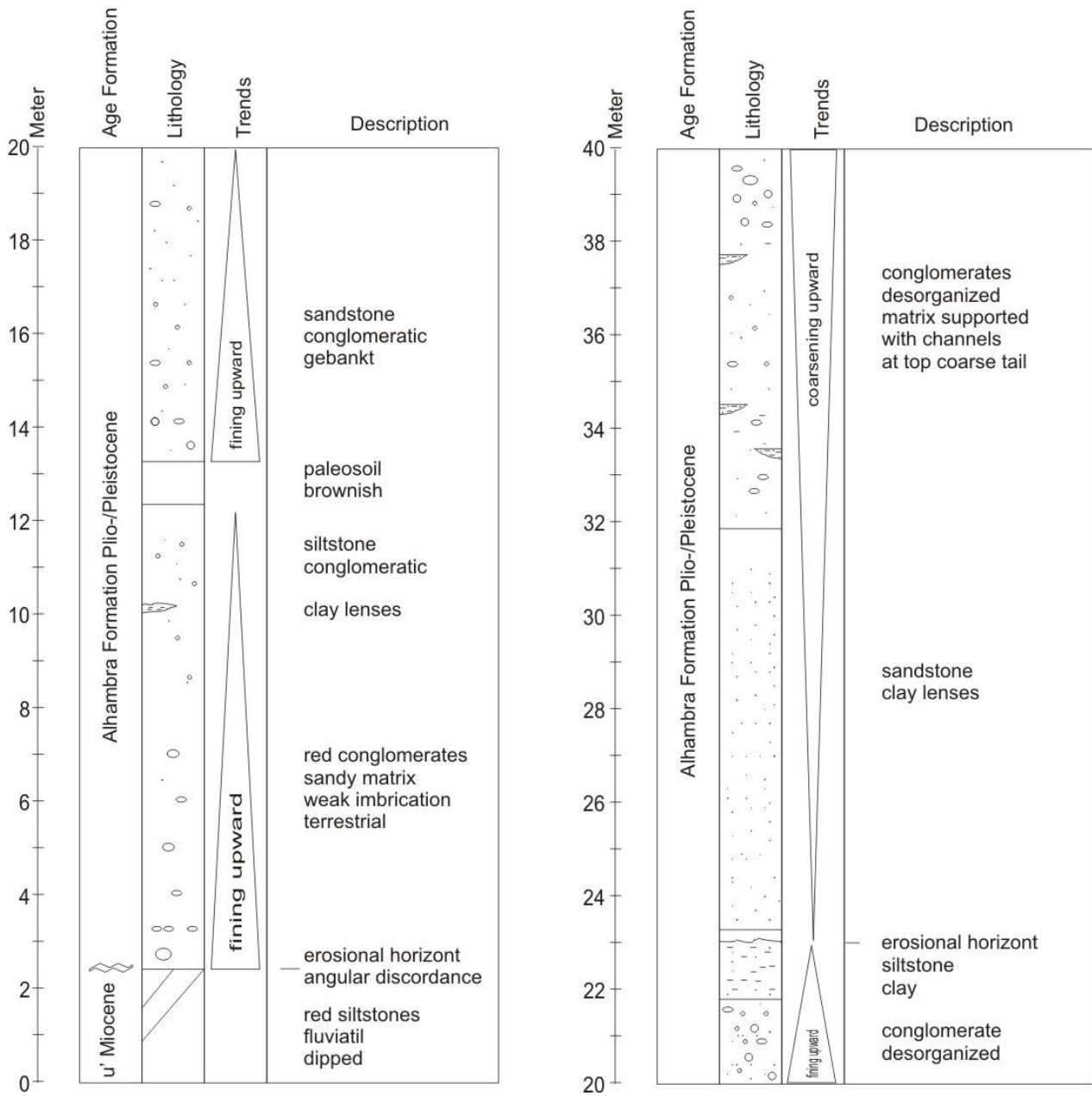
5.5 Profiles

The profile starts with the red Sandstone formation of upper Miocene age at the angular discordance between the *Alhambra* formation and the red Sandstones. A total thickness of 80 m is being described in terms of age, lithology, sedimentological trends and general descriptions. A correlation between geological markers like paleosoils between adjacent areas was not possible.

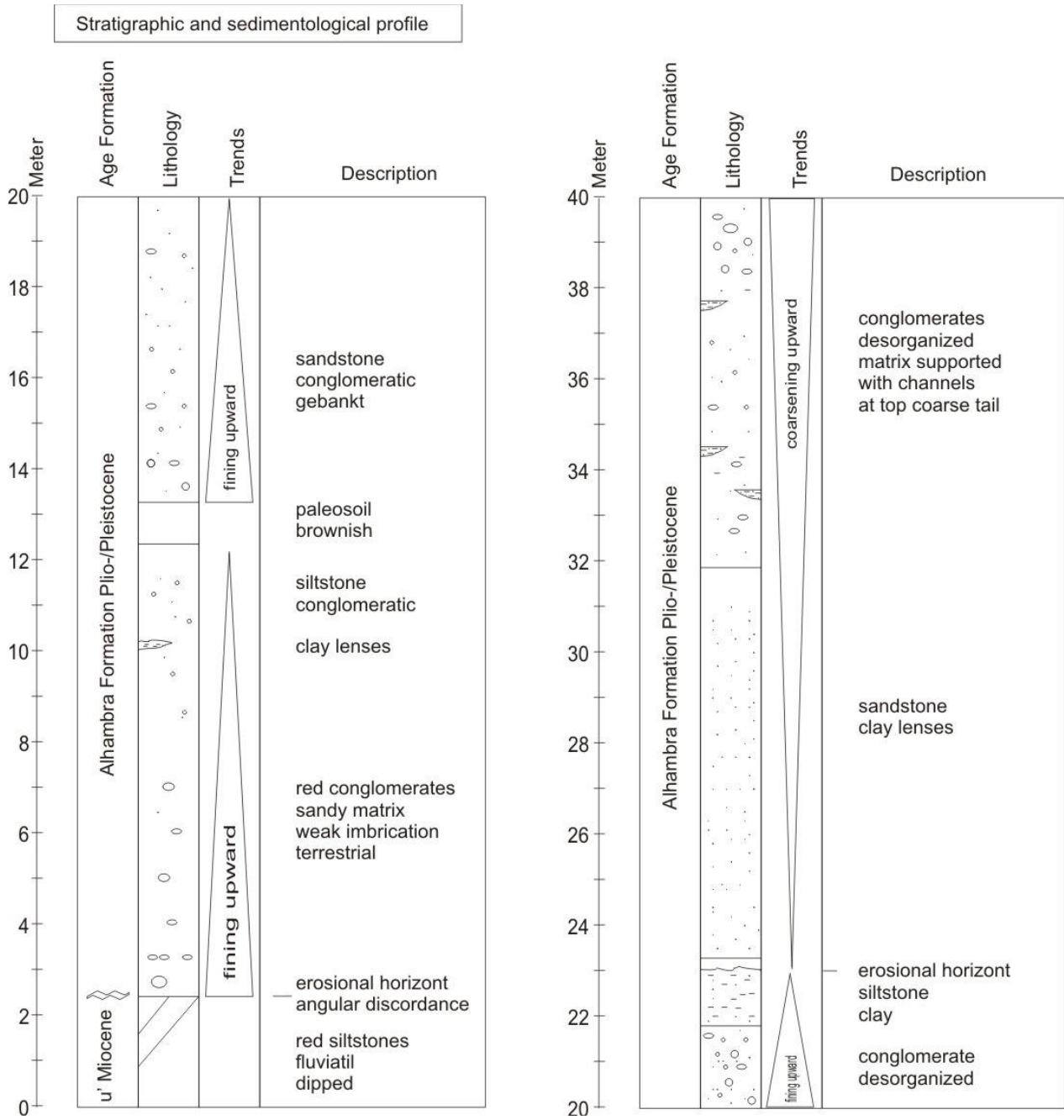
Most sedimentological trends must be described as fining upward sequences. At the end of most of the fining upward trends (paleo-) soils marking stages of low geomorphological dynamic. At the bottom of the *Alhambra* formation less but thick paleosoils can be found, while at the top of the formation several but thin paleosoils were observed. The *Alhambra* conglomerates are often disorganized, without any bedding.

Within the ‘*Alhambra Formation*’ fining upward sequences, from well-rounded clasts over sand to silty clay are common. At the top Paleosoils, marking stages of low geomorphodynamic activity, can be observed (Photo 5.12). In general soil formation can only take place in periods of geomorphodynamic stability, while active periods produce erosion/sedimentation. In the mapping area several horizons of paleosoils in the *Alhambra* Formation can be found. At the bottom of this formation few amounts but thick paleosoils have been developed, while towards the top the amount is increasing and thickness decreasing. The colours range from strong red over reddish to brownish, depending on the quantity of hematite content. In the *Alhambra* formation main soil forming processes are clay illuviation and calcification.

Stratigraphic and sedimentological profile



• Figure 5.18 Profile Ia: Rio Darro stratigraphic and sedimentological profile (0-40 m).



• Figure 5.19 Profile 1b: *Rio Darro* stratigraphic and sedimentological profile (40-80 m).

Abbreviations

°	degree
°C	degree centigrade (Celsius scale)
‰	per mil
2H	D or Deuterium
AAS	Atomic Absorption Spectroscopy
ABL	Atmospheric Boundary Layer
approx.	approximately
Arr.	Arroyo (stream)
avg.	average
Barr.	Barranco (creek, valley)
D	² H or Deuterium
d-excess	deuterium excess
Emb.	Embalse (reservoir)
ETA	actual evapotranspiration
Fte.	Fuente (spring)
FUB	Freie Universität Berlin
GMWL	Global Meteoric Water Line
GWR	groundwater recharge
ICP	Inductively Coupled Plasma
IGME	Instituto Geologico y Minero España
Man.	Manantial (spring)
masl	meter above sea level
max.	maximum
min.	minimum
MWL	Meteoric Water Line
Nac.	Nacimiento (source)
SI	saturation index
UGR	Universidad Granada
UJA	Universidad Jaen
vs.	versus
VSMOW	Vienna Standard Mean Ocean Water
WMMWL	Western Mediterranean Meteoric Water Line

-
- AGUIRRE, E., (1957). UNA PRUEBA PALEOMASTOLOGICA DE LA EDAD CUATERNARIA DE LOS CONGLOMERADOS DE LA ALHAMBRA (GRANADA). ESTUDIOS GEOLOGICOS 13, 135 - 140.
- ALLERTON, S., LONERGAN, L., PLATT, J.P., PLATZMAN E.S. AND MCCLELLAND E., (1993) PALAEOMAGNETIC ROTATIONS IN THE EASTERN BETIC CORDILLERE, SOUTHERN SPAIN, EARTH PLANET, SCI. LETT, 119, 225-241.
- ARAGUAS-ARAGUAS, L., FROELICH, K. AND ROZANSKI, K., (2000). DEUTERIUM AND OXYGEN-18 ISOTOPE COMPOSITION OF PRECIPITATION AND ATMOSPHERIC MOISTURE. HYDROLOGICAL PROCESSES, 14(8): 1341-1355.
- AZAÑÓN, J.M., GALINDO-ZALDIVAR, J., GARCIA-DUENAS, V. JABALOY, A. (2002) THE GEOLOGY OF SPAIN, ALPINE TECTONICS II: BETIC CORDILLERA AND THE BALEARIC ISLANDS GIBBONS, WES, MORENO, T., THE GEOLOGY OF SPAIN, CARDIFF THE GEOLOGICAL SOCIETY LONDON.
- AZAÑÓN, J. M. ,AZOR, A., BOOTH-REA AND TORCAL, FR (2004) SMALL-SCALE FAULTING, TOPOGRAPHIC STEPS AND SEISMIC RUPTURES IN THE ALHAMBRA (GRANADA, SOUTHEAST SPAIN) 2004, JOURNAL OF QUATERNARY SCIENCE 19(3) 219–227.
- BEDMAR, A.P. (1994) COMPOSICION ISOTOPICA DE LAS PRECIPITACIONES Y AGUAS SUBTERRANEAS DE LA PENINSULA IBERICA, CENTRO DE ESTUDIOS DE TECNICAS APLICADAS, P138:
- BIGELEISEN, J., AND M. WOLFSBERG, (1958) THEORETICAL AND EXPERIMENTAL ASPECTS OF ISOTOPE EFFECTS IN CHEMICAL KINETICS, ADV. CHEM. PHYS., 1, 15-76.
- BRAGA, J.C., MARTIN, J.M., ALCALA, B., (1990) CORAL REEF IN COARSE-TERRIGENOUS SEDIMENTARY ENVIRONMENT (UPPER TORTONIAN, GRANADA BASIN, SOUTHERN SPAIN) SEDIMENTARY GEOLOGY, 66: 135 – 150.
- CASTILLO, A. FERNANDEZ-RUBIO, R. (1985) "APLICACIÓN DE FERTILIZANTES QUIMICOS EN LA VEGA DE GRANADA. REPERCUSION EN LA CALIDAD DE LAS AGUAS SUBTERRANEAS" I CONGRESO DE GEOQUIMICA. 57-58.
- CASTILLO, A. (1986) "LAS AGUAS SUPERFICIALES Y SUBTERRANEAS EN SIERRA NEVADA (GRANADA Y ALMERIA)" EN "SIERRA NEVADA". ED. ANDALUCIA, S.A. DL: GR/694-1985. 145-169.
- CASTILLO, A. (1993) "CALIDAD AGRONÓMICA DE LAS AGUAS DE RIEGO DE LA VEGA DE GRANADA" NATURALIA BAÉTICA: 5, 91-103
- CASTILLO, A. (1995). EL EMBALSE SUBTERRANEO DE LA VEGA DE GRANADA, UNO DE LOS MAS IMPORTANTES DE ANDALUCIA. TIERRA Y TECNOLOG.A, 9, 37-42.
- CASTILLO, A. (2000) - PARQUE NACIONAL DE SIERRA NEVADA, DE CANSECO EDITORES. 2000 PARQUE NACIONAL DE SIERRA NEVADA - CLIMA E HIDROLOGIA - HIDROGEÓLOGO. INVESTIGADOR DEL C.S.I.C. INSTITUTO DEL AGUA (UNIVERSIDAD DE GRANADA).
- CELLE-JEANTON, H., TRAVI, Y., BLAVOUX B (2001), ISOTOPIC TYPOLOGY OF PRECIPITATION IN THE WESTERN MEDITERRANEAN REGION AT THREE DIFFERENT TIME SCALES, GEOPHYSICAL RESEARCH LETTERS 28, 1215–1218.
- CLARK, I. AND FRITZ, P., (1999). ENVIRONMENTAL ISOTOPES IN HYDROGEOLOGY. LEWIS PUBLISHERS. Boca Raton, 328pp
- CRAIG, H. (1961): ISOTOPIC VARIATIONS IN METEORIC WATERS. SCIENCE, 133: 1702-1703.

-
- COUTAGNE, A.(1948): ETUDE GENERALE DES VARIATIONS DE DEBITS EN FONCTION DES FACTEURS QUI LES CONDITIONNENT. 2^ŒME PARTIE: LES VARIATIONS DE DEBIT EN PERIODE NON INFLUENCEE PAR LES PRECIPITATION. LA HOULLE BLANCHE, SEPT.-OCT. 1948
- DABRIO, J.C., VERA, J.A. (1978) CARACTERISTICAS SEDIMENTARIAS DEL JURASICO SUBBETICO EN LA REGION DE ALGARINEJO – RUTE. ACT. GEOL. HISP. I – V, 8-11.
- DANSGAARD, W. (1964). STABLE ISOTOPES IN PRECIPITATION. TELLUS 16, 436-468.
- DELGADO CALVO-FLORES R, DELAGADO FLORES G, PARRAGA MARTINEZ-J, GAMIZ MARTIN-E, SANCHEZ MARANON-M, TENORIO URRIOS-MA, (1989). PROYECTO LUCDERNE. MAPA DE SUELOS. GUEJAR SIERRA. –ICONA. MINISTERIO DE AGRICULTURA, PESCA Y ALIMENTACION. UNIVERSIDAD DE GRANADA.
- DELGADO, L; SANCHEZ, L.; CASTILLO, A.; BAEZ, M.E. Y PEÑA, A. (2002) “ESTUDIO DEL IMPACTO DEL HERBICIDA BENSULFURON-METILO EN ENSAYOS DE CAMPO EN LA VEGA DE GRANADA” XIII CONGRESO NACIONAL FARMACÉUTICO
- DVWK REGELN 128 (1992): ENTNAHME UND UNTERSUCHUNGSUMFANG VON GRUNDWASSERPROBEN. VERLAG PAUL PAREY
- FAO-IGME. (1968). PROYECTO DE INVESTIGACIÓN HIDROGEOLÓGICA DE LA CUENCA DEL GUADALQUIVIR. PNUD.
- FEDOROFF, N., (1997). CLAY ILLUVIATION IN RED MEDITERRANEAN SOILS. CATENA 28, 171 – 189.
- FÜCHTBAUER, H. (1998) (EDITOR), SEDIMENTE UND SEDIMENTGESTEINE, SCHWEIZERBART'SCHE VERLAGSBUCHHANDLUNG, S.1141.
- FREEZE, R.A. AND CHERRY, J.A. (1979): GROUND WATER. PRENTIC HALL INC., NEW JERSEY.
- GARRIDO, J.R. (2003) COMPOSICION ISOTOPICA DEL VAPOR DE AGUA ATMOSFERICO EN EL SURESTE DE LA PENINSULA IBERICA, DEPARTAMENTO DE CIENCIAS DE LA TIERRA Y QUIMICA AMBIENTAL, TESIS DOCTORAL, 418
- GRAY, D.M. (1973): HANDBOOK OF PRINCIPLES IN HYDROGEOLOGY.- WATER INFORMATION CENTER INC. HUNTINGTON, N.Y.
- GÜNSTER, N., SKOWRONEK, A. (2001) SEDIMENT - SOIL SEQUENCES IN THE GRANADA BASIN AS EVIDENCE FOR LONG- AND SHORT-TERM CLIMATIC CHANGES DURING THE PLIOCENE AND QUATERNARY IN THE WESTERN MEDITERRANEAN, QUATERNARY INTERNATIONAL 78, 17 - 32
- GONFIANTINI R. (1986). ENVIRONMENTAL ISOTOPES IN LAKE STUDIES. IN HANDBOOK OF ENVIRONMENTAL ISOTOPE GEOCHEMISTRY A., VOL. 1 (ED. P. FRITZ AND J. C. FONTES), PP. 113-168. ELSEVIER.
- HAARMANN, U. (2001) : GESCHICHTE DER ARABISCHEN WELT. C.H. BECK MÜNCHEN, 786
- IAEA (2000) MEBUS GEYH NIEDERSÄCHSISCHES LANDESAMT FÜR BODENFORSCHUNG HANNOVER ENVIRONMENTAL ISOTOPES IN THE HYDROLOGICAL CYCLE PRINCIPLES AND APPLICATIONS VOLUME IV: GROUNDWATER (WWW.IAEA.ORG)
- IAEA-GNIP (2004) GLOBAL NETWORK OF ISOTOPES IN PRECIPITATION. INTERNATIONAL ATOMIC ENERGY AGENCY, VIENNA. URL: [HTTP://ISOHIS.IAEA.ORG/](http://isohis.iaea.org/). ACCESSED IN OCTOBER 2004.
- IGME (2000) PLUVIOMETRIA EN EL OBSERVATORIO DE CARTUJA - 774M – GRANADA, INTERNAL PAPER

-
- IGME (1985) MAPA GEOLOGIA, MAPA GEOLOGICO – MINERO DE ANDALUCIA (1:400 000), JUNTA DE ANDALUCIA
- IGME 5.30 (2001) NORMA DE EXPLOTACION DE LA UNIDAD HIDROGEOLOGICA 5.30 (SIERRA ARANA), INTERNAL PAPER
- IGME 5.31 (2001) NORMA DE EXPLOTACION DE LA UNIDAD HIDROGEOLOGICA 5.31 (LA PEZA) , INTERNAL PAPER
- IGME 5.32 (2001) NORMA DE EXPLOTACION DE LA UNIDAD HIDROGEOLOGICA 5.32 (DEPRESSION DE GRANADA) , INTERNAL PAPER
- IGME (2002) MODELO DE DATOS MAPA GEOLÓGICO-MINERO DE ANDALUCÍA ESCALA 1:400.000 (3ª VERSIÓN), E00-FILES.
- JOUZEL, J., MERLIVAT, L., (1984). DEUTERIUM AND OXYGEN-18 IN PRECIPITATION: MODELLING OF THE ISOTOPE EFFECTS DURING SNOW FORMATION. JOURNAL OF GEOPHYSICAL RESEARCH 89, 11749–11757.
- KAKIUCHI, M. AND MATSUO, S. (1979) DIRECT MEASUREMENTS OF D/H AND 18O/16O FRACTIONATION FACTORS BETWEEN VAPOR AND LIQUID WATER IN THE TEMPERATURE RANGE FROM 10 TO 40 °C. GEOCHEM. J. 13, 307–311.
- LOPEZ-CHICANO, J.C CERON, A.VALLEJOS, A. PULIDO-BOSCH, (2001) GEOCHEMISTRY OF THERMAL SPRING, ALHAMA DE GRANADA (SOUTHERN SPAIN), APPLIED GEOCHEMISTRY (16) 2001, 1153-1163
- MARTIN, J.M. & BRAGA, J.C. (1997). SIERRA NEVADA: HISTORIA DEL LEVANTAMIENTO DE UN RELIEVE DEDUCIDA DE LAS UNIDADES CONGLOMERATICAS DE SU BORDE. CALVO, J.P. & MORALES (ED.), AVANCES EN EL CONOCIMIENTO DEL TERCIARIO IBERICO, 117 – 120
- MARTIN, J.M. (2000) GEOLOGIA E HISTORIA DEL ORO DE GRANADA. BOLETIN GEOLOGICO Y MINERO. VOL 111-2 Y 3, 47-60.
- MAPA DIGITAL DE ANDALUCÍA 1:100.000 (1999). SEVILLA: CONSEJERIA DE OBRAS PUBLICAS Y TRANSPORTES, INSTITUTO DE CARTOGRAFÍA DE ANDALUCÍA.
- MEYER T., TESMER M. (2000): ERMITTLUNG DER FLÄCHENDIFFERENZIERTEN GRUNDWASSERNEUBILDUNG IN SÜDOST-HOLSTEIN NACH VERSCHIEDENEN VERFAHREN UNTER VERWENDUNG EINES GIS, INAUGURAL DISSERTATION, FUB
- MEYER, H. SCHÖNICKE, L. WAND, U. HUBBERTEN, H.-W. & FRIDRICHSEN, H. (2000). ISOTOPE STUDIES OF HYDROGEN AND OXYGEN IN GROUND ICE. –EXPERIENCES WITH THE EQUILIBRATION TECHNIQUE. – ISOTOPES ENVIRON. HEALTH STUD. 36 P., 133-149.
- MINISTERIO DE MEDIO AMBIENTE, EMBALSE DE CANALES (2001), CONFEDERACIÓN HIDROGRÁFICA DEL GUADALQUIVIR ZONA DE GRANADA EMBALSE DE CANALES. P: 1-2
- MINISTERIO DE MEDIO AMBIENTE, EMBALSE DE CUBILLAS (2001), CONFEDERACIÓN HIDROGRÁFICA DEL GUADALQUIVIR ZONA DE GRANADA EMBALSE DE CUBILLAS. P: 1-2
- MINISTERIO DE MEDIO AMBIENTE, EMBALSE DE QUENTAR (2001), CONFEDERACIÓN HIDROGRÁFICA DEL GUADALQUIVIR ZONA DE GRANADA EMBALSE DE QUÉNTAR- P: 1-2
- MORENO, E., SORIA MINGORANCE, J., 1988. MAPA Y MEMORIA EXPLICATIVA DE LA HOJA 1009 (GRANADA) DEL MAPA GEOLOGICO DE ESPANA A ESCALA 1 : 50.000. MADRID, 73 PP.

-
- MOSER, H., AND STICHLER, W., (1974), DEUTERIUM AND OXYGEN-18 CONTENTS AS AN INDEX OF THE PROPERTIES OF SNOW COVERS, IN INTERNATIONAL SYMPOSIUM ON SNOW MECHANICS, VOLUME 114: GRINDELWALD, SWITZERLAND, INTERNATIONAL ASSOCIATION OF HYDROLOGICAL SCIENCES, P. 122–135.
- MOSER, H., AND STICHLER, W., (1980), ENVIRONMENTAL ISOTOPES IN ICE AND SNOW, IN FONTES, J.C., AND FRITZ, P., EDS., HANDBOOK OF ENVIRONMENTAL ISOTOPEGEOCHEMISTRY, VOLUME 1A: NEW YORK, ELSEVIER, P. 141–178.
- REMENIERAS G. (1974): TRATADO DE HIDROLOGÍA APLICADA. BARCELONA; ESPANA.
- SANZ DE GALDEANO, C., PELAZ-MONTILLA, JA, LOPEZ-CASADO, C. (2003) SEISMIC POTENTIAL OF THE MAIN ACTIVE FAULTS IN GRANADA BASIN (SOUTHERN SPAIN), PURE AND APPLIED GEOPHYSICS 160, 1537-1556.
- STULL, R. B. (1988): AN INTRODUCTION TO BOUNDARY LAYER METEOROLOGY, 666 PP.
- TURC, L. (1954): CALCUL DU BILAN DE L'EAU EVALUATION EN FONCTION DES PRECIPITATIONS ET DES TEMPERATURES. PUBL. NO. 37 DES L'ASSOCIATION INTERNATIONALE D'HYDROLOGIE, ASSEMBLÉE GÉNÉRALE DE ROME, TOME III, 188-202
- VANDENSCHRIK, G., B. VAN WESEMAELA, E. FROTA, A. PULIDO-BOSCH, L. MOLINAB, M. STIEVENARD, R. SOUCHEZD (2002) USING STABLE ISOTOPE ANALYSIS (D D–D 18O) TO CHARACTERISE THE REGIONAL HYDROLOGY OF THE SIERRA DE GADOR, SOUTH EAST SPAIN” JOURNAL OF HYDROLOGY 265 43–55.
- VERHAGEN B. TH., GEYH M., FRÖHLICH K. & WITH K. (1991): ISOTOPE HYDROLOGICAL METHODS FOR THE QUANTITATIVE EVALUATION OF GROUND WATER RESOURCES IN ARID AND SEMI-ARID AREAS - DEVELOPMENT OF A METHODOLOGY. RESEARCH REPORTS OF THE MINISTRY FOR ECONOMIC COOPERATION OF THE FED. REP. OF GERMANY, 164 P.
- VISERAS, C. CALVACHE ML, SORIA JM, FERNANDEZ, J.,(2003), DIFFERENTIAL FEATURES OF ALLUVIAL FANS CONTROLLED BY TECTONIC OR EUSTATIC ACCOMODATION SPACE. EXAMPLES FROM BETIC CORDILLERA, SPAIN. GEOMORPHOLOGY 50, PP 181-202.
- WWW.JUNTADEANDALUCIA.ES (2005), CLIMATE DATA
[HTTP://WWW.JUNTADEANDALUCIA.ES/AGRICULTURAYPESCA/PORTAL/OPENCMS/PORTAL/PORTADA.JSP](http://www.juntadeandalucia.es/agriculturaypesca/portal/openCMS/portal/portada.jsp)

APPENDIX 1 (Introduction)

• Table a1.1 : List of meteorological stations, data source, data time period and mean annual precipitation.

Station ID	Station Name	X	Y	Z	Data Source	mean annual P	Time period
1	Baza	520628	4157712	814	Junta Andalucia	303.1	2000-2005
3	Loja	399051	4114478	487	Junta Andalucia	364.4	2000-2005
4	Pinos Puente	431534	4124395	594	Junta Andalucia	354.5	2000-2005
5	Iznalloz	451312	4141428	935	Junta Andalucia	475.1	2000-2005
6	Jerez	486806	4116224	1212	Junta Andalucia	287.7	2000-2005
7	Cadiar	483724	4086564	950	Junta Andalucia	426.9	2000-2005
8	Zafaraya	397421	4094617	905	Junta Andalucia	773.8	2000-2005
9	Almunecar	439612	4066365	49	Junta Andalucia	366.1	2000-2005
10	Padul	444684	4097558	753	IGME 2000	409.3	1961-1997
11	La Peza	475063	4125456	1085	IGME 2000	445.3	1961-1997
12	Diezma	470862	4130415	1233	IGME 2000	532.6	1961-1997
13	Huetor Santillan	460117	4130759	1200	IGME 2000	769	1961-1997
14	Quentar Tocon	467479	4121993	1200	IGME 2000	882.2	1961-1997
15	Pantano de	459484	4116968	975	IGME 2000	579.3	1961-1997
16	Albolote	442158	4118474	654	IGME 2000	454.9	1961-1997
17	Dilar	449558	4101990	990	IGME 2000	545.3	1961-1997
18	Dilar - Central	451862	4102743	980	IGME 2000	600.5	1961-1997
19	Padul - Agu	446633	4097027	740	IGME 2000	434.9	1961-1997
21	Lanjaron	457003	4086037	710	IGME 2000	504.7	1961-1997
22	Jayena	429750	4090025	970	IGME 2000	395.1	1961-1997
23	Granada - Base Area	443398	4109612	685	IGME 2000	376.6	1961-1997
24	Albunuelas	434660	4083124	1120	IGME 2000	775	1961-1997
25	Pinos Genil	455902	4113285	774	IGME 2000	552.9	1961-1997
26	Albergue Universitario	465226	4104772	2550	IGME 2000	738.4	1960-1997
27	Huetor Santillan	454443	4119852	1022	IGME 2000	674.3	1961-1997
28	Guejar Sierra	461335	4112718	1084	IGME 2000	604.3	1961-1997
29	Observatorio Cartuja	447308	4116447	774	IGME 2000	449	1902-1997
38	Velez Malaga	399138	4073067	49	Junta Andalucia	395.2	2000-2005

APPENDIX 2 (Background)

• Table a2.1 GWR and runoff calculation for the meteorological station Iznalloz (X 451312 Y 4141428 Z 935)

month	precipitation	temperature	ETA	runoff & recharge	ETA	runoff & recharge
	[mm]	[°C]	TURC	TURC	COUTAGNE	COUTAGNE
1	67.64	6.40	70.50	-2.86	64.94	2.70
2	49.56	6.98	51.95	-2.39	48.18	1.38
3	82.24	10.16	85.82	-3.58	79.20	3.04
4	60.12	12.14	63.11	-2.99	58.67	1.45
5	49.72	15.76	52.32	-2.60	48.90	0.82
6	8.15	23.45	8.59	-0.44	8.13	0.02
7	0.65	25.16	0.69	-0.04	0.65	0.00
8	0.24	24.52	0.25	-0.01	0.24	0.00
9	15.80	20.49	16.65	-0.85	15.73	0.07
10	76.44	14.86	80.20	-3.76	74.41	2.03
11	77.80	8.93	81.14	-3.34	74.85	2.95
12	83.52	7.05	86.67	-3.15	79.62	3.90
year	571.88	14.66	597.89	-26.01	553.52	18.36

• Table a2.2 GWR and runoff calculation for the meteorological station *Observatorio de Cartuja* (X 447308 Y 4116447 Z 774)

month	precipitation	temperature	ETA	runoff & recharge	ETA	runoff & recharge
	[mm]	[°C]	TURC	TURC	COUTAGNE	COUTAGNE
1	46.21	7.34	54.48	-2.52	50.57	1.39
2	51.96	8.12	62.28	-2.95	57.90	1.43
3	59.33	11.89	54.21	-2.67	50.60	0.94
4	51.54	14.52	40.92	-2.07	38.38	0.48
5	38.86	16.96	18.42	-0.94	17.40	0.07
6	17.48	23.95	3.58	-0.18	3.39	0.00
7	3.39	26.52	4.12	-0.21	3.91	0.00
8	3.91	24.36	26.33	-1.35	24.81	0.17
9	24.98	20.41	52.18	-2.60	48.78	0.80
10	49.58	16.12	58.53	-2.74	54.38	1.40
11	55.78	10.15	61.45	-2.70	56.83	1.91
12	58.75	7.16	18.96	-0.96	17.83	0.17
year	461.77	15.63	455.45	-21.89	424.78	8.78

• Table a2.3 GWR and runoff calculation for the meteorological station *Padul* (X 444683 Y 4097327 Z 753)

month	precipitation	temperature	ETA	runoff & recharge	ETA	runoff & recharge
	[mm]	[°C]	TURC	TURC	COUTAGNE	COUTAGNE
1	18.00	7.76	54.65	-2.53	50.73	1.39
2	52.12	8.26	62.13	-2.93	57.74	1.46
3	59.20	11.42	47.04	-2.32	43.96	0.76
4	44.72	13.19	39.72	-2.00	37.26	0.46
5	37.72	16.46	12.81	-0.66	12.11	0.04
6	12.15	22.84	0.69	-0.04	0.65	0.00
7	0.65	25.39	0.37	-0.02	0.35	0.00
8	0.35	24.82	16.76	-0.86	15.83	0.07
9	15.90	20.81	68.80	-3.35	64.07	1.38
10	65.45	16.51	69.67	-3.17	64.58	1.92
11	66.50	10.76	65.39	-2.89	60.51	1.99
12	62.50	8.32	41.85	-2.01	38.96	0.88
year	435.26	15.55	479.87	-22.77	446.77	10.33

APPENDIX

• Table a2.4 GWR and runoff calculation for the meteorological station *Pinos Puente* (X 431534 Y 4124395 Z 594)

month	precipitation	temperature	ETA	runoff & recharge	ETA	runoff & recharge
	[mm]	[°C]	TURC	TURC	COUTAGNE	COUTAGNE
1	39.84	7.11	46.50	-2.22	43.28	1.00
2	44.28	8.32	68.25	-3.17	63.36	1.72
3	65.08	11.88	43.28	-2.16	40.51	0.61
4	41.12	14.02	33.71	-1.71	31.69	0.31
5	32.00	17.66	2.42	-0.12	2.30	0.00
6	2.30	24.85	0.53	-0.03	0.50	0.00
7	0.50	26.27	0.46	-0.02	0.44	0.00
8	0.44	25.66	16.44	-0.84	15.54	0.06
9	15.60	21.91	57.53	-2.85	53.71	0.97
10	54.68	16.32	61.63	-2.87	57.23	1.53
11	58.76	10.35	74.46	-3.10	68.70	2.66
12	71.36	7.96	41.01	-1.93	38.08	1.00
year	425.96	16.03	446.23	-21.03	415.33	9.87

• Table a2.5 GWR and runoff calculation for the meteorological station *Puebla de Don Fadrique* (X 554482 Y 4192456 Z 1110)

month	precipitation	temperature	ETA	runoff & recharge	ETA	runoff & recharge
	[mm]	[°C]	TURC	TURC	COUTAGNE	COUTAGNE
1	15.56	4.02	22.90	-1.14	21.43	0.33
2	21.76	4.68	38.90	-1.90	36.31	0.69
3	37.00	8.44	32.21	-1.61	30.19	0.41
4	30.60	10.62	38.07	-1.91	35.69	0.47
5	36.16	14.11	12.28	-0.63	11.61	0.04
6	11.65	21.35	2.74	-0.14	2.60	0.00
7	2.60	23.17	15.73	-0.81	14.86	0.06
8	14.92	22.76	23.94	-1.22	22.57	0.15
9	22.72	18.39	48.22	-2.38	45.05	0.79
10	45.84	13.32	31.90	-1.58	29.82	0.50
11	30.32	7.54	42.64	-2.00	39.60	1.04
12	40.64	5.58	33.79	-1.67	31.57	0.55
year	309.77	12.83	343.32	-16.99	321.31	5.02

• Table a2.6 GWR and runoff calculation for the meteorological station *Cadiar* (X 483724 Y 4086564 Z 950)

month	precipitation	temperature	ETA	runoff & recharge	ETA	runoff & recharge
	[mm]	[°C]	TURC	TURC	COUTAGNE	COUTAGNE
1	24.56	7.36	59.63	-2.67	55.21	1.75
2	56.96	7.50	75.91	-3.35	70.23	2.33
3	72.56	10.46	53.31	-2.59	49.70	1.02
4	50.72	12.25	35.64	-1.80	33.46	0.38
5	33.84	15.68	4.69	-0.24	4.45	0.00
6	4.45	23.08	3.37	-0.17	3.20	0.00
7	3.20	24.75	0.84	-0.04	0.80	0.00
8	0.80	24.51	24.37	-1.25	22.97	0.15
9	23.12	20.14	76.32	-3.64	70.90	1.78
10	72.68	15.45	66.03	-2.99	61.20	1.84
11	63.04	9.69	111.19	-3.19	101.83	6.17
12	108.00	7.80	29.80	-1.48	27.86	0.46
year	513.93	14.89	541.09	-23.40	501.80	15.89

APPENDIX 3 (Methods)

List of all measured parameters, site types, operating persons and date of sampling.

• Table a3.1 Site information and measured parameters of Feb.04 campaign (Dr.Kohfahl/Prof.Pekdeger).

Site ID	Site name	Type	Village	IGME declaration	Sampling date	Measured parameters
SP-GR-022	Fte. Alta	spring	Sierra Nevada		05. Feb 04	T,EC,Ions, D, 180
SP-GR-023	Fte. las Viboras		Fuente las viboras			
SP-GR-024	Fte. del Hervidero		La Zubia			
SP-GR-025	Fte. la Cortijuela					
SP-GR-026	Fte. de los 16 canos		Guejar Sierra			
SP-GR-027	Fte. de Teja					
SP-GR-028	Fte. de Urquiza	Thermal spring	Durcal right tube from spectators view			
SP-GR-029	Fte. de Urquiza left		Durcal left tube from spectators view			
SP-GR-030	Fte. y Alberca de Palmones	spring	Padul	1942.6.073		
SP-GR-031	Fte. los Molinos					
SP-GR-032	Banos de la Malah	Thermal spring	La Mahala	1942.6.007	06. Feb 04	T,EC,Ions, D, 180, runoff
SP-GR-033	Fte. Grande	spring	Alfacar			T,EC,Ions, D, 180
SP-GR-022	Fte. Alta		Sierra Nevada	1941.8.002		

• Tab.a3.2 Site information and measured parameters of May 04/Feb.04 (Prof.Benavente) campaign.

Site ID	Site name	Type	Village	IGME declaration	Sampling date	Measured parameters
SP-GR-022	Fte. Alta	Spring	Sierra Nevada		12-Mai-04	T, EC, pH, D, 180
SP-GR-023	Fte. las Viboras					T, EC, pH, D, 180, runoff
SP-GR-032	Banos de la Malah	Thermal spring	La Mahala		20-Feb-04	T, EC, pH, D, 180
SP-GR-051	Instituto del agua	Rain	Agua Lluvia Instituto del Agua			

• Table a3.3 Site information and measured parameters of June – Sept. 04 campaigns (Dr.Hidalgo)

Site ID	Site name	Type	Location	Sampling date	Measured parameters
SP-GR-038	Laguna del Majano	snowmelt	desagüe en margen izq de la Laguna del Majano	27-Jun-04	T, EC, D, 180
SP-GR-039	desde Pico del Goteron		Chorrera ladera Este (desde P. del Goterón)		
SP-GR-040	Laguna de la Mosca	laguna	Laguna de la Mosca		
SP-GR-041	Collado del Ciervo	snowmelt	Agua de fusión hacia el collado del Ciervo (3122 m.)		
SP-GR-042	Ladera SO Mulhacén		Agua de fusión en Nevero de ladera SO Mulhacén		
SP-GR-043	Cumbre del Muhacén		Agua de fusión en Nevero cumbre del Mulhacén		
SP-GR-044	Circo del Veleta		Cuenca del Guarnón 1ª chorrera (más oriental) del Circo del Veleta (escombrera de las minas de siderita)		
SP-GR-045	Laguna Larga (oeste)	laguna	Nieve fundiendo en el interior de la Laguna Larga (oeste)	04-Jul-04	
SP-GR-046	Laguna Larguilla		Nevero fundiendo al Sur de la Laguna Larguilla		
SP-GR-047	7ª chorrera del Corra	snowmelt	Agua de fusión cayendo por unas roquillas		

APPENDIX

-continued- • Table a3.3

Site ID	Site name	Type	Location	Sampling date	Measured parameters
SP-GR-048	Tajos del Campanario	rio	2ª Chorrerilla por debajo de los Tajos del Campanario de las tres chorrerillas (Río Guarnón individualizado)	04-Jul-04	T, EC, D, 18O
SP-GR-049	Fusión nieve	snowmelt	Fusión nieve	22-Jun-04	D, 18O
SP-GR-053	Corral del Veleta		7ª chorrera del Corral del Veleta (SP47*)	04-Jul-04	
SP-GR-054	Nevero Río Mulhacén	snow	Penúltimo nevero Río Mulhacén	27-Jun-04	T, EC, D, 18O
SP-GR-055	Ladera SE R. Chico	snowmelt	Vereda El Chorrillo-Trevez. Agua de fusión de nevero (ladera SE R. Chico)		
SP-GR-056	Margen izq		desagüe en margen izq		
SP-GR-057	Laguna de la Caldereta	laguna	Laguna de la Caldereta, nieve fundiendo en la lagunilla		
SP-GR-180	Collado de la Carigüela	snowmelt	Collado de la Carigüela (cara S) agua de fusión del nevero	10-Jul-04	
SP-GR-181	Laguna de Aguas Verdes (algo de nieve)	laguna	Laguna de Aguas Verdes (algo de nieve)		
SP-GR-182	Lagunillos de los Machos	snowmelt	Único aliviadero del arroyo de los 3 Lagunillos de los Machos		
SP-GR-183	Laguna de los Machos	laguna	Laguna de los Machos		
SP-GR-184	Deagüe del Laguneto de la chorrera	snowmelt	Deagüe del Laguneto de la chorrera occidental de R. Seco (3)		
SP-GR-185	Laguna de Río Seco (5)	laguna	Laguna de Río Seco (5)	17-Jul-04	
SP-GR-186	San Juan, margen dcha. (nevero)	snow	San Juan, margen dcha. (nevero)		
SP-GR-187	Lagunillo de Juego de Bolos	laguna	Lagunillo de Juego de Bolos (sin salida)		
SP-GR-188	Laguna de la Caldera		Laguna de la Caldera		
SP-GR-189	Lagunillo de la Virgen 5		Lagunillo de la Virgen 5		
SP-GR-190	Lagunillos de la Virgen 2	laguna	Lagunillos de la Virgen 2	21-Jul-04	
SP-GR-191	Lagunillos de la Virgen 4		Lagunillos de la Virgen 4		
SP-GR-192	Lagunillos del Fraile de Capileira 2		Lagunillos del Fraile de Capileira 2		
SP-GR-193	Lagunillos del Fraile		Aliviadero del Lagunillos del Fraile de Capileira 1. Aporte principal de un gran cono de derrubios		
SP-GR-194	Chorrera del Molinillo	Río Dílar	Río Dílar por debajo de la Chorrera del Molinillo	28-Jul-04	
SP-GR-195	Lagunillos de la Mula (S) casi estancada	laguna	Lagunillos de la Mula (S) casi estancada	28-Jul-04	
SP-GR-196	Laguna de la Mula		Laguna de la Mula. No está aliviando, algo excavada. Muy llena de algas	28-Jul-04	
SP-GR-197	Nacimiento del Alhorí	nac.alhori	Nacimiento del Alhorí	31-Jul-04	
SP-GR-198	Laguna de Juntillas	laguna	Laguna de Juntillas (suelta muy poco agua por el aliviadero)		
SP-GR-199	Laguna de Vacares		Laguna de Vacares (restos de nevero)		
SP-GR-200	Lagunillos de las Calderetas		Lagunillos de las Calderetas 3 (ver esquema)		
SP-GR-201	Nacimiento del Río Lanjarón	Nac.Río Lanjaron	Nacimiento del Río Lanjarón	05-Aug-04	
SP-GR-202	Laguna de Lanjarón	laguna	Laguna de Lanjarón. No desagua actualmente pero esta filtrando bastante agua unos 8 m abajo		
SP-GR-203	Laguna de las Tres Puertas		Laguna de las Tres Puertas. Entra un hilillo de derrubios		
SP-GR-204	Siete Lagunas (2).		Siete Lagunas (2).	11-Sep-04	

APPENDIX

-continued- • Table a3.3

Site ID	Site name	Type	Location	Sampling date	Measured parameters		
SP-GR-205	Siete Lagunas (1).	laguna	Siete Lagunas (1).	11-Sep-04	T, EC, D, 180		
SP-GR-206	Siete Lagunas (7).		Siete Lagunas (7).				
SP-GR-207	Siete Lagunas (8).		Siete Lagunas (8).				
SP-GR-208	Siete Lagunas 10. Laguna Hondera		Siete Lagunas 10. Laguna Hondera				
SP-GR-209	Charquilla debajo de la parte alta de los Borreguiles del Puerto		Charquilla debajo de la parte alta de los Borreguiles del Puerto	17-Sep-04			
SP-GR-210	Laguna de Charca Palo. Aliviando agua y muy clara					05-Aug-04	
SP-GR-211	Laguna Bolaños						
SP-GR-212	Laguna Cuadrada						
SP-GR-213	Laguna de Najera grande						
SP-GR-214	Saliente de Lavadero Reina						
SP-GR-215	Laguna del Caballo						
SP-GR-216	Laguna del Carnero						
SP-GR-217	Laguna del Cartujo						
SP-GR-218	Laguna de las Cabras						14-Aug-04
SP-GR-219	Lagunillos de Río Seco						
SP-GR-220	Lagunillo del Veleta						
SP-GR-221	Laguneto del Veleta						
SP-GR-222	Laguneto del Veleta 2					22-Aug-04	Laguneto del Veleta (fusión, colgado, aguas claras).
SP-GR-223	Laguneto del Veleta 3						Laguneto del Veleta 2 (fusión, colgado, muy turbio).
SP-GR-224	Laguneto del Puntal de Loma Pua		Laguneto del Puntal de Loma Pua				
SP-GR-225	Laguna Martín.	laguna	Laguna Martín. Con muchas algas. Estancada.	25-Sep-04			
SP-GR-226	Nacimiento de la laguna Martín.	nac. Laguna	Nacimiento de la laguna Martín.				
SP-GR-227	Laguna 3 del Corral	laguna	Laguna 3 del Corral. Ha bajado más de 1 m. Muy turbia y verdosa.				
SP-GR-228	Laguna chica Vald. Borreguil. Sale poco agua.	laguna	Laguna chica Vald. Borreguil. Sale poco agua.				
SP-GR-229	Laguna Larguilla (Gabata)		Laguna Larguilla (Gabata). Ha bajado casi 1 metro. Desagua poco.				
SP-GR-230	Laguna Larga.		Laguna Larga. Ha bajado más de 2 m. de nivel.				
SP-GR-231	Laguna de la Mosca	Snow or snowmelt	Laguna de la Mosca. No ha bajado mucho de nivel.				
SP-GR-232	Laguna más alta de las Calderetas	Snow or snowmelt	Laguna más alta de las Calderetas. Sin entrada visible. Ha bajado 10 cm. Cristalina, poca salida.				
SP-GR-233		Snow or snowmelt					
SP-GR-038	Laguna del Majano	Snow or snowmelt	desagüe en margen izq de la Laguna del Majano		27-Jun-04		
SP-GR-039	desde Pico del Goteron	Snow or snowmelt	Chorrera ladera Este (desde P. del Goterón)				

APPENDIX

• Table a3.4 sites, type, persons, date and measured parameters of November 04 campaign (IGME staff).

Site ID	Site name	Type	Village	IGME declaration	Sampling date	Measured parameters
SP-GR-081	Camino frente Puleva	Observation well	Granada Vega	1941.7.265	16-Nov-04	T, EC, watertable, D, 18O
SP-GR-082	Romilla			1941.5.205	05-Nov-04	
SP-GR-083	Atarfe			1941.6.217	17-Nov-04	
SP-GR-084	Pedro Ruiz			1941.6.221	12-Nov-04	
SP-GR-085	Aeropuerto			1941.6.218	25-Nov-04	
SP-GR-086	Alhendin			1942.3.240	08-Nov-04	
SP-GR-087	Cullar Vega			1942.3.072	09-Nov-04	
SP-GR-088	Casa Nuevas	Well		1941.5.090	22-Nov-04	
SP-GR-089	Santa Rosa			1941.5.085	10-Nov-04	
SP-GR-090	Cort. Trevijano	Observation well		1941.7.157	26-Nov-04	

• Table a3.5 Sites, type, persons, date and measured parameters of Dec. 04 rainwater (Fernandez, IGME)

Site ID	Site name	Type	Village	IGME declaration	Sampling date	Measured parameters
SP-GR-091	Rain 975m	Rain	Guejar Sierra	-	02-Dez-04	D, 18O
SP-GR-092	Rain 1310m			-		
SP-GR-093	Rain 1500m			-		
SP-GR-094	Rain 1550m			-		
SP-GR-095	Rain 670m		Puerta oficina IGME	-		

• Table a3.6 Sites, type, persons, date and measured parameters of Feb.05 campaign (Dr.Meyer, AWI).

Site ID	Site name	Type	Description	Sampling date	Measured parameters
SP-GR-235	Snowpatch 1	Snow	Schnee, Schmelzkruste; Schneefleck Ende des Winters; vermutl. Evapo+Sublim.; Kiefernwald, NE-Hang; Nevado Filabride	19. Feb 05	D, 18O
SP-GR-236	Snowpatch 2		Schnee, unterhalb Schmelzkruste; vermutl. Evapo+Sublim.; Kiefernwald, NE-Hang; Nevado Filabride	19. Feb 05	D, 18O
SP-GR-237	Snowpatch 3		Schnee; N-Hang; in Kurve B. Viboras; Fte. de las Viboras (SP 23) nicht gefunden; Schneegrenze ~1400m	19. Feb 05	D, 18O

APPENDIX

• Table a3.7 Sites, types, persons, date and measured parameters of Vega sampling campaign feb 05.

Site ID	Site name	Type	Village	IGME declaration	Sampling date	Measured parameters
SP-GR-130	Armillá Vivero Dip	Well	Armillá	-	18-Feb-05	T, EC, pH, runoff, alkalinity, Ions, D, 18O
SP-GR-131	Cullar Vega		Cullar Vega			
SP-GR-132	Alhencira		Alhendin			
SP-GR-133	Terrazos Terragran		Pulianas			
SP-GR-134	Cort. Santa Ana	Thermal Spring	Sierra Elvira			T, EC, pH, runoff, alkalinity, Ions, D, 18O
SP-GR-135	Banos de Sierra Elvira					
SP-GR-136	Meson El Guerro	Well	Huetor de Vega			T, EC, pH, alkalinity, Ions, D, 18O
SP-GR-137	Manantial de la Reina	Spring	Santa Fe			T, EC, pH, runoff, alkalinity, Ions, D, 18O
SP-GR-138	Arroyo de salado	Surface water				T, EC, pH, alkalinity, Ions, D, 18O
SP-GR-139	Banos Santa Fe	Thermal Spring	Santa Fe, aeropuerto			
SP-GR-140	Los Fagailos	Spring	Fuente Vaqueros			T, EC, pH, runoff, alkalinity, Ions, D, 18O
SP-GR-141	Rio Cubillas	Surface water	Cubillas			T, EC, pH, alkalinity, Ions, D, 18O
SP-GR-142	Puente Rio Genil		Lachar			

• Table a3.8 Sites, type, persons, date and measured parameters of surface and precipitation.

Site ID	Site name	Type	Village	Sampling date	Measured parameters
SP-GR-037	Rio Genil	Surface water	Rio Genil Barranco de San Juan	07-Okt-04	T, EC, pH, alkalinity, ions, D, 18O
SP-GR-067	Rio Durcal		Durcal	16-Okt-04	T, EC, pH, D, 18O
SP-GR-068	Rio Genil 2		Pinos de Genil	23-Okt-04	T, EC, pH, Eh, O ₂ , D, 18O
SP-GR-069	Rio Genil 3		Granada, at Car Bridge		
SP-GR-037	Rio Genil		Rio Genil Barranco de San Juan		T, EC, pH, D, 18O
SP-GR-076	Rio Darro		Cortijo Jesus del Valle (Granada)	28-Okt-04	T, EC, pH, alkalinity, ions, D, 18O
SP-GR-069	Rio Genil 3		Granada, at Car Bridge	10-Nov-04	T, EC, pH, Eh, D, 18O
SP-GR-068	Rio Genil 2		Pinos de Genil		
SP-GR-037	Rio Genil		Rio Genil Barranco de San Juan	15-Nov-04	T, EC, pH, D, 18O
SP-GR-076	Rio Darro		Cortijo Jesus del Valle (Granada)	16-Nov-04	T, EC, pH, Eh, D, 18O
SP-GR-097	Embalse de Quentar				
SP-GR-076	Rio Darro		Cortijo Jesus del Valle (Granada)	25-Nov-04	T, EC, pH, Eh, alkalinity, ions, D, 18O
SP-GR-078	Rio Darro 2		Granada		
SP-GR-069	Rio Genil 3		Granada, at Car Bridge	04-Dez-04	T, EC, pH, D, 18O
SP-GR-068	Rio Genil 2		Pinos de Genil		
SP-GR-079	Embalse de Canales		Granada	07-Dez-04	T, EC, pH, Eh, O ₂ , D, 18O
SP-GR-078	Rio Darro 2				
SP-GR-076	Rio Darro		Cortijo Jesus del Valle (Granada)		T, EC, pH, D, 18O
SP-GR-069	Rio Genil 3		Granada, at Car Bridge	09-Jan-05	T, EC, pH, Eh, O ₂ , D, 18O
SP-GR-068	Rio Genil 2		Pinos de Genil		

APPENDIX

• Table a3.8 continued

Site ID	Site name	Type	Village	Sampling date	Measured parameters	
SP-GR-076	Rio Darro	Surface water	Cortijo Jesus del Valle (Granada)	10-Jan-05	T, EC, pH, D, 18O	
SP-GR-078	Rio Darro 2		Granada			
SP-GR-037	Rio Genil		Rio Genil Barranco de San Juan	19 Jan 05	T, EC, pH, alkalinity, ions, D, 18O	
SP GR 069	Rio Genil 3		Granada, at Car Bridge	25 Jan 05	T, EC, pH, D, 18O	
SP GR 068	Rio Genil 2		Pinos de Genil		T, EC, pH, Eh, O2, D, 18O	
SP GR 037	Rio Genil		Rio Genil Barranco de San Juan	27 Jan 05	T, EC, pH, D, 18O	
SP GR 076	Rio Darro		Cortijo Jesus del Valle (Granada)	04 Feb 05	T, EC, pH, alkalinity, ions, D, 18O	
SP GR 078	Rio Darro 2		Granada			
SP GR 096	Arroyo de Huenes		Fuente siete ojos	05 Feb 05	T, EC, pH, D, 18O	
SP GR 098	Arroyo Caballo		Pico de Caballo	13 Feb 05		
SP GR 141	Rio Cubillas		Cubillas	18 Feb 05		
SP GR 142	Puente Rio Genil		Lachar			
SP GR 138	Arroyo de salado					
SP GR 079	Embalse de Canales		Granada	19 Feb 05		
SP GR 179	Callejon del Angel		Rain	Granada Zaidin		28 Feb 05
SP GR 179	Callejon del Angel					02 Mrz 05
SP GR 037	Rio Genil	Surface water	Rio Genil Barranco de San Juan	05 Mrz 05		T, EC, pH, D, 18O
SP GR 079	Embalse de Canales		Granada			
SP GR 179	Callejon del Angel	Rain	Granata Zaidin	06 Mrz 05		
SP GR 068	Rio Genil 2	Surface water	Pinos de Genil			
SP GR 177	Rio Cubillas		Deifontes			
SP GR 178	Embalse de Cubillas		Los Cortijos			
SP GR 172	Oberlauf Alhama de Granada		Surface water	Alhama de Granada	10 Mrz 05	
SP GR 173	Unterlauf Alhama de Granada					
SP GR 171	Zulauf Hotel Alhama de Granada					
SP GR 170	Embalse Bermejales					

APPENDIX

• Table a3.9 Sites, types, persons, date and measured parameters of spring and thermal spring samples.

Site ID	Site name	Type	Village	IGME declaration	Sampling date	Measured parameters	
SP-GR-022	Fte. Alta	Spring	Sierra Nevada	-	07-Okt-04	T, EC, pH, runoff, alkalinity, ions, D, 18O	
SP-GR-023	Fte. las Viboras		Fuente las viboras			T, EC, pH, runoff, D, 18O	
SP-GR-024	Fte. del Hervidero		La Zubia			T, EC, pH, Eh, alkalinity, ions, D, 18O	
SP-GR-025	Fte. la Cortijuela		Fuente la cartijuela (la zubia)			T, EC, pH, Eh, O2, runoff, alkalinity, ions, D, 18O	
SP-GR-026	Fte. de los 16 canos		Guejar Sierra			T, EC, pH, alkalinity, ions, D, 18O	
SP-GR-033	Fte. Grande		Alfacar			1941.8.002	T, EC, pH, Eh, O2, runoff, alkalinity, ions, D, 18O
SP-GR-034	Fte. de Nivar		Nivar			1941.4.002	T, EC, pH, runoff, D, 18O
SP-GR-035	Fte. Cerro Negro					1941.3.039	T, EC, pH, D, 18O
SP-GR-036	Nacimiento Rio Darro		Colmenar			2041.5.018	
SP-GR-028	Fte. de Urquiza		Durcal right tube from spectators view			-	16-Okt-04
SP-GR-029	Fte. de Urquiza left		Durcal left tube from spectators view	T, EC, pH, alkalinity, ions, D, 18O			
SP-GR-030	Fte. y Alberca de Palmones		Padul	1942.6.073	1942.6.007	T, EC, pH, Eh, O2, alkalinity, ions, D, 18O	
SP-GR-031	Fte. los Molinos			-		T, EC, pH, Eh, O2, runoff, alkalinity, ions, D, 18O	
SP-GR-032	Banos de la Malah		La Mahala	-	-	T, EC, pH, Eh, O2, runoff, alkalinity, ions, D, 18O	
SP-GR-033	Fte. Grande		Alfacar	1941.8.002	08-Nov-04	T, EC, pH, runoff, D, 18O	
SP-GR-034	Fte. de Nivar		Nivar	1941.4.002		T, EC, pH, D, 18O	
SP-GR-035	Fte. Cerro Negro			1941.3.039		T, EC, pH, runoff, D, 18O	
SP-GR-036	Nacimiento Rio Darro		Colmenar	2041.5.018		T, EC, pH, D, 18O	
SP-GR-070	Fte. de Vita		Cogollos Vega	-	09-Nov-04	T, EC, pH, O2, runoff, D, 18O	
SP-GR-071	Fte. Teja		Alfacar				
SP-GR-072	Fte. Savina		Beas de Granada				
SP-GR-073	Fte. Agostinos		Cortijo de los Agostinos				
SP-GR-074	Fte. Carcabal		La Peza				
SP-GR-075	Fte. Nabugal						
SP-GR-022	Fte. Alta		Sierra Nevada				-
SP-GR-023	Fte. las Viboras		Fuente las viboras	T, EC, pH, D, 18O			
SP-GR-026	Fte. de los 16 canos		Guejar Sierra	T, EC, pH, runoff, D, 18O			
SP-GR-024	Fte. del Hervidero		La Zubia	-	22-Nov-04	T, EC, pH, Eh, D, 18O	
SP-GR-025	Fte. la Cortijuela		Fuente la cartijuela (la zubia)			T, EC, pH, Eh, runoff, D, 18O	
SP-GR-030	Fte. y Alberca de Palmones		Padul			1942.6.073	T, EC, pH, runoff, D, 18O
SP-GR-031	Fte. los Molinos	1942.6.007				T, EC, pH, D, 18O	
SP-GR-032	Banos de la Malah	La Mahala	-			T, EC, pH, D, 18O	
SP-GR-077	Fte. 7 ojos	La Zubia	-			T, EC, pH, Eh, D, 18O	
SP-GR-024	Fte. del Hervidero		-			05-Feb-05	T, EC, pH, Eh, O2, D, 18O
SP-GR-025	Fte. la Cortijuela	Fuente la cartijuela (la zubia)	-	-	T, EC, pH, Eh, D, 18O		
SP-GR-135	Banos de Sierra Elvira	Sierra Elvira	-	18-Feb-05	T, EC, pH, runoff, D, 18O		

APPENDIX

• Table a3.9 continued

Site ID	Site name	Type	Village	IGME declaration	Sampling date	Measured parameters	
SP-GR-137	Manantial de la Reina	Spring	Santa Fe	-	18-Feb-05	T, EC, pH, runoff, D, 180	
SP-GR-139	Banos Santa Fe		Santa Fe, aeropuerto			T, EC, pH, D, 180	
SP-GR-140	Los Fagailos		Fuente Vaquelos			T, EC, pH, runoff, D, 180	
SP-GR-022	Fte. Alta		Sierra Nevada		19-Feb-05	T, EC, pH, D, 180	
SP-GR-026	Fte. de los 16 canos		Guejar Sierra			T, EC, pH, runoff, D, 180	
SP-GR-027	Fte. de Teja					T, EC, pH, runoff, D, 180	
SP-GR-033	Fte. Grande		Alfacar			1941.8.002	T, EC, pH, D, 180
SP-GR-034	Fte. de Nivar		Nivar			1941.4.002	T, EC, pH, D, 180
SP-GR-035	Fte. Cerro Negro					1941.3.039	T, EC, pH, runoff, D, 180
SP-GR-024	Fte. del Hervidero		La Zubia		-	26-Feb-05	T, EC, pH, D, 180
SP-GR-026	Fte. de los 16 canos		Guejar Sierra			T, EC, pH, runoff, D, 180	
SP-GR-030	Fte. y Alberca de Palmones		Padul		1942.6.073	05-Mrz-05	T, EC, pH, D, 180
SP-GR-032	Banos de la Malah		La Mahala		T, EC, pH, runoff, D, 180		
SP-GR-033	Fte. Grande		Alfacar		1941.8.002	08-Mrz-05	T, EC, pH, D, 180
SP-GR-028	Fte. de Urquiza		Durcal right tube from spectators view		-	10-Mrz-05	T, EC, pH, runoff, D, 180
SP-GR-029	Fte. de Urquiza left		Durcal left tube from spectators view				T, EC, pH, D, 180
SP-GR-174	Banos Alhama de Granada	Alhama de Granada	T, EC, pH, Eh, runoff, D, 180				
SP-GR-025	Fte. la Cortijuela	Fuente la cartijuela (la zubia)		22-Mrz-05		T, EC, pH, runoff, D, 180	

• Table a3.10 Methods, devices and detection limits of hydrochemical analysis.

Ion	Method	Device	Detection limit
Ca ²⁺	AAS	Perkin Elmer 5000	0.05 [mg/l]
Cl	photometric	Technicon Autoanalyser	1.0 [mg/l]
Fe ²⁺	AAS	Perkin Elmer 5000	0.1 [mg/l]
K ⁺	Flamefotometer	Eppendorf Elex 6361r	0.1 [mg/l]
Li ⁺	AAS	Perkin Elmer 5000	0.05 [mg/l]
Mg ²⁺	AAS	Perkin Elmer 5000	0.05 [mg/l]
Mn ²⁺	AAS	Perkin Elmer 5000	0.05 [mg/l]
Na ⁺	Flamefotometer	Eppendorf Elex 6361r	1.0 [mg/l]
NO ₃	photometric	Technicon Autoanalyser	0.05 [mg/l]
SO ₄ ²⁻	photometric	Technicon Autoanalyser	0.05 [mg/l]
Sr ²⁺	ICP	Leemans	0.05 [mg/l]
δ ¹⁸ O	H ₂ Equilibrium	Delta S Massenspektrometer Finigan	± 0.8 ‰
ΔD	CO ₂ Equilibrium	Delta S Massenspektrometer Finigan	± 0.1 ‰

• Table a3.11: Determination of physical/chemical parameters and analysis methods in field.

Parameter	Method	Device
Temperature	electrometric	Multiline P4 (Fa. WTW); Temperatursonde integrated in pH Sonde SenTIX 41
pH Value (pH1 pH13)	potentiometric with automatic temperature compensation	Multiline P4 + pH Sonde SenTIX 41 (Fa. WTW)
Electrical conductivity (10 – 10 000 μ S/cm)	elektrometric with automatic temperature compensation (25 °C)	Multiline P4 + LF Sonde TetraCon 325 (Fa. WTW)
Oxygen saturation (1 – 100%)	polarographic	Multiline P4 + Sauerstoffsonde CellOx 325 + Kalibriergefäß OxiCal SI (Fa. WTW)
Redoxpotential (200 – 1000 mV)	potentiometric (Ag/AgCl Bezugsselektrode)	Multiline P4 (Fa. WTW) + Eh Sonde Pt 4805 (Fa. Ingold)
Carbonate species	in field measurement, titration with 0,1 N HCl to pH 4,3 or with 0,1 N NaOH to pH 8,2	Vollpipette (100 ml) Feldbürette, pH Meter, Becherglas
NO ₂ (0,005 – 0,1 mg/l)	in field measurement: colorimetric	Schnelltest: Aquaquant 1.4408(Fa. Merck)
NH ₄ ⁺ (0,05 – 0,8 mg/l)	in field measurement: colorimetric	Schnelltest: Aquaquant 1.4400.001 (Fa. Merck)

APPENDIX 4 (Results and discussion)

• Table a4.1 Reliability check, electrical balance and TDS values.

site	date	cations meq/l	anions meq/l	balance meq/l	balance %	EC μ S/cm	TDS
Fte. Alta	05 Feb 04	1.26	1.21	0.05	3.76	138	65.3
Fte. Alta	07 Okt 04	0.67	0.68	0.01	0.83	77	33.8
Fte. las Viboras	05 Feb 04	3.21	3.08	0.13	4.07	284	153.2
Fte. las Viboras	07 Okt 04	3.17	3.06	0.12	3.72	288	151.0
Fte. del Hervidero	05 Feb 04	3.17	3.02	0.15	4.70	286	151.5
Fte. del Hervidero	07 Okt 04	2.87	2.90	0.04	1.26	289	142.9
Fte. la Cortijuela	05 Feb 04	4.54	4.66	0.11	2.47	401	218.7
Fte. la Cortijuela	07 Okt 04	5.12	4.91	0.21	4.01	440	234.4
Fte. de los 16 canos	05 Feb 04	2.91	2.82	0.09	3.14	262	140.2
Fte. de los 16 canos	07 Okt 04	2.40	2.46	0.06	2.66	242	120.4
Fte. de Teja	05 Feb 04	3.46	3.60	0.14	4.13	315	175.2
Fte. de Urquiza	05 Feb 04	9.35	9.52	0.17	1.84	824	540.9
Fte. de Urquiza	16 Okt 04	9.01	9.24	0.23	2.54	754	521.8
Fte. de Urquiza left	05 Feb 04	8.71	8.87	0.16	1.84	785	499.7
Fte. de Urquiza left	16 Okt 04	8.32	8.63	0.32	3.79	834	481.6
Fte. y Alberca de Palmones	06 Feb 04	5.42	5.16	0.26	4.79	473	258.8
Fte. y Alberca de Palmones	16 Okt 04	5.24	5.11	0.14	2.62	505	253.5
Fte. los Molinos	06 Feb 04	6.06	5.89	0.18	2.90	533	291.0
Fte. los Molinos	16 Okt 04	5.95	5.83	0.13	2.12	630	286.6
Banos de la Malah	06 Feb 04	36.87	37.51	0.64	1.74	3090	2307.6
Banos de la Malah	16 Okt 04	33.73	33.20	0.52	1.55	3500	2077.1
Fte. Grande	06 Feb 04	4.40	4.59	0.19	4.20	415	220.2
Fte. Grande	07 Okt 04	4.55	4.74	0.19	4.15	446	225.9
Fte. de Nivar	07 Okt 04	5.10	5.33	0.23	4.49	505	271.8
Fte. Cerro Negro	07 Okt 04	4.29	4.21	0.07	1.74	412	206.8
Nacimiento Rio Darro	07 Okt 04	4.44	4.42	0.01	0.27	438	215.3
Rio Genil	07 Okt 04	1.22	1.25	0.03	2.57	136	68.5
Rio Genil 2	10 Nov 04	1.75	1.70	0.05	2.60	130	92.6
Rio Genil 3	10 Nov 04	5.27	4.95	0.32	6.09	380	266.3
Fte. de Vita	08 Nov 04	8.04	7.73	0.31	3.90	854	376.6
Fte. Teja	08 Nov 04	7.64	7.29	0.35	4.54	722	351.5
Fte. Savina	09 Nov 04	7.91	7.55	0.35	4.47	755	401.2
Fte. Agostinos	09 Nov 04	4.28	4.14	0.14	3.23	436	197.7
Fte. Carcabal	09 Nov 04	2.73	2.64	0.09	3.32	276	130.0
Fte. Nabugal	09 Nov 04	2.97	2.98	0.01	0.46	309	146.9
Fte. 7 ojos	22 Nov 04	5.19	5.36	0.17	3.27	507	252.5
Rio Darro 2	25 Nov 04	5.84	5.63	0.22	3.69	540	282.3
Arroyo Caballo	13 Feb 05	1.34	1.30	0.03	2.58	125	67.8
Pico de Caballo	13 Feb 05	0.16	0.16	0.00	0.95	13	8.4
Armillas Vivero Dip	18 Feb 05	8.52	8.76	0.23	2.72	735	428.4
Cullar Vega	18 Feb 05	11.25	11.35	0.09	0.82	828	608.8
Alhencira	18 Feb 05	6.23	6.26	0.02	0.38	575	307.9
Terrazos Terragran	18 Feb 05	21.56	21.47	0.09	0.43	1701	1268.0
Cort. Santa Ana	18 Feb 05	10.61	10.27	0.34	3.19	941	547.2
Banos de Sierra Elvira	18 Feb 05	30.69	31.93	1.24	4.04	2650	1908.7
Manantial de la Reina	18 Feb 05	12.45	12.18	0.28	2.21	1125	646.3
Arroyo de salado	18 Feb 05	170.22	161.78	8.44	4.96	15620	9899.2
Banos Santa Fe	18 Feb 05	53.42	55.89	2.47	4.62	3700	3528.3

APPENDIX – Results and discussion

• Table a4.1 continued

site	date	cations meq/l	anions meq/l	balance meq/l	balance %	EC μ S/cm	TDS
Rio Cubillas	18 Feb 05	17.46	18.16	0.70	4.00	1501	1023.7
Genil 4	18 Feb 05	16.49	16.01	0.48	2.91	1443	910.3
Callejon del Angel	28 Feb 05	0.31	0.31	0.00	0.09	22	16.8
Callejon del Angel	02 Mrz 05	0.24	0.23	0.01	4.12	20	11.8
Callejon del Angel	05 Mrz 05	0.14	0.14	0.00	1.02	45	7.1
Los Fagailos	18 Feb 05	11.64	11.46	0.18	1.56	1042	603.9

• Table a4.2 PHREEQC input file for molar Ca:Mg ratio calculation.

```
TITLE --Rainwater (Callejon del Angel) plus co2 soil
SOLUTION 1 rainwater
  units ppm
  pH 5.31
  density 1.0
  Ca 2.8
  Mg 1.1
  Na 1.4
  K 0.7
  Cl 3
  Alkalinity 7.6 as HCO3
  S(6) 4
EQUILIBRIUM_PHASES
  CO2(g) -2.0
save solution 1
END
```

```
TITLE --Equilibrate mixture with calcite only.
USE solution 1
EQUILIBRIUM_PHASES
  Calcite 0.0
SELECTED_OUTPUT (...)
END
```

```
TITLE --Equilibrate mixture with dolomite only.
USE solution 1
EQUILIBRIUM_PHASES 3
  Dolomite 0.0
SELECTED_OUTPUT (...)
END
```

```
TITLE --Equilibrate mixture with calcite and dolomite.
USE solution 1
EQUILIBRIUM_PHASES
  Calcite 0.0
  Dolomite 0.0
```

```
SELECTED_OUTPUT
-file Cc_Do_ratios_equilibrium.sel
-user_punch true
-high_precision
-reset true
-solution true
-si calcite dolomite aragonite co2(g)
-pH true
-temperature true
-ionic_strength true
-percent_error true
-charge_balance true
-molalities H+ Ca+2 CO2 HCO3- CO3-2 Mg+2
END
```

APPENDIX – Results and discussion

• Table a4.4 Field parameters, water type, saturation indices and molar Ca:Mg ratios of group 2 members.

Site	Date	Water type	pH	T (°C)	EC (µS/cm)	SI Calcite	SI Dolomite	SI Gypsum	SI Anhydrite	rCa/Mg
Fte. la Cortijuela	07-Okt-04	Mg-Ca-HCO3	8.18	8.4	440	0.60	1.11	-3.17	-3.42	0.9
Fte. Cerro Negro	07-Okt-04	Ca-Mg-HCO3	7.18	11.7	412	-0.34	-1.03	-2.58	-2.84	1.9
Fte. de Nivar	07-Okt-04	Ca-Mg-HCO3-SO4	7.44	12.2	505	-0.02	-0.37	-1.82	-2.07	1.9
Fte. Grande	07-Okt-04	HCO3	7.68	12.1	446	0.19	0.13	-2.51	-2.76	1.6
Nacimiento Rio Darro	07-Okt-04	Ca-Mg-HCO3	7.7	12.5	438	0.18	0.13	-2.48	-2.73	1.5
Fte. de los 16 canos	07-Okt-04		7.8	10.7	242	-0.26	-0.78	-2.70	-2.95	1.5
Fte. del Hervidero	07-Okt-04		7.11	10.5	289	-0.73	-1.95	-2.58	-2.84	2.6
Fte. las Viboras	07-Okt-04		7.06	10.7	288	-0.75	-1.88	-3.00	-3.26	2.0
Fte. Alta	07-Okt-04	Ca-Mg-Cl-HCO3	7.76	8.4	77	-1.61	-3.45	-4.03	-4.29	1.3
Rio Genil	07-Okt-04	Ca-Mg-HCO3-SO4	8.15	8.8	136	-0.64	-1.72	-2.66	-2.91	2.1
Fte. los Molinos	16-Okt-04	Ca-Mg-HCO3	7.45	17.1	630	0.09	0.17	-2.16	-2.40	1.1
Fte. y Alberca de Palmones	16-Okt-04		7.65	15.9	505	0.19	0.32	-2.11	-2.36	1.2
Fte. Teja	08-Nov-04		7.04	12.7	722	-0.09	-0.30	-2.72	-2.97	1.2
Fte. de Vita	08-Nov-04		7.02	14.3	854	-0.05	-0.44	-1.88	-2.13	2.0
Fte. Nabugal	09-Nov-04	Ca-HCO3	8.15	10.1	309	0.45	-0.05	-3.05	-3.31	7.0
Fte. Savina	09-Nov-04	Ca-Mg-HCO3-SO4	7.34	13.1	755	0.10	0.02	-1.52	-1.77	1.4
Fte. Agostinos	09-Nov-04	Ca-Mg-HCO3	7.67	11.1	436	0.11	-0.04	-3.00	-3.26	1.5
Fte. Carcabal	09-Nov-04		7.84	9.8	276	-0.08	-0.54	-2.87	-3.12	1.9
Rio Genil 2	10-Nov-04	Ca-Mg-HCO3-SO4	7.32	11.3	130	-1.16	-2.60	-2.49	-2.75	1.6
Fte. 7 ojos	22-Nov-04	Ca-Mg-HCO3	7.91	9	507	0.47	0.71	-2.79	-3.04	1.3
Rio Darro 2	25-Nov-04		8.16	8.9	540	0.76	1.16	-2.11	-2.37	1.8
Alhencira	18-Feb-05		7.49	15	575	0.18	0.16	-2.02	-2.27	1.6
min			7.02	8.4	77	-1.61	-3.45	-4.03	-4.29	0.9
max			8.18	17.1	854	0.76	1.16	-1.52	-1.77	7.0
average				11.4	427	-0.09	-0.49	-2.58	-2.83	2.1

• Table a4.5 Field parameters, water type, saturation indices and molar Ca:Mg ratios of group 3 members.

Site	Date	Water type	pH	T (°C)	EC (µS/cm)	SI Calcite	SI Dolomite	SI Gypsum	SI Anhydrite	rCa/Mg
Rio Genil 3	18-Feb-05	Ca-Mg-HCO3-SO4	8.1	11.5	380	0.54	0.82	-1.82	-2.07	1.57
Armillá Vivero Dip	10-Nov-04		7.31	15	735	0.08	0.09	-1.62	-1.87	1.16
Cullar Vega	18-Feb-05		7.37	14.4	828	0.25	0.16	-1.18	-1.43	2.09
Terrazos Terragran	18-Feb-05		7.03	15	1701	0.05	-0.04	-0.57	-0.82	1.39
Cort. Santa Ana	18-Feb-05		7.3	15.7	941	0.11	0.18	-1.30	-1.55	1.10
Meson El Guerro	18-Feb-05		7.54	14.1	824	0.36	0.61	-1.54	-1.80	1.23
Manantial de la Reina	18-Feb-05		7.12	15	1125	0.18	0.05	-1.29	-1.54	1.95

APPENDIX – Results and discussion

• Table a4.5 –continued-

Site	Date	Water type	pH	T (°C)	EC (µS/cm)	SI Calcite	SI Dolomite	SI Gypsum	SI Anhydrite	rCa/Mg
Los Fagailos	18-Feb-05	Ca-Mg-SO4-HCO3	7.29	14.5	1042	0.20	0.27	-1.28	-1.53	1.28
Rio Cubillas	18-Feb-05		7.77	12.4	1443	0.26	0.21	-0.80	-1.05	1.75
Puente Rio Genil	18-Feb-05	Ca-Mg-HCO3-Cl-SO4	7.22	13.7	1501	0.72	1.14	-0.91	-1.16	1.89
min				11.50	380	0.05	-0.04	-1.82	-2.07	1.10
max				15.70	1701	0.72	1.14	-0.57	-0.82	2.09
average				14.13	1052	0.27	0.35	-1.23	-1.48	1.54

• Table a4.6 Group4 saturation indices and main characteristics.

Site	Date	Water type	pH	T (°C)	EC (µS/cm)	SI Calcite	SI Dolomite	SI Gypsum	SI Anhydrite
Fte. de Urquiza	16. Okt 04	Ca-Mg-SO4-HCO3	7.6	22.5	754	0.39	0.73	1.23	1.46
Fte. de Urquiza left	16. Okt 04		7.0	22.6	785	0.27	0.58	1.27	1.50
Banos de la Malah	16. Okt 04	Ca-Na-Mg-Cl-SO4	7.2	25.5	3090	0.19	0.18	0.42	0.64
Banos Sierra Elvira	18. Feb 05	Na-Ca-Mg-Cl-SO4	7.3	32	2650	0.55	1.10	0.53	0.72
Banos Santa Fe	18. Feb 05	Ca-Mg-SO4	7.0	36.6	3700	0.23	0.37	0.02	0.18
min			7.0	22.5	754	0.27	0.58	1.27	1.50
max			7.6	36.6	3700	0.55	1.10	0.02	0.18
average				27.8	2195	0.22	0.36	0.69	0.90

• Table a4.7 PHREEQC input file for carbonate chemistry calculations, line of saturation

```
# Calculating the saturation line
SOLUTION 1 dest water in equilibration with calcite
temp 10
EQUILIBRIUM_PHASES
CO2(g) 2
Calcite 0

SELECTED_OUTPUT
file Cc_si0_t10_p 2.sel
user_punch true
high_precision
reset true
solution true
si halite calcite dolomite gypsum anhydrite aragonite co2(g)
pH true
temperature true
ionic_strength true
percent_error true
charge_balance true
molalities Fe+2 H+ Ca+2 CO2 HCO3 CO3 2 SO4 2 Cl NO3 Mg+2 Na+ K+ Fe+3
END
```

APPENDIX – Results and discussion

- Table a4.8 PHREEQC input file for carbonate chemistry calculations, open vs. closed system

SOLUTION 1 Rainwater (Granada city) plus soil co2 (2) at 10 degree.

```

units ppm
pH 5.31
density 1.0
temp 10
Ca 2.8
Mg 1.1
Na 1.4
K 0.7
Cl 3
Alkalinity 7.6 as HCO3
S(6) 4
EQUILIBRIUM_PHASES 1
CO2(g) 2.0
save solution 1
end

```

SOLUTION 2 Rainwater (Granada city) plus soil co2 (3.5) at 10 degree.

```

units ppm
pH 5.31
density 1.0
temp 10
Ca 2.8
Mg 1.1
Na 1.4
K 0.7
Cl 3
Alkalinity 7.6 as HCO3
S(6) 4
EQUILIBRIUM_PHASES 2
CO2(g) 3.5
save solution 2
end
# water encounters carbonate minerals
# under open system conditions with
# with pCO2 2
use solution 1
EQUILIBRIUM_PHASES 1
CO2(g) 2.0
Reaction
Calcite
0.002 mole in 10 steps
SELECTED_OUTPUT
file kinetic_10degree_open_p2.sel
user_punch true
high_precision
reset true
solution true
si halite calcite dolomite gypsum anhydrite aragonite co2(g)
pH true
temperature true
ionic_strength true
percent_error true
charge_balance true
molalities H+ Ca+2 CO2 HCO3 CO3 2 SO4 2 Cl NO3 HSO4 Mg+2 Na+ K+
END

```

```

# water encounters carbonate minerals
# under open system conditions
# with pCO2 3.5
use solution 1
EQUILIBRIUM_PHASES 1
CO2(g) 3.5
Reaction
Calcite
0.0005 mole in 5 steps
SELECTED_OUTPUT
file kinetic_10degree_open_p3.5.sel
user_punch true
high_precision
reset true
solution true
si halite calcite dolomite gypsum anhydrite aragonite co2(g)
pH true
temperature true

```

• Table a4.8 (continued)

```

ionic_strength true
percent_error true
charge_balance true
molalities H+ Ca+2 CO2 HCO3 CO3 2 SO4 2 Cl NO3 HSO4 Mg+2 Na+ K+
END

```

```

# water encounters carbonate minerals
# under closed system conditions with initial pCO2= 2
use solution 1
Reaction
Calcite
0.00053 mole in 5 steps
SELECTED_OUTPUT
file kinetic_10degree_closed.sel
user_punch true
high_precision
reset true
solution true
si halite calcite dolomite gypsum anhydrite aragonite co2(g)
pH true
temperature true
ionic_strength true
percent_error true
charge_balance true
molalities H+ Ca+2 CO2 HCO3 CO3 2 SO4 2 Cl NO3 HSO4 Mg+2 Na+ K+
END

```

Stable isotopes in precipitation

• Table a4.8 Stable isotopes (rain event 1)

Date	$\delta^{18}\text{O}$ (‰)	StD	δD (‰)	StD	d-excess (‰)
2.Feb.04	-7.83	0.02	-59.2	0.3	1.84

• Table a4.9 Stable isotopes (rain event 2)

Altitude (masl)	$\delta^{18}\text{O}$ (‰)	StD	δD (‰)	StD	d-excess (‰)
670	-7.08	0.02	-36.9	0.3	19.7
975	-6.08	0.02	-24.3	0.2	24.3
1310	-6.96	0.03	-29.5	0.2	26.2
1500	-6.70	0.03	-28.9	0.2	24.7
1550	-6.87	0.02	-29.7	0.3	25.3
mean	-6.74		-29.9		24.0
StD	0.39		2.6		0.8

• Table a4.10 Stable isotopes (rain event 3)

date	d^{18}O (‰)	StD	dD (‰)	StD	d-excess (‰)
28-Feb-05	-12.54	0.08	-91.21	0.28	9.11
2-Mar-05	-18.63	0.01	-142.83	0.27	6.21
5-Mar-05	-13.7	0.01	-100.79	0.05	8.81
mean	-16.17		-121.81		7.51
StD	3.49		29.73		1.84

• Table a4.11 Stable isotopes (rain event 4)

Altitude (masl)	$\delta^{18}\text{O}$ (‰)	StD	δD (‰)	StD	d-excess (‰)
1295	-4.29	0.0	-25.2	0.1	9.13
650	-2.06	0.0	-13.3	0.3	3.19
mean	-3.18		-19.24		6.16
StD	1.58		8.41		4.20

• Table a4.12 Date, Altitude (masl), $\delta^{18}\text{O}$, δD and evaporative-enrichment-corrected $\delta^{18}\text{O}$ -values of snowmelt samples.

site ID	Altitude (masl)	X (UTM)	Y (UTM)	$\delta^{18}\text{O}$ (‰)	$\delta^{18}\text{O}$ (‰) error	δD (‰)	δD (‰) error	$\delta^{18}\text{O}$ (‰) corrected	δD (‰) corrected
SP-GR-180	3192	467216	4100692	-11.55	0.06	-76.9	0.3	-11.32	-75.7
SP-GR-182	2919	468241	4100417	-10.28	0.06	-68.8	0.4	-10.58	-70.3
SP-GR-184	3018	469256	4100752	-9.98	0.1	-66.5	0.2	-10.25	-67.8
SP-GR-224	3039	467010	4100073	-8.78	0.01	-61.1	0.3	-10.48	-69.5
SP-GR-232	2917	474283	4103394	-8.27	0.09	-59.9	0.1	-11.03	-73.6
SP-GR-038	2889	471254	4100231	-10.58	0.02	-70.1	0.3	-10.50	-69.7
SP-GR-039	2589	472401	4102774	-10.33	0.05	-68.6	0.4	-10.40	-68.9
SP-GR-041	2983	471254	4100231	-10.54	0.05	-71.1	0.2	-10.99	-73.4
SP-GR-042	3211	472401	4102774	-9.31	0.05	-61.2	0.3	-9.44	-61.8
SP-GR-043	3473	472450	4101088	-8.61	0.02	-58.2	0.1	-9.63	-63.3
SP-GR-044	2860	468831	4102567	-10.24	0.05	-68.3	0.3	-10.46	-69.4
SP-GR-045	2790	470268	4101727	-9.37	0.05	-63.7	0.3	-10.34	-68.5
SP-GR-046	2787	470131	4101794	-9.5	0.06	-62.9	0.2	-9.75	-64.1
SP-GR-047				-9.64	0.03	-64.4	0.1	-10.08	-66.6
SP-GR-049		-		-9.5	0.04	-62.4	0.4	-9.54	-62.6
SP-GR-050				-9.5	0.08	-63.7	0.4	-10.08	-66.6
SP-GR-055	2689	473109	4096441	-10.53	0.04	-68.6	0.4	-9.99	-65.9
SP-GR-056	2958	471216	4100676	-10.32	0.03	-69.8	0.2	-10.91	-72.7
	min			-11.55	0.01	-76.9	0.1	-11.32	-75.7
	max			-8.27	0.1	-58.2	0.4	-9.44	-61.8
	average			-9.82	0.05	-65.9	0.27	-10.32	-68.4

• Table a4.13: Date, Altitude (masl), $\delta^{18}\text{O}$, δD and evaporative-enrichment-corrected $\delta^{18}\text{O}$ -values of *laguna* samples.

site ID	Altitude (masl)	X / Y (UTM)		$\delta^{18}\text{O}$ (‰)	$\delta^{18}\text{O}$ (‰) error	δD (‰)	δD (‰) error	$\delta^{18}\text{O}$ (‰) corrected	δD (‰) corrected
SP-GR-211	2921	463544	4098485	-7.18	0.01	-51.4	0.3	-9.76	-64.2
SP-GR-212	2909	462902	4098129	-8.91	0.04	-62.6	0.3	-10.83	-72.1
SP-GR-213	2736	461866	4097054	-9.26	0.03	-63.1	0.4	-10.32	-68.4
SP-GR-215	2851	461190	4096807	-7.89	0.04	-57.2	0.5	-10.69	-71.1
SP-GR-216	2685	461997	4099165	-10.35	0.02	-69.1	0.2	-10.56	-70.1
SP-GR-217	2687	464634	4100593	-10.38	0.03	-68.5	0.3	-10.25	-67.9
SP-GR-218	2874	469068	4100148	-8.72	0.05	-62.8	0.3	-11.30	-75.6
SP-GR-219	2823	469717	4100056	-10.23	0.04	-68.8	0.3	-10.68	-71.0
SP-GR-220	3125	467696	4100981	-10.17	0.04	-67.4	0.4	-10.23	-67.7
SP-GR-221	3068	467505	4101855	-9.67	0.02	-64	0.1	-9.85	-64.9
SP-GR-222	3093	467548	4101787	-9.3	0.08	-61.6	0.2	-9.62	-63.2
SP-GR-181	3059	467372	4100518	-10.41	0.05	-69.4	0.3	-10.56	-70.1
SP-GR-183	2881	468470	4100336	-10.48	0.06	-70.1	0.2	-10.71	-71.2
SP-GR-185	3023	469405	4100928	-9.62	0.06	-64.1	0.3	-10.00	-66.0
SP-GR-187	2868	471745	4101956	-8.72	0.08	-58.3	0.2	-9.45	-61.9
SP-GR-189	2936	466354	4101019	-9.53	0.07	-64.1	0.2	-10.18	-67.3
SP-GR-190	2950	466428	4100907	-9.94	0.02	-66.2	0.1	-10.21	-67.5
SP-GR-191	2928	466340	4100792	-10.38	0.05	-68.6	0.2	-10.29	-68.2
SP-GR-192	2899	465883	4100683	-10.26	0.04	-68.2	0.1	-10.37	-68.8
SP-GR-195	2421	463080	4102087	-9.84	0.05	-66.7	0.4	-10.62	-70.6
SP-GR-196	2495	463052	4101813	3.82	0.05	-5.3	0.2	-13.29	-90.3
SP-GR-202	2982	464525	4099331	-8.93	0.04	-61	0.2	-10.13	-67.0
SP-GR-203	2975	464393	4099293	-9.55	0.03	-65	0.2	-10.51	-69.8
SP-GR-204	3027	473494	4101370	-8.98	0.06	-63.3	0.1	-10.98	-73.2
SP-GR-205	2995	473724	4101153	-9.75	0.07	-66.7	0.2	-10.80	-71.9
SP-GR-206	2987	473465	4100967	-10.63	0.02	-69	0.3	-9.95	-65.6
SP-GR-207	2942	473513	4100647	-10.69	0.03	-70.7	0.3	-10.52	-69.9
SP-GR-208	2897	473917	4100421	-10.54	0.06	-70.7	0.4	-10.83	-72.1
SP-GR-209	2796	479054	4106645	-10.52	0.04	-71.2	0.1	-11.08	-74.0
SP-GR-223	3084	467622	4101666	-9.8	0.07	-64.9	0.4	-9.96	-65.7
SP-GR-227	3073	467593	4101655	-9.18	0.03	-60.9	0.1	-9.58	-62.9
SP-GR-228	2866	469355	4101575	-10.13	0.06	-68.2	0.1	-10.64	-70.7
SP-GR-229	2784	470141	4101803	-10.54	0.12	-70.6	0.1	-10.79	-71.8
SP-GR-230	2787	470272	4101728	-8.35	0.05	-60.4	0.2	-11.07	-73.9
SP-GR-231	2894	472135	4101784	-10.32	0.03	-68.8	0.3	-10.50	-69.7
SP-GR-040	2895	472144	4101759	-10.53	0.04	-70.5	0.3	-10.77	-71.7
SP-GR-225	2707	463599	4100546	3.18	0.04	-5.9	0.1	-12.22	-82.5
SP-GR-233	2891	474383	4103269	-6.39	0.1	-50.8	0.2	-11.13	-74.3
SP-GR-234	2880	474564	4103379	-4.16	0.03	-38.8	0.3	-10.75	-71.6
	min			-10.69	0.02	-71.2	0.1	-12.22	-82.5
	max			3.18	0.12	-5.9	0.4	-9.58	-62.9
	average			-8.66	0.05	-61.0	0.2	-10.68	-71.0

Stable isotopes in springs Time series

• Table a4.14 Fte.Cortijuela (X 458341 Y 4104600 Z 1695)

Sampling date	$\delta^{18}\text{O}$ (‰)	$\delta^{18}\text{O}$ (‰) error	δD (‰)	δD (‰) error	d excess (‰)
22 Nov 04	-8.86	0.03	-58.2	0.3	12.7
22 Mar 05	-8.96	0.02	-58.5	0.4	13.2
7 Oct 04	-8.72	0.07	-56.1	0.3	13.7
23 Mar 05	-8.96	0.01	-58.8	0.4	12.9
5 Feb 04	-8.69		-56.3		13.2
σ	0.11	0.02	1.1	0.0	0.3
\emptyset	-8.84	0.03	-57.6	0.3	13.1

• Table a4.15 Fte.Cerro Negro (X 451504 Y 4125682 Z 1115)

Sampling date	$\delta^{18}\text{O}$ (‰)	$\delta^{18}\text{O}$ (‰) error	δD (‰)	δD (‰) error	d excess (‰)
19 Feb 05	-8.14	0.02	-53.2	0.2	11.9
08 Nov 04	-8.10	0.08	-52.5	0.4	12.3
25 Mrz 05	-8.12	0.02	-53.0	0.1	12.0
07 Okt 04	-8.11	0.04	-53.2	0.1	11.7
σ	0.01	0.02	0.3	0.1	0.2
\emptyset	-8.12	0.04	-53.0	0.2	12.0

• Table a4.16 Fte.Alta (X 463724 Y 4106755 Z 2156)

Sampling date	$\delta^{18}\text{O}$ (‰)	$\delta^{18}\text{O}$ (‰) error	δD (‰)	δD (‰) error	d excess (‰)
05 Feb 04	-9.46		-63.0		12.6
07 Okt 04	-9.41	0.04	-62.5	0.1	12.8
15 Nov 04	-9.43	0.02	-63.2	0.1	12.2
19 Feb 05	-9.52	0.02	-62.7	0.2	13.5
σ	0.04	0.01	0.28	0.02	0.46
\emptyset	-9.46	0.03	-62.85	0.12	12.79

• Table a4.17 Fte.de 16 Canos (X 460592 Y 4113364 Z 1222)

Sampling date	$\delta^{18}\text{O}$ (‰)	$\delta^{18}\text{O}$ (‰) error	δD (‰)	δD (‰) error	d excess (‰)
19 Feb 05	-8.84	0.02	-58.1	0.2	12.6
07 Okt 04	-8.83	0.04	-58.8	0.3	11.8
15 Nov 04	-8.87	0.06	-58.5	0.2	12.5
05 Mrz 05	-8.97	0.01	-59.3	0.3	12.5
05 Feb 04	-8.86		-58.8		12.1
σ	0.05	0.02	0.4	0.1	0.3
\emptyset	-8.87	0.03	-58.7	0.3	12.3

• Table a4.18 Banos de la Malah (X 435500 Y 4106901 Z 752)

Sampling date	$\delta^{18}\text{O}$ (‰)	$\delta^{18}\text{O}$ (‰) error	δD (‰)	δD (‰) error	d excess (‰)
22 Nov 04	-8.57	0.02	-57.3	0.1	11.3
06 Feb 04	-8.26		-55.4		10.7
05 Mrz 05	-8.58	0.01	-57.1	0.1	11.5
16 Okt 04	-8.47	0.03	-56.0	0.2	11.8
σ	0.13	0.01	0.8	0.0	0.4
\emptyset	-8.47	0.02	-56.4	0.1	11.3

APPENDIX – Results and discussion

• Table a4.19 Fte.de Hervidero (X 452680 Y 4104908 Z 1292)

Sampling date	$\delta^{18}\text{O}$ (‰)	$\delta^{18}\text{O}$ (‰) error	δD (‰)	δD (‰) error	d excess (‰)
5 Feb 05	-8.90	0.02	-59.0	0.1	12.2
23 Mar 05	-8.91	0.01	-59.2	0.1	12.1
26 Feb 05	-8.90	0.01	-53.7	0.2	17.5
22 Nov 04	-8.93	0.02	-61.0	0.3	10.4
7 Oct 04	-8.77	0.05	-59.9	0.3	10.3
5 Feb 04	-8.81		-59.0		11.5
σ	0.06	0.01	2.3	0.1	2.4
\emptyset	-8.87	0.02	-58.6	0.2	12.3

• Table a4.20 Fte.de Teja (X 462038 Y 4115147 Z 1278)

Sampling date	$\delta^{18}\text{O}$ (‰)	$\delta^{18}\text{O}$ (‰) error	δD (‰)	δD (‰) error	d excess (‰)
05 Feb 04	-8.19		-53.2		12.3
19 Feb 05	-8.17	0.02	-53.3	0.3	12.1
15 Nov 04	-8.00	0.03	-53.7	0.3	10.3
σ	0.09	0.00	0.2	0.0	0.9
\emptyset	-8.12	0.03	-53.4	0.3	11.6

• Table a4.21 Fte.Grande (X 450942 Y 4122562 Z 1114)

Sampling date	$\delta^{18}\text{O}$ (‰)	$\delta^{18}\text{O}$ (‰) error	δD (‰)	δD (‰) error	d excess (‰)
8 Nov 04	8.38	0.02	53.8	0.3	13.2
8 Mar 05	8.40	0.02	54.0	0.2	13.2
24 Mar 05	8.45	0.01	54.0	0.2	13.6
6 Feb 04	8.38		54.2		12.9
7 Oct 04	8.35	0.02	53.2	0.3	13.6
19 Feb 05	8.41	0.01	53.4	0.2	13.9
σ	0.03	0.00	0.4	0.0	0.3
\emptyset	8.40	0.02	53.8	0.2	13.4

• Table a4.22 Fte.las Viboras (X 460619 Y 4109365 Z 1629)

Sampling date	$\delta^{18}\text{O}$ (‰)	$\delta^{18}\text{O}$ (‰) error	δD (‰)	δD (‰) error	d excess (‰)
05 Feb 04	-8.99		-59.0		12.9
07 Okt 04	-8.92	0.06	-58.5	0.2	12.9
15 Nov 04	-8.99	0.01	-58.6	0.3	13.3
σ	0.03	0.03	0.2	0.1	0.2
\emptyset	-8.97	0.04	-58.7	0.3	13.0

• Table a4.23 Fte.Molinos (X 444626 Y 4096002 Z 730)

Sampling date	$\delta^{18}\text{O}$ (‰)	$\delta^{18}\text{O}$ (‰) error	δD (‰)	δD (‰) error	d excess (‰)
06 Feb 04	8.07		52.5		12.1
22 Nov 04	8.16	0.02	53.6	0.3	11.7
16 Okt 04	8.05	0.06	54.7	0.3	9.7
σ	0.05	0.02	0.9	0.0	1.1
\emptyset	8.09	0.04	53.6	0.3	11.2

• Table a4.24 Nacimiento Rio Darro (X 454448 Y 4121644 Z 1106)

Sampling date	$\delta^{18}\text{O}$ (‰)	$\delta^{18}\text{O}$ (‰) error	δD (‰)	δD (‰) error	d excess (‰)
07 Okt 04	8.40	0.06	54.8	0.3	12.4
24 Mrz 05	8.49	0.01	54.1	0.2	13.8
08 Nov 04	8.37	0.04	53.7	0.2	13.3
σ	0.05	0.02	0.5	0.0	0.6
\emptyset	8.42	0.04	54.2	0.2	13.2

• Table a4.25 Fte. de Nivar (X 449618 Y 4124631 Z 1108)

Sampling date	$\delta^{18}\text{O}$ (‰)	$\delta^{18}\text{O}$ (‰) error	δD (‰)	δD (‰) error	d excess (‰)
24 Mrz 05	8.41	0.01	53.6	0.3	13.7
07 Okt 04	8.40	0.03	53.8	0.2	13.4
19 Feb 05	8.42	0.02	54.2	0.2	13.2
08 Nov 04	8.39	0.04	54.2	0.3	12.9
σ	0.01	0.01	0.2	0.0	0.3
\emptyset	8.41	0.03	53.9	0.2	13.3

• Table a4.26 Fte. Palmones (X 446488 Y 4097321 Z 745)

Sampling date	$\delta^{18}\text{O}$ (‰)	$\delta^{18}\text{O}$ (‰) error	δD (‰)	δD (‰) error	d excess (‰)
05 Mrz 05	-8.55	0.03	-55.9	0.4	12.5
16 Okt 04	-8.49	0.04	-56.1	0.1	11.8
06 Feb 04	-8.55		-56.0		12.4
22 Nov 04	-8.63	0.01	-57.1	0.2	11.9
σ	0.05	0.01	0.5	0.1	0.3
\emptyset	-8.56	0.03	-56.3	0.2	12.1

• Table a4.27 Fte. Urquiza (X 448212 Y 4092451 Z 650)

Sampling date	$\delta^{18}\text{O}$ (‰)	$\delta^{18}\text{O}$ (‰) error	δD (‰)	δD (‰) error	d excess (‰)	
16 Okt 04	-8.81	0.03	-57.9	0.2	12.6	
05 Feb 04	-8.79		-57.9		12.4	right tube
10 Mrz 05	-8.92	0.02	-58.2	0.3	13.1	
10 Mrz 05	-8.85	0.01	-58.2	0.2	12.6	
05 Feb 04	-8.88		-58.1		12.9	left tube
16.Okt.04	-8.78	0.03	-58.1	0.1	12.1	
σ	0.05	0.01	0.1	0.1	0.3	
\emptyset	-8.84	0.02	58.1	0.2	12.7	

Stable isotopes in surface water Time series

• Table a4.28 Darro 1 (X 453614 Y 4116883 Z 453614)

Sampling date	$\delta^{18}\text{O}$ (‰)	$\delta^{18}\text{O}$ (‰) error	δD (‰)	δD (‰) error	d excess (‰)
10 Jan 05	-8.13	0.0	-52.0	0.2	13.01
25 Nov 04	-8.22	0.0	-54.3	0.4	11.46
7 Dec 04	-8.20	0.0	-51.8	0.5	13.80
4 Feb 05	-8.06	0.0	-51.6	0.3	12.86
σ	0.06	0.0	1.1	0.1	0.84
\emptyset	-8.15	0.0	-52.4	0.4	12.78

• Table a4.29 Darro 2 (X 452134 Y 4114769 Z 820)

Sampling date	$\delta^{18}\text{O}$ (‰)	$\delta^{18}\text{O}$ (‰) error	δD (‰)	δD (‰) error	d excess (‰)
02 Apr 05	8.10	0.02	52.5	0.1	12.3
04 Feb 05	7.98	0.02	51.8	0.5	12.1
16 Nov 04	8.01	0.07	51.4	0.3	12.7
38328	8.21	0.01	52.9	0.3	12.8
38362	8.07	0.01	52.3	0.2	12.3
25 Nov 04	8.18	0.03	54.1	0.3	11.3
28 Okt 04	7.98	0.04	51.3	0.2	12.5
σ	0.09	0.02	0.9	0.1	0.4
\emptyset	8.08	0.03	52.3	0.3	12.3

• Table a4.30 Genil 1 (X 465504 Y 4110023 Z 1179)

Sampling date	$\delta^{18}\text{O}$ (‰)	$\delta^{18}\text{O}$ (‰) error	δD (‰)	δD (‰) error	d excess (‰)
07 Okt 04	-9.51	0.03	-65.2	0.3	10.9
23 Okt 04	-9.41	0.04	-64.3	0.2	11.0
15 Nov 04	-9.63	0.03	-64.9	0.2	12.1
19 Jan 05	-9.68	0.02	-65.5	0.3	11.9
27 Jan 05	-9.65	0.03	-66.0	0.2	11.2
38416	-10.27	0.01	-70.8	0.2	11.4
σ	0.27	0.01	2.2	0.0	0.5
\emptyset	-9.69	0.03	-66.1	0.2	11.4

• Table a4.31 Genil 2 (X 457130Y 4112948 Z 820)

Sampling date	$\delta^{18}\text{O}$ (‰)	$\delta^{18}\text{O}$ (‰) error	δD (‰)	δD (‰) error	d excess (‰)
23 Okt 04	-9.53	0.04	-64.10	0.40	12.14
10 Nov 04	-9.29	0.05	-63.00	0.40	11.32
04 Dez 04	-9.24	0.02	-63.10	0.20	10.82
09 Jan 05	-9.07	0.02	-61.84	0.09	10.72
25 Jan 05	-9.07	0.03	-61.68	0.37	10.88
06 Mrz 05	-9.01	0.02	-61.29	0.15	10.79
σ	0.18	0.01	0.98	0.13	0.50
\emptyset	-9.20	0.03	-62.50	0.27	11.11

• Table a4.32 Genil 3 (X 452810 Y 4112390 Z 725)

Sampling date	$\delta^{18}\text{O}$ (‰)	$\delta^{18}\text{O}$ (‰) error	δD (‰)	δD (‰) error	d excess (‰)
09 Jan 05	-8.52	0.02	-57.1	0.1	11.0
23 Okt 04	-8.49	0.04	-56.7	0.3	11.2
04 Dez 04	-8.71	0.02	-57.7	0.4	12.0
10 Nov 04	-8.35	0.04	-56.3	0.2	10.5
25 Jan 05	-8.61	0.02	-58.6	0.2	10.3
σ	0.12	0.01	0.8	0.1	0.6
\emptyset	-8.54	0.03	-57.3	0.2	11.0

• Table a4.33 Embalse Canales (X 457810 Y 4112776 Z 950)

Sampling date	$\delta^{18}\text{O}$ (‰)	$\delta^{18}\text{O}$ (‰) error	δD (‰)	δD (‰) error	d excess (‰)
04 Dez 04	-9.16	0.02	-63.3	0.3	10.0
19 Feb 05	-9.01	0.01	-61.4	0.2	10.7
05 Mrz 05	-9.01	0.02	-61.4	0.3	10.7
σ	0.07	0.00	0.9	0.0	0.3
\emptyset	-9.06	0.02	-62.0	0.3	10.5

• Table a4.34 Arr.Huenes (X 455420 Y 4104565 Z 1420)

Sampling date	$\delta^{18}\text{O}$ (‰)	$\delta^{18}\text{O}$ (‰) error	δD (‰)	δD (‰) error	d excess (‰)
23 Mrz 05	-8.93	0.01	-59.0	0.2	12.5
05 Feb 05	-8.89	0.01	-58.8	0.2	12.3
σ	0.02	0.00	0.1	0.0	0.1
\emptyset	-8.91	0.01	-58.9	0.2	12.4

Stable isotopes in single measurements

• Table a4.35 Stable isotopes in single measurements

Site Name	Type	Sampling date	Altitude (masl)	X/Y (UTM)	$\delta^{18}\text{O}$ (‰)	$\delta^{18}\text{O}$ (‰) error	δD (‰)	δD (‰) error
Camino frente Puleva	Piezometer	16-Nov-04	619	442540 4115200	-8.84	0.01	-59.30	0.20
Romilla	Piezometer	05-Nov-04	540	430100 4117700	-6.92	0.02	-48.40	0.40
Atarfe	Piezometer	17-Nov-04	550	432480 4122400	-8.52	0.03	-57.90	0.30
Pedro Ruiz	Piezometer	12-Nov-04	554	432940 4119520	-8.13	0.02	-56.80	0.40
Aeropuerto	Piezometer	25-Nov-04	584	433530 4115090	-6.33	0.04	-44.70	0.20
Alhendin	Piezometer	08-Nov-04	728	442560 4108020	-8.82	0.03	-60.30	0.30
Cullar Vega	Piezometer	09-Nov-04	647	441238 4112140	-8.96	0.01	-59.70	0.20
Cort. Trevijano	Piezometer	26-Nov-04	615	442229 4116375	-8.27	0.03	-56.60	0.30
Instituto del agua	Rain	20-Feb-04	650	447015 4116550	-7.63	0.05	-59.20	0.20
Rain 975m	Rain	02-Dez-04	975	461294 4111763	-6.08	0.02	-24.30	0.20
Rain 1310m	Rain	02-Dez-04	1310	466974 4122957	-6.96	0.03	-29.50	0.20
Rain 1500m	Rain	02-Dez-04	1500	469738 4123212	-6.70	0.03	-28.90	0.20
Rain 1550m	Rain	02-Dez-04	1550	471369 4121606	-6.87	0.02	-29.70	0.30
Rain 670m	Rain	02-Dez-04	670	447148 4114717	-7.08	0.02	-36.90	0.30
Rain at Fte. del Hervidero	Rain	23-Mrz-05	1295	452681 4104907	-4.29	0.02	-25.19	0.14
Fte. de Vita	Spring	08-Nov-04	944	448211 4126823	-7.48	0.04	-48.70	0.20
Fte. Teja	Spring	08-Nov-04	1262	455011 4124238	-8.35	0.02	-52.30	0.20
Fte. Savina	Spring	09-Nov-04	1113	463808 4120518	-8.10	0.10	-52.50	0.30
Fte. Agostinos	Spring	09-Nov-04	1362	469515 4119592	-8.55	0.05	-56.70	0.30
Fte. Carcabal	Spring	09-Nov-04	1605	471406 4120195	-8.79	0.07	-57.80	0.10
Fte. Nabugal	Spring	09-Nov-04	1471	472835 4121540	-8.69	0.04	-56.70	0.30
Fte. 7 ojos	Spring	22-Nov-04	1411	455151 4104428	-8.97	0.02	-59.20	0.40
Banos de Sierra Elvira	Spring	18-Feb-05	571	436043 4120641	-7.82	0.02	-51.82	0.14
Manantial de la Reina	Spring	18-Feb-05	563	434096 4118218	-8.39	0.01	-57.45	0.25

APPENDIX – Results and discussion

• Table a4.35 -continued-

Site Name	Type	Sampling date	Altitude (masl)	X/Y (UTM)		$\delta^{18}\text{O}$ (‰)	$\delta^{18}\text{O}$ (‰) error	δD (‰)	δD (‰) error
Banos Santa Fe	Spring	18-Feb-05	840	433992	4112505	-8.41	0.02	-55.31	0.43
Los Fagailos	Spring	18-Feb-05	542	429477	4111979	-8.44	0.02	-57.07	0.35
Banos Alhama de Granada	Spring	10-Mrz-05	760	413097	4098439	-8.26	0.02	-53.82	0.36
Rio Durcal	Surface water	16-Okt-04	647	448197	4092470	-8.42	0.02	-56.90	0.40
Arroyo Caballo	Surface water	13-Feb-05	2500	459726	4096646	-9.78	0.02	-65.30	0.38
Arroyo de salado	Surface water	18-Feb-05	740	435667	4112891	-6.53	0.01	-48.24	0.30
Rio Cubillas	Surface water	18-Feb-05	549	430629	4122035	-6.55	0.01	-45.89	0.28
Puente Rio Genil	Surface water	18-Feb-05	560	426281	4117770	-7.43	0.02	-51.48	0.12
Embalse Bermejales	Surface water	10-Mrz-05	800	421546	4093626	-5.62	0.02	-38.88	0.41
Zulauf Hotel Alhama de Granada	Surface water	10-Mrz-05	760	413112	4098400	-7.88	0.02	-50.02	0.08
Oberlauf Alhama de Granada	Surface water	10-Mrz-05	761	413016	4098208	-7.92	0.01	-50.17	0.27
Unterlauf Alhama de Granada	Surface water	10-Mrz-05	758	413134	4098444	-7.96	0.03	-50.73	0.36
Rio Cubillas	Surface water	08-Mrz-05	693	447838	4131886	-7.66	0.01	-52.25	0.23
Embalse de Cubillas	Surface water	08-Mrz-05	640	440820	4126377	-6.18	0.01	-44.42	0.30
Casa Nuevas	Well	22-Nov-04	552	430138	4123195	-6.13	0.02	-42.50	0.20
Santa Rosa	Well	10-Nov-04	555	427396	4122063	-6.64	0.02	-46.70	0.20
Armilla Vivero Dip	Well	18-Feb-05	694	444801	4109716	-8.98	0.01	-60.22	0.25
Cullar Vega	Well	18-Feb-05	654	441457	4111726	-9.16	0.00	-62.33	0.33
Alhencira	Well	18-Feb-05	814	444185	4106797	-9.15	0.02	-60.50	0.20
Terrazos Terragran	Well	18-Feb-05	724	446535	4119370	-7.81	0.01	-50.90	0.20
Cort. Santa Ana	Well	18-Feb-05	574	437121	4119131	-8.52	0.01	-57.53	0.36
Meson El Guerro	Well	18-Feb-05	719	449190	4111289	-8.91	0.03	-60.40	0.09
UGR, Facultad de Ciencias	Well	09-Mrz-05	650	446075	4115214	-8.19	0.01	-55.07	0.10